Low-temperature thermochronological and structural study of the inner Hardangerfjord area, southern Norway

Karen Cecilie Johannessen

Master of Science Thesis
in Geodynamics

Department of Earth Science
University of Bergen
2012

ABSTRACT

The origin of the mountainous topography in southern Norway is at present unresolved. Post-Devonian sediments are absent onshore, making quantification of crustal uplift and fault displacements difficult. Low-temperature thermochronological techniques can be employed to constrain the timing of vertical movements through the uppermost few kilometres of the crust and are at present the most effective means of obtaining information about the topographic evolution prior to the Quaternary glaciations. This study aims to delineate the post-Caledonian morphotectonic evolution of the inner Hardangerfjord region by the means of apatite fission track and (U-Th)/He thermochronology, in combination with inverse thermal history modelling.

Thirty-two samples derived from the steep flanks of the inner segments of the Hardangerfjord were analysed by the apatite fission track method. The resulting cooling ages range from Late Triassic to Late Cretaceous. A general positive age-elevation trend is evident, with abundant Early Cretaceous ages close to sea level and Jurassic ages on the Hardangervidda plateau. Four samples from the Eidfjord and Ulvik districts were analysed by the (U-Th)/He method, giving dominantly Cretaceous single grain ages. Fisson track age-elevation gradients and combined data from the apatite fission track and (U-Th)/He thermochronometers reveal low Jurassic-Cretaceous cooling rates in the order of ~1 °C/Ma. Large age jumps over limited horizontal distances suggest post-Middle Jurassic offset across both small-scale faults and regional structures. Offset age-elevation gradients indicate local displacements in the order of several 100 to more than 1000 metres.

Thermal history modelling reveals two distinct episodes of accelerated cooling, which can be linked to documented pulses of tectonic activity onshore southern Norway and in adjacent offshore areas. Rapid cooling (2-6 °C) is inferred for the Permo-Triassic and is consistent with rift flank uplift and accelerated denudation in connection to the development of the North Sea Basin. The Jurassic and Cretaceous periods were characterised by low cooling rates (≤ 1 °C/Ma) and relatively minor regional exhumation, suggesting that the effects of the second North Sea rift phase were not pronounced in inland areas. Localized, periodically increased exhumation rates associated with fault displacement and footwall uplift are inferred from the fission track age distribution, but are not resolved by the thermal history models. The second episode of rapid cooling (~2 °C/Ma) is constrained to the late Cretaceous-Eocene and may have been attributed to tectonic activity in relation to the North Atlantic breakup or enhanced topographic relief following thermally induced uplift triggered by the Iceland mantle plume. Distinctly different Palaeogene cooling paths for adjacent structural blocks suggest that fault activity may have continued into the Cenozoic. Considering the fission track age distribution patterns and thermal history models reported from southwestern Norway in general, it is suggested that extensive fault activity has exerted a significant control on the overall morphology of the passive margin. Pre-Eocene peneplanation and domal tectonic uplift, as has been proposed in previous studies, cannot fully account for the thermochronological data obtained in the current work.

ACKNOWLEDGEMENTS

I wish to thank my supervisors, Prof. Joachim Jacobs and Dr. Fabian Kohlmann, for excellent guidance throughout my time as a master student. Joachim is especially thanked for introducing me to the sampling scheme and for sharing his knowledge and experience in the field. Fabian has taken me through fission track analysis step by step to ensure that in the end I could present my results with confidence. Thank you very much!

I would like to thank Dr. Anna Ksienzyk for good advice and support throughout the process and for including my samples during grain selection for (U-Th)/He analysis. In addition, Anna provided me with six of her own samples, for which I am very grateful. Thanks to Vibeke Gellein Hanssen for teaching me the procedures for mineral separation. Present and former members of the Bergen Tectonics and Thermochronology research group are thanked for fruitful discussions and good times during my two years as a master student.

I would like to thank my fellow geology students at the University of Bergen, with whom I have shared five wonderful years full of memorable moments. Malene Eikås Halkjelsvik and Kari Sekkingstad are especially thanked for their very useful comments on early drafts of the thesis.

My father, Arne Johannessen, kindly volunteered to be my field assistant and is thanked for his enthusiasm and interest in my work. Special thanks to my mother, Aud Johannessen, for unlimited support and for helping out with babysitting whenever needed.

Finally, I would like to thank my boyfriend, Christian Breistein, for patiently allowing me to pursue my goals and our boys Håkon and Håvard, for always giving me something to smile about and for reminding me what, at the end of the day, is more important in life.

Bergen, 25 October 2012

Karen Cecilie Johannessen

TABLE OF CONTENTS

1. INTRODUCTION

The origin of the high topography in southern Norway is a matter of controversy. As a result of the general lack of post-Devonian sediments onshore, the timing of uplift, erosion and topographical development is difficult to constrain. Over the last few years in particular, the onshore tectonic and geomorphological evolution, especially from the Jurassic onwards, has been the focus of a heated debate. In this regard, two contrasting models have received special attention; the conventional model (hereafter referred to as the peneplanation-uplift model) that invokes Mesozoic peneplanation followed by tectonic uplift during the Cenozoic (Gabrielsen et al., 2010) and the ICE hypothesis, which portrays the present topography as a remnant of the ~410 Ma Caledonian orogen (Nielsen et al., 2009). Low-temperature thermochronological techniques have the potential of revealing essential aspects concerning the timing and magnitude of Mesozoic and Cenozoic exhumation in southern Norway. However, the data that are available at present do not provide sufficient information on recent cooling events and thus cannot differentiate between the scenarios advocated by each of the models (Ksienzyk, 2012).

The research presented in this thesis is part of the Earth System Modelling (ESM) project at the University of Bergen. Overall, the aim of the ESM project is to improve the understanding of how onshore deformation and erosion is linked to sediment transport and deposition in a passive margin setting. The present contribution attempts to provide new insights into the exhumation and tectonics of the Norwegian margin hinterland. Apatite fission track (AFT) and (U-Th)/He analysis will be utilized in order to gain new, detailed information about the cooling history of the mountainous central part of the country.

1.1 Study area

The present study focuses on the Eidfjord, Ulvik, Ullensvang and Granvin districts in the inner regions of the Hardangerfjord (Fig. 1). Geologically, this area is dominated by crystalline, Precambrian lithologies in addition to minor Cambrosilurian metasedimentary rocks and remnants of Caledonian thrust sheets. The NE-SW-trending Hardangerfjord Shear Zone dissects the Precambrian basement in the westernmost part of the field area. Following the termination of the Caledonian orogeny the Hardangerfjord Shear Zone exerted a major

control on the regional tectonic evolution (Fossen & Hurich, 2005) and may have governed landscape development by influencing denudational patterns.

Topographically, the inner Hardangerfjord region is characterized by high relief. Glacial fjords and valleys with steep flanks on both sides are incised into the undulating highlands of the Hardangervidda plateau, which has a general elevation of ca. 1000 m in the area. The highest summits in the study area rise sharply to elevations of more than 1600 m a.s.l. The small tributaries to the Hardangerfjord are generally relatively shallow compared to the main segment, which attains a depth of 700 m in the outer Sørfjord.

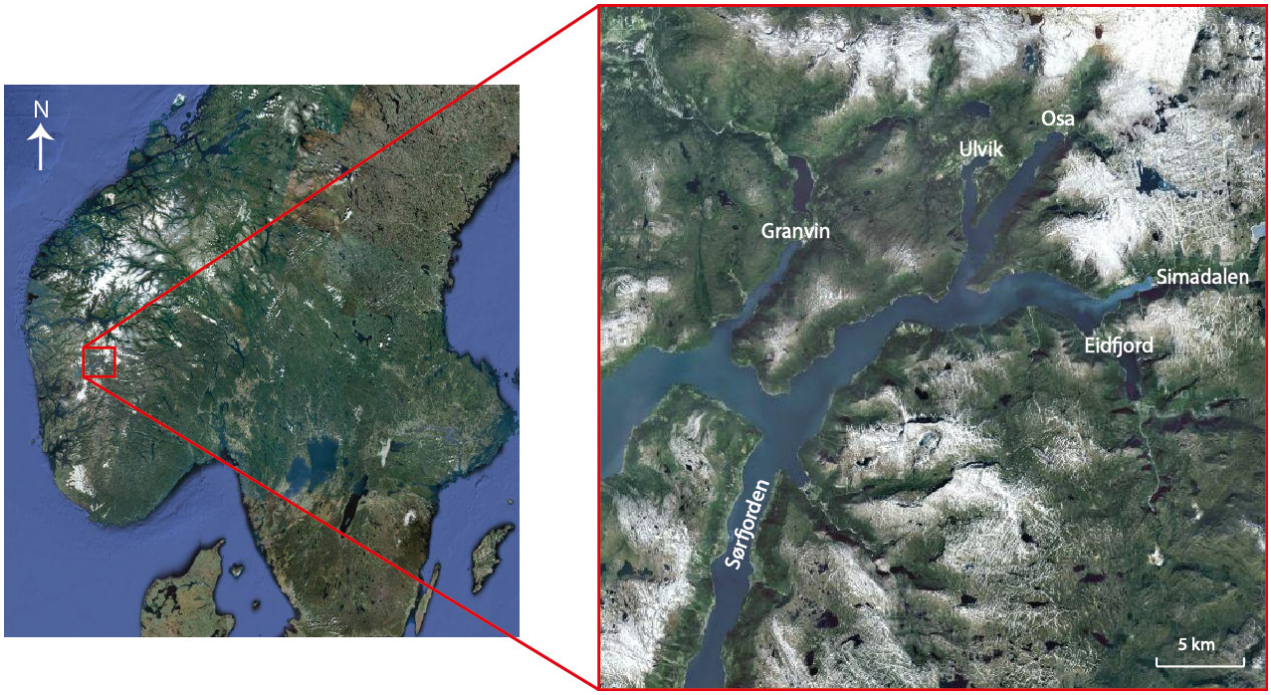

Fig. 1. Overview map of the study area, which is located in central southern Norway, directly to the west of the highest topography. The Sørfjord and the Eidfjord are the main segments of the inner portions of the Hardangerfjord. Four small tributaries extend towards the N-NE in the northern part of the outlined area.

1.2 Research objectives

The glacially shaped fjords in southern Norway offer a unique opportunity to sample across the passive margin into the hinterland at constant, low elevations. Samples collected in this manner have the potential of revealing essential aspects concerning the style of passive margin evolution. Eidfjord is regarded as one of the classical sites for low-temperature thermochronology in Norway, and a number of studies have been undertaken in this particular area (Andriessen and Bos, 1986; Rohrman, 1995; Leighton 2007). Some of the youngest

apatite fission track ages in Norway are found at low elevations in the inner regions of the Hardangerfjord. The combination of young ages close to sea level and high relief topography makes the Eidfjord and adjacent tributaries of the Hardangerfjord excellent targets for detailed studies on the timing and magnitude of the much debated post-Jurassic exhumation. Vertical sample transects are well suited for this purpose. Previous work in the region has, however, failed to provide a comprehensive representation of the exhumation history, mainly because the so called vertical profiles that have been sampled extend over significant horizontal distances (i.e. >20 km). Considerable lateral differences between samples in a vertical profile increase the risk of sampling across faults. Thermochronological data obtained from vertical profiles that are sampled in this manner may potentially contribute a distorted picture of the regional cooling history, given that structural discontinuities are not acknowledged.
Numerous brittle structures dissect the basement of the inner Hardangerfjord. Limited structural work has thus far been conducted in the area, and consequently little is known about the nature of these structures and their possible records of displacement. In order to properly describe the tectonic evolution, the importance of differential exhumation across major fault zones and small-scale structures should be assessed. This has only partly been done in previous studies undertaken in the inner Hardangerfjord region. In the present contribution, the issues associated with large horizontal distances within vertical profiles will be addressed and structural data will be included in order to provide a more comprehensive understanding of the tectonic evolution of the Norwegian margin.
The aims of the current study are:

1. To provide steeper and more detailed vertical profiles from the inner regions of the Hardangerfjord in order to obtain better constraints on the exhumation of the southern Scandes.
2. To determine whether the region has experienced episodes of accelerated cooling and confine the timing of such events.
3. To establish the significance of displacements along small-scale fault systems on the distribution of fission track ages in the study area.
4. To use thermochronological data to determine whether the Eidfjord and its tributary fjords are located at sites of major Mesozoic or Cenozoic fault activity.
5. To test the obtained results against the predictions of the peneplanation-uplift-model and the ICE hypothesis and assess the degree of correlation in each case.

1.3 Terminology

In this thesis the term exhumation is used to describe the displacement of rocks with respect to the surface, as defined by England and Molnar (1990). Exhumation occurs by means of tectonic or erosional denudation or a combination of both. Unless otherwise stated, uplift refers to the upward displacement of rocks relative to the geoid.

2. REGIONAL GEOLOGICAL SETTING

2.1 Precambrian crustal accretion

2.1.1 General setting

Southern Norway constitutes the youngest part of the Archaean to Mesoproterozoic Baltic Shield that comprises the entire Scandinavian Peninsula as well as a large area in the Kola Province of northwestern Russia. Over geological time the Baltic Shield has resided within a wide range of plate-tectonic settings and has experienced several episodes of accretion and deformation. This is reflected in the fascinating and complex geology that is apparent in Norway today.

On a global scale the most significant series of events during the Proterozoic was related to the assembly of the Rodinia supercontinent between 1.3 and 1.0 Ga. The Baltic Shield, which was situated at the equator at the time, occupied the central eastern margin of the supercontinent (Torsvik & Cocks, 2005).

2.1.2 The Precambrian in southern Norway

The basement in southern Norway evolved through numerous episodes of crustal accretion and polyphase deformation during late Paleoproterozoic to Neoproterozoic times. Two orogenic episodes are believed to be of particular importance with respect to crustal growth and reworking. The Gothian event (1.75-1.50 Ga) involved subduction-related magmatism and deformation associated with the growth of an accretionary orogen along the western margin of the Baltic Shield. Substantial portions of the basement in southern Norway were formed during this time (Gaál & Gorbatschev, 1987). The Sveconorwegian orogeny (1.14-0.90 Ga) is believed to have resulted from successive collisions between a series of Gothian crustal blocks, followed by continent-continent collision between the Baltic Shield and another large continent of which the identity is uncertain (Bingen et al., 2008). Except for the emplacement of large volumes of late- to post-orogenic granites, the Sveconorwegian orogeny involved relatively little crustal accretion. It is, however, recorded by extensive reworking of the largely Gothian basement (Gaál & Gorbatschev, 1987).

2.2 The Caledonian orogeny

2.2.1 General setting

Subsequent to the break-up of the Rodinia supercontinent at ~750 Ma the Iapetus Ocean started opening between Laurentia and Baltica (Torsvik & Cocks, 2005). Sea floor spreading in the Iapetus was accompanied by anticlockwise rotation of the Baltic Shield, resulting in a plate configuration where Norway was facing the Iapetus Ocean and the Laurentian continent (Hartz & Torsvik, 2002). In the Neoproterozoic to Ordovician Baltica experienced a prolonged period of tectonic quiescence, accompanied by extensive erosion, transgression and deposition of marine sediments over large parts of the continent. The closure of the Iapetus Ocean commenced in the Early Ordovician and culminated in the Early Devonian with the collision between Baltica and Laurentia and the creation of the Caledonian orogenic belt in western Scandinavia, Greenland and the northern British Isles (e.g. Gee et al., 2008).

2.2.2 The Norwegian Caledonides

The Caledonian orogeny involved westward subduction of the Baltoscandian margin beneath Laurentia, evident by ultra-high pressure eclogite facies parageneses in the coastal areas of the Western Gneiss Region in Norway (Dobrzhinetskaya et al., 1995; Griffin et al., 1985) and decreasing metamorphic grade of the basement towards the foreland in the southeast (Dietler et al. 1985). A number of E- to SE-verging thrusts developed on the Baltic flank of the orogen. Along some of these thrusts, the displacement of nappes amounts to several hundred kilometers (Gee et al., 2008). The Caledonian orogenic wedge consists of a number of tectonic units of diverse origin. These units have been grouped into the Lower, Middle, Upper and Uppermost Allochthons (cf. Roberts & Gee, 1985). The Lower and Middle Allochthons comprise sedimentary rocks derived from the continental margin of Baltica, in addition to detached and reworked slivers of the Precambrian basement (Stephens, 1988). The Upper Allochthon includes island-arc complexes, ophiolites and associated sedimentary successions, which in part may have originated within the Laurentian realm of the Iapetus Ocean (Pedersen et al., 1988). A Laurentian affinity has also been suggested for the Uppermost Allochthon, which mainly comprise ophiolites, arc-type granitoids and margin-proximal sediments (Roberts et al., 2007). The Caledonian nappes rest on strongly sheared Cambrosilurian metasediments that form a weak decollément zone, over which the thrust sheets have been translated (Fossen & Dunlap, 1998).

2.3 Post-Caledonian stages

Southern Norway has experienced several episodes of extension following the Caledonian orogeny. The most significant onshore deformation took place during the initial stages of the orogenic collapse in the Devonian.

2.3.1 Devonian orogenic collapse

Mode I extension: Backsliding of the orogenic wedge

The contraction associated with the Caledonian Orogeny ceased towards the beginning of Devonian times and was followed by widespread extensional tectonics. During early stages of orogenic collapse, deformation was accommodated by reactivation of the Caledonian basal thrust as a low-angle detachment (Mode I extension; Fossen, 1992, Fig. 2a). Within the phyllites of the décollement zone, Caledonian top-to-the-southeast kinematic indicators are systematically overprinted by fabrics consistent with top-to-the-northwest displacement, suggesting a transition from a compressional to a tensional tectonic regime succeeding Caledonian nappe emplacement (Fossen, 1992; Fossen & Rykkelid, 1992). The timing of the transition is constrained by mica $^{40}Ar/^{39}Ar$ thermochronology of mylonites from the base of the Jotun Nappe Complex. Hinterland-verging mylonitic fabrics are generally associated with deformational ages in the range 402-395 Ma, whereas mylonites that primarily display a top-to-the-foreland sense of shear record deformation between 415 and 408 Ma. Hence, the shift from Caledonian thrusting to post-Caledonian orogenic collapse must have been relatively swift and is likely to have taken place between 408 and 402 Ma (Fossen & Dunlap, 1998). The total displacement along the décollement during the extensional phase has been estimated to be > 20 km (Fossen & Rykkelid, 1992). According to some studies (e.g. Andersen, 1998), early stages of orogenic collapse were associated with displacement along east-dipping extensional shear zones in the easternmost parts of the hinterland, inferring foreland-directed movement along the décollement zone in this particular region. Such a scenario implies compressional tectonics in the east concomitant with extensional collapse of the hinterland and involves the development of a post-orogenic foreland fold and thrust belt. Clear kinematic evidence for top-to-the-northwest displacement in areas close to the eastern thrust front led Fossen (1992, 2000) to propose a model that involves backsliding of the entire orogenic wedge as result of a transition from convergent to divergent plate motions.

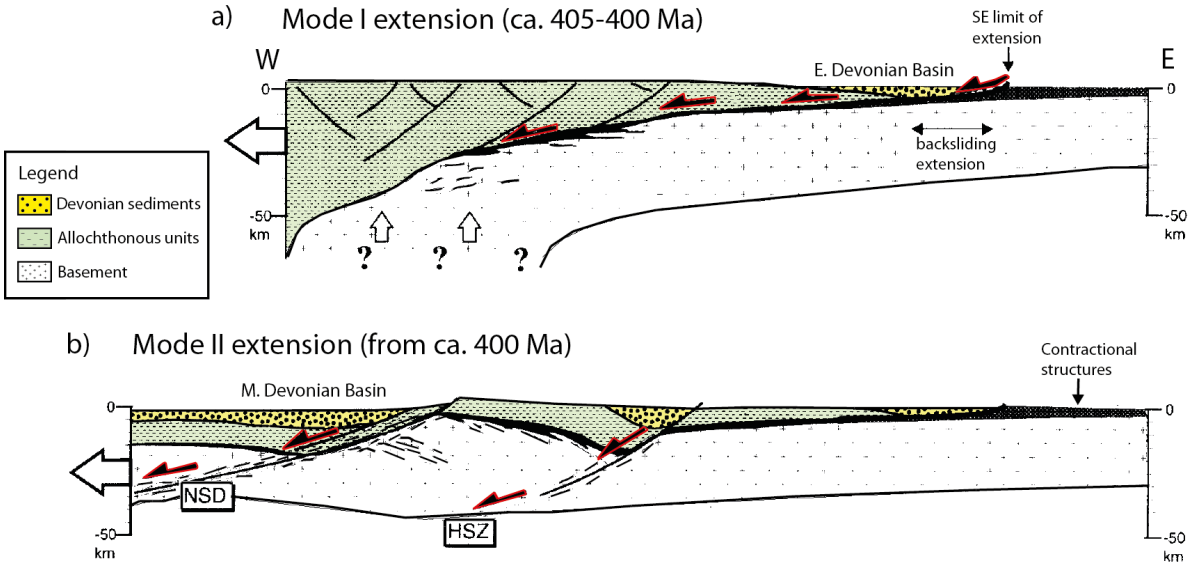

Fig. 2. Post-orogenic evolution of the Baltic flank of the Caledonides: a) Mode I: Reactivation of the basal thrust as a low-angle detachment; b) Mode II: Crustal collapse following the development of W-NW-dipping extensional shear zones. Modified from Fossen and Dunlap (1998).

Mode II extension: Development of W-NW-dipping, ductile shear zones

The translation of the orogenic wedge towards the northwest caused progressive exhumation of the hinterland accompanied with southeastward rotation of the décollement zone. Consequently, the detachment attained a shallow and locally reversed dip unfavourable for extensional reactivation (Fossen, 2000). Backsliding was followed by extensive crustal collapse associated with the development of W-NW-dipping extensional shear zones in the western parts of the hinterland (Mode II extension; Fossen, 1992, Fig. 2b). The shear zones initially formed within the ductile regime, but attained a brittle character as exhumation progressed (Andersen, 1998). Caledonian allochthons are clearly displaced by Mode II extensional structures (e.g. Milnes et al., 1988), indicating that the backsliding motion of the orogenic wedge came to a halt during early stages in the development of the ductile shear zones (Fossen, 1992). The Nordfjord-Sogn Detachment Zone (NSDZ, Fig. 3) is the largest of the post-Caledonian shear zones and juxtaposes ultrahigh-pressure rocks belonging to the Western Gneiss Region and low-grade metamorphic Caledonian allochthons with local Devonian deposits (Norton, 1986). The extensional displacement along the NSDZ is thought to be partly responsible for the exhumation of the ultrahigh-pressure lithologies that are present in the footwall. However, non-coaxial strain along the NSDZ cannot solely explain the pressure estimates and the metamorphic imprints of the exhumed eclogites. Additional mechanisms, such as erosional or extensional denudation in combination with coaxial vertical

shortening at deeper crustal levels, may account for the remaining exhumation (Krabbendam & Wain, 1997). While the other major shear zones clearly penetrate the Precambrian basement, the NSDZ has been suggested to merge with the Caledonian décollement at depth (Wilks & Cuthbert, 1994). According to Fossen (2010) the NSDZ links with the Bergen Arc Shear Zone (BASZ) to the south. Consequently, it is difficult to envision how the NSDZ could possibly be restricted to the décollement zone only. The NE-SW-trending Møre-Trøndelag Fault Zone accommodated sinistral strike-slip displacement during the Devonian orogenic collapse and acted as a transfer zone between the extensional structures in the Western Gneiss Region and W-NW-dipping shear zones, such as the Høybakken Detachment, to the northeast (Braathen et al., 2000; Séranne, 1992).

The last ductile, contractional structures evident within the Caledonian crust are large-scale, E-W-trending folds that mainly affect fluvial-alluvial Devonian basins that are situated in the hangingwall of the NSDZ, the NSDZ and coast-proximal areas of the Western Gneiss Region (Fossen, 2010). Devonian sediments are found in the synforms of these folds, while the basement crops out in the antiforms (Osmundsen, Andersen, Markussen, & Svendby, 1998). The age and tectonic significance of the E-W-trending folds are uncertain. Devonian extension and basin formation may have been accompanied by N-S contraction induced by a combination of internal stress permutations associated with exhumation and far-field stresses related to the continuing convergence between Baltica and Avalonia (Chauvet & Séranne, 1994). Alternatively, the folds may have formed in a transtensional regime developed during sinistral shear along the Møre-Trøndelag Fault Zone (Osmundsen et al., 1998) or as a result of separate compressional pulses during Late Devonian to Permian or even Mesozoic times (Eide et al., 1999; Osmundsen et al., 1998).

The Hardangerfjord shear zone (HSZ) is a NW-dipping, ductile extensional structure that can be traced from the southern margin of the Jotun Nappe southwards along the entire length of the Hardangerfjord (Fig. 3). The offshore continuation of the shear zone is represented by a set of NE-SW-trending lineaments and NW-dipping reflectors that extend through the Ling Depression, across the North Sea and possibly link up with the Highland Boundary Fault in Scotland (Færseth et al., 1995). Hence, its total length may be more than 600 km (Fossen & Hurich, 2005). The HSZ marks the transition between thick-skinned Caledonian deformation (i.e. deformation that has affected the Precambrian basement) in the hinterland of the orogen and thin-skinned deformation in the foreland. There are no indications of extensive post-Caledonian deformation of the basement to the east of the Hardangerfjord Shear Zone (Andersen, 1998). The HSZ is marked by a ca. 5 km thick

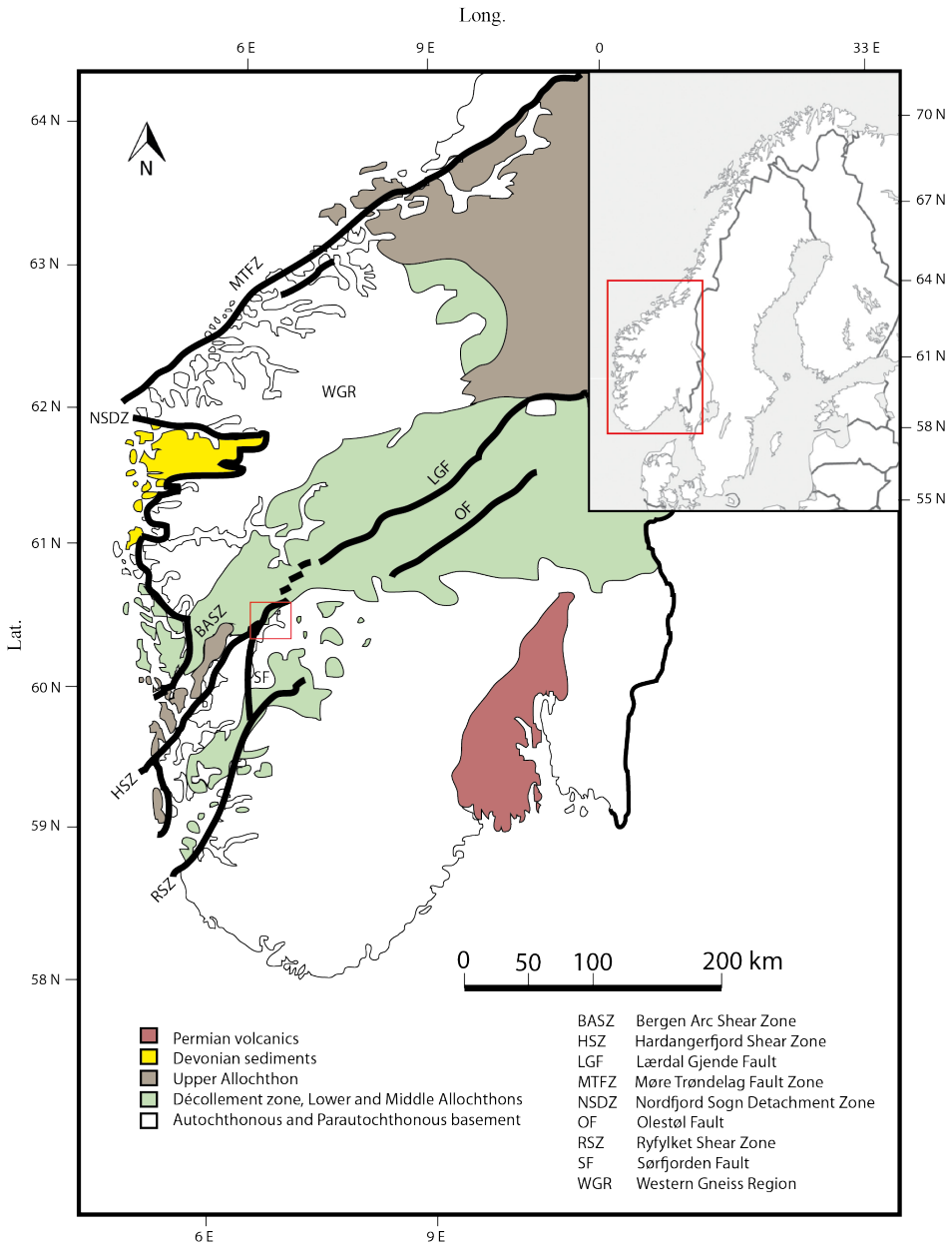

Fig. 3. Simplified geological map of southern Norway. Thick black lines illustrate the location of major faults and ductile shear zones developed or reactivated during Mode II and Mode III extensional deformation. The approximate location of the field area is indicated by red box. Redrawn after Andersen (1998) and Fossen and Hurich (2005).

package of mylonites and the estimated down-to-the-NW displacement is in the order of 10-15 km. Caledonian thrust sheets are mainly preserved in the hangingwall and are monoclinically folded in the half-graben that overlies the shear zone. Immediately to the southeast of the HSZ, the sub-Cambrian peneplanation surface deviates from the dome shaped geometry that is evident elsewhere in southern Norway (Fig. 4). This departure is a result of 800-1000 m of footwall uplift associated with Devonian extensional displacement (Fossen & Hurich, 2005).

Thermochronological constraints on Devonian exhumation

Geochronological and thermochronological studies conducted in the southwestern part of the Norwegian Caledonides generally reveal rapid cooling associated with the collapse of the Caledonian orogen. U-Pb ages obtained from eclogites of the Western Gneiss Region attest to maximum burial at depths of 50-100 km at 415-400 Ma (Kullerud et al., 1986). $^{40}Ar/^{39}Ar$ thermochronology of hornblende indicate cooling through 500 ºC between 455 and 395 Ma (Boundy et al., 1996; Fossen & Dunlap, 1998). Anomalously old ages of 439 and 455 Ma have been obtained from the Lindås nappe, which occupies a tectonostratigraphically high position within the Bergen Arcs. These ages are interpreted to reflect early phases of exhumation associated with nappe emplacement. Significantly lower ages are reported from the Western Gneiss Region, where cooling is believed to be a result of exhumation in relation to extensional movement along the ductile shear zones to the west (Boundy et al., 1996). $^{40}Ar/^{39}Ar$ biotite and muscovite ages from southern Norway are in the range 410-385 Ma, indicating relatively rapid cooling below ~350 ºC following the culmination of the Caledonian orogeny (Chauvet & Dallmeyer, 1992; Fossen & Dunlap, 1998).

Mode III extension: Brittle faulting

The displacement along Mode II ductile shear zones was followed by the development of NE-SW-trending brittle faults, designated as Mode III extensional structures (Fossen, 2000). The largest of these structures is the NE-SW-trending Lærdal-Gjende Fault System, which transects the nappe stack in central southern Norway and is interpreted as a late, upper crustal expression of the HSZ (Fossen & Hurich, 2005). Locally, the Mode III faults are found to exhibit semi-ductile features and cohesive fault rocks, indicative of a temperature of formation close to that of the brittle-ductile transition (i.e. ca. 300 ºC for felsic rocks; Fossen, 2000). U-Pb ages of ~396 Ma, obtained from titanites that formed within brittle extensional faults in the parautochthonous basement west of Bergen, are believed to reflect the timing of the onset of brittle faulting in the region (Larsen et al., 2003). Although slight local differences in the timing of the entrance into the brittle domain are likely, the high cooling rates that are characteristic for the Early Devonian (Fossen & Dunlap, 1998) imply an almost synchronous shift to Mode III deformation throughout southwestern Norway (Fossen, 2000). NE-SW-trending faults and tension veins clearly affect Middle Devonian sedimentary rocks along the west coast. The stress field responsible for post-orogenic NW-SE extension may thus have persisted throughout much of the Devonian period (Larsen et al., 2003).

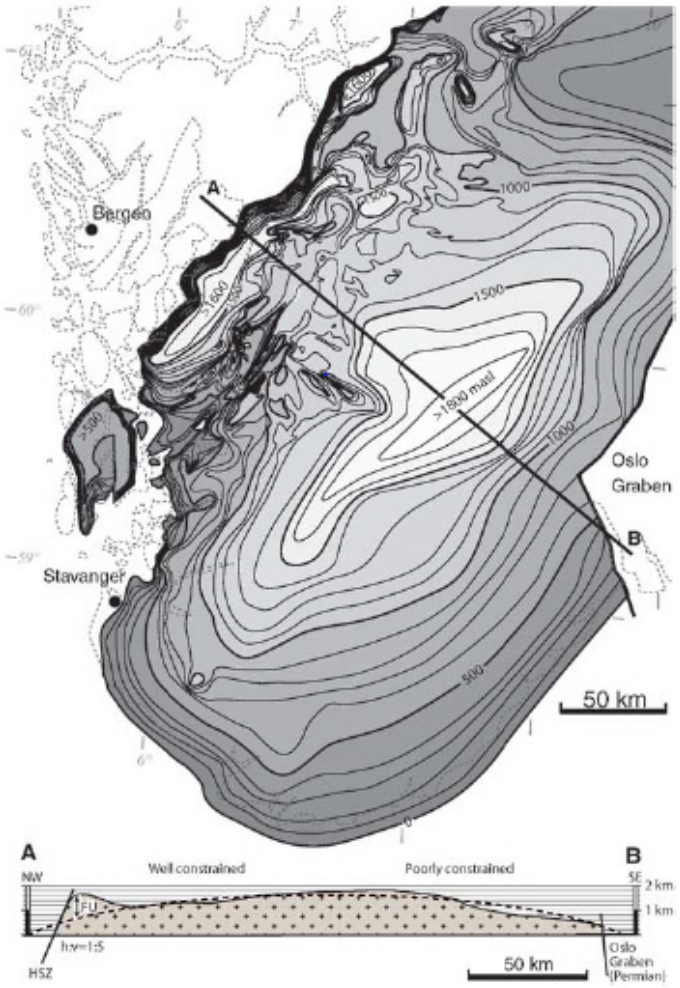

Fig. 4. Contour map of the elevation of the uppermost basement surface in southern Norway. The basement surface generally equals the sub-Cambrian peneplain and displays a dome-shaped geometry. This dome trend is disrupted in the footwall of the Hardangerfjord Shear Zone, where the peneplain reaches heights of > 1600 m asl. The deviation is particularly clear in the NW-SE-trending profile that is shown below the map. FU denotes footwall uplift and has a magnitude of 800-1000 m. From Fossen and Hurich (2005).

2.3.2 Late Devonian and Carboniferous tectonic stability

Rapid Early Devonian extensional collapse and associated cooling were followed by a prolonged period of time characterized by relative tectonic and thermal stability. By the early Carboniferous the topographic evolution was mainly controlled by surface-processes (Gabrielsen et al., 2010). $^{40}Ar/^{39}Ar$ alkalifeldspar data from the Jotun Nappe Complex and the Bergen area record sustained temperatures of 200-350 ºC from Middle Devonian times towards the end of the Carboniferous period. The Caledonian orogen may thus have remained topographically high and virtually unaffected by tectonic activity throughout Carboniferous times. This interpretation is supported by the lack of evidence for extensive deformation and metamorphism and the absence of post-Devonian onshore sediments in southern Norway

(Dunlap & Fossen, 1998). Results of $^{40}Ar/^{39}Ar$ alkalifeldspar thermochronology of samples obtained from a traverse through the NSDZ (Eide et al., 1999) agree well with the late Devonian thermal quiescence postulated by Dunlap and Fossen (1998) and are supportive of relatively slow cooling from 340 Ma until the latest Carboniferous. In addition, the data of Eide et al. (1999) indicate an episode of enhanced cooling from 360-340 Ma. This cooling event has been interpreted as a result of thermal underplating accompanied by increased topography and accelerated denudation rates. The early Carboniferous rapid cooling is contemporaneous with phases of faulting, igneous activity and development of unconformities that have been documented around the North Atlantic margin and may be correlated with the north-south folding of the Devonian basins and their substrate (Eide et al., 1999).

2.4 Late Paleozoic to Cenozoic tectonic evolution

2.4.1 Permo-Triassic rifting

Reorganization of the plate configuration during the Carboniferous-Permian resulted in a change in the regional stress state, and a rift system started to develop in northwestern Europe (Doré et al., 1999; Gabrielsen et al., 2010). Crustal stretching was accompanied by extensive volcanism, followed by thermal subsidence and development of several large basins (e.g. the Permian basins of the central and northern North Sea; Gabrielsen et al., 2010). Both the Permian Oslo Rift and the Permo-Triassic North Sea Basin are characterized by a pronounced N-S structural grain, indicative of an E-W extensional regime (Færseth et al., 1995). The formation of the Oslo Rift commenced at ~300 Ma with the development of brittle, extensional faults and simultaneous onset of volcanism. After ~240 Ma volcanic activity ceased and the rift appears to have been aborted before the beginning of Triassic times (Neumann et al., 1992). The inception of rifting in the North Sea is poorly constrained, but has traditionally been regarded as Middle to Late Permian (e.g. Færseth et al., 1995) or possibly Early Triassic (Roberts et al., 1995). Alkalifeldspar $^{40}Ar/^{39}Ar$ data from western and central southern Norway are suggestive of a Carboniferous-Permian episode of accelerated cooling, which is believed to reflect the onset of rifting in the Oslo Graben and perhaps also in the North Sea region (Dunlap & Fossen, 1998). Hence, early stages of North Sea rifting may date back to 300 Ma. The N-S-trending Øygarden Fault Complex is believed to have exerted the main control on the structural development of the North Sea during Permo-Triassic times (Færseth et al., 1995).

Onshore Permian extension is manifested by ~260 Ma, coast-parallel dolerite dykes, which crop out in the Sunnhordaland, Sotra and Sunnfjord regions (Fossen & Dunlap, 1999; Færseth et al., 1976; Løvlie & Mitchell, 1982; Torsvik et al., 1997). The dykes are generally found in association with N-S-trending brittle faults. A second generation of dolerite dykes with ages of ca. 220 Ma is contemporaneous with a Late Triassic phase of extension on the Horda Platform directly to the west of the Øygarden Fault Complex (Fossen & Dunlap, 1999). Additional evidence for tectonic activity is provided by paleomagnetic and K-feldspar $^{40}Ar/^{39}Ar$ data from fault breccias (Andersen et al., 1999; Eide et al., 1997; Torsvik et al., 1992) and K-Ar illite data from incohesive fault gouges (Ksienzyk, 2012), which indicate widespread Carboniferous-Permian to latest Permian fault activity in southwestern Norway. Permian extension was associated both with reactivation of post-Caledonian NE-SW-trending structures (e.g. Andersen et al., 1999; Torsvik et al., 1992) and with the formation, or possibly rejuvenation, of a second set of faults striking N-S (Færseth et al., 1995). A phase of Late Triassic to Early Jurassic fault reactivation has been reported from the region and appears to coincide with the intrusion of dykes at ca. 220 Ma (Ksienzyk, 2012).

2.4.2 Late Jurassic rifting and shoulder uplift

A second phase of rifting commenced in northwestern Europe in the Middle-Late Jurassic and led to the development of a triple rift system between southern Norway and the British Isles (e.g. Doré et al., 1999). The Viking Graben is the northernmost segment of this rift system, while the Central Graben and the Moray Firth Basin represent its southern branches. In contrast to the Permo-Triassic rifting, which affected the total width of the northern North Sea Basin, the Jurassic extensional phase was mainly localized to the axes of the Viking and Sogn Grabens (Færseth et al., 1995). A general NW-SE extension direction characterized the Jurassic tectonic activity in the northern North Sea. Interference between Jurassic NE-SW striking faults and pre-existing structures developed during Permo-Triassic E-W extension resulted in an overall obliquity of the rift system (Færseth et al., 1997). In addition to the development of grabens offshore, the Late Jurassic extensional phase involved rift shoulder uplift (Gabrielsen et al., 2010) and reactivation of faults onshore (Andersen et al., 1999; Eide et al., 1997; Fossen et al., 1997; Ksienzyk, 2012; Torsvik et al., 1992). There is no evidence for Jurassic igneous activity in southern Norway. Hence, the onshore effects of rifting may have been relatively mild (Fossen & Dunlap, 1999).

2.4.3 Cretaceous and Cenozoic tectonic activity

The most pronounced tectonic events in the proximity of western Scandinavia during the Cretaceous and Paleogene were related to multiphase rifting of the North Atlantic margins, which culminated with the initiation of sea-floor spreading in the early Eocene (e.g. Doré et al., 1999). From the Late Cretaceous to the Miocene far field compressional stresses induced by the Alpine collision, possibly in combination with the push exerted by the incipient ridge system in the North Atlantic, led to the inversion of old structures in the North Sea (Vågnes et al., 1998).

Due to the scarcity of onshore sediments that may serve as marker horizons, there is limited evidence for late Mesozoic and Cenozoic fault activity in southern Norway. However, results from apatite fission track thermochronology indicate significant Late Cretaceous or possibly Cenozoic extensional displacement across segments of the Møre-Trøndelag Fault Zone (Redfield et al., 2005; 2004). Similarly, thermal history modelling of thermochronological data from southern Norway has yielded different cooling histories for adjacent fault-bound blocks. This signature has been taken as an indication of possible Cretaceous or Cenozoic fault reactivation (Ksienzyk, 2012; Leighton, 2007). K-Ar illite dating of fault gouges has revealed latest Cretaceous-Paleogene reactivation of the Lærdal-Gjende Fault (Ksienzyk, 2012).

During late Pliocene and Pleistocene times large ice sheets covered Scandinavia. Following the last deglaciation approximately 11 500 years ago the region experienced significant post-glacial rebound. The glacioisostatic uplift has a dome-like character and has thus far attained a magnitude of ca. 1000 m in central southern Norway (Riis, 1996). Interior regions of Norway have continued rising until the present, and a current uplift rate of 1-4 mm/yr has been estimated (e.g. Fjeldskaar et al., 2000).

2.4.4 Neotectonics

The seismicity in Norway and adjacent offshore areas is low to intermediate. Most earthquakes occur in vicinity to the Viking Graben, along the shelf edge from the northern North Sea to Svalbard and in coastal areas of western and northern Norway (Bungum et al., 1991). Focal mechanism solutions indicate mainly normal faulting onshore, while there is a tendency for reverse to strike-slip fault reactivation in offshore areas. In western Norway and the northern North Sea region the maximum horizontal compressive stress is oriented roughly WNW-ESE. The estimated stress field is compatible with the direction of the ridge push force associated with spreading in the North Atlantic Ocean (Hicks et al., 2000). However, second

order sources of stress accumulation, such as postglacial uplift and lithospheric loading and unloading, are required to explain the overall pattern of seismic activity (Bungum et al., 1991; Fjeldskaar et al., 2000; Hicks et al., 2000). The Hardangerfjord region is among the most seismically active areas in Norway and a small number of perceptible earthquakes are typically recorded each year. Although the seismic activity is largely confined to the Sunnhordaland area, occasional earthquakes occur further to the northeast. Recent seismicity in the central Hardangerfjord region includes a magnitude 3.3 earthquake registered in Voss in March 2012 and a magnitude 3 earthquake with epicentre below Nordheimsund recorded in July 2012 (Norwegian National Seismic Network).

2.5 Mesozoic to present topographic evolution

The geomorphology of southern Norway is characterized by a low relief plateau landscape at high elevations in interior parts of the country, deeply incised glacial valleys and fjords towards the west and gentle hills towards the east. Despite the fact that essential geomorphological features, such as the undulating surfaces at high altitudes in central southern Norway, were described more than a century ago (Reusch, 1901), their origin remains a mystery. Recently, renewed attention has been called to the topographic evolution of the Southern Scandes. Two contrasting models are featured in an ongoing debate regarding the geological processes responsible for the present expression of the Norwegian mountains; the traditional and widely accepted peneplanation-uplift-model and the relatively recent ICE (isostacy-climate-erosion) hypothesis. Below follows a review of each of these models.

2.5.1 The peneplanation-uplift-model

According to the supporters of the peneplanation-uplift-model (e.g. Gabrielsen et al., 2010; Mosar, 2003) the Caledonian orogen was completely obliterated during Devonian extensional collapse and late Paleozoic and Mesozoic rifting (Fig. 5). By the Late Cretaceous southwestern Norway was flooded by a shallow sea. Except for isolated pockets of Mesozoic sediments along the western coast (e.g. Fossen et al., 1997), post-Devonian sediments are generally absent onshore and the presumed transgression is difficult to constrain. The present topography in southern Norway is believed to be a result of considerable Cenozoic tectonic uplift, followed by glacial landscape modification.

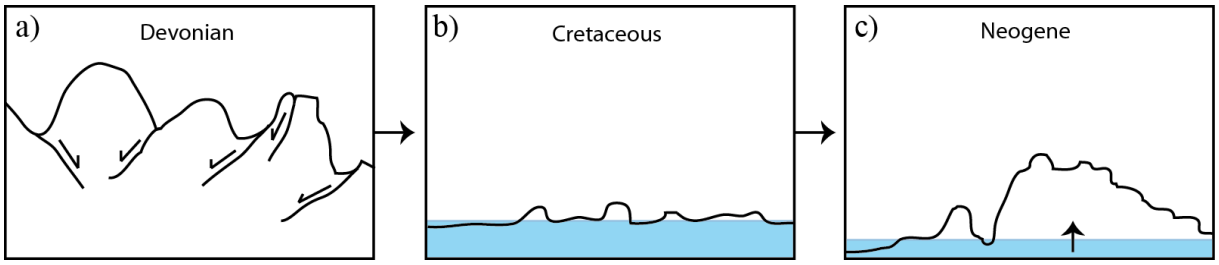

Fig. 5. The topographical evolution of southern Norway according to the peneplanation-uplift model: **a)** Devonian orogenic collapse and subsequent rifting events obliterated the Caledonian topography; **b)** By the Cretaceous or possibly early Paleogene the previously high topography in southern Norway had been reduced to a submerged peneplain with local remnant peaks; **c)** Tectonic uplift caused topographic rejuvenation during Paleogene and particularly Neogene times.

The peneplanation-uplift-model is rooted in traditional views on the development of landscape forms first presented by Davis (1889). Davis described the cyclic nature of landscape evolution and imagined that a progressive decline in surface gradients through time could lead to the development of a surface of subdued relief close to sea level. Such a surface was termed a peneplain. In the Davisian model rapid uplift of the low-relief surface would produce an elevated plateau landscape with incised river canyons. Given sufficient time this landscape would once again be graded to sea level and the cycle would be complete. The deeply eroded, undulating peneplain that is found at high elevations in interior parts of Norway was first described by Reusch (1901) and has traditionally been referred to as the paleic surface. Several different interpretations of the age of the paleic surface have been presented and a wide variety of distinct peneplains or remnants thereof have been defined. The position of the paleic surface has mainly been established through correlation of summit height envelopes, autochthonous block fields or lower elevation summit plains of greater areal extent. Doré (1992) constructed a summit envelope across southern Norway and correlated this surface with the base Paleogene surface offshore. Stuevold and Eldholm (1996) questioned the interpretation of Doré (1992) and suggested a link between the paleic surface and the offshore upper Oligocene unconformity. Riis (1996) defined the remnants of a Jurassic peneplain based on correlation of summit levels and autochthonous block fields. An additional erosional surface at an elevation of ca.1100 m was assigned a Paleocene age. Lidmar-Bergström et al. (2000) identified four erosional levels at different altitudes. Each level was interpreted as to represent an episode of erosion associated either with uplift or with a reduction of the general base level. Similar to the propositions by Riis (1996), a Mesozoic age was suggested for the upper summit envelope, while the common base at ca. 1000 m was inferred to be of Paleocene age (Lidmar-Bergström & Bonow, 2009; Lidmar-Bergström et al.,

2000). Although the exact definition of the paleic surface is a matter of some controversy, it is generally agreed that the present low-relief-high-elevation landscape is a remnant of a limited number of uplifted late Mesozoic-early Cenozoic erosional surfaces with scattered residual peaks (Gabrielsen et al., 2010).

The Cenozoic topographic rejuvenation is believed to have been tectonically induced. Several studies have aimed at revealing the cause of uplift, but hitherto no single model has gained widespread approval. Rift flank uplift associated with the opening of the North Atlantic Ocean at ~55 Ma may have been the cause of tectonic activity in southern Norway and the North Sea during Paleogene times (Torske, 1972). Thermal disturbances of the asthenosphere in connection with the passage of the Icelandic plume and flexural bulging in response to sediment loading offshore may have triggered additional uplift (Doré, 1992). However, the present topography in southern Norway cannot solely be explained as a result of these processes (Doré, 1992; Japsen & Chalmers, 2000). Hence, additional mechanisms must have been in play. It is generally agreed that a Neogene episode of tectonic activity has affected the North Atlantic region. There is, however, little consensus regarding the exact timing of the inferred uplift event and the attributes of the processes in force (Japsen & Chalmers, 2000). According to Riis and Fjeldskaar (1992) significant portions of the required uplift may have been caused by post-glacial rebound during Pliocene-Pleistocene times, possibly aided by lithospheric phase changes due to pressure release. In other studies regional compression (Cloetingh et al., 1990), astenospheric diapirism (Rohrman & van der Beek, 1996), volume expansion associated with mantle convection (Stuevold & Eldholm, 1996) and serpentinisation of the mantle (Skelton & Jakobsson, 2007) have been proposed as possible explanations for the Neogene tectonic pulse.

Several techniques have been employed in order to constrain the timing of Cenozoic uplift and erosion. Low-temperature thermochronology and its possible implications will be discussed in a later section. Overburial estimates have been used to determine the extent of erosion offshore. Missing sedimentary sections in the North Sea have generally been interpreted as an indication of subaerial exposure of shallow parts of the basin as a result of regional uplift (e.g. Japsen, 1998). Important information regarding the character and magnitude of erosion has been revealed through studies of the North Sea sedimentary record. Jordt et al. (1995) reported an Eocene-Oligocene shift in sedimentation from smectite-rich mud derived from the Shetland platform to coarse-grained sediments sourced from the Scandinavian mainland and interpreted their findings as a sign of increased topographic relief in Scandinavia following an episode of uplift in the earliest Oligocene. A similar conclusion

was drawn by Faleide et al. (2002). In addition Faleide et al. (2002) documented a clear link between the timing of deposition of eastward prograding clastic wedges and presumed episodes of Paleogene and late Neogene uplift related to rifting in the North Atlantic and glacial rebound, respectively.

2.5.2 The Isostasy-Climate-Erosion (ICE) hypothesis

While the peneplanation-uplift-model portrays the Scandes as a mainly Neogene feature, the ICE hypothesis (Nielsen et al., 2009) suggests a rather different origin for the high topography in Norway. According to Nielsen et al. (2009) tectonic denudation associated with orogenic collapse and continental rifting failed to completely destroy the Caledonian topography. Hence, significant relief remained by the end of the Jurassic extensional phase (Fig. 6). From the Cretaceous onwards surface processes exerted the main control on exhumation rates. Removal of material by erosion was compensated by isostatic rebound of a buoyant crustal root formed during the Caledonian collisional phase. The presence of a thick root beneath the orogen would imply that considerable erosion could take place without a substantial reduction in the general surface elevation. Hence, according to the ICE hypothesis the Norwegian mountains are remnants of Caledonian topography and have been subjected to a progressive reduction in regional mean elevation since Early Devonian times. Concomitant with post-extensional isostatic uplift onshore, the offshore crust, thinned by late Paleozoic and Mesozoic rifting, experienced subsidence and sedimentation. The coastline is believed to have functioned as a stable hinge zone, only mildly affected by vertical movements.

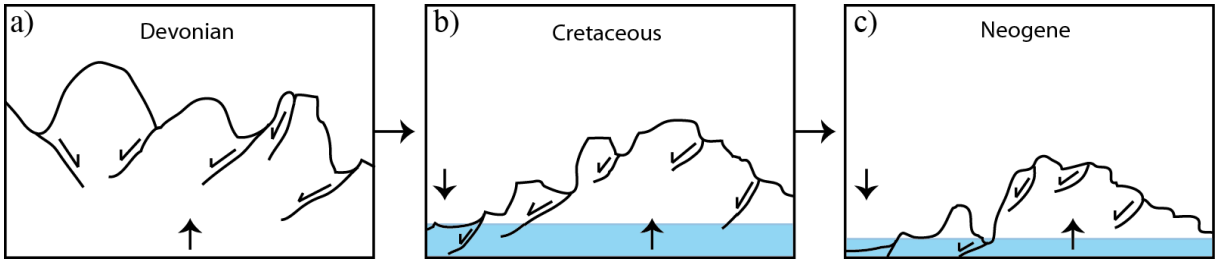

Fig. 6. The topographical evolution of southern Norway as portrayed by the ICE hypothesis: **a)** Devonian extensional collapse and Mesozoic rifting reduced the general elevation of the Caledonides; **b)** The orogenic collapse was incomplete and significant relief remained towards the end of the Mesozoic Era; **b, c)** Protracted denudation during Mesozoic and Cenozoic times was accompanied by isostatic uplift induced by a buoyant crustal root.

In the absence of peneplanation and tectonic uplift, another agent must have been responsible for the distinct geomorphology of southern Norway. Nielsen et al. (2009) interpret

the change in the nature of sedimentation in the North Sea at the Eocene-Oligocene boundary (Jordt et al., 1995) as a response to a global climatic deterioration and suggest that glaciers may have controlled the pattern of erosion in the mountainous interior of Norway. Recent studies have shown that warm-based cirques and alpine glaciers may effectively limit topography above the equilibrium line altitude (e.g. Mitchell & Montgomery, 2006), eventually producing a relatively low-relief landscape with isolated remnant peaks. Glacial erosion is aided by periglacial processes, such as frost weathering and frost-induced mass diffusion, which have been found to form flat landscape elements at high altitudes (Anderson, 2002). New, independent data by Steer et al. (2012) demonstrate that the volume eroded from the glacial fjords and valleys in western Norway is insufficient to account for the offshore Plio-Pleistocene sedimentary record. The mismatch is interpreted in terms of significant glacial erosion of low-relief surfaces at high elevations.

According to Nielsen et al. (2009) observations and data from onshore and offshore Norway are in good agreement with the ICE hypothesis. Their interpretation of a buoyant root beneath the high topography in southwestern Scandinavia is supported by the presence of significant low-density material at the base of the crust, which is manifested by a large negative Bouguer anomaly. The overburial estimates from the North Sea are explained by extensive glacial erosion during Pliocene-Pleistocene times. Nielsen et al. (2009) acknowledge the evidence for late Mesozoic and Cenozoic fault activity that has been reported from onshore southern Norway (e.g. Redfield et al., 2005) and suggest that faulting may be explained by differential isostatic readjustments as a result of regional differences in erosional unloading. Active tectonic uplift during the Cenozoic is therefore not required.

2.6 Previous fission track and (U-Th)/He studies in western Scandinavia

Three decades of thermochronological studies in Norway has resulted in a good overall coverage of fission track data, especially for apatite (Fig. 7). Although a limited number of studies were undertaken in the 1970's and early 80's (e.g. Van den Haute, 1977), the real pioneers of low-temperature thermochronology in Scandinavia were Andriessen and Bos (1986) who applied zircon and apatite fission track analysis in order to unravel the thermal history of the Eidfjord area. Three zircon fission track ages between 294 Ma and 317 Ma were obtained. No correlation was found between age and altitude. Andriessen and Bos (1986) interpreted the relatively minor difference in ages at sea level and at an elevation of 1620 m as a result of rapid cooling through the 175-225 ºC isotherm during late Carboniferous times.

Apatite fission track ages were found to increase systematically with elevation; from 110 Ma at sea level to 166 Ma at an altitude of 1620 m. Based on the fission track age patterns Andriessen and Bos (1986) estimated a total removal of 13 km of crustal material since Caledonian times and 8 km since the late Carboniferous, assuming a constant geothermal gradient of 30 ºC and effective closure temperatures of 200 ºC and 105 ºC for the zircon and apatite fission track systems, respectively. The results were combined with previously published biotite Rb-Sr and K-Ar ages of ~385 Ma and ~420 Ma, respectively (Priem et al., 1976) and were interpreted to indicate rapid uplift of the crustal column (100 m/Ma) following the termination of the Caledonian orogeny, succeeded by significantly lower uplift rates (20 m/Ma) from the latest Carboniferous onwards.

Nearly a decade later, Rohrman et al. (1995) presented an extensive apatite fission track dataset obtained mainly from central southern Norway and coast-proximal regions in western parts of the country. The Oslo rift and adjacent areas in eastern Norway were covered in a previous publication (i.e. Rohrman et al., 1994). Rohrman et al. (1995) reported mainly Triassic and Jurassic cooling ages and described a radial pattern of increasing fission track ages from the interior towards the coast and from sea level to the peaks in central southern Norway. The oldest ages (i.e. Middle to Late Triassic) were reported from the south coast, while the youngest ages in the study (i.e. Early Cretaceous) were obtained for samples from low elevations in the inner Hardangerfjord and Sognefjord regions. Along the western coast and at high elevations in the areas with the highest topography Jurassic ages were found to predominate. Four vertical profiles were included in the study, among them a profile from Eidfjord, sampled from sea level to an elevation of 1620 m (including ages from Andriessen & Bos, 1986). The reported ages range from 99 Ma to 181 Ma, and define a general trend of increasing age with elevation. Based on AFT data and thermal history modelling two major episodes of rapid exhumation were suggested: a) A Triassic-Jurassic phase that started in the east and migrated westwards. b) A Neogene uplift event characterized by domal warping of the AFT isochrons and thus greater exhumation in the interior than along the coastline. Rohrman et al. (1995) imagined that southern Norway behaved as a structurally coherent block since the Permian and remained unaffected by faulting throughout Mesozoic and Cenozoic times.

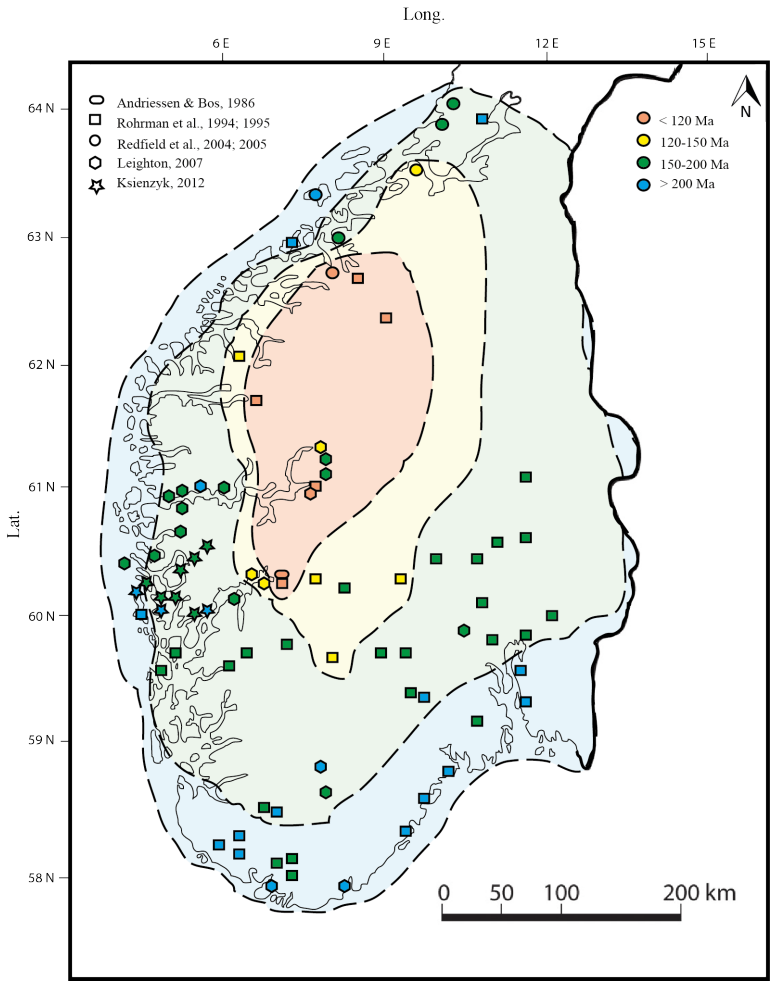

Fig. 7. A representative selection of the results obtained by previous apatite fission track studies in southern and central Norway. All ages are derived from samples located < 500 m above sea level. Age domains (faint colours) have been created by employing the contouring approach of Rohrman et al. (1995). Note that there are numerous exceptions from the general age pattern.

The domal model of Rohrman et al. (1995) was challenged by Redfield et al. (2005; 2004), who documented different Mesozoic and Cenozoic cooling histories for adjacent structural blocks bound by segments of the Møre-Trøndelag Zone. Juxtaposed ages, differing by as much as 97 Ma, were obtained across very short distances and were taken as clear indications of post-Permian fault activity. Four distinct structural blocks were identified and a general trend of increasing fission track ages towards the coast was described. The reported AFT ages range from 280 Ma in the hangingwall of the coast-proximal Hitra-Snåsa Fault to 93 Ma in the footwall of the innermost Bæverdalen Lineament (excluding samples with anomalously high Cl-contents; cf. section 3.2.3). Redfield et al. (2005; 2004) interpreted the age distribution in the area as a result of top-to-the-west normal displacement along each of the investigated faults.

In accord with the study by Redfield et al. (2005; 2004), Leighton (2007) observed large offsets of apatite fission track ages across major fault zones in southern Norway and showed that Mesozoic and possibly Cenozoic fault activity had also taken place in this region. 77 apatite fission track ages and 9 (U-Th)/He ages were reported, ranging from Permian to mid Cretaceous and Early Cretaceous to Oligocene, respectively. Based on inverse thermal history modelling Leighton (2007) suggested a Permo-Triassic phase of rapid cooling (1-5 ºC/Ma) for the entire region, generally followed by slow cooling (< 1 ºC/Ma) from the Jurassic throughout the Paleogene. A second episode of accelerated cooling commenced in the Neogene. However, considerable variations in Mesozoic and Cenozoic thermal histories were found between structural blocks.

A detailed apatite fission track record from the Bergen area was presented in a recent contribution by Ksienzyk (2012). The reported fission track ages range from 294 Ma to 160 Ma. Early to Middle Jurassic ages were found to dominate throughout the region, while most Permian and Triassic ages were obtained from the coastal area west of Bergen. (U-Th)/He dating was performed for 10 samples collected from a ca. 85 km long transect across a number of major lineaments in the northern part of the studied area. In general, the reported (U-Th)/He ages are younger than the corresponding fission track ages and range from Triassic to Cretaceous, with a majority of Early Cretaceous ages. Ksienzyk (2012) documented clear offsets of both fission track and (U-Th)/He ages across major faults in the region. The age distribution was thus suggested to be largely tectonically controlled and affected by episodes of Cretaceous and possibly Cenozoic fault activity. Thermal history models revealed constant, relatively rapid cooling (~2 ºC/Ma) during Permian to Early Jurassic times followed by slow cooling (< 1 ºC/Ma) from the Early Jurassic throughout the Cenozoic. Significantly different thermal histories were obtained for closely spaced samples derived from adjacent fault-bound blocks. Ksienzyk (2012) interpreted the rapid regional exhumation during Permian to Jurassic times as a response to rifting in the North Sea. After the North Sea rift was aborted during the latest Jurassic, the rate of uplift onshore decreased.

Over the last few years a number of apatite fission track studies have been carried out by MSc students at the University of Bergen. The work has mainly been confined to the Hordaland area and the general aims of the projects have been to determine the role of fault reactivation on differential exhumation in the region. Johansen (2008) and Tørresen (2009) dated samples from lateral transects across major lineaments in the Sotra-Bergen area and in Nordhordaland, respectively. Both studies revealed increased cooling rates in Permo-Triassic times, consistent with the proposed timing of rifting in the North Sea. Tørresen (2009) further

documented accelerated exhumation rates during the second rift phase in the Late Jurassic. A general decrease in fission track age with distance from the coast was reported by Johansen (2008) and offset fission track ages were observed across some of the major faults in the region. Magerholm (2010) and Utami (2012) focused on the area around the Hardangerfjord and attempted to establish whether the Hardangerfjord Shear Zone has been subjected to Mesozoic reactivation. While Magerholm (2010) did not observe significant differences in fission track ages across the shear zone in the Tysnes-Kvinnherad area, Utami (2012) documented a considerable offset of ages in the outermost Hardangerfjord region. In general, Early-Middle Jurassic ages were obtained from the hangingwall block and Late Jurassic-Early Cretaceous ages were reported from the footwall block.

A limited number of studies have been undertaken in southwestern Scandinavia east of the region with the highest topography. Rohrman et al. (1994) observed a pattern of continuously increasing apatite fission track ages across the Oslo Rift, from Triassic in the southeast to Jurassic in the northwest. Triassic, Jurassic and Neogene cooling phases were suggested to account for 3-4 km of post-rift denudation in the area. In southern Sweden exhumation generally occurred considerably earlier than in Norway. AFT ages are found to increase systematically from Triassic in the western part of the country to Cambrian in the east. The distribution of fission track ages has been explained by the former existence of a Caledonian foreland basin in the region (e.g. Cederbom et al., 2000).

It is beyond the scope of this thesis to give a full review of the available fission track and (U-Th)/He data from southwestern Scandinavia. Recently, Hendriks et al. (2007) presented a compilation that includes the results of the majority of fission track studies from the region. Their contribution should thus be consulted for a complete overview of the work that has been conducted over the last decades.

2.7 Geological framework of the inner Hardangerfjord area

2.7.1 Lithology

The inner Hardangerfjord region is dominated by Mesoproterozoic basement rocks that have experienced relatively little Caledonian reworking (Birkeland et al., 1997; Ragnhildstveit et al., 1994; Sigmond, 1998; Sigmond et al., 2000). Granitoids crop out over large areas and display varying degrees of deformation. Migmatitic gneisses are particularly abundant and occur throughout the region, locally in association with lenses of quartzite (Sigmond, 1998). U-Pb data on zircon from a migmatitic gneiss sampled on southeastern Hardangervidda

indicate crystallisation around 1670 Ma and attest to a high-grade metamorphic event associated with partial melting at ~1470 Ma (Sigmond et al., 2000). It is not known whether the migmatitic gneisses on the western part of the plateau share this history. Other prominent lithologies include banded orthogneisses as well as more massive varieties of granodioritic and tonalitic composition. A narrow belt of augen gneiss is exposed within the migmatites at Osafjellet in the northern part of the field area. Similar lithologies are more conspicuous elsewhere on Hardangervidda, particularly to the southwest of Hallingskarvet (Sigmond, 1998). Weakly deformed fine to medium grained granites crop out as irregularly shaped bodies along both margins of the Eidfjord and the Sørfjord and are commonly found in association with the 1540 Ma, partly migmatized meta-andesites and -dacites of the supracrustal Ullensvang group. Field relations indicate that the metavolcanic lithologies may be older than some of the gneisses (Sigmond, 1998). A dome-shaped body of coarse grained biotite granite, hereafter referred to as the Eidfjord granite (cf. Priem et al., 1976), crops out in Eidfjord and along both margins of the Simadalsfjord. The emplacement of the Eidfjord granite is related to the terminal stage of the Sveconorwegian orogeny, and the intrusion has a Rb-Sr whole-rock age of 911±35 Ma (recalculated by Andriessen and Bos, 1986; after Priem et al., 1976). Similar late- to post-orogenic granites crop out in a belt extending from Mandal in the south to Finse in the north. U-Pb zircon ages of 1100-900 Ma have been reported for these intrusions (Andersen et al., 2002).

Remnants of autochthonous and parautochthonous metasedimenary rocks, which constitute the Caledonian décollement zone, cover large areas on western Hardangervidda south of Eidfjord. The most prominent lithologies are quartzitic and calcareous phyllites and mica schists, in addition to less abundant conglomerates and marble layers of limited extent (Sigmond, 1998). Outliers of Caledonian allochthons are found locally in the same region. Northwest of the study area the vast, crystalline Jotun Nappe and associated nappes of the Lower and Middle Allochthon form a more or less continuous cover that extends for several tens of kilometers towards the Sognefjord in the north and can be traced from the Bergen Arcs in the west to the Valdres area in the east. The Hardanger-Ryfylke Nappe Complex is located to the south of the Hardangerfjord and mainly comprise Precambrian crustal lithologies with relatively strong Caledonian deformational imprints (Fossen, 1992).

2.7.2 Tectonics

The field area covered in the present study is situated in immediate vicinity of the Hardangerfjord Shear Zone, which is the largest tectonic feature in the Hardanger region. The

shear zone follows the Hardangerfjord northwestwards to the Granvin area, where it is exposed subaerially. As a result of large-scale footwall uplift and accelerated denudation in connection to the Devonian post-orogenic collapse (cf. section 2.2.1), Caledonian nappes are found merely as outliers to the SE of the shear zone where the bulk of the work presented in the present thesis has been conducted. A thick stack of Caledonian units are preserved in the down-faulted hangingwall west of Granvin. In the studied area, the onshore expression of the Hardangerfjord Shear Zone is a several km wide zone of mylonites (Fossen & Hurich, 2005). Shear zone structures are evident in the Precambrian basement from the western flank of the Granvinfjord in the west to Bruravik in the east. The HSZ may have originated in the Precambrian, but the bulk displacement is believed to have taken place in the Devonian (Fossen & Hurich, 2005). Brittle reactivation of some segments may have occurred during the Permo-Triassic rift phase (e.g. Færseth et al., 1995). At present, limited information is available regarding the Mesozoic and Cenozoic history of the HSZ. The brittle Lærdal-Gjende Fault (LGF) transects the Caledonian tectonostratigraphy in the area directly to the northwest of the Osafjord, where it forms an array of relay structures. Tectonic rejuvenation of the LGF is believed to have taken place during Permian and late Jurassic-Early Cretaceous times (Andersen et al., 1999). Evidence for Paleogene reactivation has recently been reported by Ksienzyk (2012).

The density of lineaments is generally high in the inner Hardangerfjord region and on the western side of Hardangervidda. N-S-trending fractures are particularly abundant (Gabrielsen et al., 2002). This set of structures may have formed in the Precambrian and is possibly related to the Mandal-Ustaoset Fault Zone, which can be traced across the eastern part of Hardangervidda. Although field evidence indicates that movement along the Mandal-Ustaoset Fault Zone has not taken place at least since earliest Cambrian times (Sigmond, 1985), N-S-trending structures further to the west may have been reactivated during phases of North Sea rifting or possibly even at later stages (Færseth et al., 1995). The NNE-SSW-trending Sørfjorden Fault, which coincides with a major glacially incised trough, is one of the most conspicuous lineaments in the field area. WNW-ESE and ENE-WSW-trending lineaments occur throughout the area. The WNW-ESE-trending structures are roughly parallel to major Svecofennian and Sveconorwegian suture zones and may belong to a Proterozoic fracture pattern that extends across large parts of Fennoscandia (Gabrielsen et al., 2002).

3. METHODOLOGICAL BACKGROUND

Thermochronology is the study of the thermal evolution of rocks by temperature-sensitive methods. Apatite fission track and (U-Th)/He low-temperature thermochronology are among the most widely used approaches for investigating tectonic and erosional processes that affect thermal conditions at shallow crustal depths. Both systems are sensitive towards the prevailing temperatures in the upper few kilometres of the crust. Together, the apatite fission track and (U-Th)/He systems cover the temperature range between 40 °C and 120 °C, and thus provide a unique means of obtaining thermal information that is virtually inaccessible by other radiometric methods. The following sections include a review of the essential attributes of the apatite fission track approach and a brief description of the (U-Th)/He method.

3.1 Background for the fission track method

The potential for fission track analysis as a geochronological method was first recognized in the early 1960's, following the first transmission electron microscope observation of fission tracks, which was undertaken by Silk and Barnes (1959). Pioneering discoveries were made by Fleischer, Price and Walker, whose comprehensive studies on the behaviour and significance of fission tracks (compiled in Fleischer et al., 1975), accompanied with experiments on track revelation (e.g. Fleischer & Price, 1964b; Price & Walker, 1962), led to rapid developments and recognition of the fission track method as an applicable tool in earth sciences. Early fission track studies were mainly concerned with absolute dating of impact glasses (e.g. Fleischer & Price, 1964a) and volcanic rocks (e.g. Naeser et al., 1980). The full potential for the utility of fission track thermochronology in orogenic and passive margin settings was not acknowledged until the 1980's, following the contributions of a number of workers, among them Gleadow et al. (1986) and Gleadow and Fitzgerald (1987). Progressive advances in the fission track method have, over the past few decades, led to the recognition of a number of additional applications, including sedimentary provenance and landscape development modelling (see summary by Gallagher et al., 1998).

3.1.1 Track formation mechanisms

Fission tracks are narrow damage features that are introduced into the lattices of U-bearing mineral grains upon spontaneous nuclear fission of ^{238}U (Price & Walker, 1963). Other naturally occurring radioactive isotopes, such as ^{235}U and ^{232}Th, have exceedingly long

fission-half-lives, and their contribution to track production can be neglected (e.g. Wagner & Van den Haute, 1992). The fission process involves splitting of an unstable nucleus into two daughter nuclei of slightly different mass. Every fission event is associated with a release of energy (normally about 210 MeV; Wagner & Van den Haute, 1992), out of which a substantial fraction is kinetic. Both product nuclei possess a strong positive charge and are ejected in opposite directions away from the site of fission.

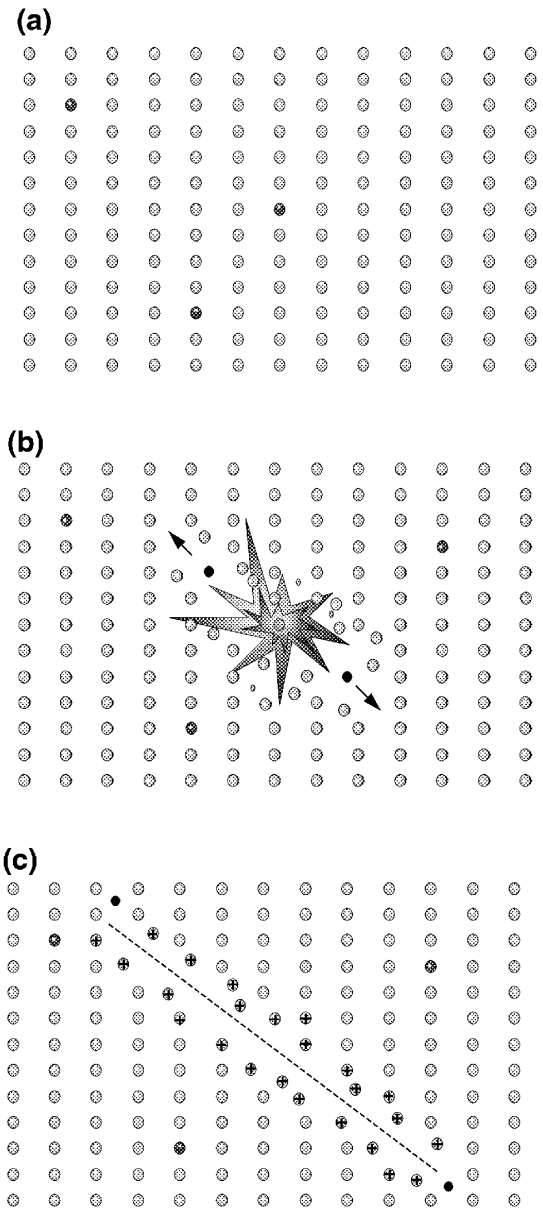

Fig. 8. The ion spike explosion model for formation of fission tracks in minerals. a) Radioactive ^{238}U (represented by dark spots) is present in trace amounts within the crystal lattice. b) Occasionaly, an ^{238}U atom undergoes spontaneous fission, which generates two heavy particles of slightly different mass. As a result of Coulomb repulsion the positively charged product nuclei recoil. While travelling through the lattice the heavy particles capture electrons from neighbouring atoms. c) The fission product nuclei leave ionized lattice atoms along their paths. These atoms repel each other and thus impose damage to the crystal lattice. Modified from Gallagher et al. (1998) after Fleischer et al. (1975).

The most widely acknowledged model for fission track generation is the ion spike explosion model (Fig. 8), put forward by Fleischer et al. (1965b). Details regarding the mechanisms behind track formation remain unknown and the model must thus be regarded as

a simplification (e.g. Gallagher et al., 1998). However, it provides a satisfactory approximation of the actual track-generating process. The ion spike explosion model attributes the formation of fission damage trails in insulating solids to the movement of highly charged, positive fission fragments through the lattice. These fission fragments capture electrons from the atoms along their trajectories. Coulomb repulsion leads to displacement of ionized lattice atoms away from the path of the fission product nucleus. The displaced atoms are relocated into nearby interstitial sites, leaving vacancies in the lattice within the damaged core region. Hence, a trail of permanent damage develops in the affected area. Elastic relaxation of the disrupted region causes straining of the immediate surroundings. The area affected by fission is thus wider than the trail of the fission nucleus itself. Eventually, ejected fission fragments lose their kinetic energy through interaction and collision with neighboring lattice atoms. The distance over which fission nuclei travel before coming to rest is dependent on the properties of the host material and on the fission fragment's mass and energy (Gallagher et al., 1998). Experimental results on apatite are generally consistent with a distance of ejection of approximately 8 μm for each of the two nuclei (Gleadow et al., 1986).

An alternative to the ion spike explosion model is the thermal spike model (Chadderton, 1988; Vineyard, 1976), which involves intense heating of the crystal lattice along the path of the fission fragment. Thermal conduction to the surroundings leaves a quenched damage core, in which lattice defects are generated. The compound spike model (Chadderton, 2003) is another, relatively recent contribution that argues for the combined effect of ionization and thermal activation. Clearly, additional studies must be undertaken before a comprehensive understanding of the processes behind track formation can be attained.

3.1.2 Track revelation

Apatite fission tracks in their natural state are extremely narrow features that rarely exceed 14 nm in width (Paul & Fitzgerald, 1992). Knowledge about the atomic-scale structure and properties of such latent (i.e. unetched) tracks has been obtained through transmission electron microscopy (e.g. Paul, 1993; Paul & Fitzgerald, 1992). Latent tracks are generally close to cylindrical in shape and are represented by a zone of amorphous material that clearly stands out from the surrounding crystalline solid (Bursill & Braunshausen, 1990). Chemical etching must be employed in order to make fission tracks visible under an optical microscope. The etchant serves to enlarge the area damaged by fission. As a result of the disordered lattice structure and low interatomic binding energy of the core of the damage zone, fission tracks

are much more susceptible to dissolution than the surrounding, undamaged apatite bulk material (Fleischer et al., 1975). The rate of etching is greater at the track tip than on the internal surface of each track, and etched tracks thus evolve into narrow, needle-like features (Wagner & Van den Haute, 1992). Due to the anisotropic nature of the apatite crystal, the efficiency of etching varies with crystallographic orientation. Etching has been found to progress most rapidly parallel to prismatic crystal faces (e.g. Green et al., 1986).

3.1.3 Characteristics of the apatite fission track system

Compared to the majority of other radiometric schemes the apatite fission track system is sensitive towards relatively low temperatures. The closure temperature in the context of fission track analysis is the temperature above which no tracks are effectively preserved. Fission tracks are generated at a constant rate even at temperatures above the upper limit of track preservation. However, such thermal conditions promote total erasure instantly after formation (Wagner & Van den Haute, 1992). The effective closure temperature of the apatite fission track system is conventionally approximated to 120 ºC. This estimate has been established through a combination of in situ borehole studies (e.g. Gleadow & Duddy, 1981; Hammerschmidt et al., 1984; Naeser & Forbes, 1976) and laboratory experiments involving extrapolation of the obtained results to geological time scales (e.g. Burchart et al., 1979; Duddy et al., 1988).

Early in the evolution of the fission track technique, Price and Walker (1963) reported partial obliteration of tracks at temperatures well below the closure temperature of the system. This trait was initially regarded as a major shortcoming that could potentially prohibit successful application of the method. Decades of studies have, however, revealed that the partial obliteration of fission tracks that occur at relatively low temperatures can be exploited in order to constrain the thermal evolution of rocks (e.g. Gleadow et al., 1986). Hence, the temperature dependence on track retention is now recognized as a key property that allows geological cooling histories to be inferred based on fission track data.

3.1.4 Objectives and applicability of fission track analysis

Apatite fission track age data from individual grain analyses provide information about the timing of the low-temperature cooling history of the host rock. Fission tracks develop continuously over time, and their formation rate is determined by the fission decay constant for ^{238}U. The number of tracks in a grain depends on both the time of residence at low temperatures and the abundance of ^{238}U. In order to obtain a fission track age for any given

grain, it is necessary to know the number of spontaneous fission tracks per unit volume, as well as the initial content of ^{238}U (e.g. Gallagher et al., 1998). While track density estimates form the basis for the calculation of a fission track age, the degree of track length reduction provides information about the time of residence at temperatures corresponding to reduced fission track stability (Gleadow et al., 1986). Both track density and length information are implemented during thermal history reconstructions (e.g. Ketcham, 2005).

Fission track analysis may be successfully applied to grains that display a wide range of ages and U-concentrations. Only in rare cases does the method prove inadequate. Young, U-poor samples generally contain very few tracks. Fission track analysis on such samples gives highly imprecise results. Conversely, for very old, U-rich samples the damage inflicted by fission fragments is extensive enough to render individual tracks impossible to distinguish (Wagner & Van den Haute, 1992).

3.2 Fission track annealing

3.2.1 External factors responsible for track shortening and obliteration

Latent fission tracks are metastable features. Compared to the surrounding, undamaged crystalline material, the tracks are in a higher energy state. Order tends to be restored within the damaged zone given sufficient time and appropriate external conditions. The process responsible for gradual restoration of the damaged crystal lattice is referred to as fading (Wagner & Van den Haute, 1992). Under the general conditions that dominate at the surface of the Earth this restoration transpires at an extremely slow rate. Studies on fission track stability have demonstrated that certain physical parameters promote progressive shortening of tracks and act to increase the rate of track obliteration. Fleischer et al. (1965a) revealed a slight increase in fading rate for fission tracks in zircons subjected to hydrostatic pressures in excess of 80 kbar. Opposite effects, involving enhanced track stability with increased pressure, have later been reported for apatite (Wendt et al., 2002). The experiments of Fleischer et al. (1965a) further indicated a connection between track segmentation and exposure to shear stress. The track-modifying process is in this case not regarded as conventional track fading, but is rather related to microscopic slip-movements. In a recent study, Hendriks and Redfield (2005) suggested increased annealing rates for apatites that have accumulated considerable radiation damage. The conclusions of Hendriks and Redfield (2005) have been challenged by a number of workers (e.g. Green et al., 2006) and must at present be regarded as highly controversial. Although numerous experiments have aimed to

provide additional knowledge on the factors responsible for track fading, several aspects regarding the physical processes in force remain incompletely understood.

Temperature has long been known to represent the parameter of greatest importance in regard to track shortening and healing (e.g. Fleischer et al., 1965a). A great effort has been made in order to describe the thermal influence on track behaviour, and as a result a rather comprehensive understanding has been attained. Fission tracks in apatite are generally unstable above 120±10 ºC (established for the Durango apatite age standard), but are sensitive towards significantly lower temperatures (e.g. Gleadow & Duddy, 1981; Naeser, 1979). Considerable variations in fission track stability have been reported for different apatite compositions (Barbarand et al., 2003a; Carlson et al., 1999; Green et al., 1986) and different cooling rates (Wagner & Reimer, 1972). The process that is responsible for thermal fading of fission tracks over time is termed annealing. Although the exact mechanism behind annealing is not entirely understood, diffusion of displaced lattice atoms and vacancies is believed to be essential (e.g. Gallagher et al., 1998; Tagami & O'Sullivan, 2005). Thermal annealing is associated with progressive track shortening and reduction in the number of observable fission tracks. Initially, tracks anneal from the tips inward. Further annealing results in track segmentation and development of healed material within the previously damaged crystal lattice (Green et al., 1986; Paul, 1993).

3.2.2 Partial annealing

Partial annealing is the process by which fission tracks shrink without being completely erased. Apatite fission tracks principally experience partial annealing between ~60 ºC and ~120 ºC (e.g. Gleadow & Duddy, 1981; Naeser, 1979). This temperature interval is associated with a progressive increase in degree of annealing and is commonly referred to as the partial annealing zone (PAZ; originally termed the partial stability zone; Wagner, 1972). Owing to track annealing at ambient surface temperatures (Donelick et al., 1990; Gleadow et al., 1986), the low-temperature boundary of the zone is difficult to establish accurately and has generally been defined as the temperature that corresponds to the maximum gradient of stability reduction (Wagner & Van den Haute, 1992).

The concept of partial annealing has conventionally been implemented during interpretation of fission track ages with depth (e.g. Fitzgerald & Gleadow, 1990). Shallow crustal depths associated with relatively low temperatures (i.e. below 60-70ºC) are characterized by essentially zero annealing and progressive accumulation of fission tracks over time. The partial annealing zone is encountered at greater depths (2-4 km, assuming a

geothermal gradient of 30 °C). At the temperature condition of the PAZ, the accumulation of new tracks is accompanied with a gradual decrease in track length and density. A fission track age reduction between 0 and 100% is expected within this zone. The zone of total annealing is localized at even greater depths (>~4 km). Within this zone no fission tracks can be retained, and the fission track age thus decreases to zero (Wagner, 1972). Since the zone of total annealing includes all temperatures for which zero track stability is inferred, it does not have a maximum temperature limit.

3.2.3 Internal parameters and their influence on annealing kinetics

The relationship between track annealing efficiency and specific properties of individual apatites is at present not fully understood. Several internal factors may potentially affect the inception and progression of annealing (e.g. Carlson et al., 1999; Donelick et al., 2005).

Chemical composition

Green et al. (1986) demonstrated a significant between-grain variation in resistance towards annealing attributed to differences in chemical composition and suggested the Cl/(Cl+F) ratio to be of particular importance. Cl-rich apatites were found to be considerably less susceptible to annealing than their F-rich counterparts. Several later studies have supported this assessment (e.g. Barbarand et al., 2003a; Carlson et al., 1999; O'Sullivan & Parrish, 1995). The impact of compositional differences on annealing is not only important with regard to the annealing rate within the PAZ, but also appears to have an effect on the closure temperature of the system (Ketcham et al., 1999). For apatite crystals with near end member compositions of F, total annealing has been reported at temperatures of ~100 ºC. Experimental results suggest that the closure temperature increases with increasing Cl-content. Particularly Cl-rich varieties may contain stable fission tracks at temperatures in excess of 160 ºC (Ketcham et al., 1999). Barbarand et al. (2003a) found that the dimensions of the unit cell profoundly affect apatite annealing properties. The actual structure of the crystal lattice is governed by the combination of ionic substituents in crystallographic sites and is thus a product of the bulk chemical composition. In addition to the Cl/(Cl+F) ratio, the content of rare earth elements (REE) in the Ca site has been observed to cause some variation in annealing behaviour. For F-rich apatite varieties, elevated concentrations of REE are associated with increased annealing rates. The reduced annealing efficiency caused by high Cl-contents appears to mask any effect of additional substitutions in Cl-rich grains.

D_{par}

The parameter D_{par}, first introduced by Donelick (1993), represents the mean maximum diameter of etch pits oriented parallel to the crystallographic *c*-axis. D_{par} essentially reflects apatite solubility, but has been proven to correspond well with annealing behaviour. Grains that exhibit low values of D_{par} (i.e. $\leq$ 1.75 μm) generally contain tracks that anneal relatively rapidly, while high D_{par} varieties are more resistant towards annealing (Carlson et al., 1999). Chemical composition appears to be a controlling factor on the diameter of etch pits and D_{par} is found to be positively correlated with wt% Cl (e.g. Burtner et al., 1994). The two parameters should, however, not be regarded as equivalent. Additional factors, such as the presence of crystallographic imperfections and ionic substitutions in the cation sites, may influence the diameter of fission track etch pits (Barbarand et al., 2003a). The etch pit parameter may in fact incorporate the combined effects of a range of ionic substitutions. Regardless of the actual size-determining factors, D_{par} has proven to be one of the most suitable measures of resistance towards annealing for individual apatites (Barbarand et al., 2003a; Donelick et al., 2005). Ideally, D_{par} measurements should be included in every thermochronological study to assess the significance of differential annealing behaviour (e.g. Carlson et al., 1999). Given the range of responses to elevated temperatures observed for individual grains, it is clear that variations in apatite annealing properties must be accounted for when the thermal histories of rocks are interpreted.

Crystallographic effects

The annealing behaviour of fission tracks in apatite is found to be highly anisotropic (Green & Durrani, 1977). Partially annealed tracks oriented at a low angle to the basal plane generally display a significantly shorter mean etchable track length than tracks that are oriented parallel to the crystallographic *c*-axis. The divergence in track length has been proven to increase systematically as annealing progresses (Donelick, 1991; Green et al., 1986). For strongly annealed samples only tracks oriented parallel to the *c*-axis may be detectable (Green et al., 1986). The general decrease in track length observed for fission tracks oriented perpendicular and at a high angle to the *c*-axis is accompanied by a reduction in track density (e.g. Green, 1988; Laslett et al., 1984; 1982). Fission track analysis may thus provide strikingly different results depending on which section of the apatite grain is considered. In order to avoid such inherent ambiguities, only apatite grains oriented with the *c*-axis parallel to the plane of view are conventionally included in the analysis (e.g. Donelick et al., 2005).

3.3 Age data

3.3.1 The external detector method

A number of different techniques can be applied in order to determine the content of ^{238}U in apatite grains for which fission track analysis is performed (see Donelick et al., 2005; Hasebe et al., 2004; Wagner & Van den Haute, 1992). At present, most fission track studies utilize the external detector method (Fig. 9), which is based on the relative abundance of U-isotopes. The ratio $^{238}U/^{235}U$ is constant in nature (Steiger & Jäger, 1977), and accordingly, the concentration of ^{238}U can be estimated by determining the abundance of ^{235}U. Fission of ^{235}U occurs at extremely low rates in nature, but is favoured when the host mineral is exposed to low-energy thermal neutrons in the vicinity of the core of a nuclear reactor (Donelick et al., 2005). Thermal neutrons rarely induce fission of ^{238}U or ^{232}Th (e.g. Donelick et al., 2005; Gallagher et al., 1998). Thus, virtually all tracks that are generated during irradiation originate through fission of ^{235}U. The common procedure is to etch the apatite grain-mount before attaching it to an essentially U-free muscovite external detector. The grain-mount and the detector are placed in direct contact before being irradiated with thermal neutrons. During irradiation some of the fission particles generated in the apatite grain cross the interface between the crystal and the detector and thereby produce tracks in the muscovite. These tracks provide an estimate of the abundance and distribution of ^{235}U in individual apatite grains. Ultimately, a fission track age is determined by establishing the relationship between the density of spontaneous tracks in the apatite and the density of induced tracks in the external detector (Gallagher et al., 1998; Tagami & O'Sullivan, 2005). The external detector method is advantageous in that it allows dating of individual grains. It can therefore successfully be applied to materials with extremely heterogeneous U-distributions or to sedimentary samples that consist of detrital grains with very different fission track ages (Tagami & O'Sullivan, 2005).

In recent years it has become increasingly more common to apply laser ablation inductively coupled mass spectrometry (LA-ICP-MS) in order to determine the ^{238}U concentrations of apatites selected for fission track analysis (Hasebe et al., 2004). The LA-ICP-MS approach is significantly faster than the conventional techniques for establishing U-contents and will likely become a routine procedure in the years to come.

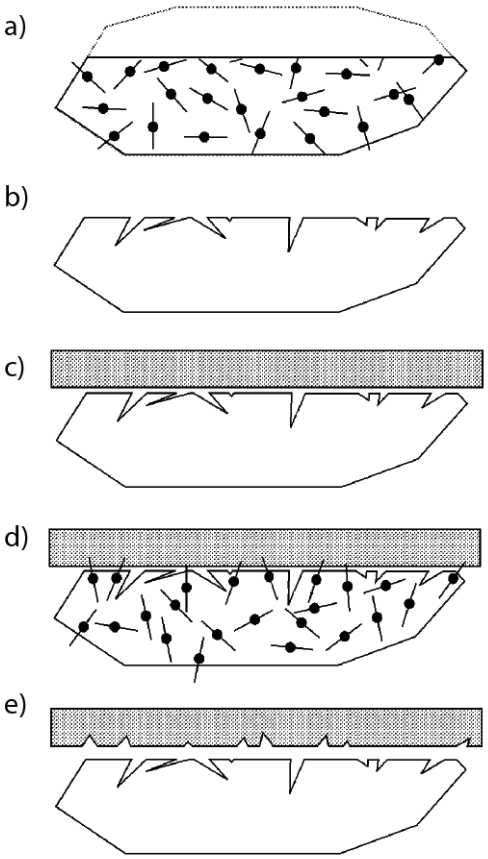

Fig. 9. The external detector method for determination of fission track age and ^{238}U concentration: a) The apatite grain mount is ground and polished to expose internal sections of individual crystals; b) Chemical etching reveals spontaneous fission tracks that are connected to the surface of the grain mount; c) A U-free mica detector is placed in direct contact with the grain mount, d) Low-energy thermal neutron irradiation induces fission of ^{235}U. Some of the fission particles cross the interface between the apatite mount and the detector; e) Chemical etching of the mica detector reveals the induced tracks. Ultimately, the grain mount displays the spontaneous fission tracks from ^{238}U, while the detector displays the induced tracks derived from fission of ^{235}U. Modified from Gallagher et al. (1998) after Hurford and Carter (1991).

3.3.2 Age equation

Basic age equation for radioactive decay

The standard formula for radioactive decay serves as the foundation for the fission track method. This equation describes the spontaneous decay of the radioactive parent atom to a stable daughter product. In its most fundamental form the equation can be written as

$$\frac{dN_P}{dt} = -\lambda N_P, \tag{3.1}$$

where dN_P/dt represents the rate of decay, which is proportional to the number of remaining parent nuclides, N_P, at any given time. The decay constant, λ, is expressed in yr^{-1}. $(N_P)_0$ gives the initial concentration of the parent atom and integration of equation 3.1 yields

$$N_P = (N_P)_0 e^{-\lambda t} \tag{3.2}$$

Equation 3.2 displays the number of remaining parent atoms at any given time, t. For convenience equation 3.2 may be rewritten as

$$(N_P)_0 = N_P e^{\lambda t} \tag{3.3}$$

The number of daughter atoms, N_D, equals the difference between the number of parent atoms initially present and the number of remaining parent nuclides. Equation 3.3 can thus be modified to

$$N_D = N_P(e^{\lambda t} - 1) \tag{3.4}$$

Equation 3.4 is the classical formula for radioactive decay, which forms the basis for the majority of geochronological methods.

Fission track age equation

The fission track approach differs from other radiometric dating methods in that spontaneous fission tracks rather than actual radiogenic nuclei represent the daughter product. A number of modifications are therefore necessary to make formula 3.4 applicable. In addition to spontaneous fission, ^{238}U experiences α-decay. Such events are much more frequent than fission, and both the decay constant for α-decay, λ_α, and the fission decay constant, λ_f, must be included in the fission track age equation. Given that the ratio $\lambda_f/(\lambda_\alpha+\lambda_f)$ is constant for ^{238}U (Wagner & Van den Haute, 1992), the basic fission track age formula can be expressed as follows:

$$N_s = \frac{\lambda_f}{\lambda_d}\,{}^{238}Ne^{\lambda_d t} - 1 \tag{3.5}$$

where λ_d is the total decay constant for ^{238}U, which incorporates the constants for both α-decay and spontaneous fission. t is the fission track age of the sample. Equation 3.5 displays the number of spontaneous tracks, N_s, (i.e. the abundance of the daughter product) as a function of the number of parent atoms (i.e. ^{238}N) and time since closure of the system. Since the ^{238}U/^{235}U ratio is constant, the number of parent atoms is related to the number of induced tracks, N_i. N_i is a function of the abundance of ^{235}U and is given by:

$$N_i = {}^{235}N\sigma_f\Phi, \tag{3.6}$$

where ^{235}N is the number of ^{235}U atoms, σ_f is the thermal neutron fission cross section and Φ is the thermal neutron flux during irradiation. The following formula for fission track age is obtained by substituting the expression for N_i into equation 3.5:

$$t = \frac{1}{\lambda_d} ln\left\{1 + \left(\frac{\lambda_d}{\lambda_f}\right)\left(\frac{N_s}{N_i}\right) I\sigma_f\Phi\right\}, \tag{3.7}$$

where I is the isotopic ratio $^{235}N/^{238}N$. Only fission tracks that intersect the polished surface of the grain mount are counted. The areal density of tracks thus serves as an estimate of the spatial density. N_s and N_i represent the number of tracks per unit volume and must be converted into the number of tracks per unit area in order to suite the frame of study. The relationship between N_s and N_i and the spontaneous and induced track densities, ρ_s and ρ_i, can be expressed as follows:

$$\frac{\rho_i}{\rho_s} = \frac{N_i}{N_s} gq \,, \tag{3.8}$$

where the parameter g is the integrated geometric factor that corrects for the difference in effective volume for track production. Tracks that intersect the surface of the grain mount are derived from an effective volume that is twice as large as the volume that has produced the tracks that are apparent on the surface of the detector. q is the factor of efficiency of registration and observation of tracks. This parameter is essentially identical during analysis of unknown samples and age standards (see paragraph below) and may be ignored given that equal criteria are applied throughout the counting process (e.g. Tagami & O'Sullivan, 2005; Wagner & Van den Haute, 1992). Taking the relationship in equation 3.8 into account, equation 3.7 can be rearranged as:

$$t = \frac{1}{\lambda_d} ln\left\{1 + \left(\frac{\lambda_d}{\lambda_f}\right)\left(\frac{\rho_s}{\rho_i}\right) qgI\sigma_f \Phi\right\} \tag{3.9}$$

The zeta calibration approach

Some of the parameters in equation 3.9 are poorly constrained or difficult to determine accurately. This is particularly the case for the fission decay constant, λ_f, and the neutron flux, Φ (e.g. Van den Haute et al., 1998). The latter has traditionally been established by measuring induced beta or gamma activity on metal activation monitors or by inducing fission in a standard glass with known U-content (Hurford & Green, 1983). The neutron flux is related to the induced track density in the dosimeter glass, denoted by ρ_d, by the empirically defined constant B:

$$\Phi = B\rho_d \tag{3.10}$$

To overcome the uncertainties in estimation of the fission decay constant and the difficulties in precision during measurement of neutron flux, Hurford and Green (1982, 1983) proposed a new calibration approach based on analyses of standards with known ages. A personal zeta

factor, ζ, should be calculated by each analyst for every mineral species that is analysed. This parameter includes both the fission decay constant and the neutron capture cross section and is given by

$$\zeta = \frac{\sigma_f I B}{\lambda_f} \tag{3.11}$$

At present, the zeta calibration method is the recommended approach for calculation of fission track ages (Hurford, 1990). In practice, the zeta factor is calculated by conducting a series of calibrations on standards of known fission track age. The following equation is used to compute the zeta factor:

$$\zeta = \frac{e^{\lambda_d t_{std}} - 1}{\lambda_d (\rho_s/\rho_i)_{std} g \rho_d}, \tag{3.12}$$

where t_{std} is the age of the standard, $(\rho_s/\rho_i)_{std}$ is the ratio of spontaneous to induced fission tracks counted on the standard and ρ_d is the estimated density of induced fission tracks derived from a dosimeter glass in the position of the standard at the time of irradiation. The fundamental fission track age equation for the zeta approach is obtained by substituting the expression for zeta in equation 3.11 by that in equation 3.12. Equation 3.9 may thus be rewritten as:

$$t = \frac{1}{\lambda_d} ln\left(1 + \lambda_d \zeta g \rho_d \frac{\rho_s}{\rho_i}\right) \tag{3.13}$$

The zeta calibration approach is of particular value because it serves to level the effect of personal variations in track recognition and counting and enables different analysts to obtain virtually identical results despite slight differences in counting techniques (Gallagher et al., 1998).

3.3.3 Age standards

The most commonly used and recommended standards for apatite fission track zeta calibration are Fish Canyon Tuff and Durango. Both apatites fulfil the requirements for age standards listed by Hurford and Green (1983); i.e. accessibility, age homogeneity, rapid post-formational cooling and compatibility of ages between several thermochronometers. The Durango apatite occurs as coarse, lemon-coloured crystals within the Cerro de Marcado open pit iron mine near Victoria de Durango, Mexico (Young et al., 1969). Based on sanidine-anorthoclase ^{40}Ar-^{39}Ar ages from two ignimbrites that stratigraphically bracket the timing of

apatite crystallisation, a reference age of 31.44 ± 0.18 Ma has been established (McDowell et al., 2005). The Fish Canyon Tuff apatite is derived from a voluminous ignimbrite field in San Juan, Colorado, for which a ^{40}Ar-^{39}Ar biotite age of 27.8 ± 0.2 Ma has been reported (Hurford & Hammerschmidt, 1985).

3.3.4 Error calculations

For a fission track age that is calculated by the zeta calibration method the error estimate, s_t/t, is mainly based on the error on the track density ratio of spontaneous to induced tracks, s_R/R, and the error on the track density of the dosimeter glasses, S_Φ/Φ. The error on the zeta value is of less importance (Wagner & Van den Haute, 1992). s_t/t is given by the following formula:

$$s_t/t = K\sqrt{(S_R/R)^2 + (S_\Phi/\Phi)^2}\,, \tag{3.14}$$

where $K \approx 1$ for samples with fission track age < 600 Ma and s_R/R may be expressed as

$$s_R/R = \sqrt{\frac{1}{N_s} + \frac{1}{N_i}} \tag{3.15}$$

The error estimates on the age and the track density ratio are given with 1σ confidence.

3.3.5 Chi-square test

Fission track counts are governed by Poisson statistics. By the application of the external detector method, a matched pair of spontaneous and induced tracks, and hence an individual fission track age, is obtained for every grain. Since the U-concentration does not affect the relation between spontaneous and induced tracks, the ρ_s/ρ_i ratio is not expected to vary significantly between grains derived from the same crystalline sample (Wagner & Van den Haute, 1992). A chi-square test has been developed in order to detect dispersion in grain ages beyond the variation allowed for a Poissonian distribution (Galbraith, 1981; Green, 1981). In effect, the test assesses whether the ratio ρ_s/ρ_i is the same for each pair of counts. The following formula is used to calculate a chi-square value:

$$\chi^2 = \frac{1}{N_s N_i}\sum_{j=1}^{n}\frac{(N_{sj}N_i - N_{ij}N_s)^2}{N_{sj}+N_{ij}} \tag{3.16}$$

N_s, N_i and n denote the total number of spontaneous and induced tracks and the total number of grains, respectively, while N_{sj} and N_{ij} represent the number of spontaneous and induced tracks in grain j. A p-value is calculated for each sample. This value reflects the probability

that the critical value of the χ^2-function at n-1 degrees of freedom and at the desired confidence level exceeds the calculated χ^2. If the p-value falls below 5%, the chi-square test is regarded as failed, and the ρ_s/ρ_i ratio is not homogenous within the sample (e.g. Galbraith, 2005). Sedimentary samples quite commonly contain a range of detrital components and are generally expected to exhibit more than one grain age population. In contrast, crystalline samples that fail the chi-square test should be treated with caution during interpretation, and a reason for the age dispersion should be sought (Wagner & Van den Haute, 1992).

The radial plot (Galbraith, 1988, 1990) is a graphical means of evaluating the distribution of individual grain ages within a sample. A standardized estimate, y, which is a function of the grain age, the standard error and the central age of all grains, is plotted against precision, x. Because the radial plot considers the precision of each calculated age, it is well suited for visual comparison of single grain fission track age estimates.

3.4 Length data

3.4.1 Track classification

Fission tracks are generally classified as semi-tracks or confined tracks according to their position relative to the polished plane of the grain mount. All tracks that intersect the polished surface are referred to as semi-tracks (Laslett et al., 1982). Such tracks have been truncated during mount preparation and do not display their full original length. Semi-track length estimates are obtained by projecting points on each track vertically up to the surface (Wagner & Storzer, 1972). The information extracted from such projected track length measurements has proven to be insufficient when it comes to resolving differences in cooling style and generally does not provide an adequate image of the true track length distribution (Laslett et al., 1994). For these reasons, the previously customary practice of measuring projected track lengths has been abandoned.

Over the last few decades considerable attention has been devoted to the study of tracks that are confined within the grain volume. Confined tracks reside fully beneath the surface of the mount and can only be reached by the etchant through conduits in the crystal lattice (Bhandari et al., 1971; Laslett et al., 1982). Lal et al. (1969) and Bhandari et al. (1971) described two major groups of confined tracks, characterized according to the nature of their conduits (Fig. 10). TINT (track in track) type tracks are connected to the surface through semi-tracks, while TINCLE (track in cleavage or crack) type tracks are reached by the etchant through cleavage planes or cracks. Donelick et al. (2005) further identified a third, minor

variety, TINDEF (track in defect), which is linked to the surface through a defect or a fluid inclusion. Measurements of confined track lengths involve significantly smaller biases than the estimation of projected track lengths (Laslett et al., 1982). Furthermore, the confined track length distribution is more sensitive to variations in the true length distribution (Gleadow et al., 1986; Green et al., 1989). Consequently, track length measurements are at present generally performed only for confined tracks that are subparallel to the polished crystal surface. Recent technological advances have incited new interest in semi-track lengths and their possible applications in fission track analysis. New software is currently on the way and will enable utilization of a combination of confined tracks and semi-tracks in order to gain more detailed thermal information (Gleadow, in press).

In order to address issues related to poor reproducibility of length data, Ketcham et al. (2007a) proposed *c*-axis projection as a means of converting individual track length measurements into an estimated value for each length in an orientation parallel to the *c*-axis. The necessity for normalisation of track angles is a direct result of the annealing anisotropy observed in apatite (cf. section 3.3.3).

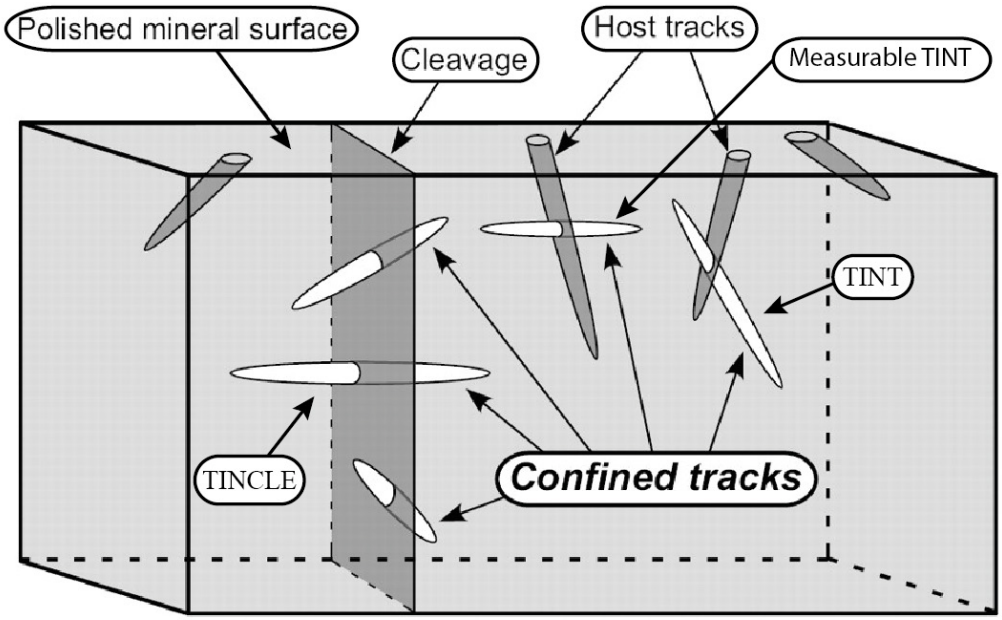

Fig. 10. A schematic illustration of various track types in an etched apatite crystal. Semi-tracks (dark grey) are truncated during grinding and polishing and their traces appear on the polished mineral surface. Confined tracks reside fully within the crystal volume. Two types of confined tracks are displayed; tracks in tracks (TINTs) and tracks in cleavage (TINCLEs). Modified from Tagami and O'Sullivan (2005).

3.4.2 Initial track lengths

The etchable length of a fission track is the specific part of the latent track that can be revealed by chemical etching under standardized conditions (Wagner & Van den Haute, 1992). Experimental studies suggest that the majority of induced tracks in apatite exhibit etchable lengths within the range 15.8 μm to 16.6 μm (Gleadow et al., 1986). Naturally occurring fission tracks in rapidly cooled volcanic rocks are generally somewhat shorter than experimentally induced tracks (Gleadow et al., 1986; Green, 1980). Consequently, some annealing must occur even at temperatures below that of the lower boundary of the partial annealing zone (Donelick et al., 1990).

3.5 Qualitative interpretation of fission track data

3.5.1 Track length distributions

The size reduction experienced by tracks at slightly elevated temperatures is highly significant for the utility of the fission track method. Each spontaneous fission track represents a different age of formation and records a specific portion of the thermal history experienced by the host rock (Gleadow et al., 1986). The length of any fission track is directly related to the prevailing temperature conditions since track formation. A great deal of information can be extracted from track length studies by establishing the relative contributions of different track length components and identifying separate generations of fission tracks. Gleadow et al. (1986) were among the first to recognize the importance of track lengths for the interpretation of fission track age data. Their study mainly concerned the discrimination of cooling styles based on track length distribution signatures. Four major spontaneous track length distribution types and corresponding thermal histories were identified (Fig. 11): 1) Relatively narrow, unimodal track length distributions associated with mean track lengths in the range 14.0 μm to 15.5 μm are generally concordant with rapid cooling followed by thermal quiescence. This specific distribution is typical for volcanic rocks, but may be attained by any rock that has experienced particularly rapid cooling through the temperature interval of enhanced track sensitivity. 2) For slowly cooled, crystalline basement rocks a distinct, negatively skewed track length distribution is characteristic. The mean track length generally ranges from 12.5 μm to 13.5 μm and the standard deviation is somewhat greater than for rapidly cooled volcanic rocks. For the track length distribution to attain the observed shape, it is essential that the basement remains thermally undisturbed. Monotonous cooling through the PAZ is thus inferred. Slow and steady cooling to ambient surface temperatures involves gradual

accumulation of tracks and progressive annealing. Partial annealing has been proven to be particularly effective in the uppermost interval of track stability, i.e. above c. 80 ºC (Gallagher & Brown, 1997). Thus, virtually no tracks formed at higher temperatures will be apparent when sufficient cooling time is permitted. The track length distribution for undisturbed basement-type samples are therefore dominated by relatively longer tracks, formed at the prevalent conditions of the low-temperature portion of the PAZ.

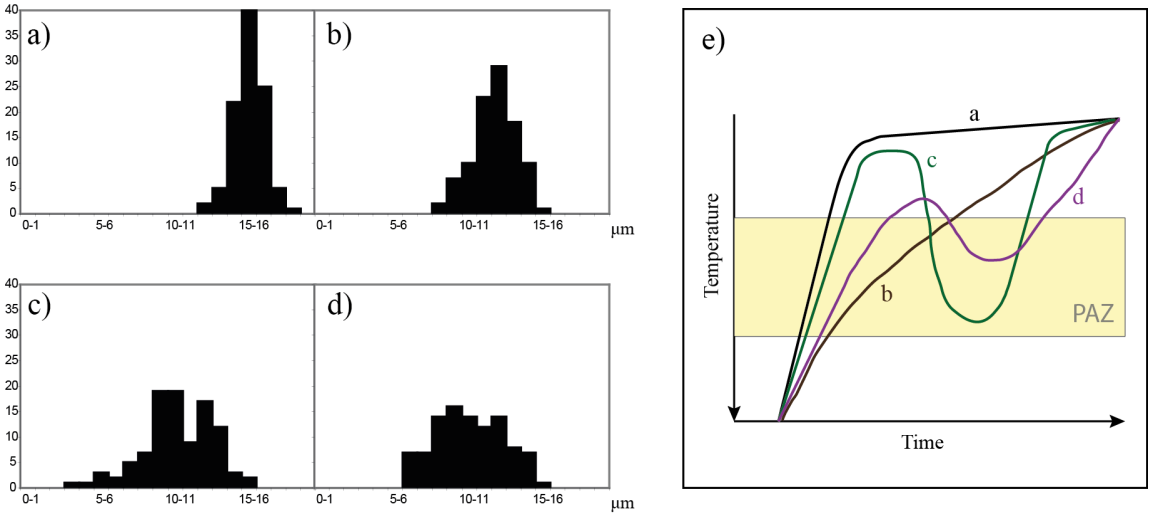

Fig. 11. Four distinct track length distribution signatures indicative of different cooling histories: **a)** Rapidly cooled volcanic type; **b)** Undisturbed basement type; **c)** Bimodal type; **d)** Mixed type. **e)** Representable cooling paths for the track length distributions in a-d. See text for details. Redrawn after Gleadow et al. (1986).

3) A bimodal distribution is expected for samples that have experienced elevated temperatures subsequent to the initial cooling. This distribution is characterized by two well-defined peaks with distinctively different means. Each peak corresponds to a particular component that records a portion of the thermal history. Tracks that formed prior to or during the thermal event have experienced a phase of enhanced annealing, and are thus shorter than tracks that were generated during and subsequent to the most recent episode of cooling. Under ideal circumstances the proportion of long tracks may reveal the extent of the period over which the rock has resided at near-surface temperatures. The size and shape of the short track-length component provides information about the duration and magnitude of the thermal event. 4) Complex cooling histories are in many cases difficult to resolve in practice. A thermal event of relatively short duration or insufficient maximum temperatures may fail to produce a clear bimodal distribution. Under such circumstances the peaks in the distribution signature merge to form a broad, unimodal distribution, characterized by a rather high standard deviation. Poorly resolved bimodal distributions are generally referred to as mixed types.

3.5.2 Geological significance of fission track ages

To a first-approximation fission track ages may be taken as to represent the time of residence at temperatures below those of the zone of total annealing (Wagner & Van den Haute, 1992). Implied in this statement is the assumption that all fission tracks that have formed over the given period of time have remained unaltered. In practice, however, the relationship between fission track age and cooling history is not straightforward, and the concept of closure temperature is not strictly valid for the fission track system (Gallagher et al., 1998). Actual closure may be represented by any temperature within the partial annealing zone (Wagner, 1972).

Fission track ages and track length distributions are related in a rather complicated manner, and a coeval evaluation of both is necessary in order to fully appreciate the geological meaning of the data. The probability of a track intersecting the polished surface of a grain is proportional to the length of the track (Laslett et al., 1982). Theoretically, a linear relationship between track length and track density reduction is expected. A reduction in length leads to a corresponding reduction in track density, and hence a lowered fission track age (Green, 1988; Laslett et al., 1994). In practice the linear relationship only holds for apatites that have experienced less than 25 % track length reduction (Green, 1988).
As a consequence of the observed track length/density relationship, the proportion of short tracks that are included during counting is not equal to the actual share of short tracks in the grain as a whole. An apatite grain that chiefly contains relatively short tracks will display a younger age than a grain with the same true number of tracks, but with a majority of long tracks. It is thus clear that the obtained fission track age for any given sample is highly dependent on the sample's time of residence and thermal evolution within the partial annealing zone (Gleadow et al., 1986; Wagner & Van den Haute, 1992). Slow cooling through the zone of partial annealing implies progressive shortening of tracks and declining probability of observing individual tracks during the counting procedure. The fission track age obtained from a sample that has experienced such a cooling path should not be taken as to indicate the exact time at which the rock attained a temperature below the closure temperature of the system. In fact, the acquired age may be significantly younger than the time of entry into the PAZ and should rather be regarded as a cooling age that reveals residence at temperatures somewhere within the PAZ at the given time (Wagner, 1972). The fission track ages of slowly cooled rocks do not reflect specific thermal events, and should thus be considered apparent ages rather than absolute ages in the conventional sense (e.g. Gleadow et al., 1986). For samples that have suffered multiple episodes of reheating, the interpretation of

fission track ages is particularly problematic (Wagner & Van den Haute, 1992). The fission track age obtained from a sample that displays a mixed or bimodal type track length distribution is typically a composite value that is not geologically meaningful when considered independently (Gleadow et al., 1986). Conversely, the fission track ages of rapidly cooled rocks may indeed be interpreted as actual cooling events. As a consequence of the dominance of long track lengths in such samples, the number of fission tracks that intersects the polished grain surface gives a good estimate of the number of tracks within the total volume of the grain (Laslett et al., 1982). For rapidly cooled rocks, the fission track method serves to establish the timing of entrance into the PAZ (Wagner, 1972).

3.5.3 Vertical profiles

Detailed information about the cooling path within a geographically restricted area can be made available through fission track analysis of a suite of samples collected from a near vertical profile. Early work by Wagner and Reimer (1972) demonstrated a positive correlation between apatite fission track age and elevation for samples from the Swiss and Italian Alps. The observed trend was interpreted as to reflect the movement of the rock column through the temperature gradient associated with increased fission track stability. Implicit in the concept of vertical profiles is the assumption that all samples have experienced the same thermal history (Gallagher et al., 2005). At any time in the geological past, rock samples derived from low portions of the profile were exposed to higher temperatures than samples that presently reside at higher elevations. Correspondingly, fission track studies of samples from drill holes demonstrate a gradual decrease in fission track age with depth, down to the point at which the age is reduced to zero (e.g. Gleadow & Duddy, 1981; Wagner et al., 1997). It has long been known that fossil partial annealing zones may be identified when fission track age data from vertical profiles are plotted against sample elevation (e.g. Fitzgerald & Gleadow, 1990; Gleadow & Fitzgerald, 1987). The base of a partial annealing zone is typically perceived as a break in slope associated with a change in the gradient of the regression line (Fig. 12). Samples below the break in slope are found to display similar fission track ages, and are therefore inferred to have experienced rapid cooling from depths associated with total annealing. The position of the break in slope itself thus represents the timing of the onset of the cooling event. All samples that presently reside at the surface have cooled through the PAZ and some degrees of partial annealing must be accounted for. Consequently, the age corresponding to the break in slope represent a minimum age for the onset of cooling (Fitzgerald et al., 1995). An exhumation rate for the period of accelerated cooling can be

calculated from the gradient of the regression line below the break in slope. Samples above the break in slope are derived from a pre-cooling fossil partial annealing zone. The gradient associated with this particular part of the age-elevation plot is not solely related to an exhumation rate, but also reflects the inherent annealing signature of the PAZ (Fitzgerald & Gleadow, 1990). The actual shape of the profile above the break in slope is dependent on the paleogeothermal gradient and the time of residence for each sample within the PAZ (Fitzgerald et al., 1995).

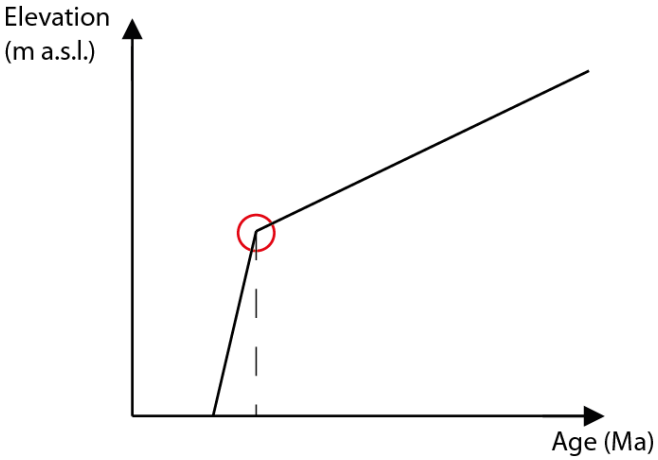

Fig. 12. Typical appearance of an age-elevation-plot from an area that has experienced an episode of rapid cooling. The break in slope (red circle) represents the timing of the onset of accelerated cooling. Similar ages are found for the lowermost part of the profile.

A number of studies (e.g. Fitzgerald & Gleadow, 1990; Gallagher & Brown, 1997) have reported track length distributions that are in good agreement with the described interpretation of the age-elevation plot. Typically, samples from below the break in slope display unimodal distributions dominated by long tracks. A track length component of this kind is conventionally taken as to indicate rapid cooling through the PAZ associated with concurrent and subsequent accumulation of fission tracks (e.g. Gleadow et al., 1986). Conversely, samples above the break in slope characteristically contain a component of shorter tracks that must have experienced partial annealing over an extended period prior to the cooling event.

For a break in slope to be identified, it is usually required that samples are collected over a significant relief. This is particularly the case in regions where a substantial period of time has lapsed since the episode of enhanced cooling. Gradual accumulation of long fission tracks is associated with a reduced proportion of short tracks. The signature indicative of residence within a fossil PAZ thus becomes less pronounced (Gallagher et al., 2005). As a result, discrete cooling events become progressively more difficult to recognize in time.

Absence of a well-defined break in slope may in some cases indicate that the region in question never experienced a cooling event of sufficient magnitude. Alternatively, the transition between the fossil PAZ and the previous zone of total annealing may be outside the range of the vertical profile.

Fission track data obtained from vertical profiles are quite commonly used to calculate the paleogeothermal gradient from the time prior to the onset of accelerated cooling. The calculations can be performed in a number of different ways depending on the characteristics of the sampled profile. Bray et al. (1992) proposed an algorithm based on weighted least-square regression of modelled maximum temperatures for sedimentary samples from a range of depths in a bore hole. Fitzgerald and Gleadow (1990) estimated the paleogeothermal gradient for a vertical profile sampled in the Transantarctic Mountains by simply dividing the total thickness of the rock column above the break in slope for the time in question by the temperature difference between the base of the PAZ and the surface. Although the approach is straightforward, significant uncertainty is introduced into the estimates if the previous stratigraphic thickness and the paleo-surface temperature are not well constrained.

3.6 Apatite (U-Th)/He analysis

The production of radiogenic He from actinide decay formed the basis of the very first attempts of establishing absolute ages through geochronology (Rutherford, 1905). At the time, the temperature-sensitive diffusive behaviour of He was not understood, and the technique became known for yielding erroneously young ages. Consequently, the (U-Th)/He scheme was abandoned shortly after its conception and received limited attention until Zeitler et al. (1987) discovered a way to quantify diffusive He loss and relate it to the cooling histories of rocks within the upper few kilometres of the earth's crust. In recent years the (U-Th)/He method has experienced a renaissance. At present the technique is a widely acknowledged tool for exploring the near-surface cooling histories of rocks and the thermal perturbations in the uppermost crust. Assuming a cooling rate of 10 °C/Ma, the effective closure temperature of the (U-Th)/He system is ~70 °C (e.g. Farley, 2002). Given its sensitivity towards lower temperatures, the (U-Th)/He system effectively compliments apatite fission track analysis. Used together the two methods have the potential of revealing detailed information regarding the timing and style of cooling through the uppermost 1-4 km of the crust.

3.6.1 ^{4}He generation in apatite

The (U-Th)/He method is based on ingrowth of ^{4}He (α-particles) produced by the series decay of ^{238}U, ^{235}U and ^{232}Th. In addition, minor amounts of ^{4}He are generated by the decay of ^{147}Sm. The total amount of accumulated ^{4}He depends on the concentration of the radioactive parent nuclides, the α decay constants, λ, and the time, *t*, since closure of the system and is expressed as

$$^{4}He = 8\,^{238}U\left(e^{\lambda_{238}t}-1\right)+7^{235}U\left(e^{\lambda_{235}t}-1\right)+6^{232}Th\left(e^{\lambda_{232}t}-1\right), \quad (3.17)$$

where all isotopic abundances are given as present-day values. The constants that precede each of the isotopic abundances represent the number of alpha particles generated in the individual decay chains. ^{147}Sm normally produces undetectable amounts of ^{4}He and is ignored in the formula. Equation 3.17 assumes that no non-radiogenic ^{4}He is present in the crystal.

3.6.2 ^{4}He diffusion behaviour

He retention in crystals is governed by thermally activated volume diffusion processes. In apatite, He diffusion obeys a linear Arrhenius relationship that is given by

$$\frac{D}{a^2}=\frac{D_0}{a^2}e^{-E_A/RT} \quad (3.19)$$

(Fechtig & Kalbitzer, 1966), where D is the diffusivity and D_0 is the diffusivity at infinite temperatures. "a" denotes the diffusion domain radius, and E_A, R and T represent the activation energy (≈ 33 ± 0.5 kcal/mol for the Durango apatite; Farley, 2000), the gas constant and the temperature, respectively. In the case of the Durango apatite, for which the majority of studies on He diffusivity has been undertaken, the diffusion domain is represented by the entire grain (Farley, 2002). From equation 3.19 it is evident that the diffusivity increases with temperature. According to Fick's first Law (Fick, 1855), diffusion is driven by the He concentration gradient in the crystal. A high concentration gradient (i.e. a substantial difference in He concentration between the crystal rim and the internal portions of the grain) promotes rapid He loss. Thus, diffusion is most effective in old grains or grains with high abundances of parent nuclides. Fick's first Law is conventionally written as

$$F=-D\frac{\partial C}{\partial x}, \quad (3.20)$$

where F denotes the mass flux, D the diffusivity and $\partial C/\partial x$ the concentration gradient (concentration, C, divided by distance, x). Fick's second Law (Fick, 1855) describes the

change in concentration with time as a function of the concentration gradient. For objects with spherical geometries Fick's second Law is given by

$$\frac{\partial C}{\partial t} = D\left(\frac{\partial^2 C}{\partial r^2} + \frac{2}{r}\frac{\partial C}{\partial r}\right), \tag{3.21}$$

where r is the radius of the sphere. The (U-Th)/He age equation presented in section 3.6.1 does not account for diffusional loss of He subsequent to its formation. In order to prove useful in the context of (U-Th)/He thermochronology, equation 3.17 must be combined with Fick's Laws of diffusion. The following equation gives an expression for the amount of He retained in a crystal at a given time, *t*, provided that the crystal experiences continuous accumulation and thermally dependent diffusive loss of radiogenic He:

$$\frac{\partial\, {}^4He(r,t)}{\partial t} =$$

$$8\,\lambda_{238}{}^{238}U\,(t) + 7\lambda_{235}{}^{235}U(t) + 6\lambda_{232}{}^{232}Th(t) + \frac{D(t)}{a^2}\left(\frac{\partial^2\, {}^4He(r,t)}{\partial r^2} + \frac{2}{r} \times \frac{\partial\, {}^4He(r,t)}{\partial r}\right) \tag{3.22}$$

3.6.3 Effective closure temperature and partial He retention

The effective closure temperature of the (U-Th)/He system is a function of cooling rate and mineral grain size and varies between ~55 °C and ~75 °C. As described by Dodson (1973), the closure temperatures of thermochronometers in general are positively correlated with cooling rates, meaning that rapidly cooled rocks record higher closure temperatures than slowly cooled rocks. Experimental studies have documented this relationship for the (U-Th)/He system (Farley, 2000). Mineral grain size exerts a significant effect on the closure temperature. Small grains have shorter holding times than larger grains and consequently record cooling through lower temperatures. In apatite, the shortest pathway for He diffusion is perpendicular to the *c*-axis, and the prism radius is therefore the most relevant parameter when considering variations in effective closure temperature (Farley, 2002).

The (U-Th)/He system is in general particularly sensitive to temperatures between ~80 °C and 40 °C (Wolf et al., 1998). This specific interval is termed the partial retention zone (HePRZ) and is characterized by progressive loss of He from the apatite crystal through diffusion. Apatite (U-Th)/He ages reflect the thermal history of a sample in the HePRZ. At temperatures above 80 °C He escapes to the surroundings more rapidly than it is produced and the age remains zero. Below 40 °C virtually all generated He is retained in the crystal and gas accumulates over time, causing a progressive age increase. The HePRZ represents the temperature range, over which (U-Th)/He ages change most dramatically with temperature.

Eventually, samples residing within the partial retention zone achieve equilibrium between He production and loss and a steady state He age is attained (Wolf et al., 1998).

3.6.4 Alpha-ejection

Alpha-particles produced by radioactive decay of the actinides possess relatively high kinetic energies, which allow them to travel a substantial distance within the apatite crystal before coming to rest. As a result, parent and daughter nuclei are spatially separated. The initial energy and the lattice density determine the exact distance an alpha particle is capable of travelling (Farley et al., 1996). In apatite, the α-stopping distance is between ~18.8 μm and ~22.3 μm, depending on which parent nuclide is considered (Ketcham et al., 2011).

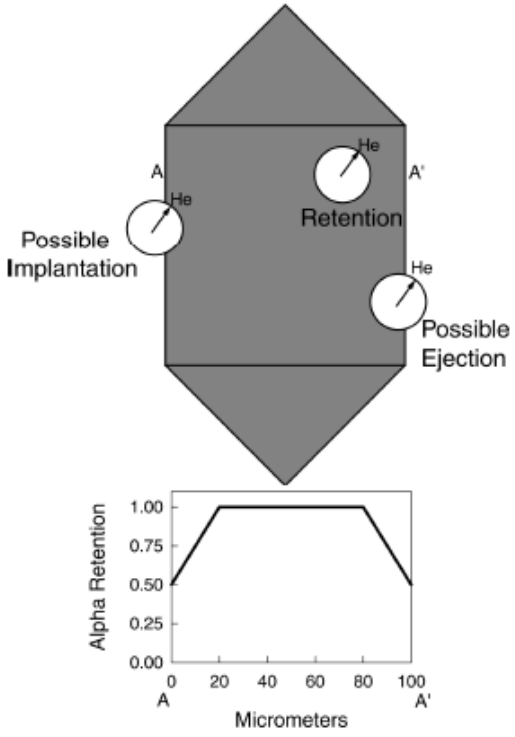

Fig. 13. Schematic illustration of three possible outcomes of long α-stopping distances: α-retention, α-ejection and less frequent α-implantation. Circles represent sites at which the α-particle may come to rest, while arrows indicate possible particle trajectories. α-ejection may occur if the parent nuclide is situated less than a stopping-distance from the rim. The lower plot displays the probability of alpha retention along a cross-section through the grain. From Farley (2002).

There are three possible outcomes of alpha decay with regard to He retention (Fig. 13; Farley, 2002): 1) Alpha-particles are retained in the grain regardless of particle trajectory, provided that the parent nuclide is positioned more than ~20 μm from the grain edge. 2) If the parent nuclide is located within a stopping distance from the crystal surface, there is a probability that the α-particle may be ejected from the grain. Whether the produced He is ejected or retained in the crystal depends on the particle trajectory. The probability of ejection rises to its maximum when the parent nuclide is located at the edge of the grain. 3) Alpha-decay occurring in the neighbouring grains or in the surrounding matrix may cause implantation of

He into the apatite. Alpha-particle implantation is generally not considered to have a pronounced effect on the concentration of He in individual grains.

Alpha-ejection effects represent a major challenge for the (U-Th)/He method since underestimation of the amount of retained He leads to measured ages that are considerably younger than the true ages. To account for α-ejection in apatite, Farley et al. (1996) presented a parameter that effectively corrects for the loss of He from the portion of the grain that is located less than a stopping-distance from the crystal surface. The F_T correction factor incorporates the surface to volume ratio of the grain and the α-stopping distance and is given by

$$F_T = 1 - \frac{S}{4} \times \beta \ , \tag{3.23}$$

where S is the alpha stopping distance and β is expressed as

$$\beta = \frac{2.31L+2R}{RL^{-1}} \tag{3.24}$$

L represents the crystal length, while R denotes the half prism width of the apatite. The grain dimensions are crucial when considering the importance of alpha-ejection for individual apatites. Small grains have large surface to volume ratios and are particularly influenced by reduced ages as a result of He loss. The alpha-ejection correction entails a homogeneous spatial distribution of parent nuclides within the apatite crystal. A corrected (U-Th)/He age is obtained by dividing the single grain raw-age by the F_T factor (Farley et al., 1996).

3.6.5 Pre-analytical requirements

A number of pre-analytical requirements must be fulfilled to ensure successful application of the (U-Th)/He method. The characteristics of the apatite crystals selected for analysis is of great importance and must be thoroughly assessed. Ideally, (U-Th)/He analysis should be performed on intact, euhedral grains, for which the physical dimensions are easy to determine. Cracks should be avoided since they represent pathways for rapid He diffusion loss and may cause ages that are too young (Farley, 2002). The greatest problems during (U-Th)/He analysis arise from the presence of small U-Th-rich mineral inclusions within the analysed apatite grains (Lippolt et al., 1994). Mineral inclusions of zircon and monazite may contribute significant He to the analysis, but generally remain undissolved after the standard dissolution processes that are employed prior to U-Th-measurements (cf. section 5.4). The excess He is thereby not accounted for by increased concentrations of parent nuclides and the resulting (U-

Th)/He ages are anomalously old. Grains with recognizable mineral inclusions can normally be avoided by careful inspection under a binocular microscope prior to analysis. This approach is, however, not fully adequate for grains that contain sub-microscopic inclusions (Belton et al., 2004). The (U-Th)/He method inherently assumes a homogeneous distribution of parent nuclides in the crystal. Zoned grains are problematic because of their unpredictable retentivities. Reduced He retention is expected if the bulk of the U and Th in the crystal are concentrated along the rim. This particular zoning pattern causes (U-Th)/He ages that are too young. Conversely, increased retention and erroneously old ages are expected for grains with U-Th-rich cores (Farley et al., 1996). Since He production may vary significantly from the core to the rim, alpha-ejection correction is normally not fully successful for zoned grains (Hourigan et al., 2005).

4. FIELDWORK AND SAMPLING

As part of the current study, 31 samples were collected for apatite fission track and (U-Th)/He analysis during July-September 2011. 6 additional samples were collected by A. Ksienzyk in 2007 and 2008.

4.1 Sampling strategy

The geological map Odda 1:250 000 by Sigmond (1998) was consulted during the development of a sampling strategy. The ideal lithology for maximum apatite yields and good quality grains is a medium- to coarse-grained, biotite-rich granitic gneiss. As such lithologies are quite common in the field area, sampling was not to any significant degree restricted by the availability of suitable rocks. From a total of 31 samples 30 were obtained from the Precambrian basement. The autochthonous and parautochthonous phyllites of the décollement zone were largely avoided, since low apatite yields are generally expected for fine-grained metasedimentary rocks. Fig. 14 displays a representative selection of the lithologies chosen for sampling.

4.1.1 Vertical profiles

The aim during the fieldwork component of the current project was to attain evenly distributed samples from a range of elevations without sampling over significant horizontal distances within each profile. In order to provide detailed information regarding the cooling of the area, and concurrently manage to cover a sufficient elevation, the vertical spacing between samples was set to approximately 200 m. Since the low-elevation samples were expected to contain most information on the latest cooling events, the sample density in the lowermost parts of the profiles are generally higher.

Three vertical profiles were sampled, each positioned on a steep flank of one of the fjords in the area (Fig. 15). Transect one is located to the northeast of Osafjorden and is referred to as the Osa profile. Eight samples (KJ-1 to KJ-8, KJ-26 and BG-14) were obtained along a steep, curvy road up to Rundavatnet. Another two samples (KJ-24 and KJ-25) were collected from the gentle hills between the road and the peak Nipahøgdi to the northwest.

Fig. 14. A selection of the sampled lithologies: a) Augen gneiss with large (~5 cm) feldspar porphyroclasts, sampled on Osafjellet (sample no. KJ-26); b) Stromatic migmatite from the southeastern flank of Onen near Kjeavatnet (KJ-19); c) Strongly foliated biotite gneiss from Osa (KJ-31); d) Quartzitic phyllite with quartz segregations, sampled close to the summit of Nipahøgdi (KJ-24); e) Coarse-grained Eidfjord Granite from Simadalen (KJ-23); f) Massive, medium-grained granite from Bruravik (KJ-27).

Transect number two, hereafter referred to as the Kjeåsen profile, is located southeast of transect one, on the Eidfjord-side of the prominent summit Onen. Three samples (KJ-23, KJ-29 and KJ-30) were obtained along a steep hiking trail from sea level in Simadalsfjorden to Kjeåsen. Further sampling was conducted along a slightly gentler gradient from Kjeåsen to an elevation of 1226 m asl on the southeastern side of Onen. Four samples (KJ-19 to KJ-22) were collected from this part of the profile. Transect three, which is designated as the Bu profile, is located on the southern side of Eidfjorden and extends from sea level near Brimnes towards the southeast. Seven samples (KJ-12 to KJ-18) were collected along a steep gradient from sea level to an elevation of nearly 1000 m asl. An additional sample (KJ-28) was obtained from the peak Vatnasetenuten on the Hardangervidda plateau.

4.1.2 Additional samples

Scattered sampling close to sea level was conducted in order to reveal possible juxtaposition of AFT ages across the Eidfjord and its tributaries and shed light on the more recent cooling history of the area. The additional samples KJ-9, KJ-10, KJ-27, BG-13, BG-16, BG-26, BG-27 and BG-53 were all collected from road outcrops located within 50 m of sea level.

4.2 Field measurements and structural mapping

At each sample location the most prominent joint directions were measured. The fracture spacing was recorded in order to assess the influence of advective and convective heat transfer. Field observations and measurements were combined with aerial photographs to reveal the presence of large scale structures, and lineament maps were produced in order to determine possible sites where faulting may have caused juxtaposition of thermochronological ages.

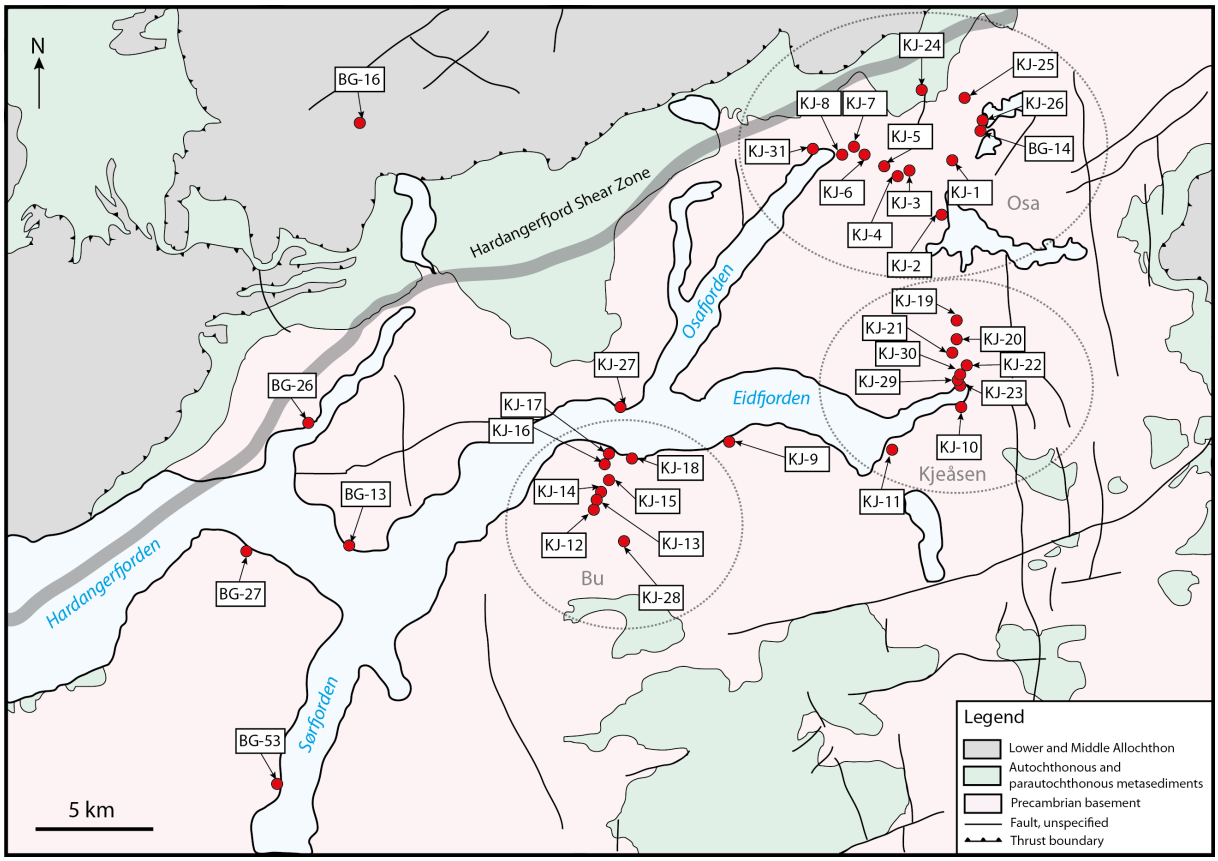

Fig. 15. Overview of sample locations. Three vertical profiles were sampled as part of the current study; the Osa profile (furthest to the north), the Kjeåsen profile (on the northern flank of the Simadalsfjord, some kilometers south of the Osa profile) and the Bu profile (further to the east on the southern side of the fjord). Additional sampling was conducted close to sea level. Samples with BG numbers were collected by A. Ksienzyk in 2007 and 2008.

5. ANALYTICAL PROCEDURE

5.1 Sample preparation

From 31 collected samples from the Eidfjord-Ulvik area, 30 were prepared for analysis. Sample preparation was conducted at the University of Bergen from August to December 2011.

5.1.1 Mineral separation

Approximately 4 kg of in situ rocks were collected for each sample. The samples were downsized to relatively small pieces in the field in order to avoid the risk of contamination that is associated with the use of a jaw crusher or a chopping block in the laboratory. Standard procedures for mineral separation were employed in order to isolate apatite. Initially, gravel-sized fragments were disaggregated in a Pulverisette 300 disc mill and the product was sieved. The <315 μm fraction was collected and the heavy mineral constituents were separated from the bulk of lighter, rock forming minerals on a Wilfley table. Magnetic separation was performed for the heavy fraction, using a Frantz magnetic separator set at 0.3 A, with forward and side slopes of 15 °. The non-magnetic components were further separated based on their specific gravities. A sodium polytungstate (SPT) solution with a density of ca. 2.87 g/cm^3 was used for this purpose. In order to separate weakly magnetic minerals like titanite from the non-magnetic, apatite-bearing fraction, the remaining heavy components were run through the Frantz magnetic separator at 1.2 A. Finally, the separate was introduced into diiodomethan (DIM), which has a density of 3.3 g/cm^3. The purpose of this step was to separate apatite from heavier minerals like zircon and pyrite. After the described steps had been performed, relatively pure apatite extracts had been obtained for most samples.

5.1.2 Grain mount preparation

Prior to mounting, the apatite extracts from each sample were sieved through a mesh cloth with mesh widths of 100 μm. For apatite-rich samples only the >100 μm fraction was used for analysis. Grains of apatite were mounted in epoxy and ground in order to expose internal sections of each grain. Subsequently, the grain mounts were polished with 6μm and 3μm diamond polish, before finally being hand-polished for 60 seconds with 0.05 μm Al_2O_3 powder.

5.1.3 Etching of latent tracks in apatite

For the current study, each sample was etched in 5 molar nitric acid (HNO_3) for 20 seconds at 20 ± 1ºC, following the scheme proposed by Green et al. (1986) and Gleadow et al. (1986). Immediately following etching, the mounts were washed in water and ethanol. The samples were left to dry at slightly elevated temperatures (i.e. ~40 ºC) to ensure full evaporation of any remaining etchant.

5.2 Thermal neutron irradiation

5.2.1 Preparation and irradiation

Subsequent to etching and drying, each sample was covered with a muscovite external detector and wrapped tightly with adhesive tape. Thermal neutron irradiation was conducted at the Garching Forschungsreaktor FRM II at the Technical University of Munich on the 21st of February 2012, using a thermal neutron flux of 1 x 10^{16} neutrons/cm^2. The neutron flux was monitored by a series of IRMM-540R dosimeter glasses with a known U-concentration of 15 ppm. Prior to irradiation, these glasses were paired with muscovite detectors and placed in front and at the end of the sample stack. An additional dosimeter glass was placed in the middle of the sequence.

5.2.2 Post-irradiation procedure

Subsequent to irradiation, the samples required nearly 4.5 months of cooling in order to reach a radioactivity below 5.0 μSvh^{-1}, which is regarded as safe for handling. Before the adhesive tape was removed, each sample-mica pair was pierced with five pin holes that are necessary as reference points. Induced tracks in mica were revealed through etching in 40 % hydrofluoric acid (HF) for 20 minutes at room temperature. After etching, the mica detectors were left in running water overnight to remove HF residue. Before analysis, each mount and the corresponding mica detector were glued on a standard petrological glass slide (Fig. 16). The mica was placed on top of a second glass so that the surfaces of the grain mount and the detector would attain approximately the same height. Finally, a small copper-grid crosshair was attached to the glass slide below the lower left corner of the mica.

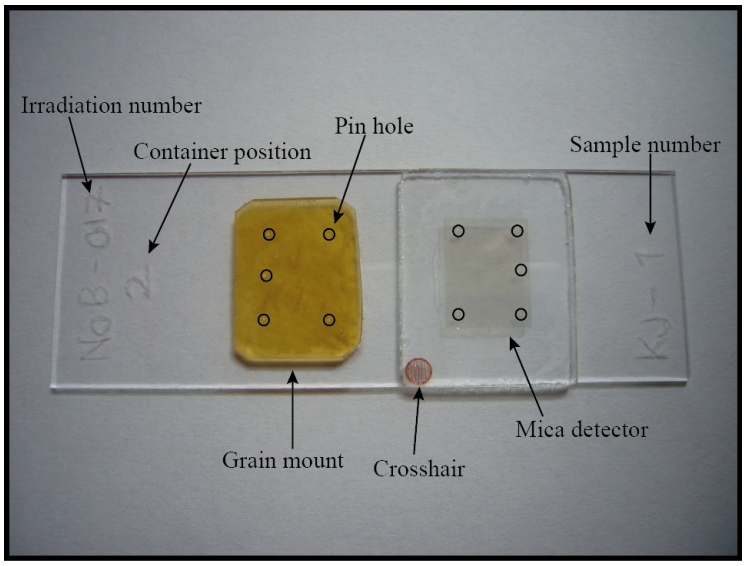

Fig. 16. Photograph of prepared glass slide with apatite grain mount and mica detector. Irradiation number, sample number and container position are displayed on the slide. Pin holes are encircled. The crosshair is used as the initial reference point during the development of a computer-generated coordinate system that correlates individual apatites with their corresponding prints.

5.3 Analytical steps

Training, calibration and analyses were executed in the fission track laboratory at the University of Bergen from January to August 2012. In total, 32 samples were analysed.

5.3.1 Equipment

Fission track analysis was performed with an Olympus BX51 optical microscope, equipped with a CalComp Drawing-board III digitizing tablet and a computer-controlled Kinetek stage, run by the FTstage software by Dumitru (1993). A cursor with a light-emitting diode (LED) was used for length measurements.

5.3.2 Counting of dosimeter glasses and estimation of ρ_d

Prior to zeta calibration and fission track analysis the detectors of the dosimeter glasses were counted in order to estimate the decrease in track density with distance from the neutron source. Throughout the analytical process, counting was performed in transmitted light and with a magnification of 1250 x. 25 grids, arranged in a 5x5 pattern, were counted on the detector of each dosimeter glass. After counting was completed, the density of induced tracks in the detector, ρ_d, was calculated for each dosimeter glass. The ρ_d values were placed

according to the position of the dosimeter glasses during irradiation, and a general track density trend was estimated for each batch using linear regression.

5.3.3 Counting technique for age standards and samples

Equal procedures were implemented both during counting of age standards for zeta calibration and samples. Prior to counting it is important to obtain a good alignment between the mount and the detector. The external detector displays a mirror image of the apatite grains in the mount (Fig. 17). This mirror image generally appears as a limited area with significantly higher track density than the surrounding mica. In order to establish a coordinate system for the FTstage software, identical points on the grain mount and the detector must be correlated. A series of reference points are used for this purpose. Pin holes function as coarse reference points and allow approximate alignment. Further correlation of fine reference points, such as tiny U-rich zircon inclusions within apatite grains or even small zircons in the mount, are required for a precise alignment.

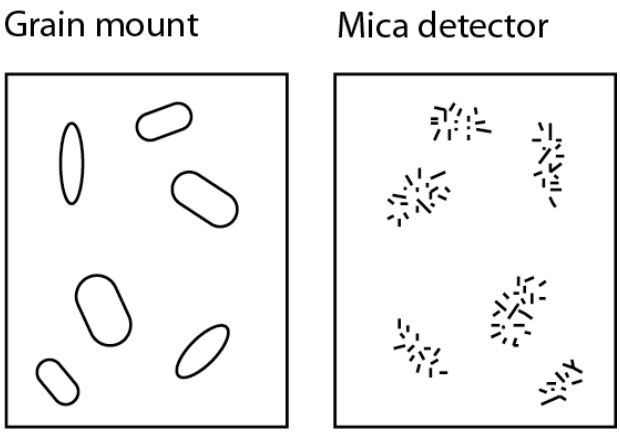

Fig. 17. Schematic illustration of a sample-detector pair. The prints in the mica represent a mirror image of the apatites in the grain mount.

Following conventions, only grains oriented parallel to the crystallographic *c*-axis were analysed. These grains are easily recognizable in reflected light because of their parallel etch pits. Grains with countable surface areas big enough to accommodate at least 25 squares were taken as qualified for analysis. The number of squares used during counting of individual grains was recorded and an equal number of squares were counted on the print. Twenty grains were counted in each sample and in nine of ten age standards. For samples containing big grains, several non-overlapping grids were counted within the same grain.

Fission tracks were identified and separated from dislocations and other features based on the following criteria (presented by Fleischer & Price, 1964b): 1) Etched fission tracks are always straight. Dislocations commonly appear as bent or spiral-shaped track-like features. 2) The length of fission tracks is limited. Abnormally long features are almost certainly not tracks and should thus be excluded during the counting procedure. 3) Fission tracks should not display a preferred orientation. Arrays of parallel features are typically made up of dislocations rather than tracks. Prior to counting, the quality of individual grains was assessed and grains that were found to contain dislocations were excluded. Truncated dislocations are in some cases impossible to distinguish from fission tracks and may cause erroneous results if counted. Strongly fractured and zoned grains, as well as grains with obvious inclusions, were omitted whenever possible.

5.3.4 Zeta calibration procedure

According to the recommendations of the IUGS Subcommission on Geochronology (Hurford, 1990), a minimum of five analyses should be implemented during the zeta calibration procedure. At least two different age standards should be included, and the mounts on which analyses are performed should represent several different irradiations. In the current study five grain mounts of Durango apatite and five mounts of Fish Canyon Tuff were analysed in order to establish a personal zeta value. A zeta value and a corresponding standard deviation were calculated for each analysis, using the software TrackKey (Dunkl, 2002). The final zeta was calculated as the weighted mean of the individual values, using the open source Meanzeta program by Mark Brandon.

5.3.5 Calculation of fission track ages

The TrackKey software (Dunkl, 2002) was used to calculate fission track ages. In addition to the arithmetic mean age, a pooled age and a central age is reported. The central age is the weighted mean of the log normal distribution of individual grain ages and will be used throughout this study. A chi-square and a *p*-value are calculated from the density parameters for single grains.

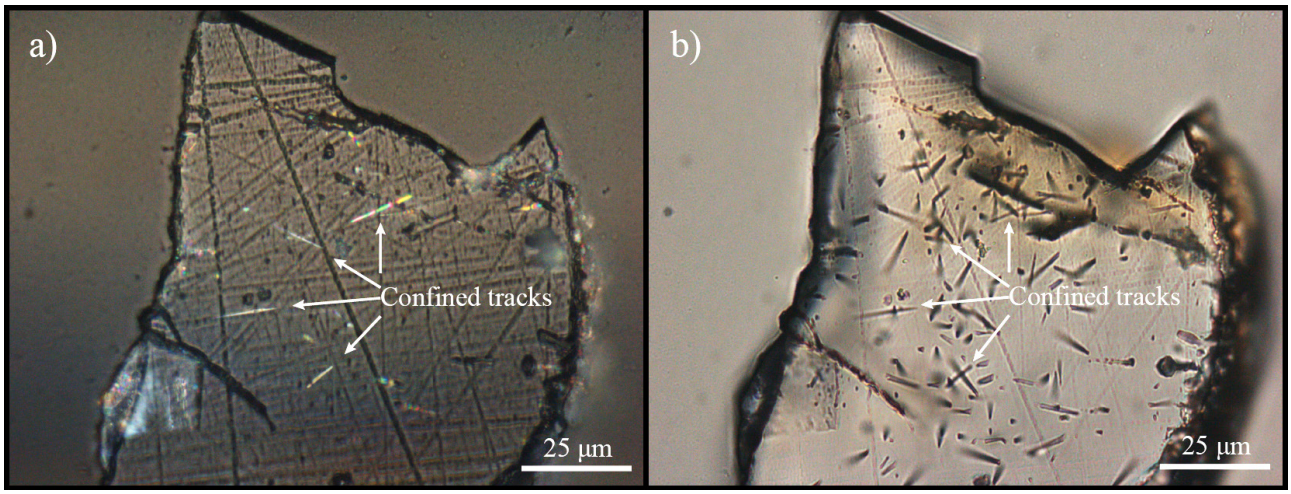

Fig. 18. Recognition of horizontally confined tracks: **a)** Reflected light: Confined tracks are easily identified because of their bright appearances. Four tracks are readily evident; **b)** Transmitted light: Confined tracks are simultaneously focused on both ends. The track in the upper left portion of the grain appears to be shallowly dipping, since it is not perfectly focused along its entire length. Conduit tracks are visible for all four confined tracks. The uppermost track is dissected by a fracture and is therefore classified as a TINCLE.

5.3.6 Track length and D_{par} measurements

All measurements were performed with a magnification of 2000 x. Fission track length data were obtained by measuring horizontally confined tracks with the LED. These tracks have a bright and easily recognizable appearance in reflected light (Fig. 18a) and are simultaneously focused along their entire lengths (Fig. 18b). Ideally, 100 track lengths should be measured for each sample in order to produce a statistically sound and robust thermal model (e.g. Donelick et al., 2005). The crystallographic *c*-axis was marked for each analysed grain (Fig. 19), and the angle between the *c*-axis and the measured track was recorded. Some TINCLEs are unusually resistant towards annealing and may drive the length distribution towards a greater mean (Jonckheere & Wagner, 2000). Following the recommendation of Barbarand et al. (2003b), only TINT-type tracks were therefore included in this study. As a consequence of the etching anisotropy in apatite (cf. section 3.1.2), fission track etch pits most commonly exhibit elliptical shapes and are aligned with the maximum diameter parallel to the *c*-axis. Five D_{par} values and their corresponding D_{perp} values (i.e. widths of etch pits perpendicular to the *c*-axis) were measured for each counted grain and three additional values were attained for every grain that had been selected for track length measurements.

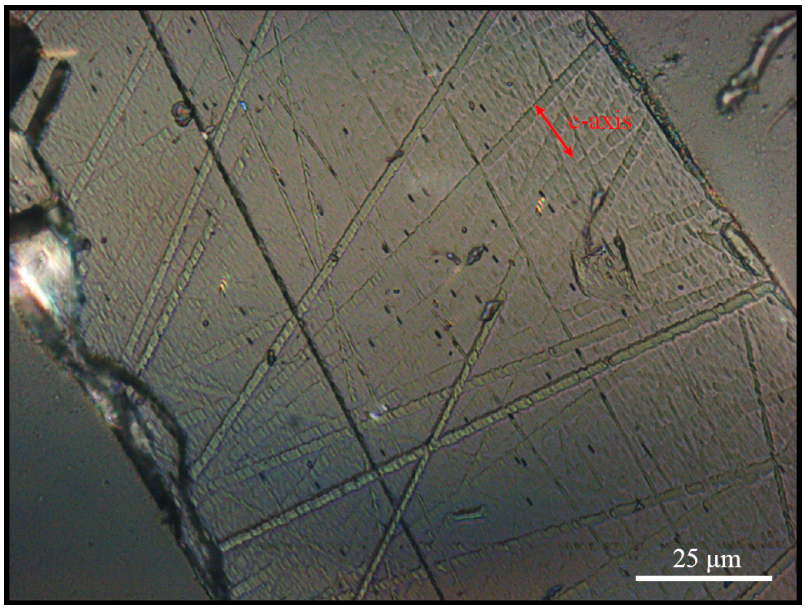

Fig. 19. Etch pits aligned parallel to the crystallographic c-axis (red line).

5.4 (U-Th)/He analysis

Four samples were selected for (U-Th)/He analysis, two from the Osa profile and two from the Kjeåsen profile. In order to reveal important aspects regarding the low-temperature cooling history over a relatively large elevation span, one sea level sample and one sample from Hardangervidda was included from each of the profiles. In addition to sampling location, general apatite quality was taken into consideration during the selection process. Sample properties were assessed by studying mineral inclusion densities and zoning characteristics in the fission track grain mounts.

(U-Th)/He analysis was performed at the Geoscience Centre at the University of Göttingen, Germany, during July and August, 2012. Prior to apatite selection, crystals from each of the samples were carefully studied under binocular and petrographic microscopes in order to reveal the presence of problematic features, such as mineral inclusions and cracks. Three grains with good crystal morphologies were hand-picked from each sample (grain selection was performed by A. Ksienzyk). All selected crystals appeared to be free of inclusions and microfractures. The length and width of each apatite was measured and the grains were packed in separate platinum capsules. He-degassing was performed under vacuum in a sealed furnace by heating the sample to ca. 870 °C for 20 min with an infrared diode laser. A hot blank was established prior to every analysis and measurements on the Durango apatite age standard were performed regularly for control. Subsequent to degassing, the obtained ^{4}He was spiked with a known amount of 99+% ^{3}He and purified with a

SAES Ti-Zr getter at 450 °C. The isotopic ratio analysis was performed with a Hiden triple-filter quadrupole mass spectrometer, equipped with an ion counting detector. Re-extraction of He was executed in order to quantify excess gas derived from mineral inclusions within the apatite. Following re-extraction, the platinum capsules were retrieved from the vacuum chamber. Each apatite grain was then dissolved in 2% nitric acid and spiked with a solution containing known concentrations of ^{235}U and ^{230}Th. The isotopic ratios in the solution were measured by a Perkin Elmer Elan DRC ICP-MS with an APEX micro flow nebuliser, and the ^{238}U, ^{232}Th and Sm contents were calculated from the obtained ratios. Alpha-ejection correction was performed for all the calculated (U-Th)/He ages, following the recommendation of Farley et al. (1996).

5.5 Thermal history modelling strategy

Thermal history modelling was performed with the software HeFTy 1.7.5 (Ketcham, 2005). Single grain fission track ages, track length measurements and etch pit diameters function as basic parameters for modelling. The HeFTy program develops a forward model to predict the outcome of a given thermal history for an assumed starting condition (e.g. regarding apatite annealing resistance) and utilizes this model in an inverse sense to find an appropriate time-temperature-path based on the ending conditions (i.e. the calculated age and the observed track length distribution). The annealing model of Ketcham et al. (2007b) was applied as a basis for estimation of kinetic behaviour. D_{par} was selected as kinetic parameter. The confined track lengths were corrected by *c*-axis projection, as proposed by Ketcham et al. (2007a). D_{par} values were used to calculate a default initial mean track length and the length reduction in the standard was set to 0.893.

From 32 samples analysed by the fission track method, 11 were selected for thermal history modelling. 20 counted grains, 100 track length measurements and a sufficient number of D_{par} values had been obtained from all except for one of these samples. The Monte Carlo search method with random subsegment spacing was employed to identify possible time-temperature paths. While establishing an inverse model, the HeFTy program tests a large number of cooling paths against the input data. From all possible cooling paths that were identified, 100 good time-temperature paths and a weighted mean curve were determined for each sample, with uncertainties given as 1σ error.

6. RESULTS

The following subchapters report the results obtained from apatite fission track analysis of 32 samples and (U-Th)/He dating of 4 samples from the inner Hardangerfjord. Detailed studies of fracture patterns have been undertaken in order to create a structural framework that may aid the interpretation of the thermochronological data. The results of the structural investigations are therefore presented first.

6.1. Brittle structures

Structural complexity characterizes the inner Hardangerfjord region. The field area explored in the present study extends across several major linear features, including a number of fjords and deeply incised glacial valleys. Several of the lineaments that have been identified from aerial photographs have been found to coincide with zones of high fracture density observed in the field. The nature of the large-scale, densely spaced fractures in the region is largely unknown and has received limited attention in the past. It is not known whether the structures record displacement and when and how movement may have occurred. Because of the general absence of marker horizons and shear sense indicators these issues are not readily addressed. Furthermore, the steep terrain that characterizes the area makes detailed observations and recognition of brecciated material or fault gouge difficult. In order to avoid premature assumptions about possible displacements while presenting the results, all large-scale brittle structures are consistently referred to as fractures or lineaments rather than faults. Because the sensitivity ranges of the apatite fission track and (U-Th)/He systems are well below the temperatures associated with the brittle-ductile transition for rock forming minerals, only brittle structures are included in the present contribution. Folds and ductile shear sense indicators may reveal interesting aspects regarding the Precambrian and Caledonian geological evolution in particular, but pre-date thermochronological ages by several hundred Ma to > 1.5 Ga (Sigmond, 1998) and are not regarded significant for the results obtained in the current study.

Two fracture sets appear to be particularly well-represented in the inner regions of the Hardangerfjord; the first set running N-S and the second set trending NE-SW. Additional E-W- and NW-SE-trending structures are evident locally. In the current study the most prominent joint directions have been recorded at most sample locations. In addition, the

orientation of particularly pronounced fracture zones has been measured on several sites in the field area. Individual orientations are listed in Appendix A together with the sample information and a stereographic plot of all measured brittle structures is presented in Fig. 20a. In the following sections the field area is subdivided into areal domains (Fig. 20b) in order to facilitate the recognition of the most pronounced fracture systems and the detection of local differences in structural patterns. Special emphasis is put on the areas in which vertical profiles were sampled, and a map of lineaments is presented from each of these areas. The lineament maps have been produced by careful study of aerial photographs, partially in combination with field observations. Some of the identified lineaments coincide with river trajectories. Although rivers generally follow weak zones in the substrate, it is not given that all rivers in the area are located on sites of major fracture zones. Therefore, river trajectories have been treated with caution and are only indicated where they make up clearly defined lineaments that parallel other structures in the region or continue across valleys. However, the fracture pattern in the inner Hardangerfjord region is found to correspond well with the orientation of fjords and valleys, and many rivers appear to coincide with recognized fractures. All stereographic plots presented in the following sections have been drawn in Stereonet 7 by Allmendinger et al. (2012). Aerial photographs have been obtained from Norge i Bilder and digital elevation models are taken from Norgeskart.

a)

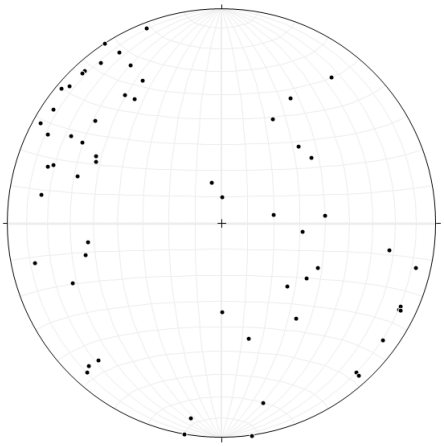

b)

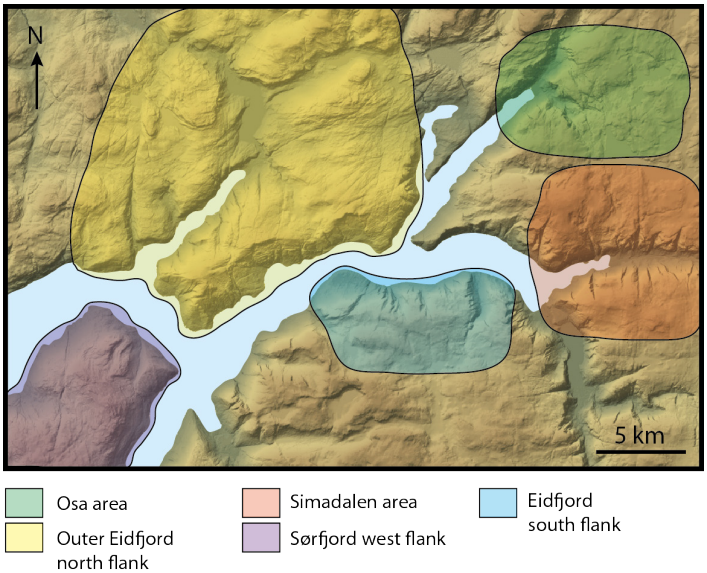

Fig. 20. a) Equal area lower hemisphere stereographic plot showing the poles to of all measured joints in the inner Hardangerfjord region. Moderately to steeply SE-dipping structures are particularly abundant. An additional set of N-S- to NE-SW-trending, mostly W-NW-dipping fractures is found throughout the area. **b)** Overview map showing the areal domains in which structural data have been collected.

6.1.1 The Osa area

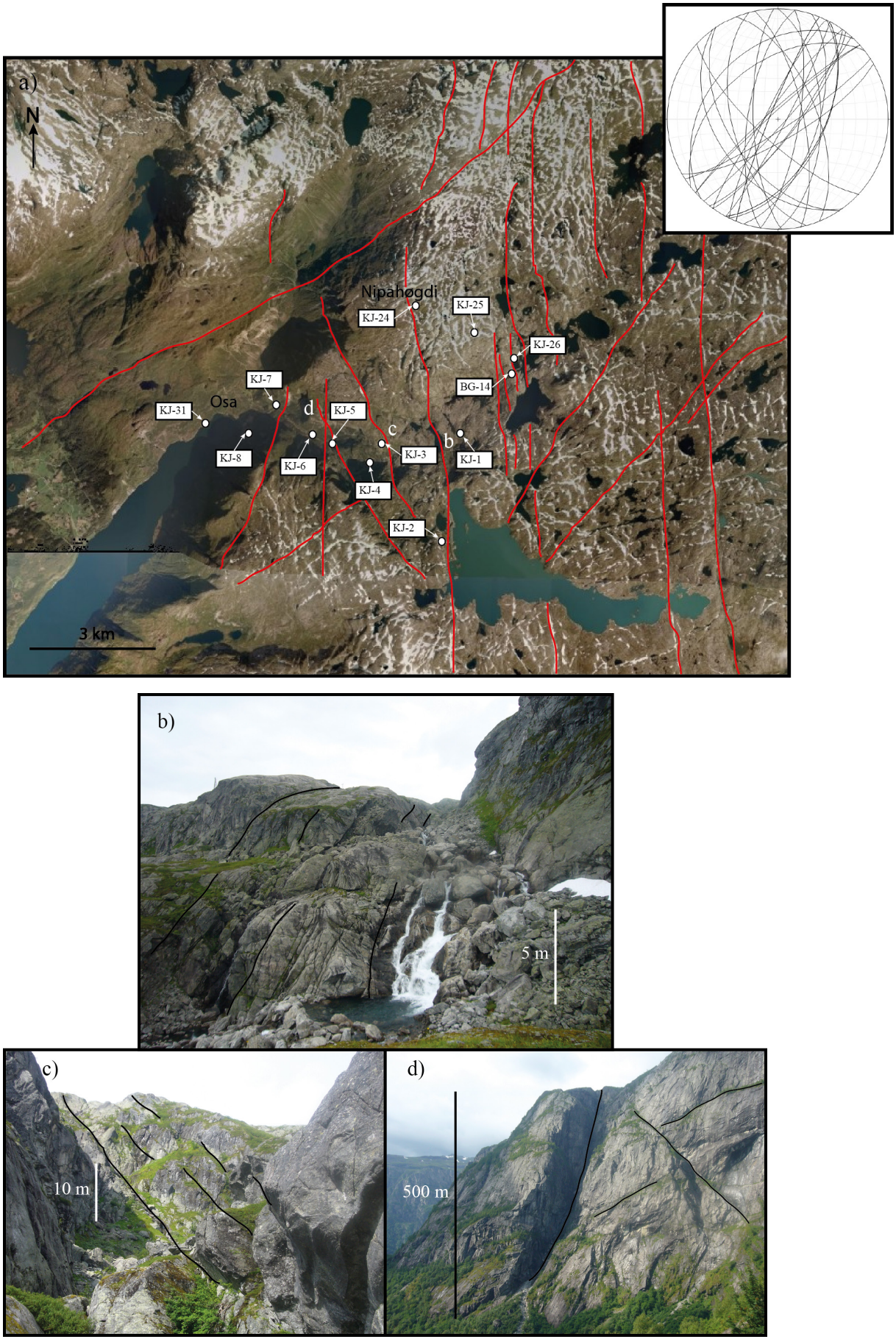

Fig. 21. (Previous page) **a)** Aerial photograph of Osa in the northernmost part of the field area. Lineaments are marked by red lines. The area is dissected by numerous fractures, but only the most obvious lineaments are included here. Three main fracture sets are apparent: 1) N-S-trending; 2) NE-SW-trending; and 3) NNW-SSE-trending. The fracture zones that are shown in b, c and d are indicated by letters. **b)** Zone with densely spaced SW-dipping joints (orientation: 146/53) located between the sampling localities of KJ-1 and KJ-3. Similarly oriented joints are apparent over an extended distance perpendicular to the strike, but the density is particularly high in vicinity to the river portrayed in the photograph. View towards the NNW. **c)** E-dipping fractures (orientation: 000/ 58) that coincide with a major topographical depression. Photograph is taken directly to the E of the sampling location of KJ-3. View towards the NNW. **d)** Large-scale fracture zone with a steep dip towards the SE. Traces of additional brittle structures with different orientations are apparent on the steep cliff face. Measurements of fracture orientation could not be obtained. View towards the WNW from the road near the sampling site of KJ-4.

The lineament density is particularly high around Osa. A variety of fracture orientations are evident, reflecting the complexity of the structural geology in this area. From the lineament map and the stereographic plot in Fig.22a, a limited number of main fracture sets can be determined. N-S- trending lineaments are predominant in the eastern part of the area. Densely spaced fractures belonging to this set are evident both towards Hardangerjøkulen in the east and Eidfjord in the south. The large-scale N-S-trending lineaments correspond to a set of steeply W- and locally E-dipping joints that are apparent in the field. In the northernmost part of the area, two subvertical, oppositely dipping NNE-SSW-trending fracture systems are dominant. An additional regional set of steeply dipping, NE-SW-trending structures roughly parallels the trend of the Osafjord. Directly to the SE of the fjord this fracture set is mainly represented by SE-dipping structures. NW-dipping structures are present, but less abundant. Intermediately NW-dipping fractures occur locally and may represent a conjugate array to the pervasive SE-dipping set. A number of intermediately to steeply dipping, NNW-SSE-trending structures extend across the valley between Nipahøgdi and Kyrelvfjellet (Fig. 21b), where the majority of the samples in the study were collected.

6.1.2 The Simadalen area

The area around Simadalen is dissected by a number of major N-S-trending structures, which are evident both on the aerial photograph and the stereographic plot in Fig. 22a. These structures belong to a regional set of relatively large subvertical fracture zones. Individual lineaments can be traced from the Simadalen area northwards to Osa (c.f. Fig. 21a) and probably even over significantly greater distances. Subvertical, both E- and W-dipping joints are dominant in

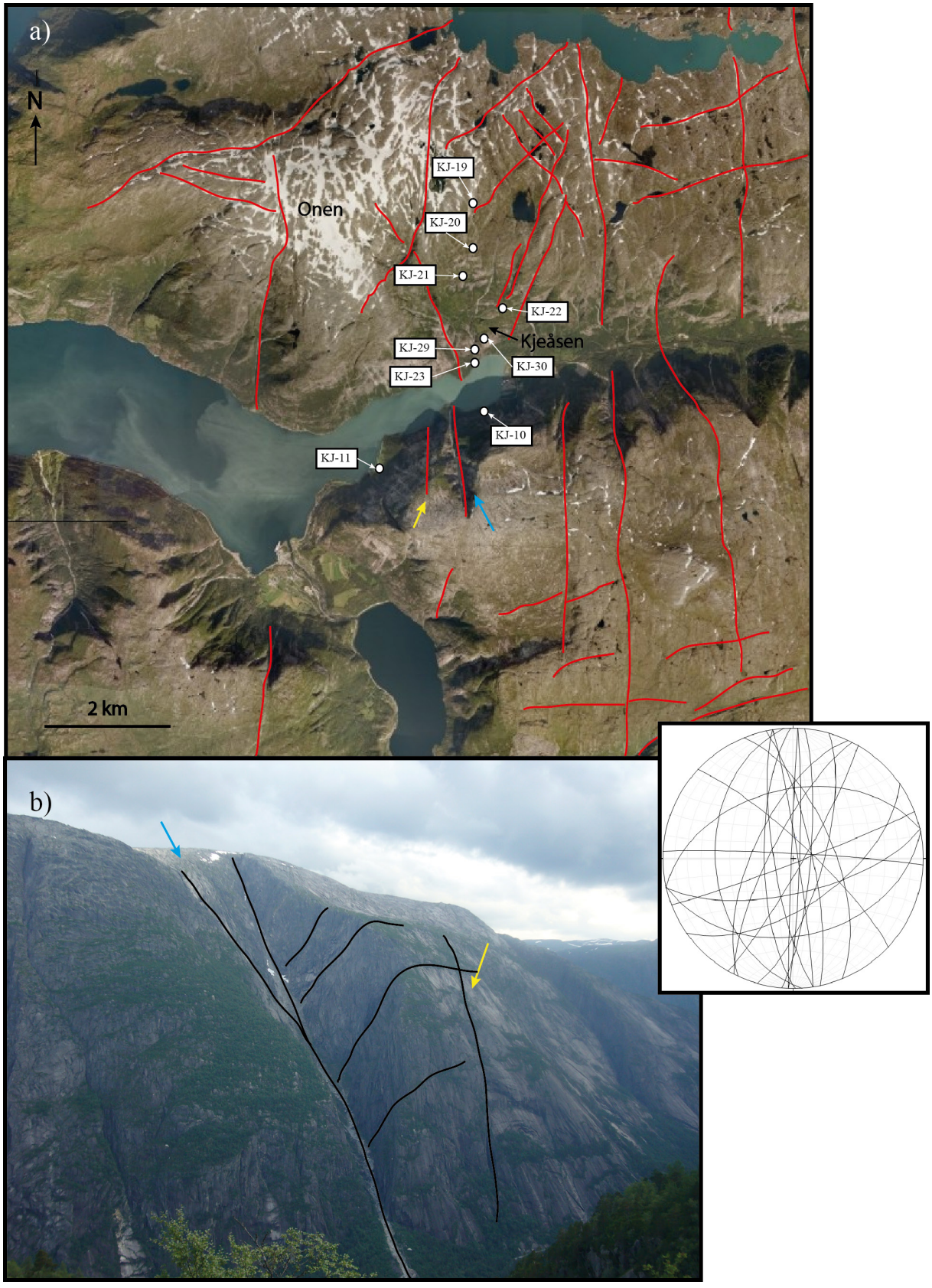
a)
N
Onen
KJ-19
KJ-20
KJ-21
KJ-22
Kjeåsen
KJ-29
KJ-30
KJ-23
KJ-10
KJ-11
2 km
b)

Fig. 22. (Previous page) **a)** Aerial photograph of Simadalen and surrounding areas. Lineaments are marked by red lines. As in the Osa area to the north, N-S-trending structures are particularly conspicuous. Due to the very limited topographical effect on the map-view traces, the majority of the N-S-trending fractures in the area appear to be subvertical or steeply dipping. This assessment is confirmed by the field measurements that are displayed in the stereographic plot. A possible W-dipping structure crosses Simadalen in the right part of the image. Additional fracture systems include a NE-SW to ENE-WSW-trending set, with individual structures that parallel the Simadalsfjord, and a second set consisting of structures that vary in orientation between W-E and WNW-ESE. NW-SE-trending lineaments are abundant in the area directly to the north of Kjeavatnet (i.e. northeast of KJ-19). Note the location of the lineaments that are portrayed in b (blue and yellow arrows). **b)** Steeply dipping to subvertical, roughly N-S-trending fracture zones in the southern flank of Simadalen (blue and yellow arrows). Note the array of moderately to steeply SE-dipping structures that are evident in the depression associated with the major fracture zone (blue arrow). View towards the SSW from the Hardangervidda plateau north of Kjeåsen.

the mountains north of Kjeåsen, from which the majority of the measurements presented in the stereographic plot in Fig. 22a were obtained. Although not visible on the aerial photograph, numerous SE-dipping fractures clearly dissect the southeastern flank of Simadalen (Fig. 22b). Similarly oriented NE-SW-trending joints are present on the northwestern side of the valley, and several lineaments that are evident on the aerial photograph may possibly belong to the same fracture system. Fig. 22a reveals the presence of additional W-E to WNW-ESE-trending lineaments that clearly parallel the trend of the Eidfjord, suggesting that the fjord may coincide with a major fracture zone.

6.1.3 The Eidfjord south flank

Two main lineament populations are evident in the mountainous area south of Bu (Fig. 23a). Subvertical NW-SE- to NNW-SSE-trending fractures are mainly recognized around Vatnasetenuten (Fig. 23b), while NE-SW-trending structures are abundant throughout the area. Field observations from the eastern side of Vatnasetenuten across the valley to Skoddedalsfjellet (central right part of image) have revealed a general pattern of SE-dipping joints and fracture zones (Fig. 23c). Most of the measurements displayed in the stereographic plot in Fig. 23a were obtained from this area, and the SE-dipping fractures may therefore be slightly over-represented with respect to structures with other orientations. The structural pattern that predominates in the outer portions of the Eidfjord south flank deviates from that observed in the Osa and Simadalen areas in that N-S-trending lineaments are not as readily evident. An ENE-WSW-trending lineament is found to cross the vertical profile directly to the southeast of Bu. This structure has a similar orientation to one of the dominant fracture sets in the Simadalen area.

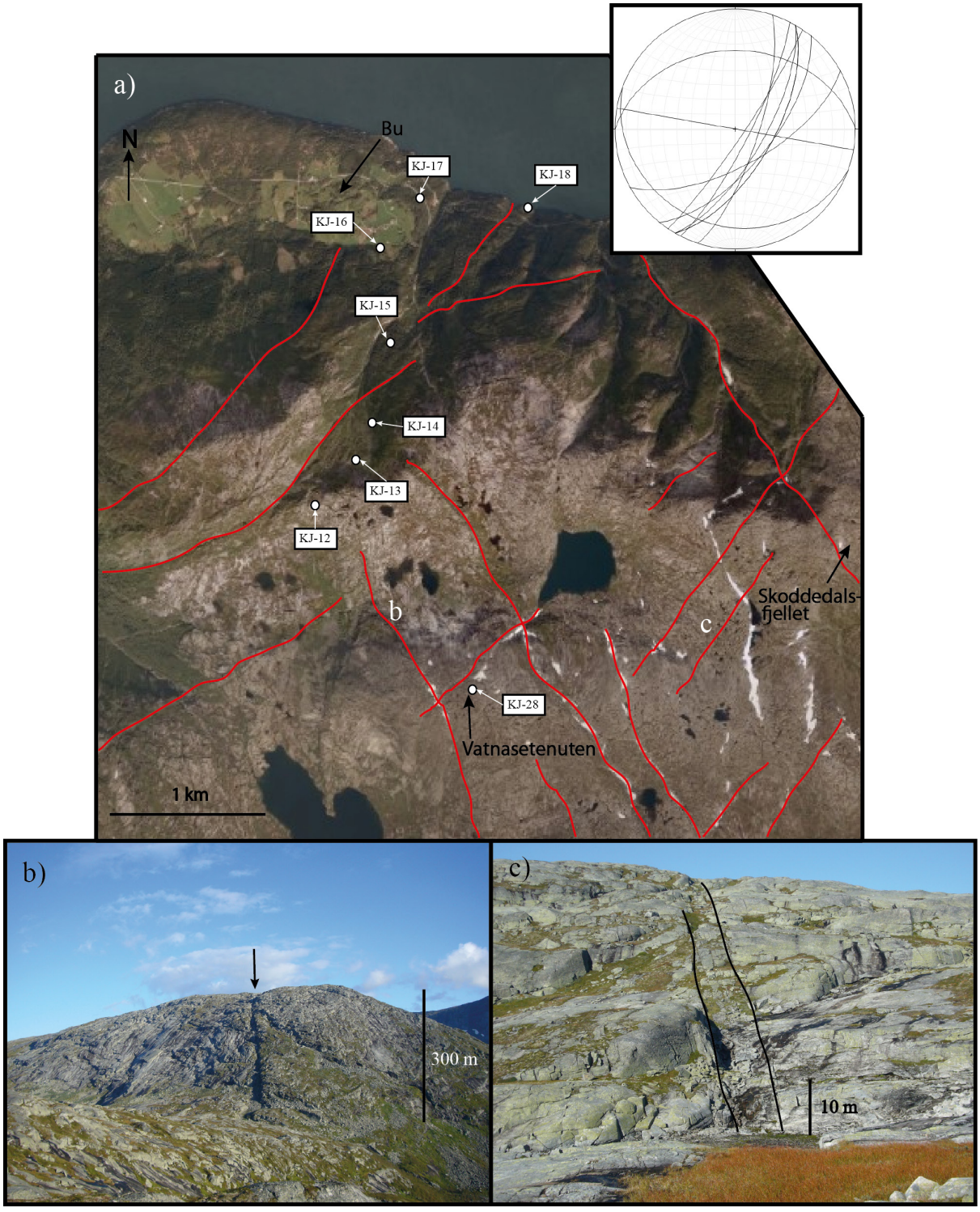

Fig. 23. **a)** Aerial photograph of the Bu area on the southern side of the Eidfjord. Lineaments are marked by red lines. Two fracture orientations are dominant: NW-SE and NE-SW. The fracture zones portrayed in b and c are indicated by letters. **b)** Large-scale NNW-SSE-trending fracture that dissects Vatnasetenuten to the west of KJ-28. No measurements of fracture orientation could be obtained. View towards the SSE from the sampling location of KJ-12. **c)** SE-dipping fracture zone (orientation: 030/70) between the summits of Vatnasetenuten and Skoddedalsfjellet. Similarly oriented joints, although less densely spaced, are apparent over great distances. View towards the NE from the eastern flank of Vatnasetenuten.

6.1.4 The outer Eidfjord north flank

NE-SW-trending joints with steep, southeasterly dips are dominant on the northern flank of Eidfjorden in the Granvin and outer Ulvik areas. A second set of subvertical, WNW-dipping fractures may correspond to the orientation of the NNE-SSW-trending Sørfjorden Fault to the south. Joint measurements from the outer portion of the Eidfjord north flank are presented in Fig. 24a.

6.1.5 The Sørfjord west flank

Four main fracture sets are recorded in the Sørfjord west block (Fig. 24b), including a subvertical set of SE-dipping joints that is pervasive throughout the field area and a well-represented W- to NW-dipping set that may possibly relate to the Sørfjord Fault. A secondary set of roughly E-W-trending joints with shallow dips towards the S is observed in the Jåstad area. NW-SE-trending joints with intermediate dips towards the SW are not abundant elsewhere in the field area, but are pronounced on the western flank of the Sørfjord.

a) b)

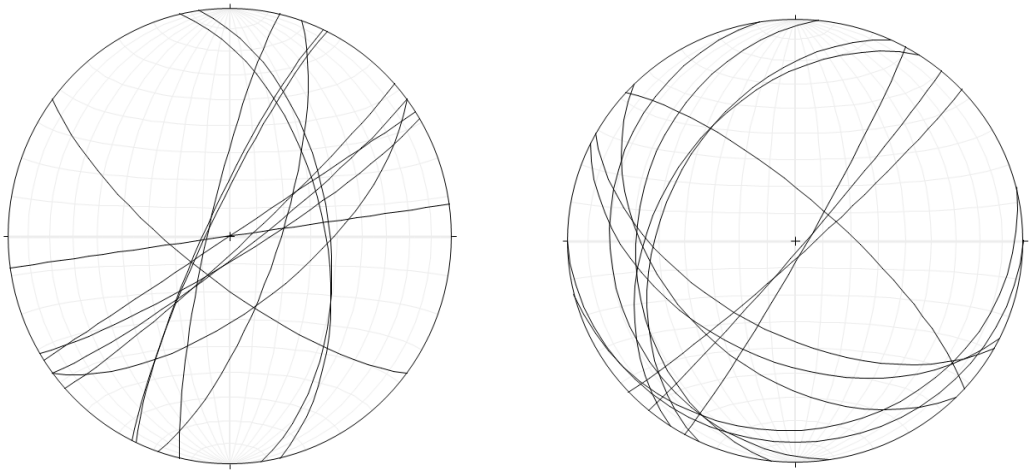

Fig. 24. a) Measurements from joints in the Granvin and outer Ulvik areas north of the Eidfjord. Subvertical, SE-dipping fractures are common. NNW-SSE-trending and NNE-SSW-trending sets are represented by fewer measurements. **b)** Joint measurements obtained west of the Sørfjord. The main fracture sets are NE-SW-, WNW-ESE-, NNE-SSW- and E-W-trending.

6.2 Apatite description

6.2.1 Apatite yields

Precambrian lithologies derived from the autochthonous basement in the inner Hardangerfjord region are generally rich in apatite (Fig. 25). Sufficient grains were obtained from all gneissic rocks and most granites sampled as part of the current study. The only low-grade metasedimentary lithology included in the study, sample KJ-24, yielded very few apatite grains, but still a sufficient amount for analysis. Four of the samples derived from the Eidfjord granite in Simadalen, KJ-10, KJ-23, KJ, 29 and KJ-30, were found to contain considerable amounts of fluorite. Fluorite is quite common in granites from southern Norway and represents a challenge during mineral separation, since it is difficult to isolated from apatite through standard heavy liquid and magnetic separation procedures. Hand-picking of apatite crystals was attempted in order to acquire a sufficient amount of grains, but was ultimately unsuccessful.

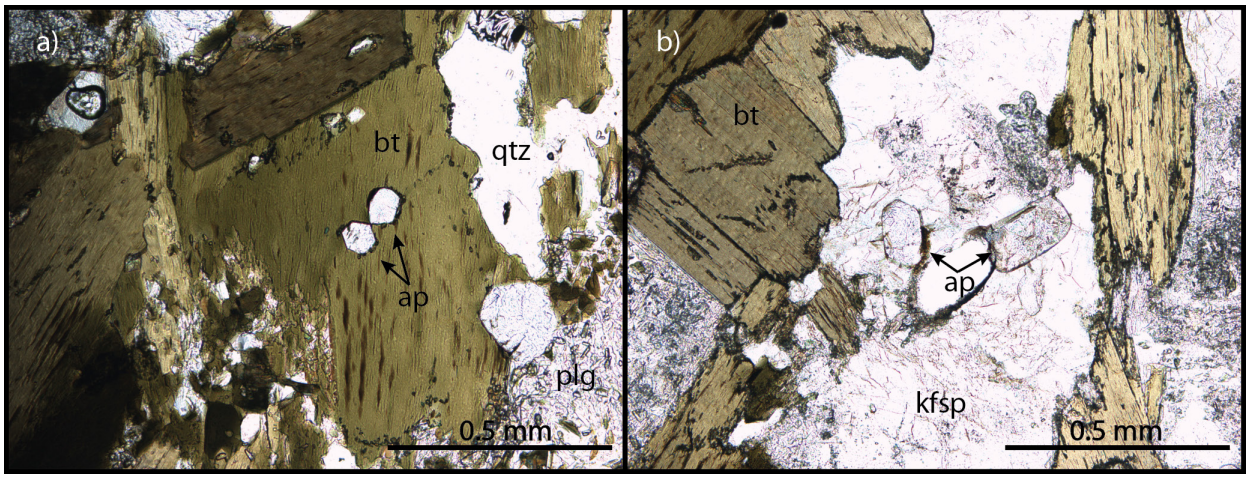

Fig. 25. Thin sections from two of the analysed samples (plane polarised light): a) Apatite grains situated within biotite in granodioritic gneiss (KJ-3). The left apatite is oriented with the c-axis perpendicular to the plain of view and displays a characteristic hexagonal cross-section; **b)** Ideomorphic to slightly rounded apatites in granite (KJ-11). Apatite grains reside within K-feldspar.

6.2.2 Grain quality

The grain quality of the samples analysed in the current study is highly variable (Fig. 26). Most samples contain relatively large apatite crystals. Euhedral, rounded and elongated grains are common, although broken fragments of large crystals are abundant in some samples. A number of samples, most notably KJ-12 and KJ-15, contain grains that display a brown discolouration, which is frequently accompanied by densely spaced, parallel, black lines (Fig.

26a). This particular trait is extremely problematic during counting, since fission tracks are barely visible through the disrupted surface. Another major problem in the analysed grains is zoning, which is a very common feature in apatites obtained from southern Norway. Apatites derived from gneissic lithologies generally display a particularly pronounced concentric zoning. U-rich cores are most abundant, although a few samples predominantly contain grains with U-rich rims. Some U-rich mineral inclusions (e.g. zircon and monazite) are present in most samples, but generally do not affect the analysis. Abundant mineral inclusions are found in some samples. Normally, these inclusions are easily recognizable and can be avoided during counting. Poor quality grains with weakened crystal lattices have a tendency to fracture during mount preparation. Cracks limit the countable surfaces of the grains, and strongly fractured and scratched apatites are therefore difficult to analyse. A restricted number of cracked grains are found in most mounts. These grains can be excluded from the analysis, given that the mount contains a sufficient number of intact apatites. In a few samples the damage caused by cracks and scratches is extensive enough to potentially affect the counting results (see Table 1). The majority of analysed samples from the inner Hardangerfjord area are U-poor. Low-U-concentrations are generally associated with low track densities, which severely limit the number of confined tracks available for track length measurements. 100 confined track-in-tracks should be measured in order to fulfil the criterion for thermal history modelling. This number of measurements is rarely possible to obtain for samples with U-concentrations below 15 ppm. Zoned grains, which may contain sections of particularly high track density, are normally avoided during the counting procedure. As a result, the U-concentration estimated from the induced track density does not necessarily give a correct impression of the typical U-content of grains in the sample. Table 1 displays the general quality and characteristics of the individual samples, listed according to sampling area and affiliation to a vertical profile. The grain quality of a representative range of samples is documented in Fig. 26.

Table 1. Apatite quality for individual samples.

Sample no.	General grain quality	Zoning	Mineral inclusions	Cracks and scratches	U-concentration [ppm]
Vertical profiles					
Osa					
KJ-1	Good	X			8.0
KJ-3	Good	X			5.5
KJ-4	Intermediate		X		7.2
KJ-5	Good				8.7
KJ-6	Intermediate	X	X		4.4
KJ-7	Poor		X		4.1
KJ-8	Poor	X	X		10.3
BG-14	Intermediate	X	X	X	10.6
KJ-24	Poor		X		0.7
KJ-25	Good	X			10.8
KJ-26	Good	X			9.4
KJ-31	Poor	X		X	5.2
Bu					
KJ-12	Poor			X	9.4
KJ-13	Good				24.1
KJ-14	Intermediate	X			31.9
KJ-15	Poor	X			13.6
KJ-16	Good	X			8.7
KJ-17	Intermediate	X			8.6
KJ-18	Intermediate	X			13.4
KJ-28	Poor				19.3
Kjeåsen					
KJ-11	Good	X			10.3
KJ-19	Good	X			10.6
KJ-20	Intermediate	X	X		10.5
KJ-21	Intermediate	X	X		14.8
KJ-22	Good	X			11.5
Additional samples					
Sørfjord west flank					
BG-27	Intermediate	X			17.7
BG-53	Good				4.5
Inner Eidfjord south flank					
KJ-9	Intermediate	X			8.5
Outer Eidfjord north flank					
KJ-27	Intermediate				17.0
BG-16	Poor			X	18.7
BG-26	Intermediate	X			21.4
BG-13	Good				9.8

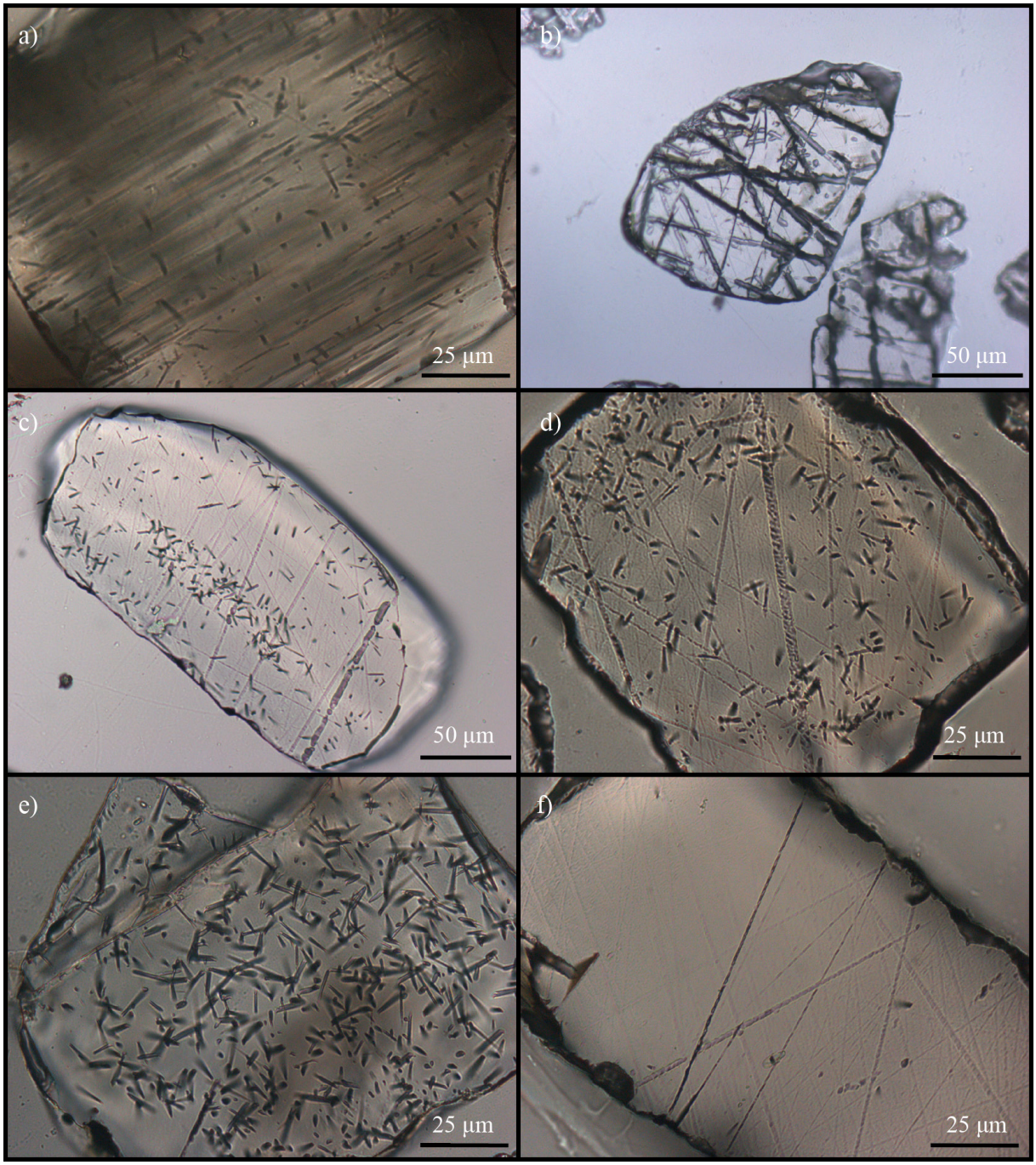

Fig. 26. Photomicrographs of a selection of apatites from the analysed samples: **a)** Poor quality apatite grain typical of KJ-15 from Bu. The exposed crystal surface is obscured by a set of parallel dark lines. Similar grains occur in several samples. **b)** Strongly scratched and fractured grains common in BG-16 from Skår. Fission tracks are not readily evident; **c)** Concentric zoning of apatite from KJ-19, Kjeavatnet. This particular grain is characterized by a U-rich core and a rim with a slightly elevated U-concentration; **d)** Zoning in apatite from KJ-14, Bu, evident by a core of relatively low track density surrounded by a concentric zone of higher track density; **e)** Relatively high track density typical of KJ-28, Vatnasetenuten; **f)** Low U-concentration reflected by a very low track density (only three tracks evident), KJ-24 from Nipahøgdi.

6.3 Pre-analytical calculations and calibrations

6.3.1 Track density gradients

Three IRMM-540R standard glass mica detectors were counted for each of the three irradiation batches included in the study and track density gradients were obtained by applying linear regression to the ρ_d values calculated for each standard glass (Fig. 27). The calculated ρ_d values range from 16.66 x 10^5 cm^{-2} to 21.26 x 10^5 cm^{-2} and a decreasing gradient with distance from the neutron source is found for all irradiations. A complete list of the container positions of individual samples and their respective ρ_d values is enclosed in Appendix B.

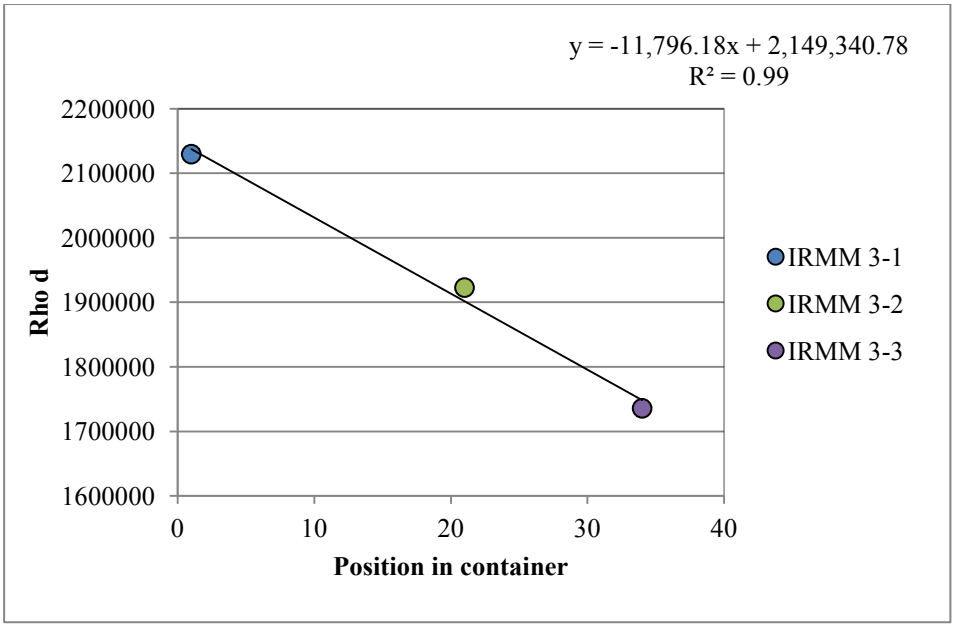

Fig. 27. ρ_d gradient for the NoB-017 irradiation tube, in which all KJ samples were included. The equation used for the calculation of individual ρ_d values is displayed in the upper right corner. IRMM 3-1 has the highest ρ_d and was located closest to the neutron source during irradiation.

6.3.2 Zeta calibration

A personal zeta value of 251.61 ± 7.02 was calculated as the weighted mean of ten analyses on Durango and Fish Canyon tuff standards. The calibration results obtained from individual age standards are displayed in Fig. 28 and details regarding each calculation are listed in Table 2.

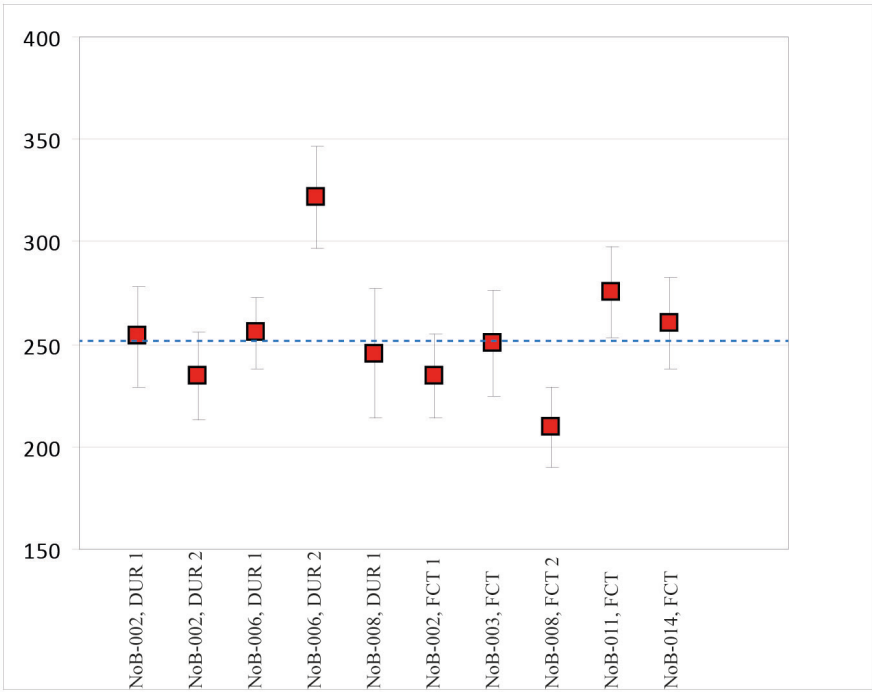

Fig. 28. Individual zeta values with 1σ error bars. The stippled blue line represents the weighted mean zeta. All calculated values except for NoB-006, DUR 2 and NoB-008, FCT 2 overlap when considering their errors. NoB-006, DUR 2 is less weighted than the remaining analyses due to its comparatively high zeta value.

Table 2. Zeta calibration results for AFT age standard analysis.

Irradiation	Standard no.	Number of crystals	Spontaneous		Induced		Dosimeter		Zeta
			ρs (10^5)	Ns	ρi (10^5)	Ni	ρd (10^5)	Nd	(Ma ± 1σ)
NoB-002	DUR 1	20	1.623	127	10.990	860	16.797	9223	253.7 ± 24.6
NoB-002	DUR 2	20	1.623	146	10.159	914	16.827	9223	234.3 ± 21.3
NoB-006	DUR 1	20	2.383	261	20.909	2290	21.617	5811	255.5 ± 17.5
NoB-006	DUR 2	20	2.492	195	27.348	2140	21.460	5811	322.0 ± 25.0
NoB-008	DUR 1	15	1.412	70	11.280	559	20.495	8071	245.3 ± 31.5
NoB-002	FCT 1	20	2.413	157	16.970	1104	16.767	9223	234.5 ± 20.6
NoB-003	FCT	20	2.479	109	20.081	883	18.088	9944	250.5 ± 25.9
NoB-008	FCT 2	20	2.196	136	16.679	1033	20.258	8071	209.6 ± 19.6
NoB-011	FCT	20	2.126	185	17.549	1527	16.755	6971	275.4 ± 22.2
NoB-014	FCT	20	2.183	173	14.791	1172	14.548	8054	260.4 ± 21.9
							Weighted mean zeta		**251.6 ± 7.0**

i) All age standards were analysed by the external detector method (c.f. sections 3.3.1 and 3.3.2), applying a 4π/2π geometry correction factor of 0.5.

ii) The following ages were adopted in the calculations:

Durango (Dur) = 31.4 ± 0.5 Ma (McDowell & Keizer, 1977), Fish Canyon Tuff (FCT) = 27.9 ± 0.5 (Hurford & Hammerschmidt, 1985).

iii) Individual zeta values are weighted according to the magnitude of their errors and their disparity with respect to the remaining values.

6.4 Apatite fission track analysis

The AFT ages obtained in the current study range from 97 to 221 Ma, with a majority of ages between 120 and 170 Ma. Except for the Late Triassic KJ-24 and the Late Cretaceous BG-16 all ages are Jurassic or early Cretaceous. The youngest sample, BG-16 (97 Ma), is derived from the Precambrian basement at Skår northwest of Granvin and is the only sample collected from the hangingwall of the Hardangerfjord Shear Zone. KJ-24, which is derived from the parautochthonous décollement zone at Hardangervidda north of Osa, exhibits the oldest age (221 Ma).

Single grain ages for all samples are displayed in radial plots in Appendix C. The span in grain ages within individual samples is typically between 80 and 100 Myr. As expected, the youngest ages are displayed by grains within the young samples BG-16, BG-26 and KJ-8, and cluster around 80 Ma. KJ-24 exhibit single grain ages as old as 445 and 860 Ma. Possible reasons for these anomalously old ages are discussed in section 8.1.2.

Mean track lengths (MTL) were measured for eleven evenly distributed samples and display a limited range of values between 10.41 ± 0.25 μm and 11.66 ± 0.23 μm. Except for BG-26, for which only 63 horizontally confined tracks were recognized, all samples selected for track length measurements fulfil the criterion of 100 measured track-in-tracks.

Customary D_{par} measurements were performed for all samples, resulting in mean values between 1.18 and 1.69. The limited range of attained D_{par} values suggests that all samples have similar chemical compositions. Their ages are thus regarded as comparable. Most of the analysed apatites from the inner Hardangerfjord region display rather low D_{par} values, which are believed to reflect near end-member fluorapatite compositions. The requirement of five measured D_{par} values per analysed grain was met in most samples. Due to the extremely low track density observed in the apatites of KJ-24, five measurements were not accomplished in all grains within this sample.

The following sections contain a presentation of the full results obtained from apatite fission track analysis, subdivided into vertical profiles. Additional samples are grouped according to structural domains. The results obtained from AFT analysis of individual samples are presented in Table 3 and Fig. 29 displays the age and location of all samples included in the study. A cross-section with the obtained AFT results is presented for each vertical profile. The approximate locations of the sketched cross-sections are shown in Fig. 30.

Table 3. Apatite fission track data.

Sample no.	Elevation	No. of	Spontaneous		Induced		Dosimeter		Central age ± 1σ	$P(\chi^2)$	MTL ± 1σ	SD	No. of	Mean Dpar	SD Dpar	U
	(m a.s.l.)	grains	ρs (10^5)	Ns	ρi (10^5)	Ni	ρd (10^5)	Nd	(Ma)	(%)	(µm)	(µm)	tracks	(µm)	(µm)	(ppm)
BG-13	25	20	6.840	600	13.155	1154	18.914	8071	123 ± 8	30.3	N/A	N/A	0	1.62	0.10	10
BG-14	1060	20	11.654	679	13.610	793	16.942	6971	184 ± 12	67.8	N/A	N/A	0	1.34	0.10	11
BG-16	510	20	10.043	743	21.952	1624	16.895	6971	97 ± 5	36.6	N/A	N/A	0	1.55	0.09	19
BG-26	25	20	12.957	916	25.546	1806	16.661	6971	105 ± 5	80.1	10.41 ± 0.25	2.00	100	1.50	0.12	21
BG-27	130	20	12.898	1099	23.555	2007	19.072	8071	130 ± 6	95.6	11.43± 0.18	1.82	63	1.31	0.09	18
BG-53	5	20	2.944	227	5.370	414	18.993	8071	130 ± 11	98.0	N/A	N/A	0	1.18	0.09	4
KJ-1	950	20	7.508	708	12.090	1140	21.257	7923	166 ± 11	21.2	N/A	N/A	0	1.40	0.08	8
KJ-3	750	20	5.119	483	7.949	750	21.140	7923	169 ± 11	58.1	N/A	N/A	0	1.45	0.13	5
KJ-4	550	20	6.722	692	10.763	1108	21.022	7923	163 ± 9	87.5	N/A	N/A	0	1.47	0.07	7
KJ-5	330	20	7.864	708	12.563	1131	20.904	7923	163 ± 9	82.8	N/A	N/A	0	1.59	0.10	9
KJ-6	200	20	3.170	304	6.237	598	20.786	7923	132 ± 10	99.6	N/A	N/A	0	1.51	0.07	4
KJ-7	105	20	3.081	274	5.757	512	20.668	7923	138 ± 11	99.1	N/A	N/A	0	1.53	0.07	4
KJ-8	45	20	6.179	357	14.28	825	20.550	7923	111 ± 9	12.2	10.59 ± 0.25	2.47	100	1.51	0.09	10
KJ-9	30	20	6.067	510	12.051	1013	20.432	7923	128 ± 8	49.4	N/A	N/A	0	1.48	0.10	8
KJ-11	15	20	6.963	755	14.683	1592	20.314	7923	120 ± 7	32.7	11.51 ± 0.19	1.86	100	1.46	0.07	10
KJ-12	980	20	9.446	569	13.779	830	20.196	7923	172 ± 13	5.2	N/A	N/A	0	1.27	0.12	9
KJ-13	790	20	22.592	2264	34.128	3420	20.078	7923	165 ± 7	24.3	N/A	N/A	0	1.57	0.10	24
KJ-14	640	20	24.665	1822	44.726	3304	19.960	7923	137 ± 6	24.2	10.90 ± 0.24	2.37	100	1.47	0.13	32
KJ-15	440	20	9.806	770	18.644	1464	19.842	7923	131 ± 10	0.1	N/A	N/A	0	1.59	0.08	14
KJ-16	190	20	7.568	523	11.909	823	19.724	7923	155 ± 10	33.7	N/A	N/A	0	1.67	0.10	9
KJ-17	100	20	5.709	397	11.173	777	19.606	7923	125 ± 9	94.0	N/A	N/A	0	1.49	0.10	9
KJ-18	1	20	8.092	701	15.93	1380	19.488	7923	124 ± 8	27.3	11.22 ± 0.19	1.95	100	1.55	0.10	13
KJ-19	1225	20	9.674	801	13.769	1140	19.370	7923	169 ± 10	56.8	11.52 ± 0.20	1.95	100	1.50	0.12	11
KJ-20	1025	20	9.186	829	13.907	1255	18.662	7923	153 ± 8	73.7	N/A	N/A	0	1.38	0.07	10
KJ-21	805	20	9.919	906	18.513	1691	18.544	7923	124 ± 7	26.9	10.93 ± 0.20	2.04	100	1.39	0.08	15
KJ-22	605	20	8.010	829	14.899	1542	18.426	7923	123 ± 7	66.2	N/A	N/A	0	1.38	0.09	11

Table 3 (continued). Apatite fission track data.

Sample no.	Elevation	No. of	Spontaneous		Induced		Dosimeter		Central age ± 1σ	$P(\chi^2)$	MTL ± 1σ	SD	No. of	Mean Dpar	SD Dpar	U
	(m a.s.l.)	grains	ρs (10^5)	Ns	ρi (10^5)	Ni	ρd (10^5)	Nd	(Ma)	(%)	(µm)	(µm)	tracks	(µm)	(µm)	(ppm)
KJ-24	1345	20	0.890	76	0.913	78	18.308	7923	221 ± 36	98.7	N/A	N/A	0	1.35	0.12	1
KJ-25	1210	20	9.773	837	13.895	1190	18.190	7923	159 ± 9	96.8	11.11 ± 0.26	2.60	100	1.33	0.10	11
KJ-26	1050	20	8.262	780	11.800	1114	18.073	7923	155 ± 10	6.2	N/A	N/A	0	1.50	0.07	10
KJ-27	50	20	11.25	958	21.761	1853	17.955	7923	116 ± 6	99.6	10.55 ± 0.18	1.76	100	1.40	0.08	17
KJ-28	1310	20	19.547	1961	24.791	2487	17.837	7923	175 ± 8	10.7	11.66 ± 0.23	2.32	100	1.65	0.08	19
KJ-31	15	20	3.555	366	6.275	646	17.719	7923	125 ± 9	78.3	N/A	N/A	0	1.47	0.08	5

i) ρ = track density in 10^5. N = number of counted tracks,

ii) Apatite analysis by the external detector method, using a 4π/2πgeometry factor of 0.5.

iii) Calculations performed by applying an IRMM-540R zeta of 251.6 ± 7.0.

iv) $P(\chi^2)$ = probability value of the chi-square function at n-1 degrees of freedom, where n = No. of crystals. The chi-square test is passed when $P(\chi^2) \geq 5$ (Galbraith, 1981).

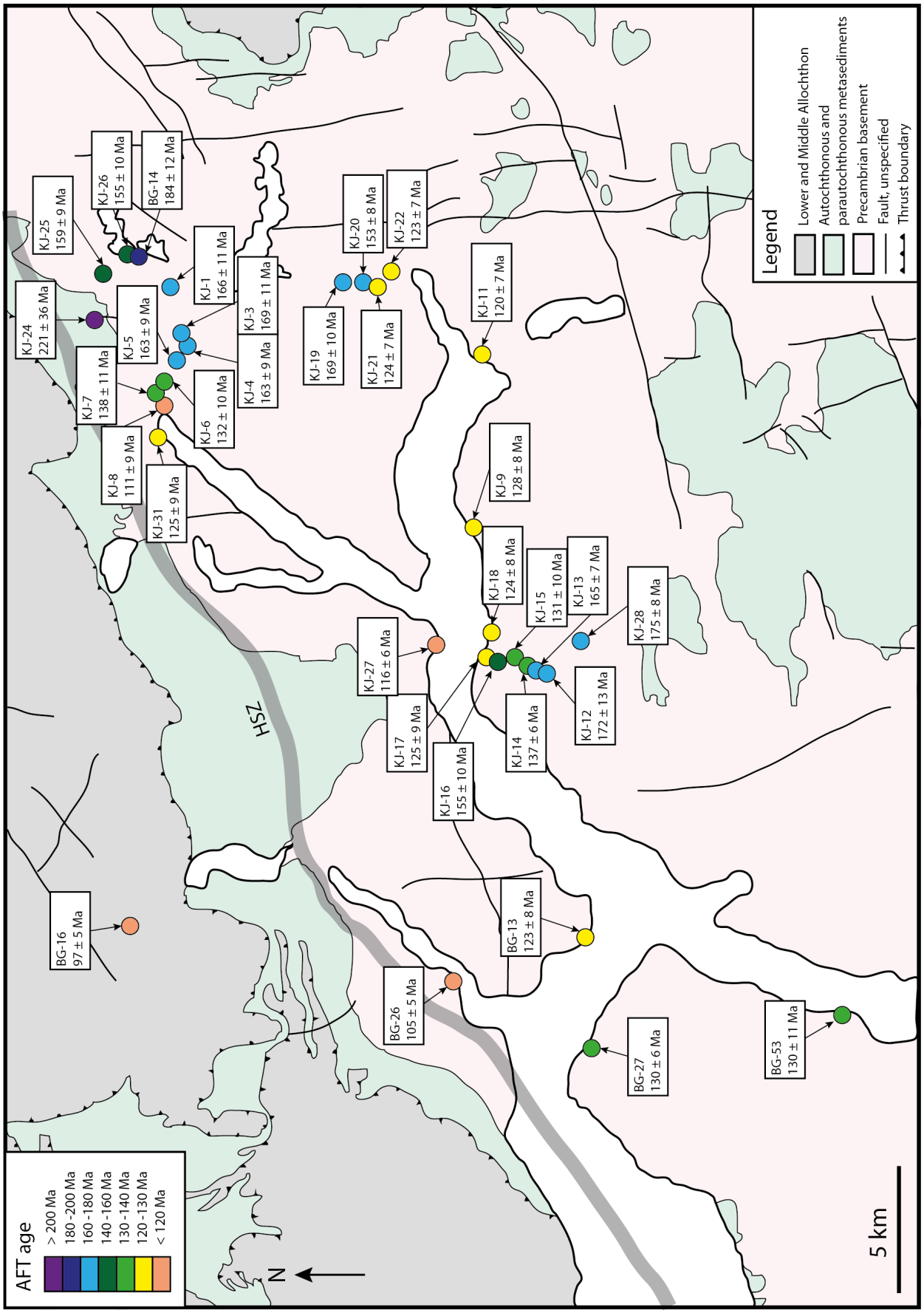

Fig. 29. Simplified geological map of the study area (after Sigmond, 1998) with sample locations and apatite fission track ages.

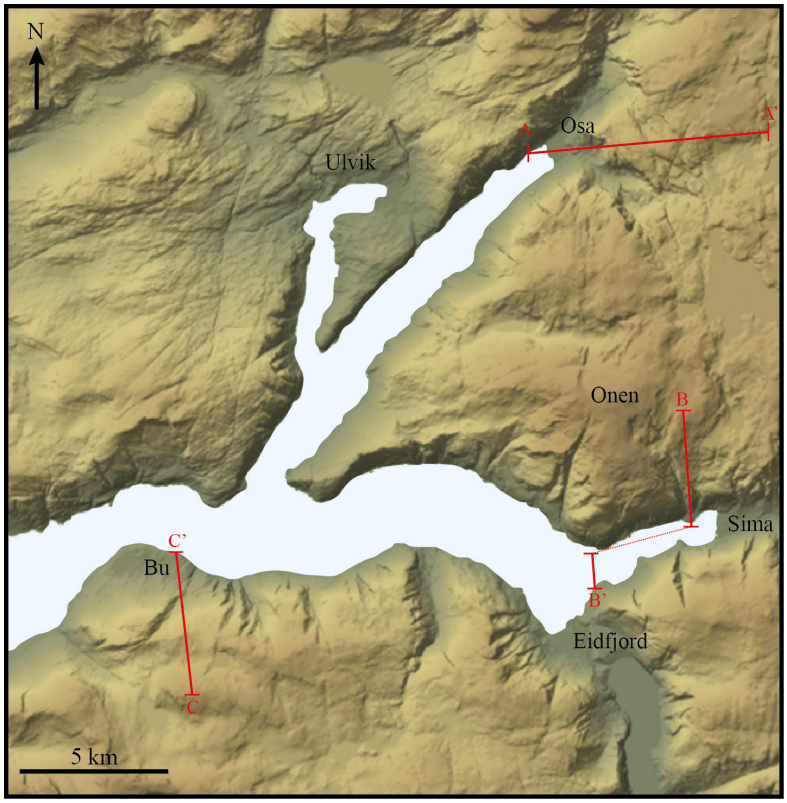

Fig. 30. Location of sketched profiles: A-A' = Osa; B'B' = Kjeåsen; C-C' = Bu. The Kjeåsen profile is divided into two segments in order to incorporate KJ-11, which is located several kilometers southwest of the remaining samples in the profile.

6.4.1 Osa profile

The Osa profile comprises 12 samples collected over a relief of 1330 m and displays a wide range of AFT ages from 111 ± 9 to 221 ± 36 Ma. A general positive correlation between age and elevation is evident (Fig. 31). The lowermost 200 m of the profile are characterised by Early Cretaceous ages. A great span of ages from Albian (KJ-8) to Valanginian (KJ-7) is observed across minor vertical distances. KJ-31 is the only sample obtained from the northwestern flank of the Osafjord and displays an age of 125 ± 9 Ma. This age overlaps within 1σ error with all ages obtained from the lower part of the profile on the opposite flank. In the middle part of the Osa transect, between 332 and 948 m asl, a very limited variation in age is observed with increasing elevation, and Middle Jurassic ages are found to predominate. Significantly greater variation is evident in the uppermost part of the profile, which encompasses samples derived from various elevations on the Hardangervidda plateau. BG-14 records an age of 184 ± 12 Ma, which is the second oldest age obtained in this study. The adjacent samples, KJ-25 and KJ-26, exhibit relatively young ages of 159 ± 9 Ma and 155 ± 10

Ma, respectively. The top sample, KJ-24, is characterized by an exceptionally old age of 221 ± 36 Ma. Taking the markedly high error into consideration, this age is found to overlap with the age of BG-14, which was collected further to the east and 288 m below KJ-24. Confined track lengths were measured for KJ-8 and KJ-25, yielding MTLs of 10.59 ± 0.25 µm and 11.11 ± 0.26 µm, respectively. The spatial relation between the samples in the Osa profile are shown together with the results from the AFT analysis in Fig. 32.

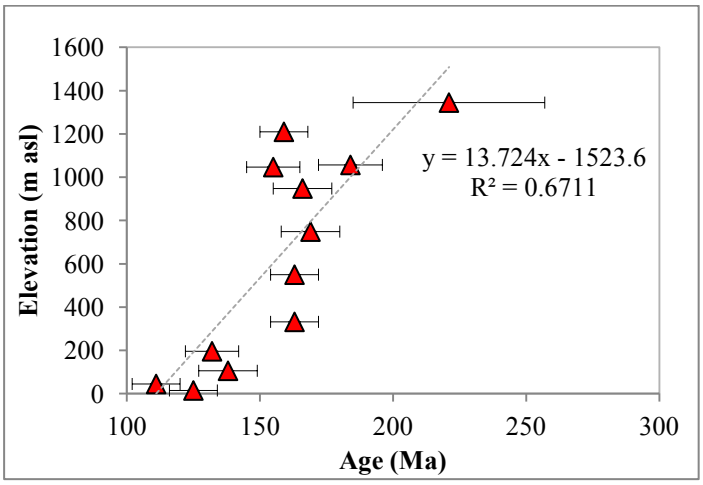

Fig. 31. Age-elevation plot for the samples from the Osa profile. A general trend of increasing ages with elevation is apparent. Some samples deviate significantly from this trend, in particular two young samples collected at high elevations (KJ-25 and KJ-26) and two relatively old samples collected from the lower part of the profile (KJ-5 and KJ-7). Error bars are 1σ.

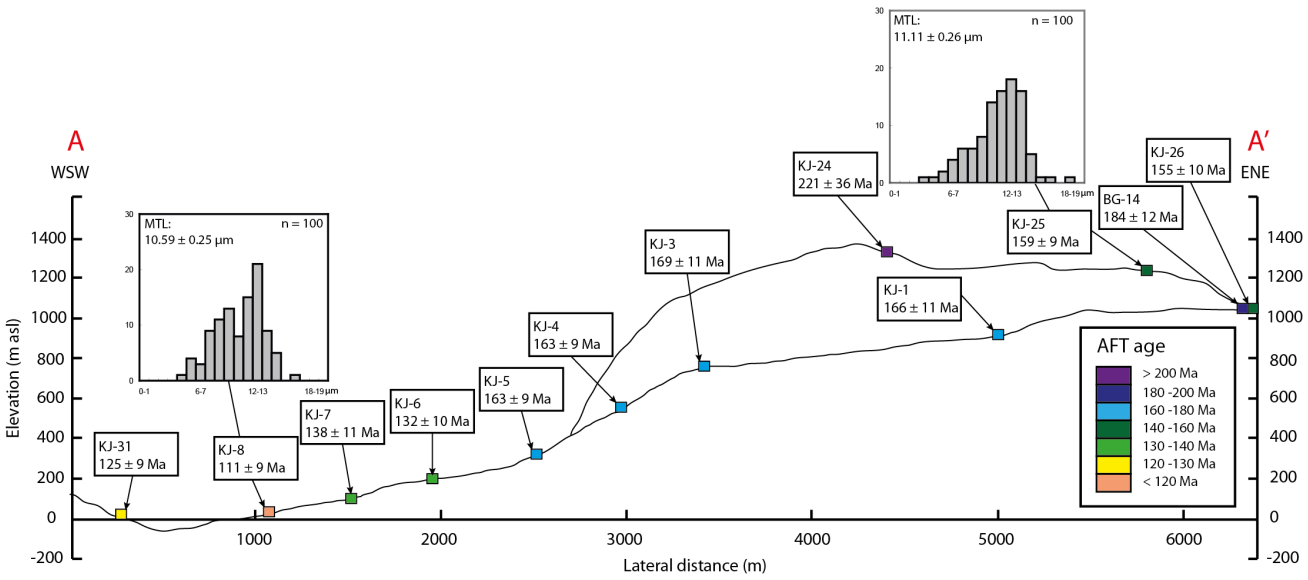

Fig. 32. Sketched profile from Osa, with sample locations, ages and track length distributions indicated. Note that the figure displays two topographical features, namely the valley that extends E-W from Osa to Rundavatnet and the Nipahøgdi summit that is located to the north of (behind) the valley.

6.4.2 Kjeåsen profile

The Kjeåsen profile originally comprised seven samples collected from sea level to an elevation of 1226 m. None of the three lowermost samples in the transect yielded sufficient apatite for AFT analysis (cf. section 6.2.1). Hence, KJ-11 from Eidfjord/outer Simadalen is included in the discussion in order to facilitate the establishment of an age-elevation relationship. The AFT ages from the Kjeåsen profile range from 120 ± 7 Ma to 169 ± 10 Ma. All samples collected from sea level to an elevation of 604 m asl exhibit Aptian ages spanning from 120 ± 7 Ma to 124 ± 7 Ma. A perfect correlation between age and elevation is observed, although limited age variation is recorded by this specific portion of the profile. In fact, when 1σ errors are taken into consideration the ages of KJ-11, KJ-22 and KJ-21 are found to overlap. The uppermost samples reveal a strong trend of progressively increasing AFT ages with elevation and display a greater span of ages over approximately the same relief as the lowermost portion of the profile. KJ-19 exhibit the oldest age in the transect, while KJ-20, sampled approximately 200 m below KJ-19, has an age of 153 ± 8 Ma. Track lengths were measured for three samples from the Kjeåsen profile. The middle sample, KJ-21, has a short MTL of 10.93 ± 0.20 µm, while the top and lowermost samples KJ-19 and KJ-11 display similar MTLs of 11.52 ± 0.20 µm and 11.51 ± 0.19 µm, respectively. Fig. 33 shows the age-elevation trends that are apparent in the Kjeåsen profile. In Fig. 34 the obtained data for individual samples are presented in a cross-section.

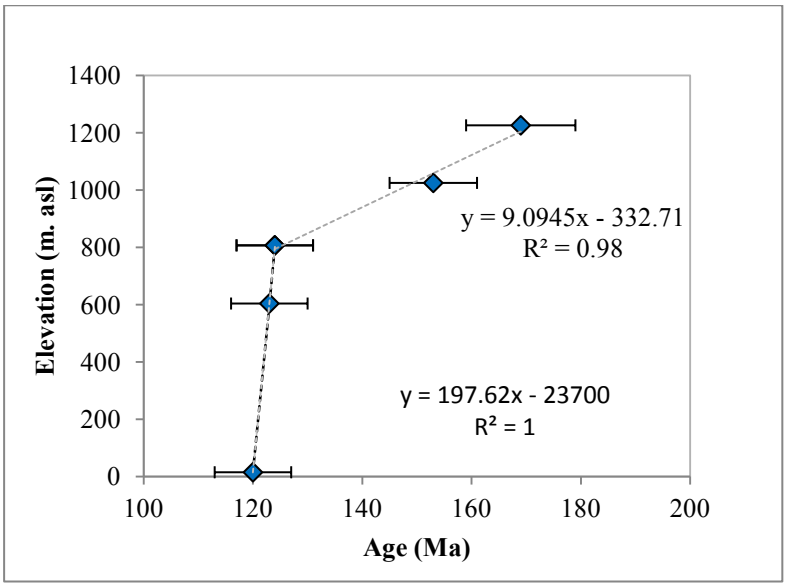

Fig. 33. Age-elevation relationship in the Kjeåsen profile. The profile may be divided into two distinct segments that both show excellent correlation between age and elevation.

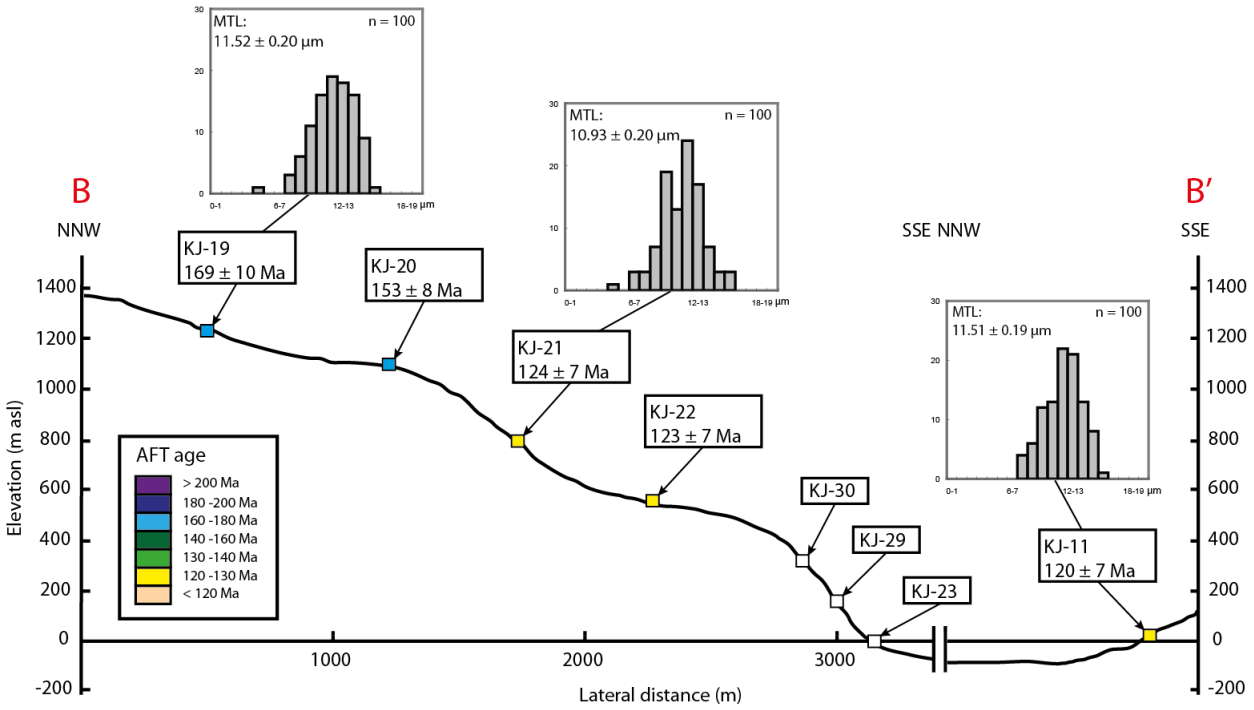

Fig. 34. Sketched profile from Kjeåsen, with topography, position of samples, ages and track length distributions. Note that KJ-11 is located far southwest of the remaining samples (see Fig. 29). The actual distance between KJ-23 and KJ-11 is thus significantly greater than the apparent distance in the figure. KJ-23, KJ-29 and KJ-30 yielded insufficient apatite for analysis.

6.4.3 Bu profile

The Bu profile consists of eight samples collected from sea level to an elevation of 1310 m. The obtained ages span from 124 ± 8 to 175 ± 8 Ma, with the oldest age displayed by KJ-28 from Vatnasetenuten. KJ-18 is the lowermost sample and exhibits the youngest age. A fairly strong positive correlation between age and elevation is evident (Fig. 35). Except for KJ-16, all samples collected below 700 m asl record Early Cretaceous cooling ages that increase systematically with elevation. A discontinuity in the general age-elevation trend is present between KJ-14 (137 ± 6 Ma) and KJ-13 (165 ± 7 Ma), where AFT ages are found to jump abruptly from Early Cretaceous in the lower portion of the profile to Middle Jurassic in the upper part of the transect. Similar age-elevation gradients are apparent within both segments. KJ-16 is derived from an elevation of 189 m asl and displays an unexpectedly old AFT age of 155 ± 10 Ma. This sample thus deviates from the otherwise well-defined age-elevation trend that is characteristic of the lower portion of the transect. Track lengths were measured in three of the samples in the Bu profile. The lowermost sample, KJ-18, and the top sample, KJ-28, exhibit MTLs of 11.22 ± 0.19 µm and 11.66 ± 0.23 µm, respectively, while the middle sample, KJ-14, has a shorter MTL of 10.90 ± 0.24 µm. The data obtained from the Bu profile

are presented in an age-elevation plot in Fig. 35 and according to sample position in the cross-section in Fig. 36.

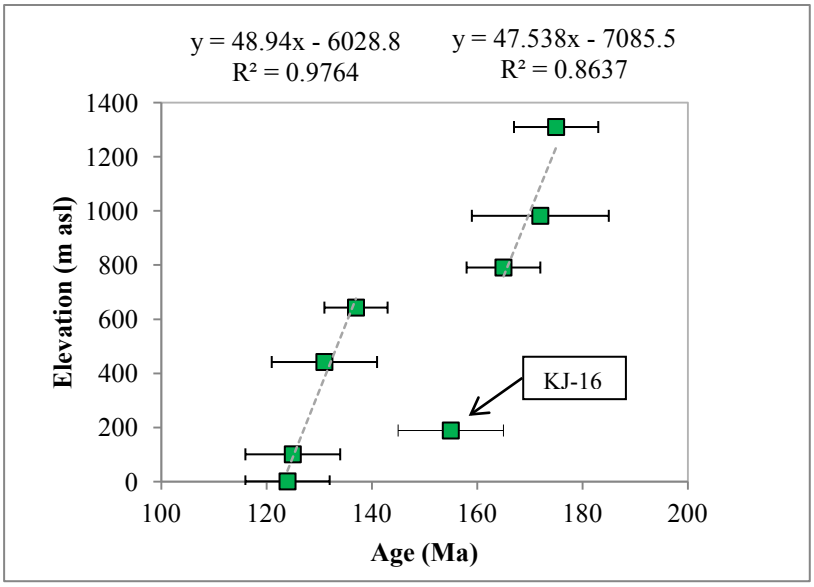

Fig. 35. Age-elevation plot from Bu. Good correlation between age and elevation is found when the lower and upper portions of the profile are considered separately. KJ-16 has a considerably older age than its neighbouring samples and is excluded from the linear regression.

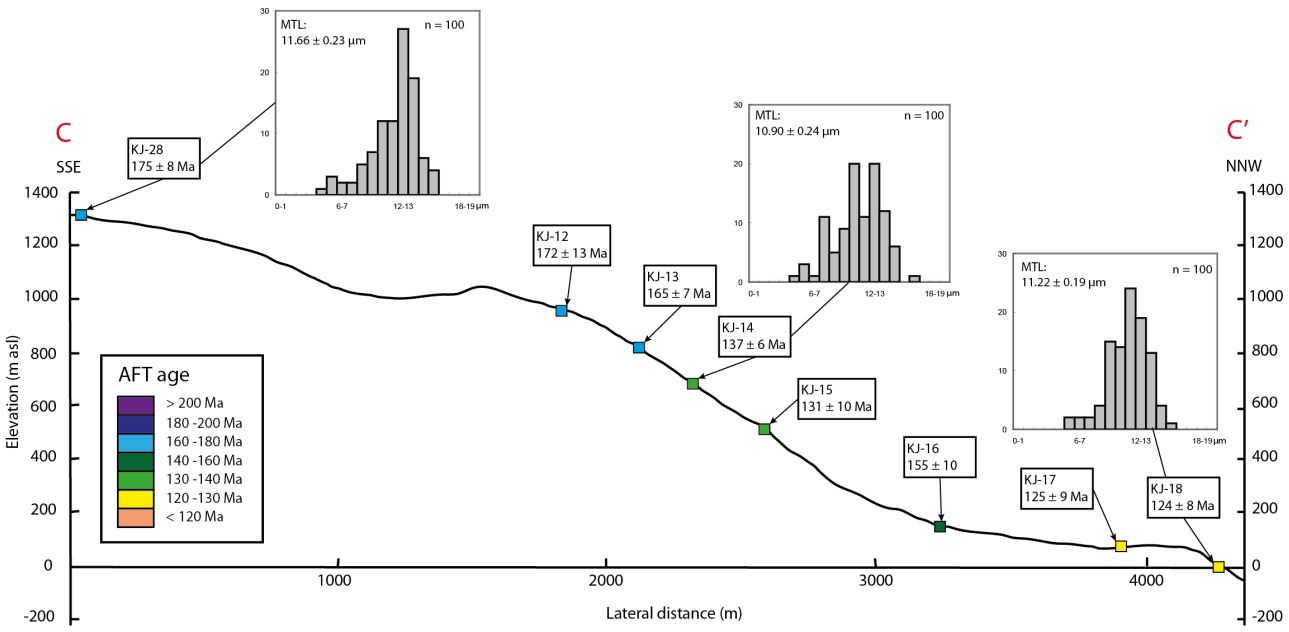

Fig. 36. Sketch of the Bu profile, showing topography, sampling locations, AFT ages and track length distributions.

6.4.4 Additional samples

Sørfjord west flank

BG-27 and BG-53 are both derived from the Sørfjord west block and exhibit similar AFT ages of 130 ± 6 and 130 ± 11 Ma, respectively. An MTL of 11.43 ± 0.18 μm is obtained for BG-27.

Inner Eidfjord south flank

KJ-9 is the only sample collected outside a vertical profile in the Eidfjord area. An age of 128 ± 8 Ma is obtained for this sample. Similar ages are evident at low elevations along the entire southern margin of the Eidfjord.

Outer Eidfjord north flank

KJ-27 from Bruravik displays an AFT age of 116 ± 6 Ma and a short MTL of 10.55 ± 0.18 μm. Compared to KJ-18, which is derived from the opposite margin of the Eidfjord in Bu, KJ-27 records a slightly younger age. However, the ages overlap when errors are considered and thus cannot be regarded different from a statistical point of view. The samples collected from the western margin of the Granvinfjord have the youngest ages of all samples analysed in the present study. BG-26 from the outer Granvinfjord records an age of 105 ± 5 Ma, while BG-16 from the valley northwest of Granvin displays an even younger age of 97 ± 5 Ma. BG-16 is derived from an elevation of 511 m asl and is thus significantly younger than comparable samples elsewhere in the study area. 63 confined track lengths were measured in BG-26. The resulting MTL of 10.41 ± 0.25 μm is the shortest value obtained in the study. BG-13 is derived from the Oksen peninsula directly across the Hardangerfjord from BG-27 and has a relatively young age of 123 ± 8 Ma.

6.5 Interaction of AFT data

6.5.1 Age and elevation

When considered independently all three vertical profiles show a moderate to strong correlation between age and elevation, as demonstrated in section 6.4. In Fig. 37 all ages obtained in the study are considered together. As would be expected in a structurally complex area such as the inner Hardangerfjord, the joint plot reveals significantly greater scatter than the plots created from individual profiles. A general trend of progressively increasing ages with elevation is, however, discernible. In an attempt to detect changes in the AFT age pattern

across the Eidfjord, all samples are colour-coded, reflecting their relative position north or south of the fjord. A pronounced difference is observed in the lowermost part of the plot. Close to sea level AFT ages are consistently younger on the north flank than on the south flank, although most ages overlap when 1σ errors are accounted for. At higher elevations no distinct pattern is apparent, and the variation in AFT age that is evident for samples collected at similar elevations is independent of sample position north or south of the fjord. As a result of the comparably old ages at sea level on the south flank, the general age-elevation trend obtained from this block displays a steeper gradient than that obtained from the Eidfjord north block.

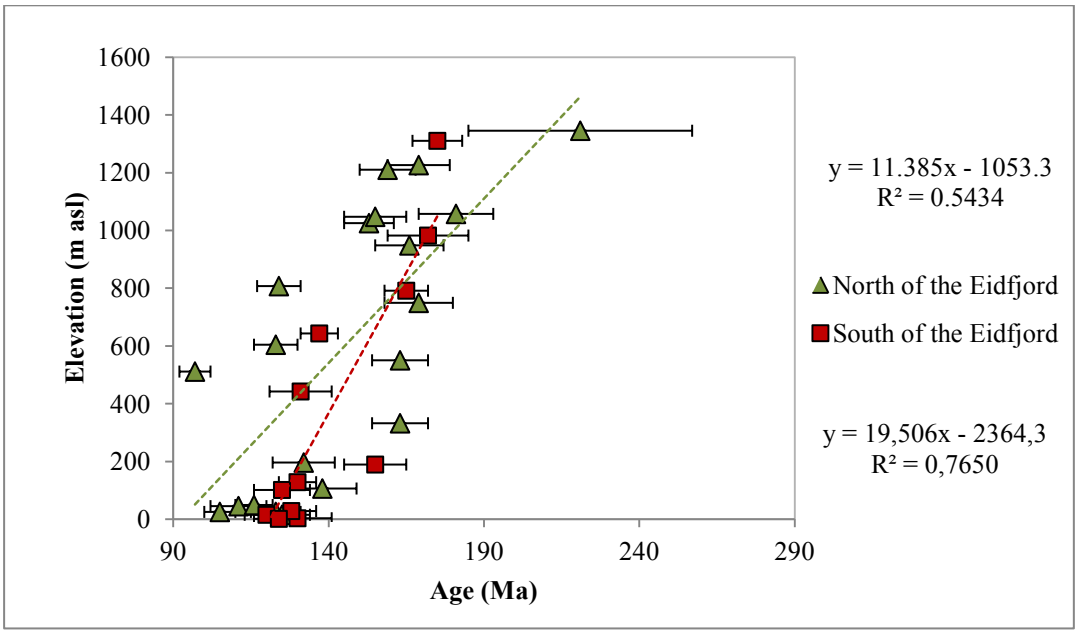

Fig. 37. Age elevation relationship for samples collected north (green) and south (red) of the Eidfjord. Regression lines are displayed for each group and indicate weak and moderate correlation for the north block and the south block, respectively. The greater scatter of data observed for the north block possibly results from the incorporation of two vertical profiles under this population, whereas the south block only encompasses one vertical profile and thus displays a more consistent relationship. See text for further details.

6.5.2 Age and mean track length

Mean track lengths of 11 samples are plotted against fission track age in Fig. 38. A strong positive correlation between MTL and age is observed for the samples derived from the Eidfjord north block. No trend is apparent among the samples from the south block, although the two oldest samples are compatible with the pattern observed north of the fjord. The three youngest ages from the south block deviate from the linear trend as a result of their relatively long MTLs.

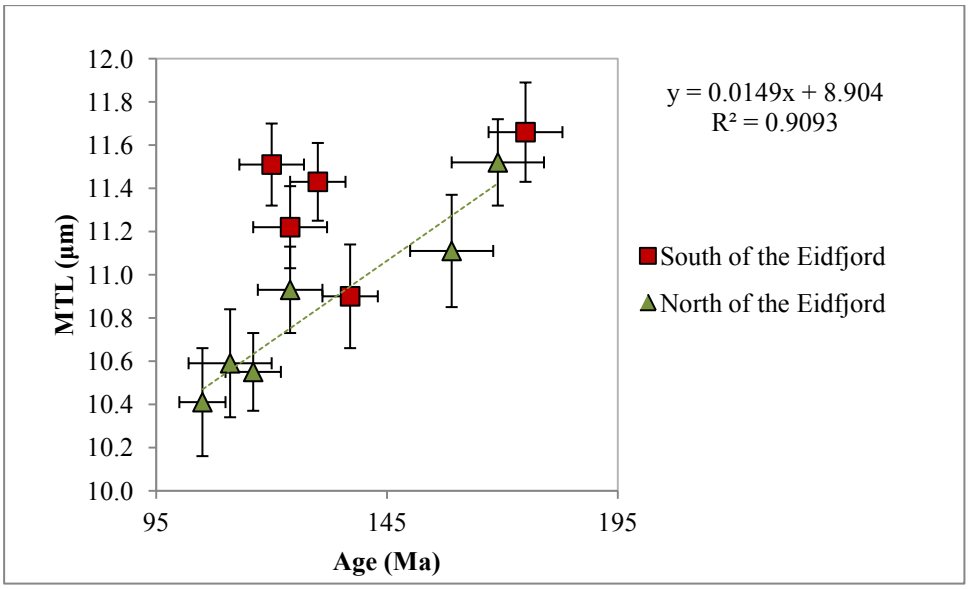

Fig. 38. Relationship between mean track length (µm) and AFT age (Ma). A progressive increase in MTL with increased age is evident north of the Eidfjord. The samples from the southern flank do not reveal the same relationship. Note that the regression line is based on the data from the north block only. The coefficient of determination is 0.91 and thus indicates good correlation. Error bars are 1σ for both axes.

6.5.3 Mean track length and elevation

Fig. 39 reveals a general increase in MTL with elevation. This is not surprising, considering the established correlation between age and MTL together with the general link between age and elevation. The three lowermost samples from the southern block correspond to the young samples in Fig. 39 and do not comply with the observed linear trend.

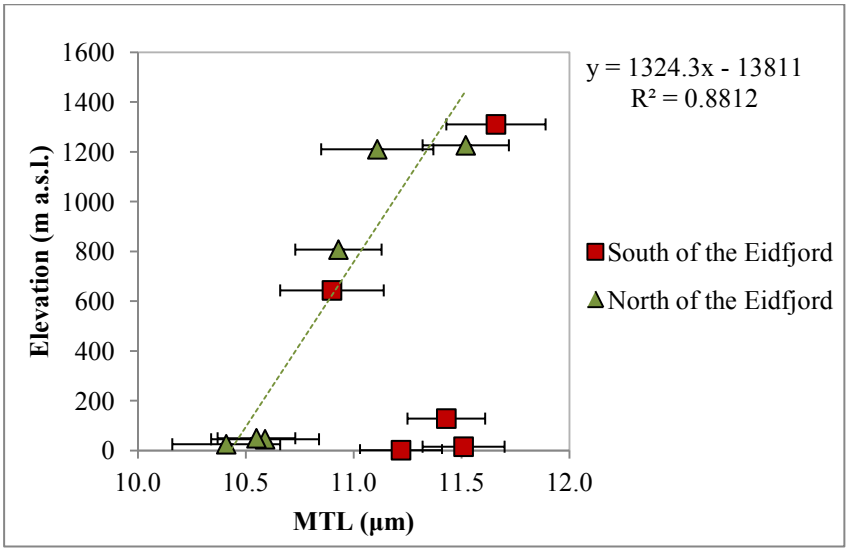

Fig. 39. Relationship between MTL (µm) and elevation (m a.s.l.). Good correlation is evident for the samples from the north flank of the Eidfjord. The data from the south flank are rather ambiguous. Note that the regression line is drawn for the data from the north flank only. Error bars are 1σ.

6.5.4 Age and mean etch pit diameter (D_{par})

In order to assess the influence of compositional differences on annealing behaviour, AFT ages are plotted against mean etch pit diameters for all samples (Fig. 40). As a result of the sampling scheme applied in the current study a general comparison of age and D_{par} may inadvertently incorporate additional variables that are not accounted for, e.g. changes in elevation. Elevation has been shown to exert a primary control on the AFT age pattern in the region (cf. section 6.4) and may possibly mask the impact of D_{par}. In an attempt to filter the age variability caused by the range of sample elevations from the potential effect of D_{par}, the sample population is divided into two groups according to elevation. Samples collected within 500 m of sea level have been regarded as comparable in previous studies (e.g. Hendriks et al., 2007), and an altitude of 500 m is thus set as the boundary between the groups. No correlation between AFT age and mean D_{par} is apparent in any of the age groups, and the compositional influence on differential annealing is inferred to be minor. This result is not unexpected given the modest range of mean D_{par} values observed.

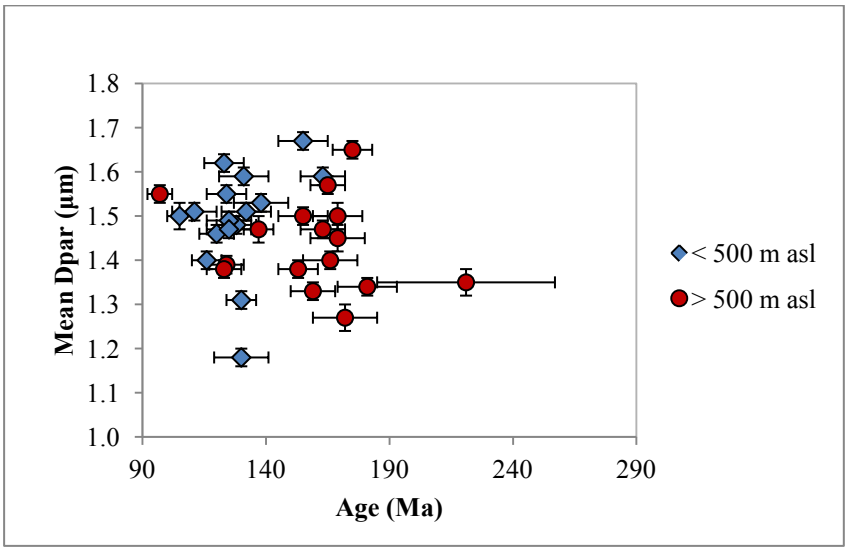

Fig. 40. Relationship between mean etch pit diameter (µm) and AFT age (Ma) for samples collected below (blue) and above (red) 500 m. a.s.l. No correlation is evident in either of the groups. Error bars are 1σ.

6.6 (U-Th)/He analysis

Four samples were dated with the (U-Th)/He method as part of the present study. For reasons that will be discussed in section 8.1.3, the uncorrected He ages are believed to be more reliable than the F_T-corrected ages and will be reported throughout the chapter. The obtained

single grain ages range from 69 Ma to 170 Ma, with a majority of Late Cretaceous ages close to sea level and Early Cretaceous ages on Hardangervidda. The full results from the (U-Th)/He analysis are presented in Table 4. In Fig. 41 the obtained single grain ages are displayed together with the corresponding fission track ages. F_T-corrected ages are included for comparison.

Table 4. Apatite (U-Th)/He data.

Sample no.	Elevation (m a.s.l.)	He (ncc)	1σ (%)	U (ng)	1σ (%)	Th (ng)	1σ (%)	eU [ppm]	Sm (ng)	1σ (%)	F_T	Uncorr. He age (Ma)	F_T-corr. He age (Ma)	1σ (Ma)	Prism rad. (µm)
KJ-8	45	0.499	2.5	0.037	2.4	0.015	2.6	11.7	0.169	5.6	0.70	99	141	8	54
		1.813	1.9	0.094	1.9	0.045	2.4	32.4	0.243	5.5	0.70	140	200	10	52
KJ-11	15	0.444	2.4	0.035	2.4	0.051	2.4	13.1	0.255	5.6	0.71	75	106	6	56
		0.461	2.6	0.039	2.3	0.061	2.4	18.8	0.262	5.5	0.73	69	93	5	58
		1.444	2.0	0.090	1.9	0.140	2.4	20.6	0.649	5.4	0.74	93	125	6	63
KJ-19	1226	2.425	1.9	0.098	1.9	0.113	2.4	23.1	0.871	5.4	0.74	151	204	9	61
		0.757	2.3	0.039	2.3	0.042	2.5	5.3	0.629	5.4	0.78	115	147	6	74
		1.859	2.0	0.098	1.9	0.088	2.4	14.4	0.930	5.4	0.78	120	155	6	70
KJ-25	1210	1.091	2.1	0.067	2.0	0.029	2.5	12.3	0.451	5.5	0.76	115	150	7	65
		1.176	2.0	0.047	2.2	0.032	2.5	17.1	0.251	5.5	0.68	170	252	14	49

Amount of ^{4}He is given in nano-cubic-cm at standard temperature and pressure. Amounts of radioactive elements are given in nanograms, with standard errors in percent. eU is the effective U-concentration in ppm (eU = [U] + 0.235 [Th]). F_T-correction according to Farley et al. (1996).

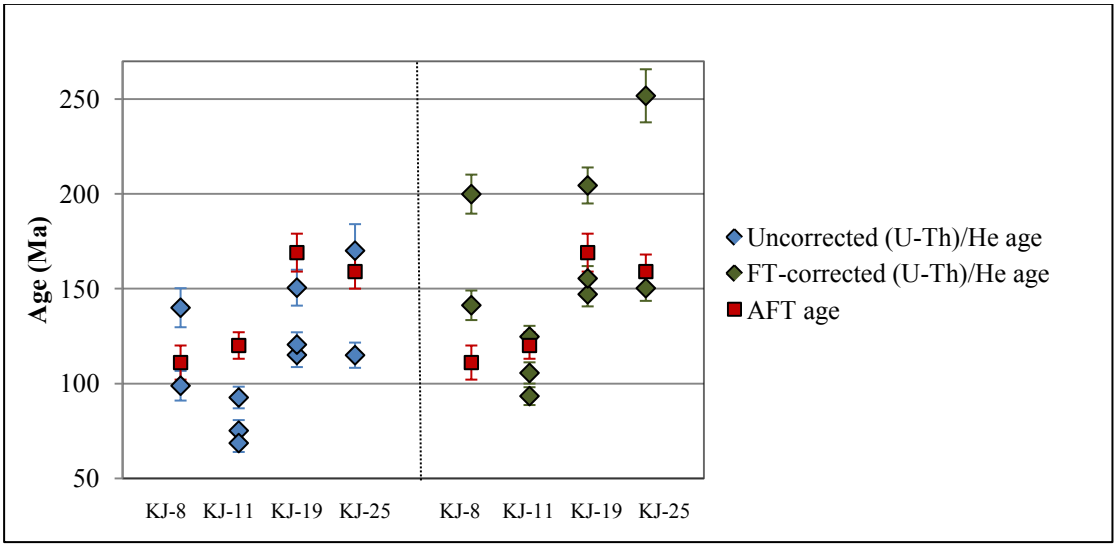

Fig. 41. Uncorrected (U-Th)/He ages (left) and F_T-corrected (U-Th)/He ages (right) displayed with their corresponding AFT ages. The majority of the uncorrected (U-Th)/He ages are younger than the ages obtained from fission track analysis performed on the same samples. In both KJ-8 and KJ-25 one single grain (U-Th)/He age is found to be older than the AFT age. The F_T-corrected ages show a greater spread within individual samples. Five grains display corrected (U-Th)/He ages that are older than the AFT ages. Error bars are 1σ.

From the samples collected as part of the Kjeåsen profile, KJ-11 from sea level and KJ-19 from the Hardangervidda plateau were dated by the (U-Th)/He method. KJ-11 shows relatively good reproducibility, evident by a spread in single grain ages of only 24 Ma. A mean age of 78 ± 7 Ma is obtained from this sample. The scatter is significantly greater for KJ-19. Two of the analysed grains display rather similar ages of 115 ± 6 Ma and 120 ± 6 Ma, while the third grain exhibits a considerably older age of 151 ± 9 Ma. Due to its incongruence with respect to the remaining ages, the oldest age is considered unreliable and will be excluded from further considerations. A mean age of 118 ± 4 Ma, obtained from the two youngest grains, will be implemented as a constraint in the AFT thermal history models in chapter 7.

Both samples included from the Osa profile, KJ-8 and KJ-25, show poor reproducibility of single grain (U-Th)/He ages. Only two grains from each sample were successfully analysed. For both samples the third grain analysis was discarded as a result of U- and Th-concentrations below the detection limit. Given the large scatter in ages observed for the remaining pairs of analysed grains (41 Ma and 55 Ma for KJ-8 and KJ-25, respectively) no valid conclusion regarding the timing of cooling through the HePRZ can be drawn for either of the samples. The (U-Th)/He results from the Osa profile will therefore not be discussed further.

Fig. 42 shows uncorrected (U-Th)/He ages plotted against effective U-concentrations for each analysed grain. A general increase in single grain ages with concentration of radioactive isotopes is evident. Possible reasons for this pattern and its interpretational implications will be discussed in section 8.1.4.

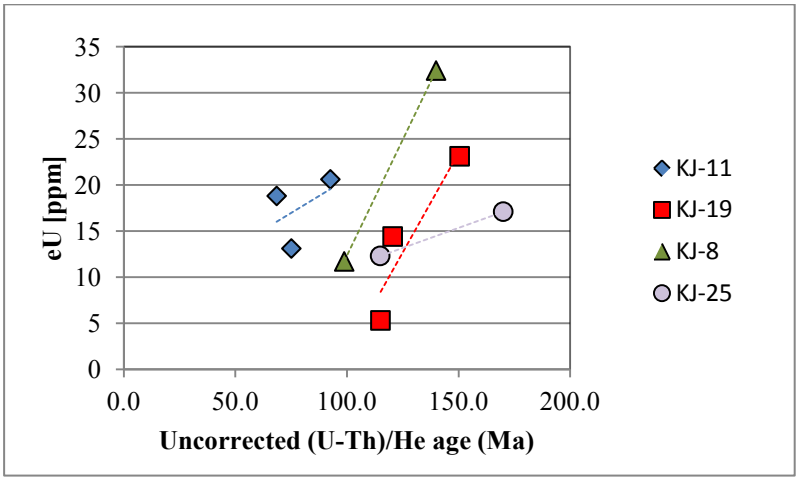

Fig. 42. Relationship between effective U-concentration and uncorrected (U-Th)/He age for individual grains. A positive correlation is evident for all samples, although the scatter is minor for the youngest sample, KJ-11.

6.7 Summary of results from AFT and (U-Th)/He analyses

When all the analytical results presented in the previous subchapters are considered together, some distinct trends appear: Early Cretaceous AFT ages predominate close to sea level, while Jurassic ages are recorded by most samples from the Hardangervidda plateau. Strikingly consistent ages, generally within the range 111-130 Ma, are evident at low elevations throughout the study area. However, the samples collected close to sea level north of the Eidfjord systematically display younger AFT ages and shorter MTLs than samples at corresponding elevations from the southern margin of the fjord. This pattern is not as pronounced at higher elevations. The (U-Th)/He system records cooling through the 70-40 °C temperature interval in the Early Cretaceous on Hardangervidda and in the Late Cretaceous at low elevations, i.e. roughly 40-50 Ma later than the ages obtained from the fission track analyses. Possible explanations for the observed patterns of AFT and (U-Th)/He data will be discussed in chapter 8.

7. THERMAL HISTORY MODELLING

7.1 Thermal constraints

Constraints must be applied to the HeFTy models in order to confine the cooling paths according to the limitations given by previous geochronological work conducted in vicinity of the study area. Any constraint applied to the model must be justified by geological observations or independent data. A basic set of constraints, encompassing start and end conditions, is required for the software to run properly and is included in all models. In the present study zircon fission track data from Eidfjord (Andriessen & Bos, 1986) are applied as the initial constraint. The reported ages indicate rapid cooling through 175-225 ºC at 306 ± 22 Ma. Similar results have been obtained from the same area in a more recent study by Leighton (2007). The closure temperature of the zircon fission track system is poorly constrained and has been found to vary according to cooling history. An average late Carboniferous-Late Jurassic cooling rate of 0.5 °C/Myr was calculated from the zircon and apatite fission track data of Andriessen and Bos (1986) and applied to the field-based relationship between closure temperature and cooling rate proposed by Bernet (2009). This approach resulted in an estimated closure temperature of the zircon fission track system of 200°C, which corresponds to the value adopted by Andriessen and Bos (1986). The zircon fission track data from Eidfjord record nearly identical ages over a range of elevations, allowing the same boundary condition to be applied to all the models, regardless of sampling altitude. An assumed present-day mean surface temperature of 7 ± 3 ºC was applied to the thermal history models as the final constraint. Where available, (U-Th)/He ages obtained in the present study were set as a third constraint. For samples derived from the Hardangervidda plateau, additional constraints were introduced to some models in order to test the viability of the peneplanation-uplift model. For simplicity, these constraints are described in detail together with the model descriptions in chapter 7.3.

7.2 Models with start and end constraints only

7.2.1 Osa profile

Inverse thermal modelling was performed for KJ-8 and KJ-25 from the Osa profile (Fig. 43). The sea level sample, KJ-8, reveals rapid cooling into the PAZ in Permo-Triassic times, followed by slow cooling (~0.1 °C/Ma) within the upper portion of the PAZ from the Late Triassic-Early Jurassic onwards. A slight increase in cooling rate is recorded in the upper part of the PAZ in the Paleogene. The relatively high proportion of short confined tracks in this sample is reflected by a long time of residence in the PAZ and a late exit at 40 Ma. Rapid cooling (1-3 °C/Ma) is suggested for the last 40 Myr. The modelled thermal history of the top sample, KJ-25, suggests entrance into the PAZ between the Permian and the earliest Late Triassic and involves rapid cooling until the Middle-Late Triassic. Slow cooling (~0.1 °C/Ma) at temperatures below 80 °C is inferred from the Late Triassic until the Early-Late Cretaceous. The sample appears to exit the PAZ at ~80 Ma, i.e. 40 Ma earlier than KJ-8. Accelerated cooling is suggested for the Cenozoic, but appears to have commenced already in the Late Cretaceous.

7.2.2 Kjeåsen profile

Thermal history modelling was performed for three samples from the Kjeåsen profile, including KJ-11 from Eidfjord/outer Simadalen (Fig. 44). The two lowermost samples, KJ-11 and KJ-21, record rapid cooling into the PAZ between the Permian and the Early-Middle Jurassic. In a similar manner as for the samples from the Osa profile, slow cooling is evident from the Jurassic throughout most of the Cretaceous. For KJ-11 the upper boundary of the PAZ is encountered at ~60 Ma. Gradually enhanced cooling rates are suggested from the Paleogene onwards, with particularly high rates inferred for the last 20 Myr. Interestingly, the middle sample, KJ-21, is found to cool out of the PAZ at ~40 Ma, i.e. at a later stage than the lowermost sample. The thermal history model indicates progressively increasing cooling rates from 50 Ma until a stable rate of ~2 °C is attained at 20 Ma. A similar pre-Cretaceous thermal history is evident for the top sample, KJ-19. Slow cooling is suggested until 80 Ma when the sample crosses the upper boundary of the PAZ. Accelerated cooling is inferred for the Cenozoic.

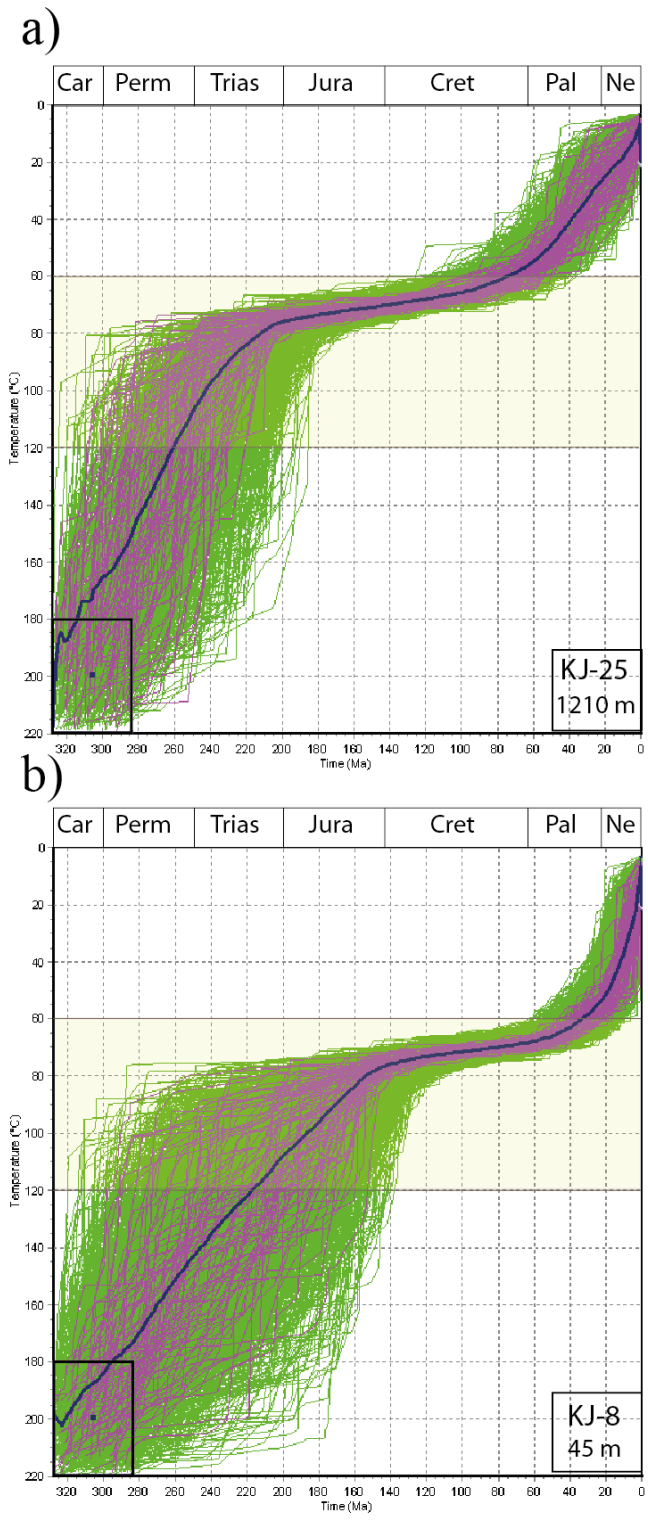

Fig. 43. Results from inverse thermal history modelling of the Osa samples, with constraints implemented as boxes. Acceptable t-T-paths are marked in green, while 100 good paths are indicated by purple curves. One dark blue curve is displayed in each model and represents the weighted mean path. The temperature interval of the PAZ is marked in pale yellow. Proposed thermal histories of **a)** KJ-25 and **b)** KJ-8. Both models indicate rapid cooling into the PAZ in the Permian-Triassic, followed by a prolonged interval of residence in the upper PAZ. Note that KJ-8 requires a later exit from the PAZ than KJ-25. See text for further details.

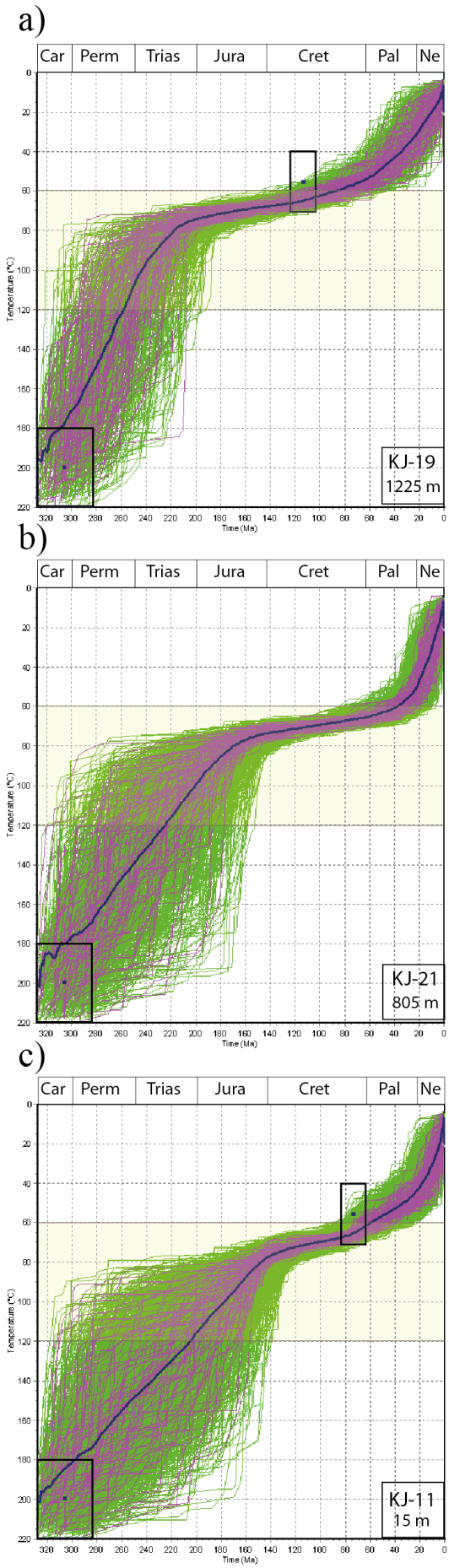

Fig. 44. Thermal history models for the Kjeåsen samples. **a)** KJ-19 **b)** KJ-21 **c)** KJ-11. Colour-coding as in Fig. 43. All samples record rapid cooling into the PAZ within the time interval from the Permian to the Early Jurassic. In the high-temperature portions of the models, the good paths are confined to a narrower age interval at high elevations than close to sea level. The latest exit from the PAZ is suggested for KJ-21. See text for further details.

7.2.3 Bu profile

Thermal history models were generated for samples KJ-18, KJ-14 and KJ-28 from the Bu profile (Fig. 45). The sea level sample, KJ-18, records rapid cooling (1-5 °C/Ma) until the Jurassic, succeeded by slow cooling through the upper portion of the PAZ. Enhanced cooling rates are observed as the sample crosses the upper boundary of the PAZ at ~50 Ma. In comparison, the middle sample, KJ-14, reveals an earlier entrance into the PAZ and an extended time of residence between 80 and 60 °C. The proposed cooling paths indicate exit from the PAZ at 60 Ma. In contrast to the other modelled samples in the study area, KJ-28 reveals continuous, relatively slow cooling from the Late Triassic until the present, albeit with slightly increased cooling rates during the last 40 Myr. According to the inverse model, the sample cooled out of the PAZ at 110 Ma, which is considerably earlier than the proposed exits of samples from similar elevations on the north flank of the Eidfjord.

7.2.4 Additional samples

Thermal history models were produced for three samples from the outer Eidfjord area (Fig. 46). BG-27 from the Sørfjord west block appears to have cooled into the PAZ concurrently with the other modelled samples collected from low elevations, i.e. between the Permian and the Early Jurassic. A shift between rapid and slow cooling is suggested in the Jurassic at temperatures of ~80 °C. The sample records an early exit from the PAZ at ~80 Ma, and thus appears to have cooled out of the sensitivity range of the apatite fission track system significantly earlier than all other sea level samples included in the study. BG-26 from the opposite margin of the Hardangerfjord reveals a strikingly different thermal history. Because of its short MTL, the sample is bound to have remained in the PAZ for an extended period of time. A late exit from the PAZ at 20 Ma implies an abrupt change from slow (~0.3 °C/Ma) to rapid (2-3 °C/Ma) cooling in the Miocene. KJ-27 displays a similar thermal history to that of BG-26, but appears to have experienced lower temperatures during the entire interval between ~160 and 20 Ma.

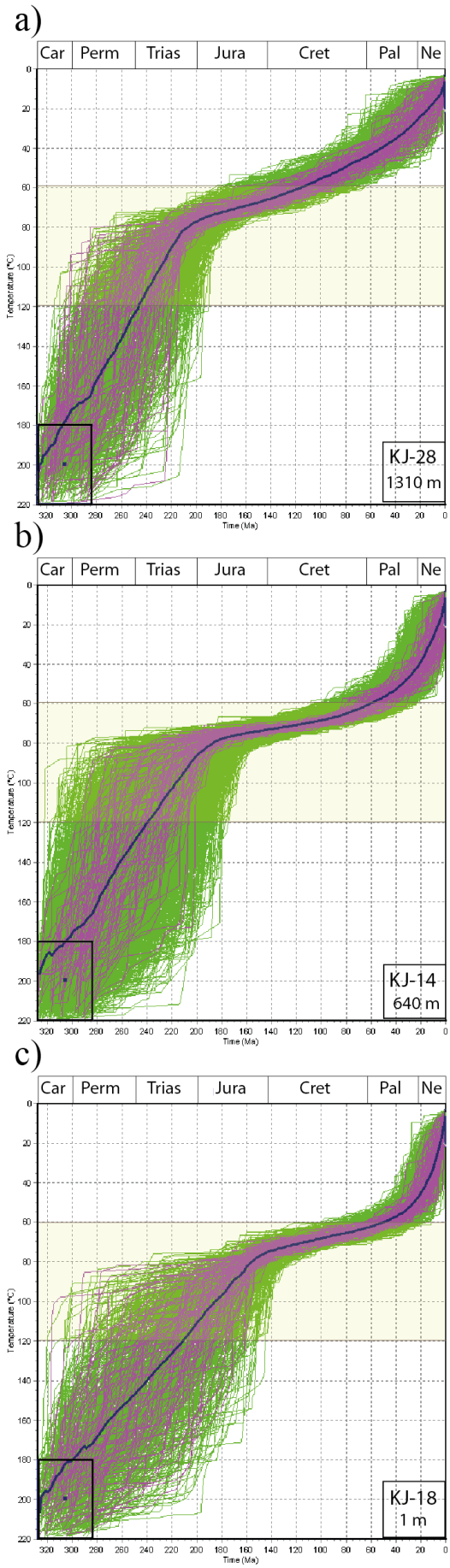

Fig. 45. Inverse thermal models based on AFT data obtained from the Bu profile. The samples are arranged according to their elevations: **a)** KJ-28; **b)** KJ-14; **c)** KJ-18. Note the progressively earlier exit from the PAZ with increasing altitude. The proposed thermal history model for KJ-28 indicates cooling out of the PAZ already in Albian times. See text for further details.

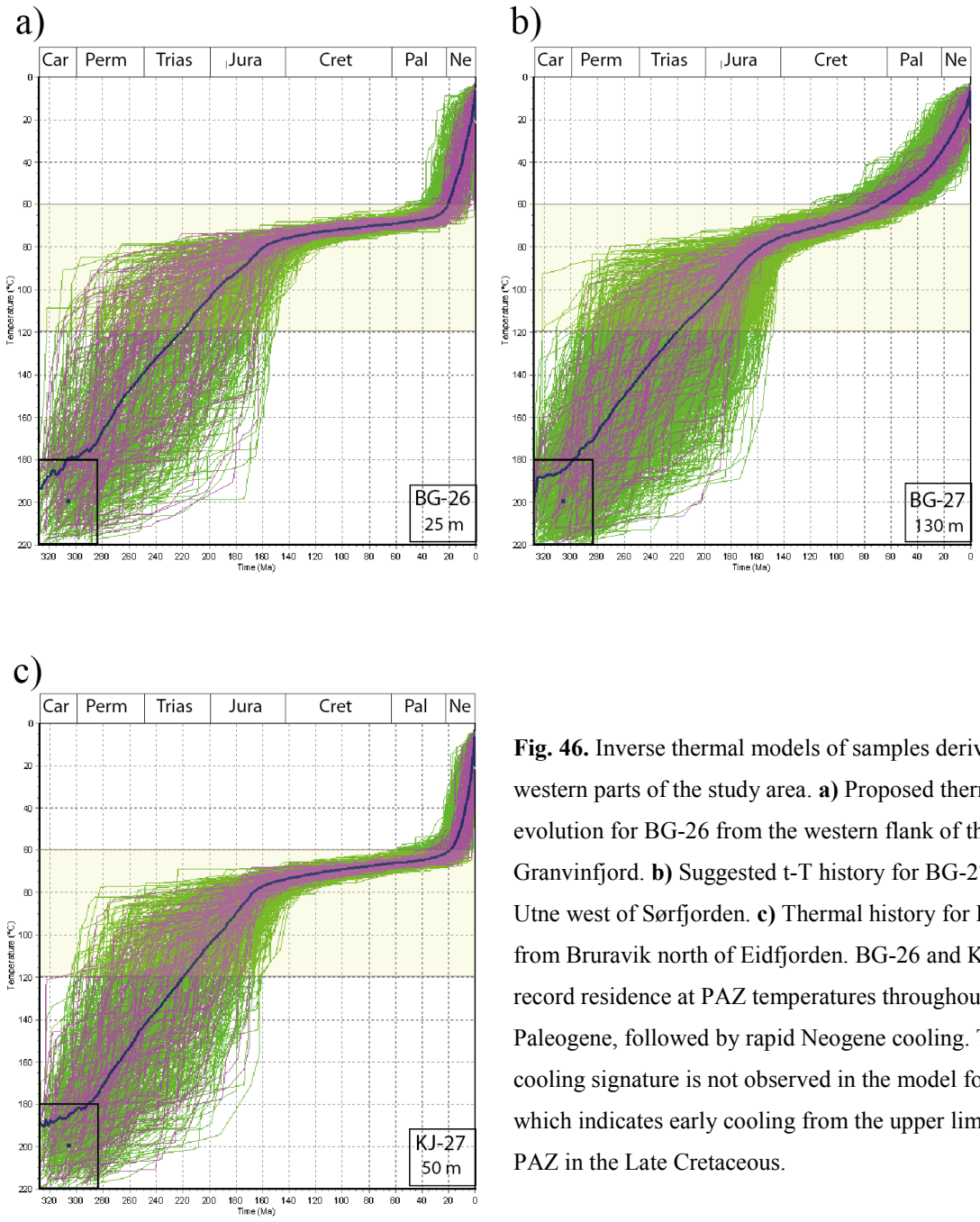

Fig. 46. Inverse thermal models of samples derived from western parts of the study area. **a)** Proposed thermal evolution for BG-26 from the western flank of the Granvinfjord. **b)** Suggested t-T history for BG-27 from Utne west of Sørfjorden. **c)** Thermal history for KJ-27 from Bruravik north of Eidfjorden. BG-26 and KJ-27 both record residence at PAZ temperatures throughout the Paleogene, followed by rapid Neogene cooling. This cooling signature is not observed in the model for BG-27, which indicates early cooling from the upper limit of the PAZ in the Late Cretaceous.

7.2.5 Comparison of models

Some general trends are shared by the majority of the thermal history models presented in the previous subchapters, i.e. rapid Permo-Triassic cooling into the PAZ followed by slow cooling through the temperature interval between 80 °C and 60 °C and, finally, accelerated cooling starting in the Late Cretaceous-Paleogene. There are some exceptions to this general pattern. KJ-28 from a high elevation in the Bu profile records a virtually linear cooling trend from the latest Triassic onwards and is found to cool out of the PAZ already in the Early

Cretaceous. The modelled thermal histories of KJ-27 and BG-26 from the outer Eidfjord north flank indicate slow cooling until the Neogene when the samples are suggested to cool out of the PAZ. Interestingly, the samples from the Eidfjord north flank consistently record a later onset of accelerated cooling, and hence a later exit from the PAZ, than samples from corresponding elevations on the south flank. The similarities and differences between the modelled thermal histories are illustrated in Fig. 47.

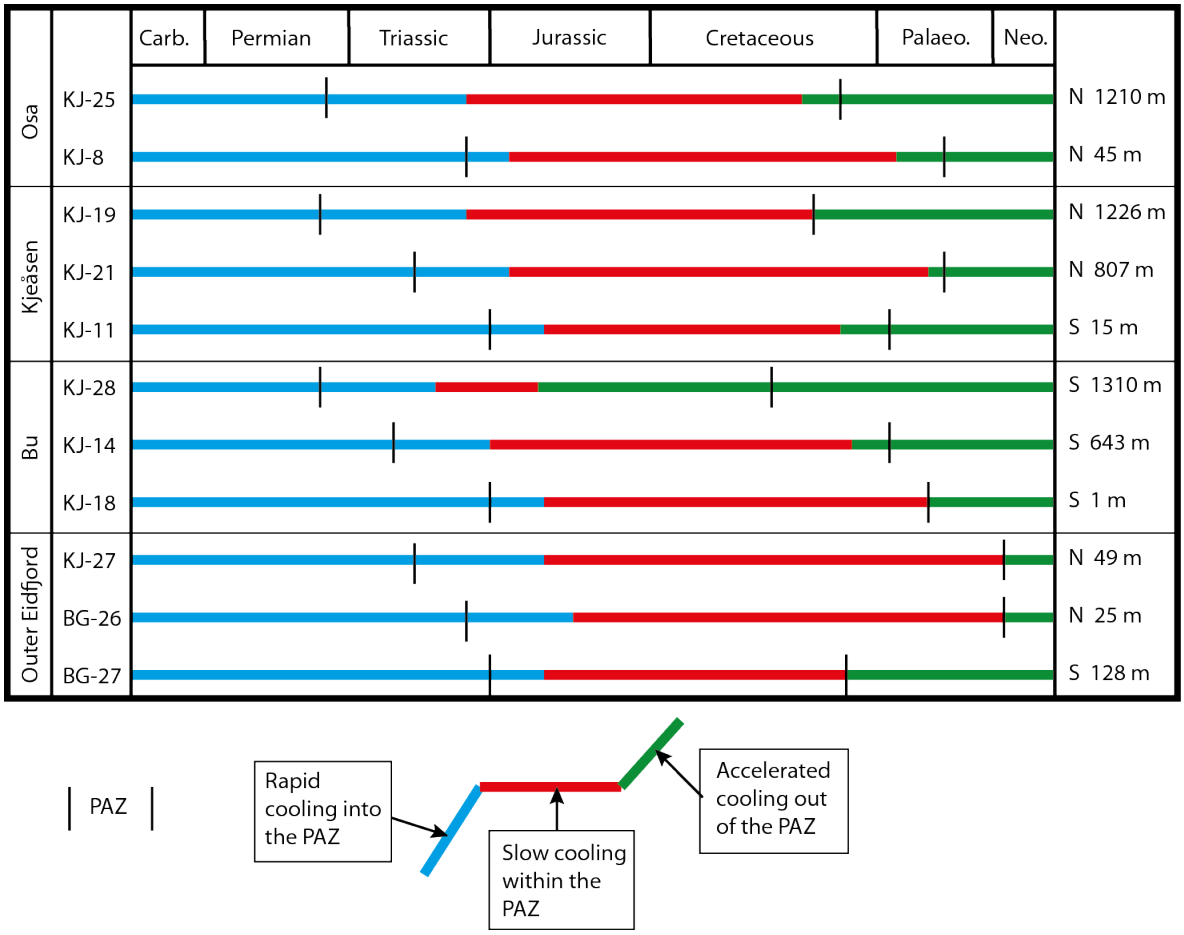

Fig. 47. Schematic comparison of modelled cooling paths. The exact time of cooling into the PAZ is difficult to determine. Here it is estimated from the weighted mean path. Although poorly constrained, the change from rapid to slow cooling rates appears to have taken place in the Late Triassic-Early Jurassic. The onset of the most recent rapid cooling is confined to the Cretaceous-Paleogene in most models. Note the differences in the timing of exit from the PAZ for samples from the Eidfjord north flank (marked N) relative to samples from the south flank (marked S). Sample elevations are displayed in the right column.

7.3 Alternative models

7.3.1 Paleocene peneplanation and reburial

Additional constraints were applied to some models in order to force the samples to the surface in the Paleocene, following the interpretations of Lidmar-Bergström et al. (2000) and Riis (1996) (cf. section 2.4.1). The time at which the samples attained surface temperatures (0-20 °C) was set to 70-50 Ma and a second box between 70 Ma and the present and 20-80 °C was implemented to allow reheating. Due to their proximity to the assumed Paleocene surface, KJ-19, KJ-25 and KJ-28 were chosen to test the outlined combination of constraints. The modelled t-T history of KJ-19 (Fig. 48a) reveals relatively rapid cooling (1-2 °C/Ma) to surface temperatures in the latest Early Cretaceous to Paleocene, followed by reheating to maximum temperatures of 80 °C in the Eocene-Oligocene. A consistent cooling rate of 1-2 °C/Ma is suggested for the most recent portion of the thermal history. Similar thermal histories are evident for KJ-25 and KJ-28 (Appendix E).

In order to test the possible prolonged existence of a peneplain without a sedimentary cover, the constraint that implies reheating was removed from the modelled t-T history of KJ-19, thus forcing temperatures below 20 °C from the entire interval between 50 Ma and present time (Fig 49b). The attempt of generating a model that supports this scenario is clearly not fully successful, considering that the proposed good paths enter the box towards the very end of the time interval given by the constraint. It is thereby apparent that the constraint is forcing a model that is not well-suited to the data.

7.3.2 Mesozoic peneplanation and reburial

A wide range of ages has been suggested for the peneplain in southern Norway (c.f. section 2.4.1). In order to acknowledge the previous literature on this topic, further constraints were added to the basic model of KJ-19 to force the sample to the surface at various times during the Mesozoic (Fig. 49). Given the required time of residence in the PAZ for the samples to acquire the observed track length distributions, reburial is a necessity. Consequently, two series of constraints were included in the models. The first constraint accounts for cooling to surface temperatures (i.e. 0-30 °C) and is implemented as a series of boxes that span 20 Ma and altogether cover the time interval between 160 and 60 Ma. According to Fossen et al. (1997), the coastal regions of southwestern Norway were transgressed in Oxfordian times. Hence, only post-Middle Jurassic peneplanation scenarios are tested. Reburial is accounted for by applying a large box that extends from the youngest age limit of the first constraint to

the present and from 30-100°C. It is evident that cooling to surface temperatures prior to 140 Ma implies high cooling rates throughout much of the Jurassic, while later cooling involves residence within the PAZ until the Cretaceous period, followed by accelerated cooling prior to the inferred peneplanation. Relatively rapid reheating to temperatures between 60 °C and 80 °C is suggested in all models, although the steepness of the curve increases as the constraints are moved towards younger ages. Late Jurassic and Early Cretaceous peneplanation scenarios imply residence within the PAZ for as much as 60 Myr following reburial. All models suggest stable, moderately high cooling rates (0.6-1 °C/Ma) after the peak temperature of the reheating event (i.e. between the Early Cretaceous and the Eocene). In order to document the thermal effects of the Mesozoic peneplanation scenario, similar constraints have been tested for additional samples from the Hardangervidda plateau. The obtained models are enclosed in Appendix E.

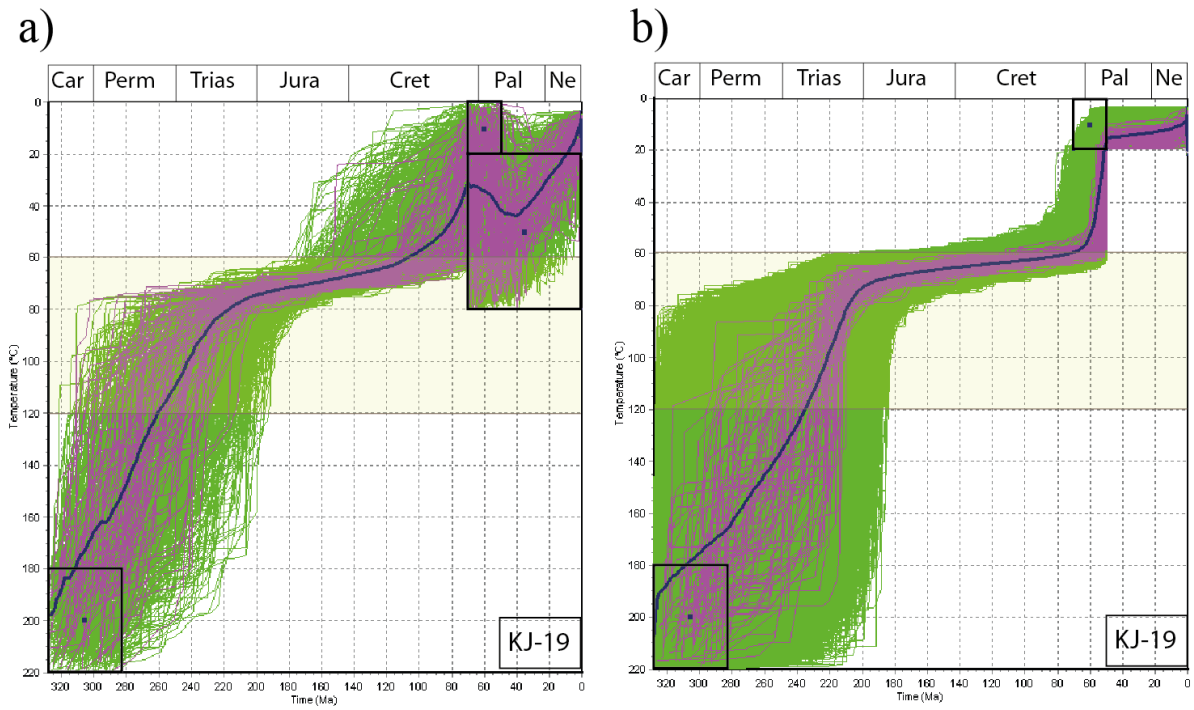

Fig. 48. Thermal history models of KJ-19, with additional constraints according to the peneplanation-uplift-model: **a)** Surface temperatures in the Paleocene and subsequent reheating to temperatures between 20 °C and 80 °C **b)** Paleocene surface temperatures without subsequent reheating. The model infers nearly instantaneous cooling from the PAZ at ~ 60 Ma, followed by thermal quiescence.

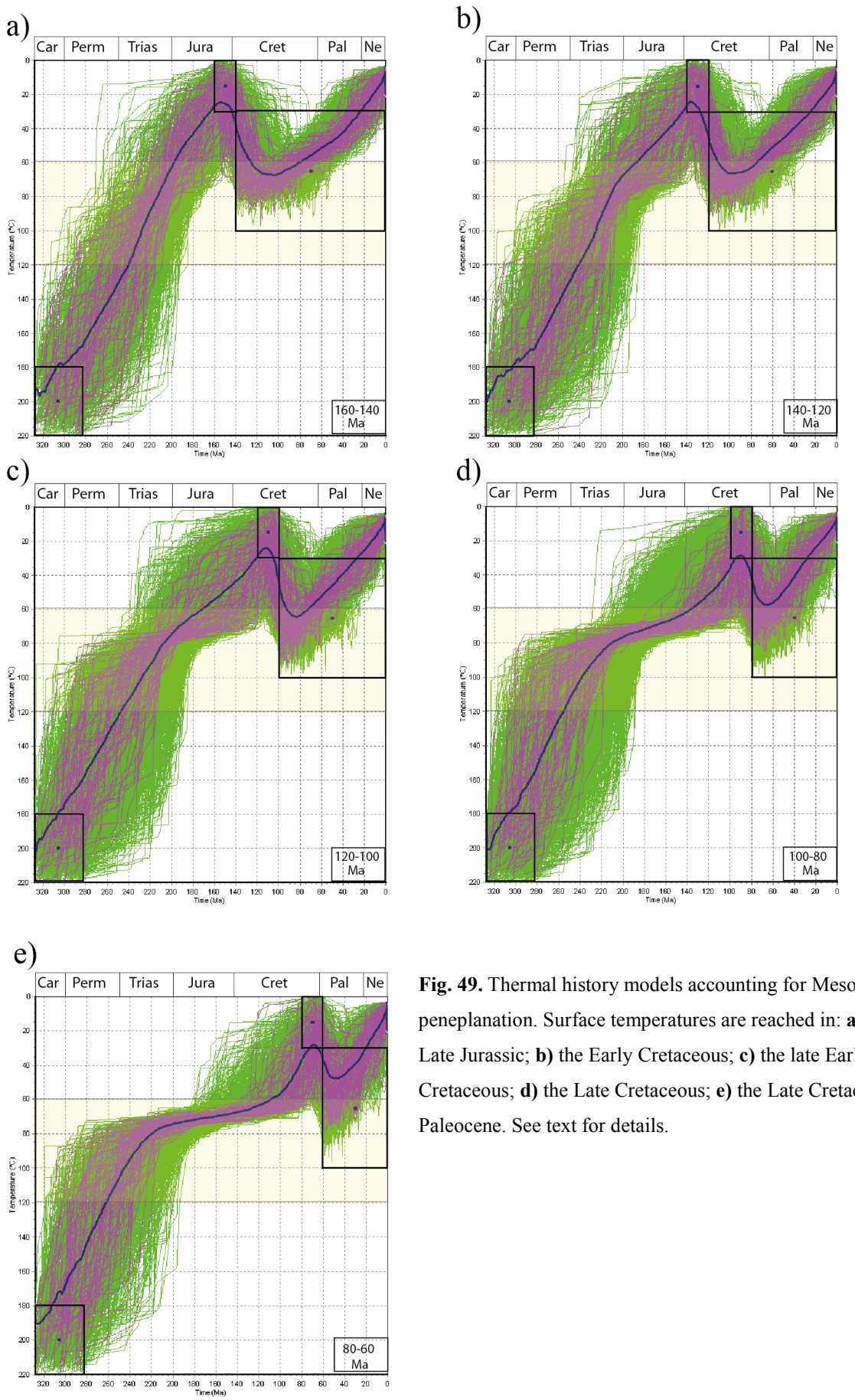

Fig. 49. Thermal history models accounting for Mesozoic peneplanation. Surface temperatures are reached in: **a)** the Late Jurassic; **b)** the Early Cretaceous; **c)** the late Early Cretaceous; **d)** the Late Cretaceous; **e)** the Late Cretaceous-Paleocene. See text for details.

8. INTERPRETATION AND DISCUSSION

The analyses performed during the course of the present study have resulted in thirty-two fission track ages, two (U-Th)/He ages and a range of thermal history models. In the following sections the quality and possible implications of the obtained data will be addressed. In order to create a basis for interpretation, the first section will assess the influence of data quality and analytical bias on the obtained results. This is followed by the interpretation of fission track and (U-Th)/He data, thermal history models and observed structures. The obtained results will then be compared with the results from previous studies undertaken in the vicinity of the study area and local and regional exhumation histories will be proposed. Finally, the thermochronological results will be compared to the predictions of the peneplanation-uplift model and the ICE hypothesis.

8.1. Assessment of data quality

8.1.1 AFT ages

The quality of the results obtained from fission track analysis is highly dependent on the specific characteristics of the analysed samples. One of the factors that may lead to systematic errors is inhomogeneous U-distributions within the analysed grains. A considerable proportion of the analysed samples were found to contain strongly zoned grains. If counting is performed on the U-poor section of a zoned grain, imprecise alignment may shift the grid towards the print of the U-rich portion of the crystal, thus causing an overestimation of ^{238}U and a grain age that is too young. Gradual changes in the density of tracks are not always easily detectable and the effect of zoning on the resulting ages is therefore not readily assessed.

The errors on the fission track ages obtained in the study are generally very low (i.e. typically between 5% and 8% of the calculated central age), possibly reflecting the good quality of the majority of the analysed grains. KJ-24 has an older age and a considerably higher error than all other samples included in the study (i.e. 16 % of the central age). The main reason for this is probably the extremely low U-content of this sample (cf. Fig. 26f). Few counted tracks give an imprecise ratio of the spontaneous to induced track density that may be prone to significant variability between grains. The thermal effect of the Caledonian orogeny caused total resetting of the apatite fission track system throughout southwestern

Norway (inferred by reset 40Ar/39Ar ages; e.g. Fossen & Dunlap, 1998), and pre-Caledonian ages are thus not expected for samples from the inner Hardangerfjord region. It is assumed that the Ordovician and Precambrian ages obtained from individual apatites in KJ-24 reflect the uncertainties associated with the analysis of extremely U-poor samples.

The chi-square test is passed by all samples analysed in the study with the exception of KJ-15 (Table 3). A failed chi-square test indicates the presence of more than one grain age population. KJ-15 is a granitic lithology obtained from the Precambrian basement and all grains are thus expected to have experienced identical cooling histories. The failed chi-square test is therefore inferred to reflect analytical complications rather than real differences in grain ages. KJ-15 was found to suffer from particularly poor grain quality (cf. Fig. 26a), which may have affected the counting results.

Sample BG-16 from the Granvin area exhibits a young AFT ages that deviate from the general age pattern observed in the inner Hardangerfjord region (i.e. Barremian to Aptian ages at sea level north of the fjord and progressively increasing ages with elevation). The particularly young age of BG-16 is surprising, considering that the sample was collected at an elevation of 500 m asl and is expected to have cooled out of the PAZ relatively early compared to the majority of sea level samples from the area. Difficulties were encountered during the analysis of BG-16 as the surfaces of most grains were found to be obscured by numerous cracks and scratches (cf. Fig. 26b). The scratched crystal surfaces lower the perceptibility of spontaneous tracks significantly, thus causing a decrease in the apparent AFT age. For analytical reasons the age of BG-16 is therefore considered a minimum age, and the sample will be treated with caution during the discussion of the possible geological implications of the data obtained in the study.

8.1.2 Mean track lengths

The generally low U-concentration that characterises the apatites from the basement of the inner Hardangerfjord region limits the number of samples suitable for confined track length measurements. 100 measured track lengths were obtained for 10 samples. In BG-26 only 63 tracks could be measured, and therefore the thermal history model generated from this sample is less robust than the remaining models.

The reproducibility of apatite fission track length data was assessed in a recent contribution by Ketcham et al. (2009). As part of this study a number of different analysts were invited to measure track lengths in two pre-selected grain mounts. The resulting MTLs and track length distributions were found to show great scatter. It is thereby clear that the

track length measuring procedure is significantly affected by biases introduced by the analyst, and the estimated MTLs hold considerable uncertainty. According to Ketcham et al. (2009), an important part of the problem is related to the lack of an efficient calibration procedure. Commonly, the analyst fails to recognize short confined tracks and the resulting MTL is driven towards a high value. The fact that long confined tracks are more likely to intersect surface tracks contributes to this bias (Laslett et al., 1982). In the present study the obtained track length distribution signatures are found to be dominated by rather short tracks, evident by MTLs within the range 10.41 ± 0.25 μm to 11.66 ± 0.23 μm. Problems associated with overestimation of MTLs thus appear to have been avoided. Instead, the recognition of the total lengths of some of the measured tracks was impeded by poorly defined track tips. F-rich apatite varieties, which are predominant in the analysed samples, have particularly low etching efficiencies. Consequently, local underetching of tracks may be a problem and the obtained track length distributions may possibly contain an overly high proportion of relatively short tracks.

8.1.3 Inverse thermal history models

Inverse thermal modelling is a useful tool for acquiring knowledge about the regional cooling style. However, thermal history models do not by any means provide the ultimate solution to the thermal evolution of the analysed samples. The models present a range of possible cooling histories and can be used as a guide to which conditions are required for the sample to attain its specific AFT characteristics. As demonstrated in chapter 7, the suggested time-temperature paths are highly dependent on the constraints applied to the model. Hence, a model is no better than the assumptions that constitute its basis. The low-temperature thermochronological data from which a model is generated, are subject to analytical biases that introduce additional errors. Track length distribution signatures exert a major impact on the suggested cooling paths. An MTL that is biased towards a low value will force the model to suggest a long residence time within the partial annealing zone. Conversely, an overestimated MTL entails rapid cooling through PAZ temperatures. In the inner Hardangerfjord region there are no independent observations or data that reveal aspects of the thermal history from the time of closure of the zircon fission track system to the present. It is not justifiable to introduce additional constraint solely to restrict the paths, and consequently, a vast range of possible cooling histories are supported by the data. In the present study, additional thermal constraints have been implemented in order to test a range of geological

scenarios proposed in previous studies. The purpose of this approach is to determine the degree to which the data are in agreement with the inferred geological processes.

8.1.4 (U-Th)/He ages

Two (U-Th)/He single grain analyses yielded unreliable ages due to U- and Th-concentrations below the detection limit. For the remaining grains the total analytical error ranges from 2.4 % to 3.2 %, which is regarded as acceptable. The poor reproducibility observed for the samples KJ-8 and KJ-25 may be attributed to a variety of factors, including the presence of minute mineral inclusions and other impurities. Differential zoning characteristics alone are not sufficient to account for the spread in single grain ages, but may contribute to the mineralogical bias. Normally, He re-extraction signatures are expected to be indistinguishable from blank levels. Excess He in the crystal subsequent to the main degassing may indicate the presence of U-Th-rich mineral inclusions within the analysed grain (Farley, 2002). Two of the grains from sample KJ-19 yielded slightly elevated He re-extraction values (Appendix D). As explained in section 3.6.5, mineral inclusions introduce parentless He to the apatite crystal and thus increase the grain age. Although no inclusions were detected in the crystals prior to analysis, a potential effect of excess He derived from foreign mineral species cannot be ruled out completely.

The alpha-ejection correction of Farley et al. (1996) requires a homogeneous U-Th-distribution and may not provide a good representation for the samples from the inner Hardangerfjord region. Pronounced concentric zoning is evident for both the samples that show reliable (U-Th)/He results. KJ-19 principally displays grains with U-rich cores and relatively wide, U-poor rims. The U-distribution pattern in KJ-11 is more complex, with thin, concentric zones of extremely high U-concentration within a bulk material characterized by a rather low content of U. Since the samples included in the study generally exhibit increasing concentrations of parent nuclides from the rim towards the core, the F_T- correction will overestimate alpha-ejection, and the corrected (U-Th)/He ages will be too old. In comparison, uncorrected (U-Th)/He ages do not account for alpha-ejection from the U-poor rim and will be too young. Considering the higher contribution of He from the core of the grain relative to the rim, the uncorrected age is suggested to represent the best approximation for the samples analysed in the present study. Fig. 50 illustrates the influence of zoning on the corrected (U-Th)/He age for typical grains from KJ-11 and KJ-19.

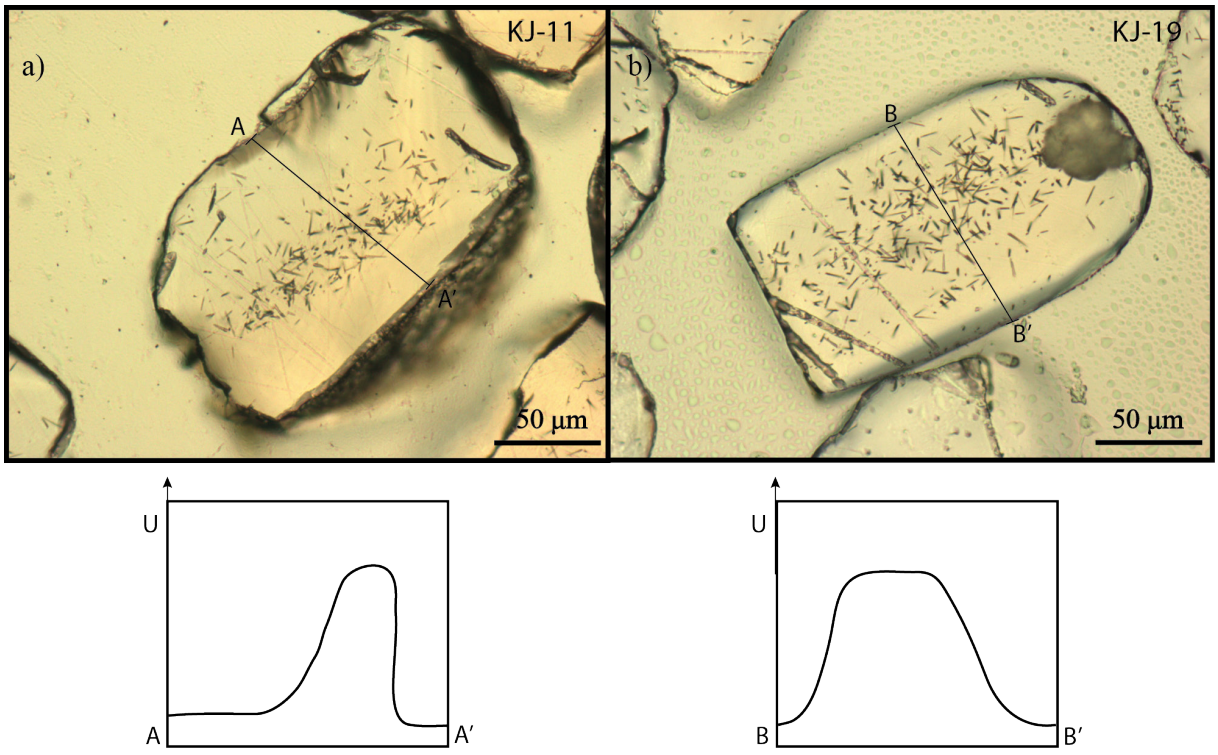

Fig. 50. Typical zoned apatites from KJ-11 and KJ-19 with qualitative U-distribution profiles: **a)** Grain from KJ-11. Elevated U-concentration is evident in the core region. The rim is characterized by a very low track-density, which implies that the effect of alpha-ejection is limited; **b)** Apatite from KJ-19. This grain displays a wider U-rich core than the grain in a. The outermost U-poor rim is generally more than a stopping distance (i.e. ~20 µm) wide and the effect of alpha-ejection is probably not pronounced. Both distribution patterns are associated with over-corrected (U-Th)/He ages when applying the approach of Farley et al. (1996).

The (U-Th)/He system records cooling through lower temperatures than the AFT system and is generally expected to yield younger ages. When considering the uncorrected (U-Th)/He ages, this relationship holds for most grains. However, some single grain ages are found to be considerably older than the corresponding AFT ages. This is obviously challenging to explain, since it implies earlier cooling through the PAZ than through the HePRZ. As discussed above, anomalously old (U-Th)/He ages may be attributed to minute mineral inclusions and to some extent zoning. Additionally, internal factors that influence the production and retention of He in apatite may lead to erroneous results. Based on step-heating diffusion experiments, Shuster et al. (2006) discovered that the effective closure temperature of the (U-Th)/He system increases with concentration of radiogenic He. Alpha recoil damage may impede He diffusion, which ultimately leads to (U-Th)/He ages that are too old. This effect is believed to be most pronounced for old samples that have accumulated extensive radiation damage. A general positive relationship between effective U-concentration (eU) and

(U-Th)/He age is found for the samples analysed in the present study (Fig. 42). As expected from the He trapping model of Shuster et al. (2006), the relationship is least pronounced for the youngest sample, KJ-11. It is thus concluded that the cumulative effect of radiation damage may have significantly affected the retentive properties of the analysed grains, causing overestimated (U-Th)/He ages. The degree to which this process has influenced the results is not known and the presumably reasonable ages obtained from KJ-11 and KJ-19 will still be discussed in terms of their geological implications in following sections.

8.2 Interpretation of apatite fission track and (U-Th)/He data

All samples measured in the present study display wide confined track length distributions and short mean track lengths that are suggestive of slow cooling through the PAZ. The obtained fission track ages are therefore interpreted as apparent ages that record cooling through the temperature interval between 120°C and 60 °C. As a result of the presumed slow ascent through the crustal depths associated with PAZ temperatures, the cooling and exhumation rates obtained from the vertical profiles partly reflect the relative positions of the samples within the PAZ (cf. Fitzgerald & Gleadow, 1990; Gallagher et al., 1998). Based on the heat flow data of Pascal et al. (2010), a low present-day geothermal gradient of ~20 °C is estimated for the inner Hardangerfjord region. Similarly low paleogeothermal gradients have previously been calculated for the Mesozoic (e.g. Leighton, 2007). Hence, a gradient of 20 °C is inferred for the Jurassic-Cretaceous and is implemented in the cooling rates presented in following sections. The supposedly low geothermal gradient implies relatively limited temperature differences between samples in the vertical profile and justifies the estimation of cooling rates based on age-elevation relationships. Nevertheless, the lowermost samples are inferred to have resided at higher temperatures throughout the cooling history and are more strongly affected by annealing-related age reduction. Consequently, the cooling rates presented below may be slightly underestimated.

Several studies have stressed the influence of topography on isotherms and its potential effect on low-temperature thermochronometers such as AFT and particularly (U-Th)/He (House et al., 1998; Mancktelow & Grasemann, 1997; Stüwe et al., 1994). Isotherms are generally found to be far apart beneath ridges and closely spaced beneath valleys (e.g. Stüwe et al., 1994). The high-relief topography that characterises the inner Hardangerfjord region could potentially have a pronounced effect on the position of isotherms in the uppermost crust. However, the main geomorphological features in southwestern

Norway were attained during a series of glaciations between ca. 2.5 Ma and 11.5 ka (Nesje & Whillans, 1994), and thus post-date the youngest AFT and (U-Th)/He ages obtained in the present study by more than 94 Ma and 66 Ma, respectively. Although fjords and glacial valleys were likely carved into pre-existing topographic lows, extreme longevity is required for the topographic features to be preserved over the time interval in question. The position of the isotherms may have shifted significantly since the samples entered the PAZ and the HePRZ, and the topographic effect, if any, is difficult to assess. Consequently, the deflection of isotherms is not taken into account in the interpretations presented below.

8.2.1 Osa profile

Samples collected at high elevations are generally inferred to have cooled through the isotherms at an earlier stage than samples collected close to sea level and apatite fission track ages are therefore expected to increase with altitude. In the Osa area the complete picture is, however, much more complex. The middle-upper part of the profile displays nearly identical ages (from 155 ± 10 Ma to 169 ± 11 Ma) over a relief of > 850 m. Significant scatter is found across short vertical distances in the lowermost and particularly the uppermost portions of the transect. As described in chapter 6.1.1 the Osa area is characterised by numerous lineament populations and displays a generally high fracture density. The distribution of fission track ages is thus suggested to be strongly influenced by faulting (Fig. 51). Differences in cooling ages for adjacent fault-bound blocks are expected where the displacement is of sufficient magnitude to be resolved by the AFT method. The ages obtained from opposite sides of major lineaments in the Osa area generally do not differ by more than their 1σ errors. Consequently, the fission track record is not conclusive with regard to fault activity, but the disordered and locally inverted age-elevation relationship strongly suggests displacement along some of the observed lineaments. KJ-26 and BG-14 are relatively closely spaced, but record significantly different AFT ages of 155 ± 10 and 184 ± 12 Ma, respectively. From the aerial photograph in Fig. 51 it is clear that the two samples are separated by a distinct N-S-trending lineament. It could be argued that down-to-the-west displacement along this structure may have caused exhumation of rocks from deeper crustal levels in the eastern block, thus causing the young age of KJ-26. However, further field observations are required to validate this interpretation. It should be noted that BG-14 is significantly older than KJ-25 (159 ± 9 Ma), which is derived from a higher elevation to the west. The possibility for differential exhumation across mainly N-S trending structures in the area between the samples cannot be ruled out, considering the high density of lineaments with such attributes to the east of the Nipahøgdi peak. The middle

part of the profile is dissected by several major NW-SE- to N-S-trending structures. Two pronounced lineaments are evident between KJ-1 and KJ-3. KJ-3 is derived from a lower elevation than KJ-1, but displays a similar age (169 ±11 Ma, as opposed to the age of 166 ± 11 Ma obtained from KJ-1). Juxtaposition across one or both of the intervening structures is conceivable. The inferred faults are found to exhibit opposite dip directions. It is therefore not clear which sense of movement is required to produce the observed age pattern, and the effects of the individual structures cannot be determined. A substantial jump in AFT age is found between KJ-5 (163 ± 9 Ma) and KJ-6 (132 ± 10 Ma) in the lower part of the profile. The age difference may be attributed to down-to-the-east extensional displacement along a N-S-trending fault that extends across the valley between the sampling localities. The age obtained from KJ-31 on the northwestern margin of the Osafjord (125 ± 9 Ma) is slightly older than the age of KJ-8 (111 ± 9 Ma) from a higher elevation on the opposite

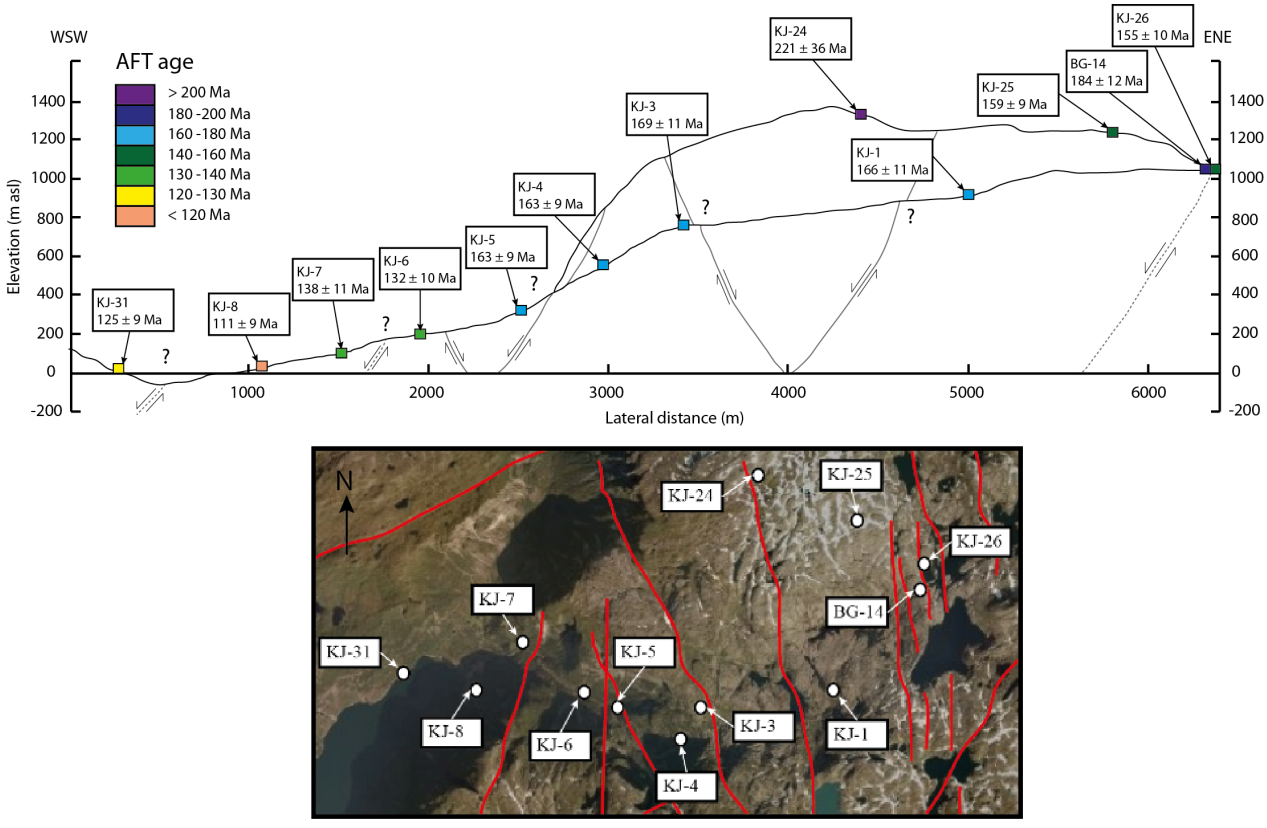

Fig. 51. Interpretation of the AFT ages from the Osa profile, illustrated schematically. Stippled lines indicate insufficient field data for determination of fault orientation. The proposed sense of shear along individual structures is based on the fission track ages of the fault-bound blocks. Question marks indicate that the presumably offset ages overlap within error. Consequently, the data are not conclusively in favour of fault displacement. A section of the aerial photograph from Osa is shown for comparison.

margin, and thereby suggests down-to-the-northwest displacement across the fjord. However, the ages overlap within error and differential exhumation cannot be substantiated. The juxtaposed AFT ages in the Osa profile require Middle-Late Jurassic or later reactivation of structures. Assuming that faulting in general causes enhanced denudation of the up-faulted block, the pattern of ages is concordant with mainly extensional displacement. Since no apparent age-elevation gradient can be established, the magnitude of displacement for the individual faults cannot be determined. The complex pattern of brittle structures in the Osa area makes it difficult to assess which of the individual fault populations may have been reactivated during post-Middle Jurassic times. Offset fission track ages are observed across N-S-, NW-SE- and possibly NNE-SSW – NE-SW-trending lineaments.

The MTLs obtained from the Osa samples KJ-8 and KJ-25 are 10.59 ± 0.25 μm and 11.11 ± 0.26 μm, respectively. According to the general shape of the cooling paths obtained from the thermal history models, both samples experienced rapid cooling into the PAZ in the Permian-Early Jurassic, followed by protracted, slow cooling (cf. Fig. 42). This cooling history would imply a prolonged time of residence in the PAZ for the lower sample, KJ-8, and thus reduced track lengths as a result of extensive annealing. The observed relation between MTL and elevation is therefore reasonable. Interestingly, KJ-8 displays a bimodal track length distribution. According to Gleadow et al. (1986) bimodal distribution signatures are generally associated with reheating events. Potential causes of reheating include reburial by sediments, thermal disturbances in relation to intrusions and hydrothermal circulation along fault systems. Reburial is considered highly unlikely as a cause of the observed bimodal distribution in KJ-8, considering that KJ-25 does not record reheating. There is no evidence for igneous activity onshore southern Norway since the Triassic. Hydrothermal circulation in the densely spaced brittle structures in vicinity to the Osafjord may potentially have caused enhanced annealing of fission tracks in KJ-8. It is, however, uncertain whether numerous, short episodes of hydrothermal heating could have produced two distinct peaks in the track length distribution histogram.

8.2.2 Kjeåsen

From the age-elevation plot in Fig. 33, a break in slope is apparent at 124 Ma. An abrupt change in the slope of the regression line, from steep in the lower portion of an age-elevation plot to gentle at higher elevations, has traditionally been interpreted as an indication of a recent episode of accelerated exhumation (e.g. Gleadow & Fitzgerald, 1987; cf. chapter 3.5.3). The upper portion of the Kjeåsen profile records an apparent cooling rate of ~0.2

°C/Ma, which is very slow compared to the rate of ~5.4 °C/Ma obtained from the lower part. Late Cretaceous accelerated cooling is not recorded elsewhere in the study area, nor has it been recognized by independent means. It is thus important to assess whether the apparent break in slope represents a real cooling event. For basement rocks that have cooled relatively rapidly from temperatures below those of the PAZ (i.e. samples from the lower part of the profile), the expected MTL is normally >14 μm (Gallagher & Brown, 1997). Samples that record prolonged residence within the PAZ (i.e. samples derived from the portion of the profile above the break in slope) are expected to exhibit shorter MTLs and wider track length distributions. The uppermost and lowermost samples from the Kjeåsen profile display nearly identical MTLs of ~11.5 μm. Since the short MTL of KJ-11 is not in concord with rapid cooling through the PAZ, an Early Cretaceous episode of accelerated cooling is considered unlikely. This interpretation is corroborated by the thermal history models from the Kjeåsen samples, which do not support enhanced cooling rates at ~120 Ma (cf. Fig. 44). In fact, thermal quiescence and residence within the upper PAZ is required throughout the Early Cretaceous in order to produce the observed track length distributions. Provided that the age-elevation trend observed for the Kjeåsen samples is not a result of a cooling event, other geological processes must be responsible for the nearly identical ages obtained from the lower 800 m of the transect. As demonstrated for the Osa profile in the previous section, faulting can produce unrealistically steep and locally reversed age-elevation gradients. The age distribution in the Kjeåsen profile is thus interpreted to be a result of fault-related differential exhumation. For reasons discussed in section 8.3.4, it is reasonable to infer that the inner portion of the Hardangerfjord may function as a major structural discontinuity. In order to reveal the nature of the identified discontinuity and evaluate its possible implications for the tectonic evolution of the area, it is necessary to consider the results from all vertical profiles and additional samples jointly. Thus, the thermochronological results from the Kjeåsen profile will be further elaborated when the combined exhumation history of the entire inner Hardangerfjord region is discussed in chapter 8.6. As a first-order assessment, the AFT age pattern obtained from the Kjeåsen profile may be interpreted as an indication of down-to-the-southeast displacement across the Simadalen segment of the structure. A throw of ~750 m is inferred from the age of KJ-11 and the age-elevation gradient in the upper part of the profile. Assuming a general error of ± 10 Ma on the fission track ages, the minimum throw that can be detected by the AFT data from the Kjeåsen profile is ~250 m. This estimate assumes that the samples from the northern margin of the Simadalsfjord have not been juxtaposed subsequent to the time of entry into the PAZ. A small number of NE-SW - NNE-SSW-trending

lineaments are found to dissect the upper part of the sampled profile (see Fig. 22). Due to limited field data from these structures, no inference about dip direction and sense of movement can be made. Differential exhumation across these structures may potentially have contributed to the very shallow age-elevation gradient observed for the upper part of the Kjeåsen profile (Fig. 52). However, the low apparent cooling rate may also reflect actual, very slow exhumation during Middle Jurassic-Early Cretaceous times. Assuming that all samples derived from the northwestern margin of the Simadalsfjord have experienced the same thermal history, an apparent cooling rate of 0.3 °C/Ma and an exhumation rate of 14 m/Ma are estimated.

The MTLs obtained from the Kjeåsen profile are within the range 10.93 ± 0.20 µm - 11.52 ± 0.20 µm. Wide track length distributions are obtained for all samples and reveal complex cooling histories that involve prolonged residence within the PAZ and possibly episodes of mild reheating. The MTL of KJ-11 from sea level south of the Simadalsfjord (11.51 ± 0.19 µm) is significantly longer than the MTL of KJ-21 obtained from an elevation of 807 m asl on the opposite flank (10.93 ± 0.20 µm). This relation implies a longer period of residence in the PAZ for KJ-21 and suggests later juxtaposition of the fjord flanks, possibly as a result of down-to-the-southeast displacement across the Simadalsfjord. Hence, the MTLs for the Kjeåsen profile are in good agreement with the interpretations drawn from the AFT ages.

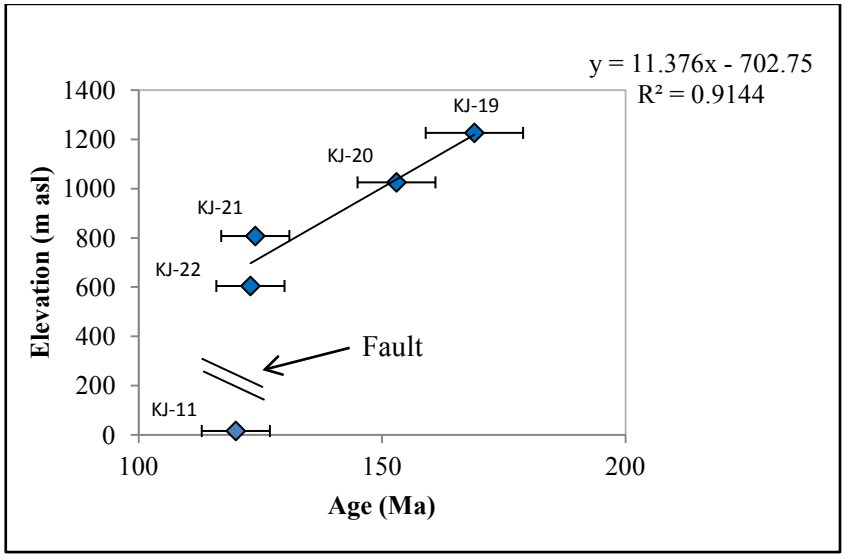

Fig. 52. Interpretation of the age-elevation relationship of the Kjeåsen profile. The lowermost sample, KJ-11, is located on the southern margin of the Eidfjord, which is suggested to coincide with a major crustal discontinuity. The samples from higher elevations on the north flank are inferred to record steady cooling through the PAZ.

The spatial separation between the sea level sample, KJ-11, and the Hardangervidda sample, KJ-19, is large and the obtained (U-Th)/He data unfortunately do not provide detailed information on the cooling path of the Simadalen area. In order to shed light on aspects of the post-Jurassic thermal evolution, the (U-Th)/He ages can be combined with the data from fission track analysis. The mean (U-Th)/He ages of KJ-11 and KJ-19 are younger than the obtained AFT ages by ~40 and ~50 Ma, respectively, and indicate cooling through the temperature interval between 80°C and 40° C in the Cretaceous. By assuming lowered effective closure temperatures for the AFT and (U-Th)/He systems during slow, monotonous cooling (cf. Dodson, 1973), an average cooling rate of < 1 °C/Ma is calculated for the Middle Jurassic-Late Cretaceous. This estimate is in accord with the rate obtained from the AFT data in the upper part of the profile and the thermal history models. (U-Th)/He data have the potential of revealing further information on the timing of faulting along the Simadalsfjord. If down-to-the-southeast fault activity occurred mainly before the (U-Th)/He signatures of the samples were attained, equal (U-Th)/He ages would be expected from corresponding elevations on both margins, and the temporal separation between the AFT age and the (U-Th)/He age would be greater on the southeastern flank than on the northwestern flank. The nearly similar separation found on both flanks of the fjord may indicate significant post-Early Cretaceous differential exhumation. However, the credibility of this assessment is greatly reduced due to the generally poor reproducibility of (U-Th)/He ages achieved in the current study.

8.2.3 Bu

In general, the Bu profile shows a good correlation between age and elevation, but there is a marked discontinuity in the trend between 640 m and 790 m asl. The good age-elevation correlation that is evident when the upper and the lower portion of the profile are considered separately possibly indicates common cooling histories for all samples within each of the segments. The relatively young AFT ages below ~640 m asl imply that the lower part of the profile records later exhumation than what would be expected from the cooling trend of the upper portion of the transect. The observed distribution may possibly reflect faulting along a structure that extends across the Bu valley and divides the profile between KJ-13 and KJ-14 (Fig. 53a). It should be noted that no such structure is readily evident from the lineament map in Fig. 23. The two segments of the age-elevation plot record strikingly similar gradients, which further support the interpretation of differential exhumation as a result of faulting. KJ-16, with its Late Jurassic age, does not fit into this interpretation, and hence must be classified

as an outlier. The legitimacy of such an assessment is questionable, considering the absence of analytical explanations for the old age of KJ-16. Alternatively, the observed distribution of AFT ages may be explained by down-to-the-west displacement across a roughly N-S-trending structure that divides the profile into two distinct blocks (Fig. 53b). Interestingly, the comparably younger samples are all located further to the east than the older samples. Pronounced, densely spaced NNW-SSE-trending lineaments are observed directly across the Eidfjord in the Bruravik area. Whether these structures continue across the fjord and dissect the southern flank is not known for certain, but structures belonging to the NNW-SSE - NNE-SSW-trending system generally appear to make up large-scale discontinuities that can be traced across considerable lateral distances in the inner Hardangerfjord region. It is considered likely that such faults may also dissect the Bu area, although aerial photographs do not immediately reveal the presence of a distinct lineament, across which the AFT ages may have been offset. As evident from Fig. 53b, KJ-16 fits excellently into the age-elevation trend of the westernmost samples. KJ-28 is derived from Vatnasetenuten and is the easternmost sample included in the profile. Despite its location within the presumed eastern block, KJ-28 records an old age that is compatible with the age-elevation gradient of the western samples. From the aerial photograph in Fig. 23 it is clear that KJ-28 is separated from the remaining samples in the profile by several additional lineaments. Although their records of displacement are unknown, it is considered likely that differential movement across some of these structures may have produced a slightly different exhumation history for KJ-28 than for the other samples derived from the presumed western block. Regardless of which fault is interpreted to have caused the distinct difference between the two segments of the profile, the AFT age pattern implies a throw of ~1200 m. The Caledonian thrust boundary, which clearly predates the recorded faulting in the Bu area, is located at rather similar elevations throughout western Hardangervidda. Consequently, the estimated throw appears to be unreasonably large. In this respect, it should be noted that the calculations are based on the age-elevation gradient determined by regression and do not account for the errors on individual ages. AFT ages may be applied in order to constrain the timing of displacement. The youngest age recorded in the down-faulted block is assumed to reflect the maximum age at which displacement would produce different AFT signatures across the fault. Thus, faulting must have occurred during the time interval between the latest Jurassic and the present. As a result of the relatively steep age-elevation gradient, the minimum detectable throw calculated for the Bu profile is ~950 m, i.e. significantly greater than for the Kjeåsen profile. An apparent

cooling rate of 1 °C is estimated for the Middle Jurassic-Early Cretaceous. This corresponds to an exhumation rate of 49 m/Ma.

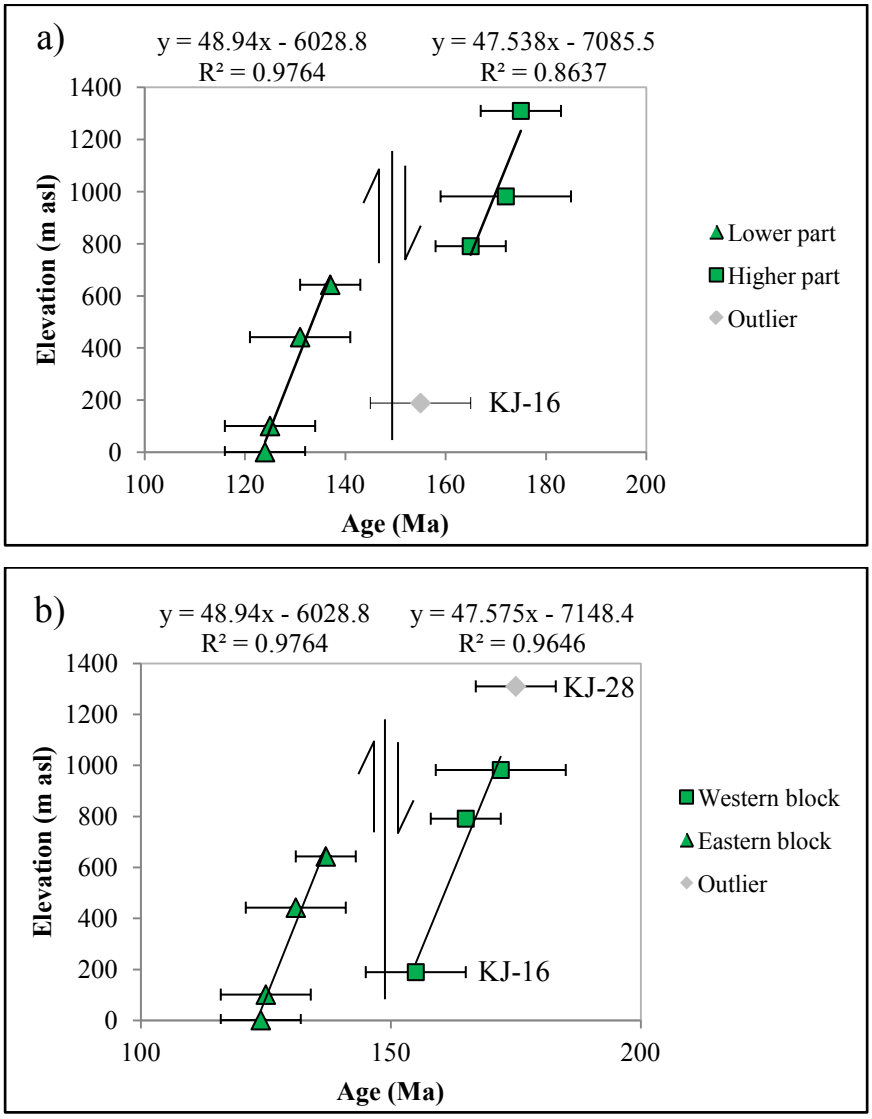

Fig. 53. Possible interpretations of the Bu profile: **a)** Age-elevation relationship explained in terms of down-to-the-south movement along a fault that crosses the Bu Valley between KJ-14 and KJ-13. The age of KJ-16 is not consistent with this interpretation. Accordingly, KJ-16 is assumed to be an outlier. **b)** Scenario involving down-to-the-west movement along a presumably N-S-trending fault. KJ-28 (marked outlier) is located far from the other samples and may belong to a third structural block.

KJ-18 from sea level near Brimnes and KJ-28 from Vatnasetenuten at 1310 m asl both show wide track length distributions that are skewed towards the higher values of the track length diagram. KJ-18 is believed to have resided within the PAZ for a longer period of time than KJ-28. This is reflected by its shorter MTL. Unexpectedly, the middle sample, KJ-14, displays the shortest MTL obtained from the profile. KJ-14 is assumed to have resided at

lower temperatures than the sea level sample throughout the inferred slow cooling in the Jurassic-Cretaceous and should thus have experienced less annealing. It should be noted that the track length distribution of KJ-14 contains three frequency peaks. Trimodal track length distributions are normally not encountered, and it is difficult to envision which thermal history could have produced this distinct signature. Hence, it is considered likely that the MTL of KJ-14 is affected by significant analytical bias, possibly as a result of particularly poor perceptibility of track tips.

8.2.4 Summarised interpretation of vertical profiles

Assuming that the Kjeåsen profile is best explained by juxtaposition across the Simadalsfjord, there are no indications of any rapid cooling events within the time interval defined by the obtained ages. Thermal history modelling of samples from the inner Hardangerfjord region suggests possible accelerated cooling during the Cenozoic. It is thus considered likely that rocks residing below the PAZ prior to the assumed cooling event are not yet exposed at the surface. In a typical age-elevation diagram, the sampled profiles are therefore inferred to plot above the break in slope.

8.2.5 Additional samples

An easily noticeable feature in the AFT record from the inner Hardangerfjord region is the remarkably young ages and short track lengths obtained from the samples from the Granvin area. For analytical reasons, the age of BG-16 may be unreasonably young (cf. section 8.1.1) and is not taken into account in the following discussion. BG-26 from the western flank of the Granvinfjord displays an age of 105 ± 5 Ma and is considerably younger than the majority of nearby samples. Interestingly, the sampling site of BG-26 is situated within internal portions of the HSZ. Numerous densely spaced lineaments are found in association with the shear zone in this area. These parallel features may represent brittle structures developed during late stages of Caledonian orogenic collapse (Fossen & Hurich, 2005). The abnormally young age of BG-26 is interpreted as a result of Mesozoic reactivation of the NE-SW-trending fracture set, accompanied by convective heat transfer from circulating meteoric water along the fault surfaces. Previous studies (e.g. Wölfler et al., 2010) have shown that hydrothermal fluids of sufficient temperature may affect the apatite fission track system by partially resetting ages and track length signatures. Heat transfer principally affects a narrow zone in immediate vicinity to the fault surface. The timing of hydrothermal alteration is constrained by the obtained fission track age. For BG-26 this implies post-Early Cretaceous fault reactivation.

Mylonitic fabrics related to the Hardangerfjord Shear Zone have been reported from the Bruravik area (Fossen & Hurich, 2005), from which the relatively young sample KJ-27 was obtained. In a similar manner as for BG-26, KJ-27 may potentially have been influenced by hydrothermal activity associated with brittle reactivation of structures within the deformation zone of the HSZ. High fracture densities (generally dm-m scale spacing between joints) are observed throughout the studied area. In this respect, the sampled outcrops in Granvin and Bruravik do not differ substantially from the inner Hardangerfjord region in general, and the fracture densities of the sampling sites of BG-26 and KJ-27 cannot unequivocally explain why these samples in particular would have been affected by hydrothermal fluid flow. All four remaining samples collected outside the vertical profiles record cooling through the PAZ in the Early Cretaceous (120-130 Ma).

8.3 Interpretation of inverse thermal history models

8.3.1 Rapid Permo-Triassic cooling

The thermal history models presented in chapter 7 indicate rapid cooling during the Permo-Triassic, consistent with the timing of the earliest, well-documented North Sea rift phase (e.g. Færseth et al., 1995) and with previous thermochronological studies from southern Norway (Andriessen & Bos, 1986; Dunlap & Fossen, 1998). Rift flank uplift associated with basin development is suggested as the dominant cause of the high exhumation rates. An average Permo-Triassic cooling rate of 2-6 °C/Ma is calculated from the basic thermal history models from the inner Hardangerfjord region. In general, the pre-Jurassic cooling is found to be poorly constrained, and a precise estimate is difficult to obtain. The time prior to the Early Jurassic is not resolved by the AFT ages, and hence there is no basis for comparison of cooling rates inferred from thermal history models and age-elevation gradients.

8.3.2 Jurassic-Cretaceous thermal quiescence

The shift from rapid cooling in association with the first phase of rifting to the lower cooling rates found for the Jurassic-Cretaceous is not well constrained by the thermal history models, but is tentatively pinned to the Late Triassic-Early Jurassic. A great scatter is observed between the 100 good paths identified in each model, especially at high temperatures. Consequently, the range of feasible ages for the break in slope exceeds 100 Ma. Low cooling rates (< 1°C/Ma) appear to have characterised the inner Hardangerfjord region at least until the early Late Cretaceous. Enhanced Late Jurassic cooling is not confirmed by any of the

models, suggesting that the Jurassic North Sea rifting did not significantly affect onshore areas inland of the coastal region. Previous studies have suggested a minor effect of the Jurassic rift phase even in coast-proximal areas (e.g. Færseth et al., 1995), which is corroborated by the lack of evidence for post-Triassic igneous activity onshore (Fossen & Dunlap, 1999).

8.3.3 Cenozoic accelerated cooling

A second phase of accelerated cooling appears to have commenced in the inner Hardangerfjord region in the latest Cretaceous-Paleogene, i.e. approximately concomitantly with the breakup of the North Atlantic and the arrival of the Iceland mantle plume (Doré et al., 1999; Skogseid & Lunt, 2012).The inflection point of the cooling paths is found in the uppermost part of the PAZ for most models. Thus, the thermal evolution following the shift in cooling rate occurs outside the sensitivity range of the AFT method and cannot be inferred. The majority of the presented models display accelerated cooling in the most recent geological past. Neogene cooling is a well-known modelling artefact in thermal history models from apatite fission track data (Redfield, 2010 and references therein) and has previously been observed in models from areas where recent cooling is not supported by independent geological observations (e.g. Danišík et al., 2012). The sensitivity range of the fission track system does not extend beyond the boundaries of the PAZ, and the modelled cooling paths at temperatures below 60 °C should merely be regarded as vague suggestions. However, the short MTLs and exceptionally young ages obtained from the samples BG-26 and KJ-27 from the outer Eidfjord north block imply prolonged residence within the PAZ. According to the modelled thermal history of BG-26, the sample did not exit the PAZ until 20 Ma. Rapid, recent cooling is thus *required* to account for the data. As discussed in section 8.2.5, the samples from the Granvin area may have been influenced by convective heating associated with the circulation of hydrothermal fluids along brittle faults within the HSZ. Hydrothermal activity may have produced a complex thermal history that is not accounted for by a simple model. If hydrothermal heating did occur, it is likely to have involved several brief episodes of reheating to temperatures in excess of 100 °C, thus causing a reduced fission track age and a track length distribution containing a majority of short tracks. Although the thermal history models of BG-26 and KJ-27 imply residence within the PAZ until ~20 Ma, the samples may therefore have been exhumed to shallower crustal levels before this time. For samples derived from sea level and to a lesser degree intermediate elevations, Pliocene-Pleistocene glacial erosion is believed to account for a substantial part of the most recent

cooling. Assuming that ~1 km of overburden was removed from the inner fjord arms during the last 2.5 Ma, the particularly high cooling rate inferred for temperatures below ~35 °C reflects fjord incision rather than general uplift and denudation. This effect explains why samples collected at low elevations require more rapid Neogene cooling than samples from the Hardangervidda plateau.

8.3.4 Differences between thermal history models

Provided that the crustal column experienced undisturbed cooling through the isotherms, it is expected that samples at higher elevations (i.e. shallower paleodepths) cooled to surface temperatures at an earlier stage than samples from low elevations. In the thermal history models from the studied vertical profiles this relationship is reflected by a later exit from the PAZ for sea level samples than for samples from the Hardangervidda plateau.

A small, but systematic difference between the timing of exit from the PAZ is evident across the Eidfjord (Fig. 54). Irrespective of elevation, the samples from the south flank record earlier exhumation than corresponding samples from the opposite flank. Taking both fission track ages, track length data and proposed thermal histories into consideration, it is suggested that the north flank of the Eidfjord has experienced a cooling history that deviates from that of the south flank. Hence, the Eidfjord is interpreted to represent a major structural discontinuity. While the sea level samples from the south flank of the fjord record cooling from the PAZ at ~50-80 Ma, none of the corresponding samples from the north flank appear to have cooled below temperatures of 60 °C prior to ~40 Ma. Paleogene or later differential exhumation is thus required. The Kjeåsen profile is particularly interesting in this respect, because it comprises samples derived from both margins of the Simadalsfjord. In order to account for the obtained fission track age and track length data, KJ-21 from the middle part of the profile on the north flank of the fjord requires a later exit from the PAZ than the sea level sample KJ-11 derived from the southern margin. Despite its location in the outer Simadalsfjord, KJ-11 appears to share the thermal history of the samples in the Bu profile, thus supporting the interpretation that the inner portion of the Hardangerfjord coincides with a major structural boundary. Interestingly, the samples from the southern margin of the fjord record higher cooling rates than the samples from the northern margin throughout the Jurassic-Cretaceous interval of relative thermal quiescence. The differences are marginal, but consistent.

As described in section 8.2, the average cooling rate calculated from the apatite fission track ages from the vertical profiles is significantly higher for the Bu profile than for the Kjeåsen profile. From the thermal history models a cooling rate of < 1 °C/Ma is evident for

both blocks, thus supporting the estimate of 0.3 °C/Ma from the Simadalen area. The calculated 1 °C/Ma from Bu is a little higher than the rate indicated by the models. However, the suggested t-T- paths represent a range of feasible cooling paths only, and the apparent discrepancy does not imply that the models are incompatible with the estimated rate. In addition, the calculated cooling rates are dependent on the assumed paleogeothermal gradient, which unfortunately is poorly constrained. Possible exhumation scenarios and tectonic causes of the differential AFT signatures will be discussed in section 8.6.

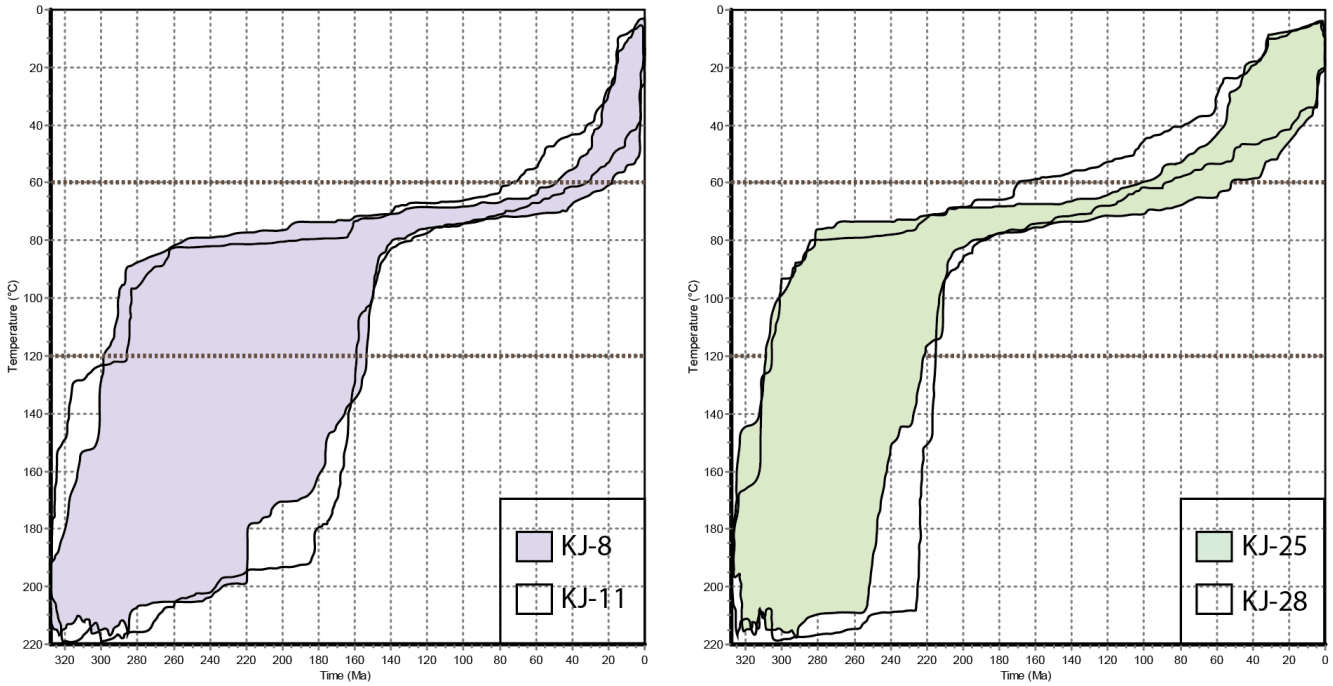

Fig. 54. Differential cooling across the Eidfjord evident from thermal history model path envelopes (good paths only): **a)** Comparison of the suggested thermal histories of KJ-8 (purple) and KJ-11 (transparent) from sea level on the north flank and on the south flank, respectively. A marginally higher Cretaceous cooling rate and an earlier exit from the PAZ is evident for KJ-11; **b)** Proposed thermal histories of KJ-25 (green) from the north block and KJ-28 (transparent) from the south block, both collected on the Hardangervidda plateau. KJ-28 appears to have resided at lower temperatures throughout the entire interval between the Early-Middle Jurassic and the present and records cooling through the upper boundary of the PAZ at an earlier stage than KJ-25. The boundaries of the PAZ are marked by dashed brown lines.

8.4 Interpretation of structural data

From the interpretations presented in the previous sections, it is possible to assess which structures may have been reactivated during the time interval between the Jurassic and the present. In Fig. 55, lineaments are grouped into six populations that are found to correspond

with the orientations of the main segments of the Eidfjord and its tributaries. The majority of the fracture sets are probably legacies from Precambrian times, with possible formation of new structures during post-Caledonian extensional collapse and Permo-Triassic rifting (Gabrielsen et al., 2002). NE-SW-trending lineaments (set I) are abundant in the immediate vicinity of the HSZ in the Granvin and Ulvik areas and appear to have formed in the same stress field as the shear zone. Subvertical to steeply southeasterly dipping fractures, which are found to be dominant in Granvin, may represent a conjugate set to the moderately dipping HSZ and related brittle structures with dips towards the northwest. NW-dipping structures belonging to set I are less conspicuous east of Osa and appear to be absent on the Eidfjord south flank. Due to the generally low sample density west of the Osafjord where set I structures are most abundant, the obtained fission track data do not provide any direct indications of whether this set has been reactivated during the Mesozoic or Cenozoic.

N-S-trending structures (set II) appear to have accommodated more displacement than any other set since the Middle-Late Jurassic. The obtained fission track data suggest that significant movement along regional N-S-trending faults has affected both structural blocks bounding the Eidfjord. Considerable down-to-the-west displacement along a presumably N-S-trending structure is suggested from the fission track data from the Bu area. In the Osa area offset ages are evident across several N-S-trending lineaments. AFT results obtained from Måbødalen south of the Simadalsfjord (Leighton, 2007) indicate down-to-the-west displacement along an array of faults that extend across the valley northwards to the Osa area. Large-scale N-S to NNW-SSE-trending structures have been identified throughout the Hardangerfjord area and in the coastal region near Bergen. Movement along this set has been found to postdate the NE-SW-trending faults formed in connection to the post-Caledonian collapse (Fossen & Hurich, 2005; Larsen et al., 2003). The data obtained in the present study confirms this relationship for the inner Hardangerfjord and suggest reactivation of the N-S-trending set subsequent to the Middle Jurassic.

The NE-SW-trending Osafjord (set III) exhibits an orientation that differ from that of the set I structures and is thus suggested to be unrelated to the Hardangerfjord Shear Zone. From Fig. 55 it is evident that the Osafjord is linked with the Bu valley to the south of the Eidfjord. There is no conclusive evidence for reactivation of this structure on either flank of the fjord. Similarly oriented lineaments are abundant in the Bu and Osa areas, but the available data are insufficient to resolve possible differential exhumation across these structures. Ages from sea level samples are quite similar across the NNE-SSW-trending Sørfjord, although slightly older ages are evident on the west flank. When comparing the

thermal history models of KJ-18 from the east block with that of BG-27 from the west block, it is apparent that the latter sample records considerably earlier cooling from the PAZ. Later exhumation of the east block implies down-to-the-west displacement across the fjord. The same sense of movement has been inferred by Leighton (2007), based on the identical pre-Neogene thermal histories obtained from samples from distinctly different elevations on the opposite margins. At present, the fission track record from the Sørfjord margins is incomplete. More samples, particularly from the eastern flank, are required to confirm differential exhumation across this particular segment of the Hardangerfjord.

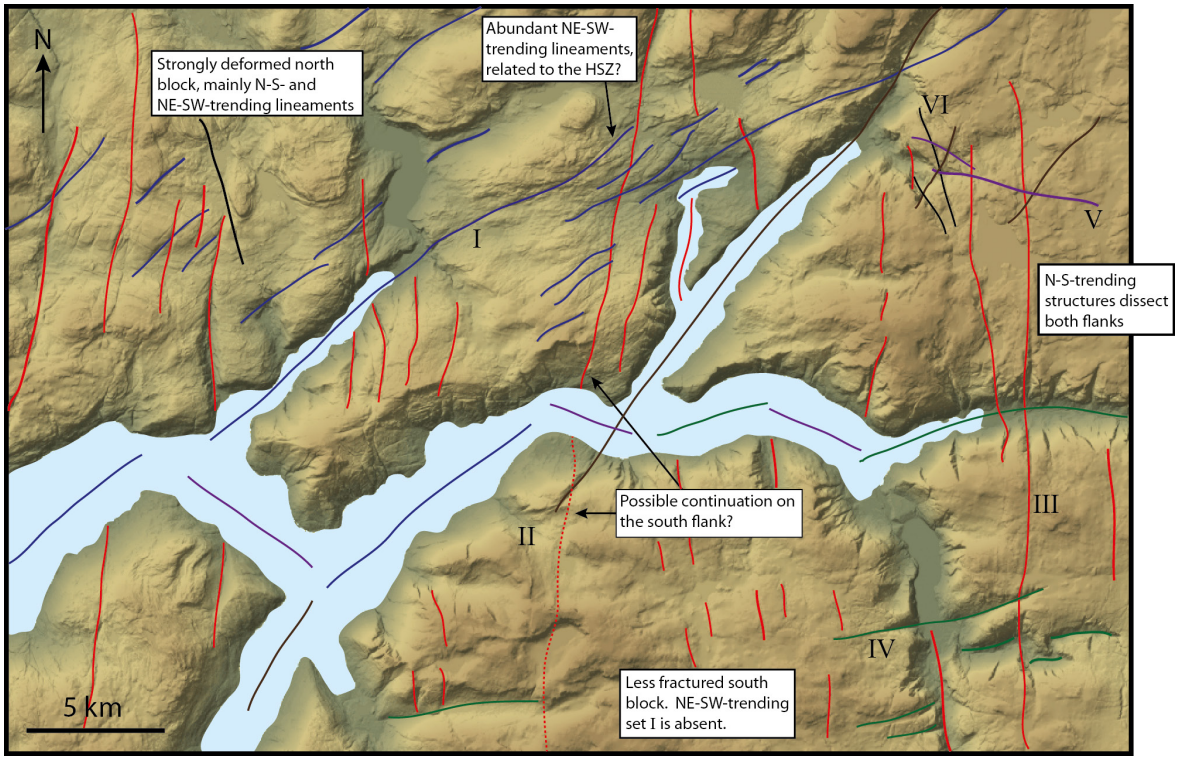

Fig. 55. Digital elevation model with main lineament orientations. The observed lineaments are divided into six sets: Set I (dark blue) is suggested to represent brittle structures related to the HSZ. Set II lineaments (brown) parallel the Osafjord. Set III (red) encompasses structures that vary in orientation between NNW-SSE and NNE-SSW. This set is well-represented on both margins of the Hardangerfjord. The NNE-SSW-trending structure that is marked by a stippled line south of the Eidfjord, represents the fault that is interpreted to have caused the offset AFT ages in the Bu profile. The Simadalen segment of the Eidfjord and similarly oriented structures constitute set IV (green). Lineaments belonging to this set are most abundant south of the Eidfjord. Set V (purple) and VI (black) lineaments are less common.

The Eidfjord comprises a number of segments, with trends varying between and ENE-WSW (set IV) and WNW-ESE (set V). Set IV lineaments are most pronounced south of the Hardangerfjord and directly north of Simadalen. Consistent offset and systematic differences

in MTLs and modelled cooling paths may suggest different exhumation histories for the structural blocks bounding the fjord to the north and south, although the fission track ages are not conclusive with regard to juxtaposition. Except from a potentially greater offset across the Simadalsfjord (cf. section 8.2.2), the fission track results do not resolve dissimilarities in displacement between the different segments of the Eidfjord.

The fission track record does not conclusively imply displacement along the NNW-SSE-trending structures that transect the Osa area (set VI), although the steep age-elevation gradient may suggest differential vertical movement of structural blocks within the vertical profile.

8.5 Comparison with previous studies

8.5.1 Apatite fission track thermochronology

The apatite fission track data obtained in the present study are generally in good agreement with the results from previous work conducted in the inner Hardangerfjord region (i.e. Andriessen & Bos, 1986; Leighton, 2007; Rohrman et al., 1995). Andriessen and Bos (1986) analysed two samples derived from the Simadalen and Eidfjord areas. A third sample was collected from the top of Hardangerjøkulen, some distance from the field area covered in the present contribution. Their lowermost sample yielded an age of 110 ± 18 Ma, which corresponds well to the age of 120 ± 7 Ma obtained from the nearby sample KJ-11. Ages of 134 ± 8 Ma and 166 ± 31 Ma were obtained for samples from elevations of 700 m and 1620 m asl, respectively. In comparison, Middle Jurassic-Early Cretaceous and Early-Middle Jurassic ages were found to dominate at similar elevations in the present study. Thus, the results are found to be compatible.

The study by Leighton (2007) comprises eleven samples obtained within or proximal to the area covered in the present work, and the reported ages range from 129 ± 7 Ma to 178 ± 7 Ma. Overall, these ages agree reasonably well with the results presented herein, although Leighton (2007) generally obtained significantly older ages for samples from low elevations. The study includes a vertical profile sampled from sea level in Eidfjord along the road through Måbødalen. Interestingly, some of the youngest samples (~140 Ma) are found at relatively high elevations on the Hardangervidda plateau, while ages of ~170 Ma predominate within the lowermost 300 m of the profile. According to Leighton (2007), this inverted age-elevation relationship may be a result of faulting. It is here suggested that the structures that offset the AFT ages in the profile sampled by Leighton (2007) belong to the same N-S-

trending set that dissects the Simadalen and Osa areas to the north (cf. sections 6.1.1 and 6.1.2).

The MTLs reported by Leighton (2007) range from 11.40 ± 0.38 μm and 12.32 ±0.17 μm and are generally found to be 0.7-1.0 μm longer than the MTLs presented in the current work. The differences are systematic and presumably reflect dissimilarities associated with the analytical approach (cf. Ketcham et al., 2009), rather than pronounced local variations in cooling histories. Through thermal history modelling Leighton (2007) revealed two episodes of rapid cooling, confined to the Permo-Triassic and the Neogene. Similar cooling paths are evident in the majority of the models presented in this thesis.

The ages obtained in the current study are in good agreement with the results of Rohrman et al. (1995), whose study included five apatite fission track ages from the Eidfjord area. All samples were collected as part of a vertical profile sampled along the road through Måbødalen. Ages between 98 ± 8 Ma and 181 ± 19 Ma were reported and a relatively good correlation between age and elevation was observed. The sea level samples of Rohrman et al. (1995) yielded ages of 98 ± 8 Ma and 113 ± 8 Ma, i.e. slightly younger, but within error of the majority of sea level samples presented in the present work (ranging from 105 ± 5 Ma - 130 ± 11 Ma). In both studies, Early-Middle Jurassic ages were obtained from the Hardangervidda samples. The MTLs of Rohrman et al. (1995) range from 11.5 ± 0.2 μm close to level to 13.1 ± 0.1 μm at the Hardangervidda plateau, and are thus significantly longer than those obtained in the present study. However, Rohrman et al. (1995) did not employ a standard etching protocol (cf. Rohrman, 1995), and their MTLs are therefore not reproducible. According to Gleadow et al. (1986) and Donelick et al. (2005), consistency in etching conditions between different samples is crucial, and the elucidation of thermal history information based on track lengths may be rendered invalid if this requirement is not met. Based on thermal history modelling, Rohrman et al. (1995) suggested Triassic-Jurassic and Neogene pulses of accelerated cooling. In the present study the first rapid cooling is confined to the Permian-Triassic and may be linked to the rifting of the North Sea. Similarly high Permo-Triassic cooling rates have previously been documented throughout southwestern Norway (Ksienzyk, 2012; Leighton, 2007). Rohrman et al. (1995) put considerable emphasis on the latest portion on the cooling history, i.e. from ~30 Ma onwards, and argued for rapid Neogene cooling resulting from 1-2 km of domal tectonic uplift. The proposal of a Neogene uplift event was largely based on the generally high proportions of short tracks measured in the samples from the Eidfjord area. Neogene accelerated cooling is also suggested by some of

the models generated in the current study. However, substantial portions of the Cenozoic thermal history occur outside the temperature range resolved by the fission track method. Hence, the most recent parts of the proposed cooling paths should not be regarded conclusive and consequently should not be used as a basis for a model for topographic evolution. In an effort to produce a regional fission track record for southern Norway, the study of Rohrman et al. (1995) largely failed to resolve local differences in cooling signatures. Clearly, their domal uplift model does not successfully describe the pattern of AFT ages in the inner Hardangerfjord region. The model suffers from the implicit presumption that southern Norway behaved as a coherent block since Permian times and is flawed in that it does not account for the documented structural control on the distribution of apatite fission track ages. Offset fission track ages are observed across minor distances and fault activity is not only confined to large, mapped structures. Considerable displacement along small-scale faults clearly contributes to the complex exhumation history of the rift margin.

8.5.2 Quality of vertical profiles

The current study includes three vertical profiles that each covers a relief of ~1300 m. All transect have been constructed with the purpose of obtaining closely spaced samples, and consequently, the maximum lateral sampling distance within each profile do not exceed 7 km. In previous studies (i.e. Leighton, 2007; Rohrman et al., 1995), the requirement for restricted lateral separation of samples has been assigned less importance, resulting in vertical profiles that extend over distances of 20-30 km. Where the distance between samples is large enough to stretch across several possible faults, important information regarding differential exhumation, and thereby aspects of the tectonic evolution, may be overlooked. The complexity of the profiles revealed in the present work stresses the necessity for closely spaced samples and demonstrates the advantages of sampling the steepest profile, rather than the profile with the easiest accessibility. Even with the sampling strategy employed in the current study, the obtained vertical profiles are not ideal. Unfortunately, none of the profiles are found to provide a common thermal history for all samples, and thus do not reveal detailed information about the continuous cooling path of the crustal column over a significant time span. The main reason is the ubiquitous presence of closely spaced structural discontinuities in the inner Hardangerfjord region. A broad spectrum of fracture orientations is identified, thus making it difficult to determine and isolate the influence of individual faults on the thermochronological results. Potentially, less disturbed profiles may be sampled in structurally less complex areas located further to the east of the Hardangerfjord Shear Zone.

8.5.3 (U-Th)/He analysis

Few studies have thus far involved (U-Th)/He analysis of samples from southern Norway. The present thesis presents the first attempt of dating samples from the inner portions of the Hardangerfjord by the (U-Th)/He method. Leighton (2007) obtained a majority of Late Cretaceous uncorrected (U-Th)/He ages from the Sognefjord region to the north of the present study area. The majority of the samples in the study were found to suffer from poor reproducibility, resulting in high uncertainties. No distinct age increase was observed with distance from the coast, as has been documented for the AFT system. In fact, some of the youngest ages (i.e. Eocene) were obtained from the outer portion of the fjord. By applying thermal history modelling, Leighton (2007) found that the reported (U-Th)/He ages were incompatible with the thermal history inferred from the AFT record. Problems with incompatible AFT and single grain (U-Th)/He ages have also been encountered in the present study, suggesting that the (U-Th)/He ages obtained from southern Norway may be significantly influenced by radiation-enhanced He retention or other factors that complicate the analysis. Ksienzyk (2012) obtained F_T-corrected single grain ages from the Bergen area ranging from Middle Triassic to Late Cretaceous. A majority of Early Cretaceous ages were reported, i.e. similar to the results obtained in the present study. Apatite fission track ages are generally found to be significantly older in the Bergen area than in the inner fjord regions. The age differences between the coast and the interior appear to be less pronounced for the (U-Th)/He system. This may suggest greater exhumation directly inland of the Hardangerfjord Shear Zone in the Jurassic, followed by relatively uniform cooling throughout southwestern Norway from the Cretaceous onwards. The present (U-Th)/He record from the inner Hardangerfjord region comprises two sample ages only. Hence, further data from the interior are clearly required to draw any valid conclusions.

8.6 Proposed exhumation history for the inner Hardangerfjord

8.6.1 General notions

From the wide track length distributions and short MTLs obtained in the current study it is apparent that the thermal history of the inner Hardangerfjord region is characterised by prolonged time intervals dominated by slow cooling. All analysed samples are inferred to have experienced similar, protracted cooling histories. Local variations in AFT ages and MTLs are suggested to be a result of differential exhumation attributed to periodic fault activity. The obtained apatite fission track data provide information about the thermal

evolution from the Permian until the Paleogene. Consequently, this specific time interval will be the focus in the following attempt to reconstruct the exhumation history of the study area.

The rapid cooling rates obtained through thermal history modelling suggest that the Permian and Triassic periods were associated with significant unroofing of the inner Hardangerfjord region. Evidently, the effect of the North Sea rifting was pronounced even in areas situated far from the coastline. While flexural rebound effects induced by rifting may have led to regional exhumation of the rift shoulder (cf. van der Beek et al., 1994), down-to-the-northwest extensional reactivation of the Lærdal-Gjende Fault and affiliated structures (Andersen et al., 1999) is believed to have controlled local exhumation patterns by causing enhanced denudation of the uplifted footwall blocks. Leighton (2007) estimated significantly lower Permo-Triassic exhumation rates for the hangingwall of the LGF (20-40 m/Ma) relative to the footwall (40-90 m/Ma), which clearly demonstrate significant displacement and probably repeated reactivation of the brittle segment of the HSZ during the development of the North Sea rift. The area studied in the current work is located in the transition zone where the ductile shear zone disappears beneath the Caledonian thrust sheets and the first clear indications of brittle overprint are evident. Although Permo-Triassic reactivation of the ductile southwestern portion of the HSZ has been proposed (Færseth et al., 1995) there is no conclusive evidence for post-Devonian brittle displacement (Fossen & Hurich, 2005). The Permo-Triassic cooling rate inferred from the thermal history models for the inner Hardangerfjord samples suggest an exhumation rate of >100 m/Ma in the footwall of the shear zone, assuming a geothermal gradient of 20 °C. Taking this comparably high exhumation rate into account, it is considered likely that Permo-Triassic brittle reactivation of the inner Hardangerfjord segment may have taken place. The onshore expression of the Permo-Triassic rift phase thus appears to have been related to both regional rift flank uplift and extensive reactivation of post-Caledonian structures resulting in differential denudation of adjacent fault-bound blocks.

From the thermal history models presented in chapter 7.1, the Jurassic and Cretaceous periods appear to have been characterised by general thermal quiescence. However, the fission track record suggests episodes of accelerated cooling, possibly associated with fault-related uplift and denudation. Such local cooling events of limited magnitude are not resolved by the thermal history models. The distribution of fission track ages in the inner Hardangerfjord area reveals significant age differences over short lateral distances and suggests post-Middle Jurassic-Early Cretaceous fault activity. Paleomagnetic and radiometric data from fault rocks obtained from Hordaland and adjacent regions indicate reactivation of

structures during Late Jurassic-Early Cretaceous times (Andersen et al., 1999; Eide et al., 1997; Fossen et al., 1997; Ksienzyk, 2012; Torsvik et al., 1992). It is considered likely that the fault activity documented in the current study is confined to roughly the same time interval. Hence, although the North Sea rift phase appears to have had a limited effect on the regional exhumation rate, extensive fault reactivation is suggested to have exerted a major control on local exhumation patterns.

Fission track ages, track length distributions and thermal history models generally indicate later exhumation of the northern side of the Eidfjord relative to the southern side. Samples obtained from similar elevations on opposite margins of the fjord display slightly offset cooling paths in the upper PAZ (see Fig. 54), suggesting that juxtaposition may have taken place subsequent to the time at which the sea level samples cooled out of the sensitivity range of the AFT method. It is thus considered plausible that the observed differential cooling signatures are in part attributed to Cenozoic episodes of fault reactivation. The most obvious explanation for possible tectonic rejuvenation during the Cenozoic is the rifting and subsequent opening of the North Atlantic Ocean in the Paleocene-Eocene. Hence, the juxtaposition of structural blocks in the Eidfjord area is assumed to partially be a result of Late Cretaceous-Paleogene fault activity. This interpretation is supported by previously published K/Ar illite data that indicate reactivation of the Lærdal-Gjende Fault at ~60 Ma (Ksienzyk, 2012). No further record of Paleogene fault reactivation is available from southwestern Norway. In this context, it is essential to note that most previous studies attempting to date fault activity (e.g. Andersen et al., 1999; Larsen et al., 2003) have focused on cohesive fault rocks. Cohesive breccias and cataclasites are generally believed to originate from brittle processes operating at greater crustal depths (Sibson, 1977) and are thus not expected to record the most recent episodes of fault activity. The present-day seismicity around the Hardangerfjord implies ongoing periodic reactivation of brittle structures in the area. Faulting related to differential glacio-isostatic compensation may account for a portion of the recorded seismic activity. The stress induced by sea-floor spreading in the North Atlantic is, however, suggested to be of greater importance (Hicks et al., 2000), thus indicating that southern Norway may have been subjected to active tectonic processes throughout the Cenozoic.

8.6.2 Detailed structural evolution of the study area

Two scenarios are proposed to explain the pattern of differential exhumation that is evident from the obtained fission track data and thermal history models. These scenarios are not necessarily mutually exclusive. A combination of both interpretations may well represent the best reconstruction of the structural evolution of the inner Hardangerfjord region.

Scenario I: Footwall uplift of the Eidfjord north block

The observed distribution of fission track age data and MTLs in the inner Hardangerfjord region may be explained by a simple model that involves juxtaposition across a fault that is presumed to underlie the Eidfjord (Fig. 56). The AFT record is consistent with down-to-the-south-southeast displacement across this structure: Younger fission track ages and shorter MTLs are found north of the fjord, thus implying later exhumation of the north block relative to the south block. The AFT ages obtained from equal elevations on the opposite flanks generally overlap within errors. This implies that the presumed fault has accommodated moderate displacement during post-Middle Jurassic-Early Cretaceous times. Fission track ages from the Kjeåsen profile reveal potentially greater displacement along the Simadalen segment (cf. section 8.2.2). However, no fission track ages are available from low elevations on the northern margin of the Simadalsfjord and the fission track record from the area is therefore insufficient to confidently draw a conclusion. There are no direct indications of the character of faulting along the Eidfjord. However, southwestern Norway has been situated in an overall extensional tectonic regime since the Paleozoic (Doré et al., 1999) and previous work has confirmed extensional movement along major structures in the coastal regions (e.g. Fossen et al., 1997). Normal displacement is thus considered most feasible for the inner Hardangerfjord region and the fault that follows the Eidfjord is suggested to be south-southeasterly dipping. This interpretation is supported by structural data, which show a predominance of SE-dipping joints and possible faults on both sides of the fjord (cf. Fig. 20a). The large, SE-dipping fracture zones that dissect the south flank of the Simadalsfjord may represent secondary brittle structures formed in vicinity to the presumed main fault, which underlies the fjord. Footwall uplift related to the suggested down-to-the-south-southeast displacement may partly be responsible for the complete erosion of the Caledonian nappes on the north flank. However, the Eidfjord north block also borders the HSZ, which is known to have accommodated extensional displacement in the order of 10-15 km since Devonian times (Fossen & Hurich, 2005), and the bulk uplift and erosion is probably attributed to movement along this structure.

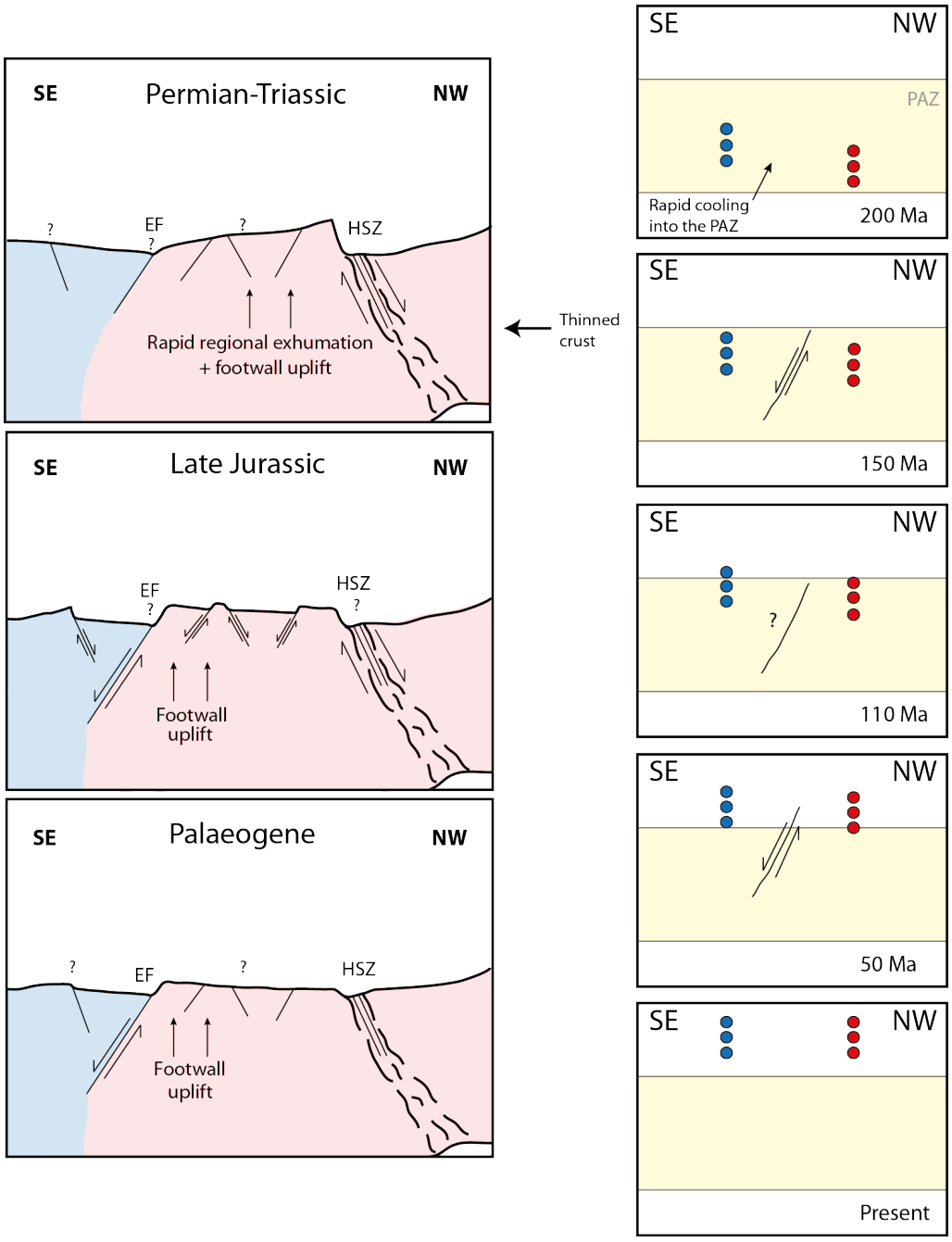

Fig. 56. Proposed structural evolution of the inner Hardangerfjord region according to scenario I. The general thermal evolution of the analysed vertical profiles are displayed to the right: **a)** The Permo-Triassic was characterised by rapid regional exhumation related to the rifting in the North Sea and localized accelerated exhumation associated with footwall uplift of along the HSZ. At this time the inner Hardangerfjord samples cooled into the PAZ. **b)** Extensive small-scale reactivation of structures affected the area during the Middle-Late Jurassic-Early Cretaceous. By the latest Early Cretaceous, rocks derived from the Hardangervidda plateau south of the Eidfjord had cooled out of the PAZ. **c)** Cenozoic reactivation of the Eidfjord Fault (EF) and related footwall uplift resulted in accelerated exhumation of the north block. The samples from the north flank, which had resided at deeper crustal levels throughout the Mesozoic, were then juxtaposed to their southern counterparts. Since the paleotopography of the area remains largely unknown, no distinct topography is indicated.

Scenario II: Internal deformation of the Eidfjord north block

The scenario presented in Fig. 56 fails to explain the higher apparent cooling rate of the Eidfjord south block throughout the Jurassic and Cretaceous. Repeated reactivation of a south-southeast-dipping structure beneath the Eidfjord would result in more efficient denudation of the footwall block in the north and thus imply higher cooling rates in this part of the study area. Both fission track age-elevation gradients and thermal history models indicate more rapid cooling south of the fjord. The Eidfjord north block is dissected by densely spaced lineaments with a wide range of orientations (see Fig. 55). Offset fission track ages in the Osa area in particular, are suggestive of extensive fault activity. Complex internal deformation, possibly involving rotation of local fault-bound blocks, may represent one viable explanation for the apparently lower cooling rates obtained from the northern margin of the Eidfjord (Fig. 57). It is important to note that the fission track ages obtained from the north flank are not exclusively younger than the ages from the south flank. Locally, the ages from the Osa profile are found to be significantly older than ages at similar elevations in the Bu profile. Oppositely dipping faults are suggested to produce local horst-graben structures, resulting in particularly old AFT ages (e.g. KJ 24 and KJ-5) in the down-faulted blocks. Rocks from deeper crustal levels are exposed in the up-faulted blocks, giving younger ages (e.g. KJ-1 and KJ-6). In comparison to the northern margin of the Eidfjord, the southern margin appears to display a smaller number of pronounced structures with less variable trends, and may thus be less affected by local differences in vertical crustal movement. Hence, the deviating AFT records obtained from the opposite margins of the Eidfjord may reflect more extensive differential exhumation across small-scale structures within the northern structural domain. According to this interpretation, movement along a presumed large-scale fault that follows the trend of the fjord is not necessary to account for the obtained data. There is no obvious explanation for the inferred variations in structural style, but it may be speculated whether the documented change in crustal architecture across the HSZ (Hurich & Kristoffersen, 1988) may have had an effect on the deformation of the footwall in the immediate vicinity to the shear zone.

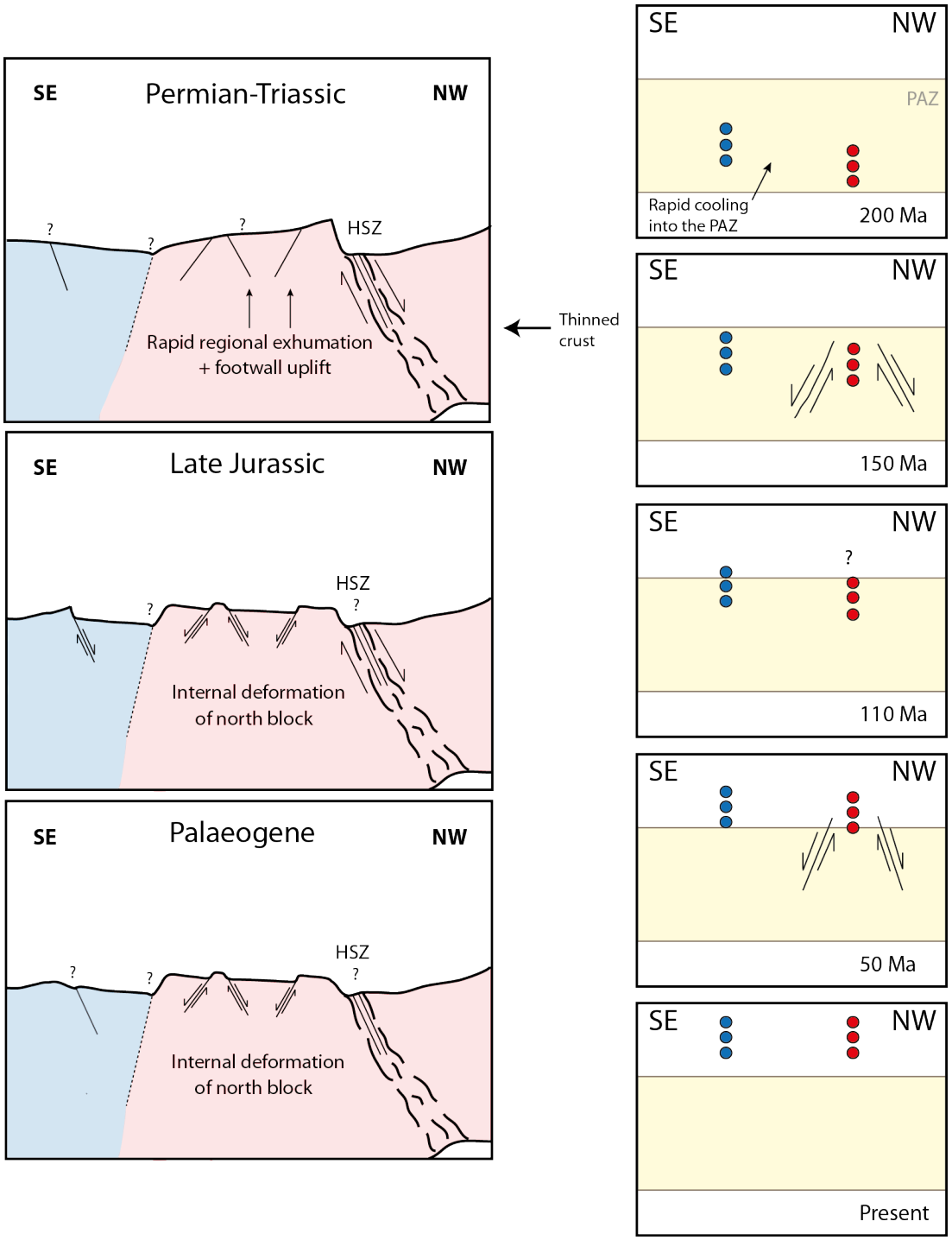

Fig. 57. Exhumation history of the inner Hardangerfjord region according to scenario II: **a)** Rapid Permo-Triassic exhumation as in scenario I. **b)** Extensive fault activity during the Middle-Late Jurassic-Early Cretaceous affected both flanks of the Eidfjord. **c)** Continued internal deformation of the north block during the Cenozoic produced a complex pattern of apatite fission track ages, reflecting differential denudation across small-scale structures. There are no indications of whether faulting affected the south block at this time.

8.7 Regional perspective

The long-term evolution of passive continental margins reflects a complex interplay between tectonics, denudation, drainage patterns and lithological controls (Gallagher et al., 1998). In the following paragraphs, the evolution of the Norwegian margin will be discussed in terms of traditional models for passive margin landscape development.

Three main classes of passive margin landscape evolution models have been proposed in order to explain the development of margins characterised by a low-elevation coastal plain separated from a high-elevation inland plateau by a prominent escarpment (Fig. 58a-c): Downwarp models (Ollier & Pain, 1997) describe passive margin development in terms of flexure of a rigid lithosphere and imply limited fault activity. Maximum removal of material and young fission track ages are expected directly seaward of the escarpment, while the interior is characterised by negligible denudation and thus old ages. Scarp retreat models (Gilchrist & Summerfield, 1990) explain margin formation by an initial phase of extensional faulting followed by inland retreat of the fault scarp and imply a progressive increase in fission track ages from the coast towards the interior. Limited vertical denudation and old ages are expected inland of the escarpment. Initial extensional faulting is also invoked by the pinned divide class models (Kooi & Beaumont, 1994), which depict a drainage divide situated inland of the fault scarp. Incision by seawards draining streams leads to vertical denudation of the coastal region and development of a new escarpment that coincides with the position of the pinned drainage divide. The pinned divide models predict young AFT ages close to the coastline, while the oldest ages occur at the locus of the drainage divide. Moderate denudation is inferred for the region inland of the fault scarp. Despite some essential differences, all three models generally predict old fission track ages along the rift flank and in the hinterland, while younger ages are expected seaward of the scarp. Together, these models have been found to successfully describe the AFT age distributions from a wide variety of passive margins worldwide (Gallagher & Brown, 1997; Gallagher et al., 1998). The data presented in the current contribution covers a geographically restricted area and do not independently provide information on the style of margin evolution in southern Norway. However, valuable information can be obtained by combining the ages presented in this thesis with the results from previous studies undertaken in coast-proximal areas of southwestern Norway. Fission track data from the Bergen and Sunnhordaland areas are generally consistent with relatively early exhumation to shallow crustal levels (Ksienzyk, 2012; Leighton, 2007; Rohrman et al., 1995). Samples from coast-proximal regions are typically characterised by Triassic-Jurassic

ages and intermediate mean track lengths in the order of 12-14 μm. Permian ages are evident locally, but are largely restricted to the outermost coastline. In comparison, the data collected in the present study reveal relatively late exhumation of the margin hinterland, evident by mainly Jurassic-Cretaceous fission track ages and short mean track lengths. According to Mosar (2003), the North Atlantic rift shoulder is delineated by the Hardangerfjord Shear Zone and its northwards continuations, implying that the HSZ separates the coastal domain affected by rifting from the relatively undisturbed rift margin. This interpretation is substantiated by a documented change in the thickness of the crust across the Hardangerfjord Shear Zone, from 28 km in the hangingwall to 34 km in the footwall (Hurich & Kristoffersen, 1988), suggesting that the coastal region may have been subjected to rift-related crustal thinning. According to Mosar (2003) the locus of rifting shifted northwards to the final position of the breakup after the North Sea rift was aborted in the earliest Cretaceous, but the position of the rift flank in southern Norway remained stationary. The inner Hardangerfjord region is located in the footwall of the HSZ and is thus suggested to form the outermost rift flank. Taking the observed regional age distribution into consideration, the traditional models for passive margin evolution described above do not provide a satisfactory approximation of the development of the North Sea rift margin. The ages obtained from coastal regions are clearly not significantly younger than the ages from the Hardangervidda plateau, as would be expected from scarp retreat and pinned divide scenarios. The fault activity documented by the present and previous low-temperature thermochronological studies is not compatible with flexural downwarping. Furthermore, the Jurassic ages obtained from the escarpment (i.e. the Hardangervidda plateau) are much younger than the ages predicted by the downwarp model. Hence, the fission track data from southwestern Norway suggest that the evolution of the North Sea margin is more complex than the scenarios portrayed by the landscape development models. There are several possible reasons for this: The Norwegian margin has been subjected to polyphase rifting, culminating with opening of the Atlantic Ocean in the Eocene (e.g. Mosar, 2003). In-between the individual rift phases, the margin has experienced changes in the orientation of the stress field (Færseth et al., 1995), which has complicated the structural evolution. The traditional landscape development models furthermore fail to account for pre-rift structural inheritance. This is critical, considering that the Precambrian structural grain is believed to have exerted a major control on the tectonic development of the North Sea rift and the Norwegian margin (Doré et al., 1999; Færseth et al., 1995; Gabrielsen et al., 2002).

The general pattern of fission track ages from the Bergen-Hardangerfjord region reveals progressively later exhumation from the coastal regions towards the interior. As pointed out by Ksienzyk (2012) the AFT age distribution in southern Norway appears to be largely structurally controlled. It is suggested that landscape development has been governed by mainly down-to-the-west displacement along large-scale extensional structures in association with the Permian and Mesozoic rift phases (Fig. 58 d). Local exceptions to the general trends are abundant both in coastal and inland areas and are suggested to reflect differential vertical movement across small-scale structures, as is extensively documented for the inner Hardangerfjord region. Larger-scale structures with easterly dip directions (e.g. the Hjeltefjord Fault Zone; Fossen, 1998) are found to produce locally reversed age distribution patterns (cf. Ksienzyk, 2012).

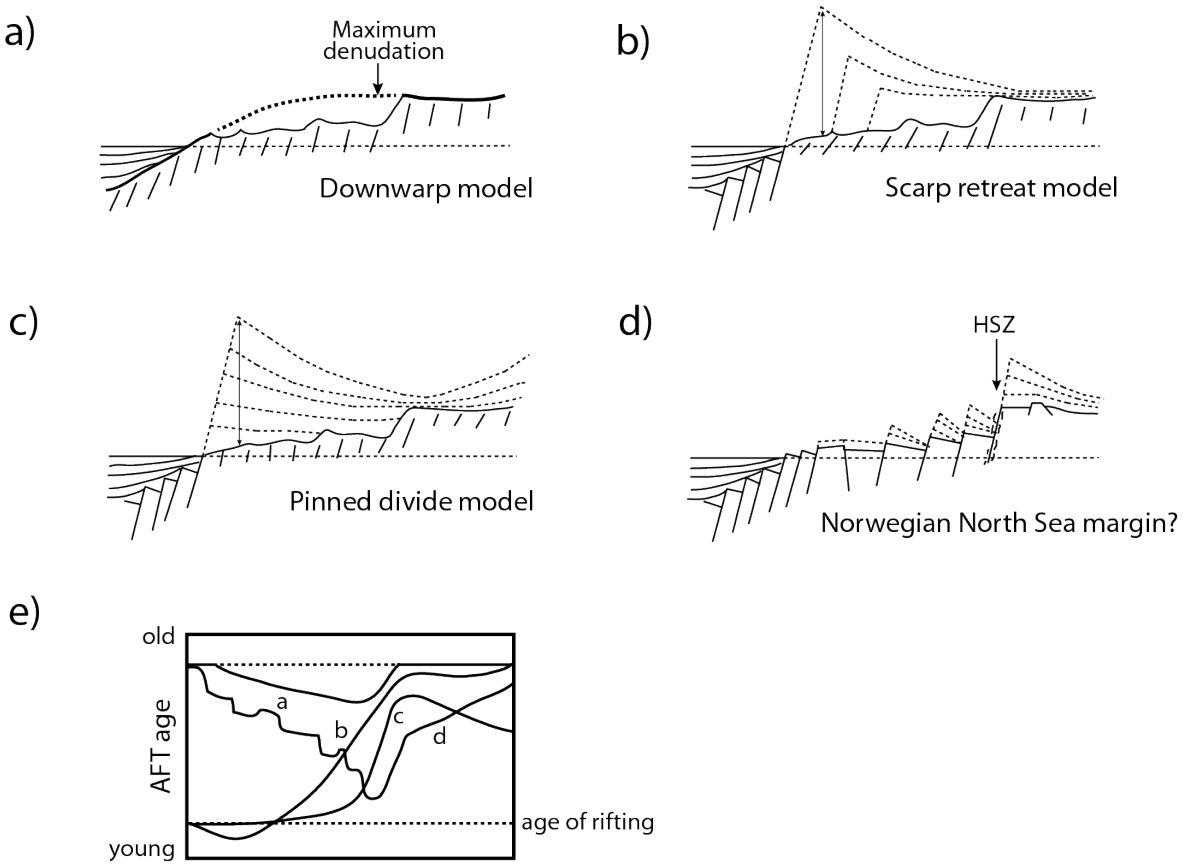

Fig. 58. (Previous page). Models for passive margin landscape evolution: **a)** Downwarp model: margin development as a denudational response to lithospheric flexure. **b)** Scarp retreat model: initial extensional faulting followed by landward retreat of the escarpment. **c)** Pinned divide model: vertical denudation of the initial rift flank from fluvial incision. **d)** Suggested evolution of the North Sea margin: denudation patterns are controlled by differential vertical movement of fault-bound blocks. **e)** Predicted AFT ages with distance from the coast for each of the presented models. The lowermost stippled line is taken to correspond to the North Atlantic rift phase in the Paleogene. According to the interpretation by Mosar (2003), the rifting of the Norwegian margin was initiated in the North Sea in the Permian and culminated with the North Atlantic breakup in the Eocene. In order to be comparable to the passive margin evolution models, which do not incorporate fjord incision, the portrayed age pattern inland of the escarpment is representative of the ages obtained from the Hardangervidda plateau. a-c and e are redrawn after Gallagher et al. (1998).

8.8 Comparison with models for topographic evolution

Although the peneplanation-uplift model and the ICE hypothesis present distinctly different views on the timing of landscape development, similar fission track signatures are expected for both scenarios. The most important clues as to how the Norwegian landscape formed probably lie in the Paleogene and particularly Neogene cooling paths. Unfortunately, most of the Cenozoic thermal evolution of the inner Hardangerfjord samples is outside the sensitivity range of the apatite fission track method and cannot be inferred. Even samples obtained from low elevations within the innermost Hardangerfjord represent crustal levels that are too shallow to provide detailed information on recent cooling events. However, some information is available through thermal history modelling. Below follows a discussion of the alternative thermal history models presented in chapter 7.2 and an assessment of the compatibility between the AFT data and each of the models for topographical evolution.

In order to determine the thermal effect of peneplanation, a number of different cooling scenarios were tested against the AFT results from the Hardangervidda plateau. The models that were created to account for the Mesozoic peneplanation scenario are generally found to display prolonged episodes of pronounced cooling. High Cretaceous cooling rates are proposed by some of these models. Rapid cooling during the Cretaceous period is not supported by independent geological observations, which suggest tectonic quiescence from the time of the termination of the North Atlantic rift phase in the earliest Cretaceous until the onset of rifting in the North Atlantic in the Paleogene (e.g. Færseth & Lien, 2002). There are no indications of any major tectonic events capable of causing regional enhanced exhumation within this time interval. In all models that force surface temperatures during the Mesozoic, reheating to temperatures of 60-90 °C is required, thus suggesting reburial by up to ~3 km of

sediments. Paleocene peneplanation, as suggested by Riis (1996) and Lidmar-Bergström et al. (2000), implies accelerated cooling commencing at ~60 Ma. The suggested cooling event is found to correspond with the initial stages of the North Atlantic break-up and the timing of cooling is therefore considered geologically reasonable. For southern Norway, which borders the intracratonic North Sea Basin, the effects of margin flexure during the initial stages of sea-floor spreading may not have been pronounced (Doré, 1992). The gradient indicated by the cooling paths may therefore be unrealistically steep. In a recent contribution, Skogseid and Lunt (2012) presented new evidence for significant dynamic uplift of the North Atlantic realm in relation to the arrival of the Iceland mantle plume at ~62 Ma. Thermally induced uplift with a magnitude of 500-2500 m may partly explain the accelerated cooling in the Late Cretaceous-Paleogene, although the magnitude of uplift, and thus the denudational response, is disputed (Hartz et al., 2012). Rapid reburial is required for the samples to achieve temperatures of ~80 °C in the Paleocene-Eocene. According to the thermal history model in Fig. 48a, the basement must have been buried by > 2 km of sediments less than 20 Myr after having reached surface temperatures. Such a scenario implies relatively high sedimentation rates, which suggest total submergence of the western part of the Hardangervidda plateau during the Paleocene-Eocene. Consequently, accommodation space must have been generated by post-rift thermal subsidence of the outer portion of the rift flank, possibly in combination with general down-to-the-west displacement across major structures. Due to the scarcity of onshore sediments, the inferred reburial is not readily verified by independent geological observations. The Bjorøy Formation, described by Fossen et al. (1997), represents a rare pocket of Mesozoic sediments onshore southern Norway. The formation comprises upper Jurassic sedimentary rocks and unconsolidated sands and was discovered within a fault zone during the construction of a subsea tunnel in the Sotra region west of Bergen. Seismic data from the area suggest that the sediments were deposited discordantly on the gneissic basement. Hence, the presently exposed rocks in this area were already at the surface in the Late Jurassic. The occurrence of coal fragments and the assemblages of pollen and spores within the sediments testify to a near-shore marine depositional environment. According to Fossen et al. (1997), this suggests that the present coast-proximal areas of southwestern Norway were flooded following a Late Jurassic marine transgression that started offshore. At a first glance, the proposed transgression appears to be compatible with the thick sedimentary cover that is required to account for the fission track data from the Hardangervidda plateau. However, vitrinite reflectance data obtained from coal within the Bjorøy Formation were found to indicate a maximum burial depth of 1 km (Fossen et al., 1997). AFT thermal history

models of basement samples derived from the same area suggest reheating to 40-65 °C in the Cretaceous-Paleogene (Ksienzyk, 2012) and are thus in fair agreement with the conclusion drawn from the vitrinite reflectance analysis. Interestingly, all thermal history models with additional constraints presented in the present study suggest considerably greater burial depths for the Hardangervidda plateau. This is unexpected since the coastal region presumably would have been affected by the transgression at an earlier stage than inland areas.

Without allowing for reheating, the constraint that forces surface temperatures in the Paleocene is found to produce a model that is poorly supported by the data. This is evident by a low goodness of fit value of 0.47 for the track length distribution inferred by the best-fit cooling path. In comparison, the best-fit paths in most models with start and end constraints only display goodness of fit values in excess of 0.80 for both track length distribution and age data. According to the thermal history model in Fig. 48b, the Hardangervidda samples must have experienced a cooling rate of ~8 °C/Ma around 60 Ma in order to reach the surface in the Paleocene. This rate is regarded unreasonably high, even with rift flank and plume-induced uplift operating in conjunction. Based on the obtained model, Paleocene peneplanation and subsequent sustained residence close to the surface is therefore considered unlikely.

All attempts of generating thermal history models without inferred reburial and with surface temperatures constrained to pre-Paleocene time intervals were unsuccessful. This clearly demonstrates that Mesozoic peneplanation followed by limited sedimentation is not in accordance with the AFT data from the Hardangervidda plateau. Furthermore, the (U-Th)/He data obtained from KJ-19 indicate cooling through HePRZ temperatures in the Early Cretaceous and are incompatible with prolonged residence at the surface prior to ~100 Ma.

The present study documents extensive post-Middle Jurassic displacement along faults in the inner Hardangerfjord region. Considerable fault activity is suggested for the time interval between the Middle-Late Jurassic and Early Cretaceous. Differential Cenozoic thermal histories for adjacent fault-bound blocks indicate possible later reactivation. The peneplanation-uplift model does not provide an answer to how the paleic surface, presumably formed during the Late Cretaceous or Paleogene (Doré, 1992; Gabrielsen et al., 2010; Lidmar-Bergström et al., 2000; Riis, 1996), has remained intact throughout episodes of post-formational fault activity. Fault displacements in the order of several hundred meters (as is required for faulting to be resolved by AFT data) would be expected to offset the paleic surface and thus produce pronounced local relief. However, no indications of preserved up-faulted blocks have been described. Provided that the Hardangervidda plateau at some stage

was covered by several kilometres of sediments, it would be reasonable to expect remnants of preserved sedimentary rocks in down-faulted blocks and fault zones. Thus far, no such sedimentary pockets have been identified.

The track-length distributions of the Hardangervidda samples are unimodal, positively skewed and display a wide range of track lengths, resulting in rather high standard deviations. These features are generally associated with mixed distribution signatures, which are traditionally interpreted to indicate a prolonged or complicated thermal history within the partial annealing zone (Gleadow et al., 1986). A bimodal track length distribution is generally expected for rocks that have been subjected to a distinct reheating episode, such as that portrayed by the model in Fig. 48a. Forward modelling of KJ-19 (Appendix F) indicates that a bimodal track length distribution would only be pronounced for peak reheating temperatures between 90°C and 100 °C. Thus, the absence of two well-defined peaks in the track length distribution diagrams of the samples from the Hardangervidda plateau does not necessarily preclude reburial of the basement by substantial volumes of sediments during Paleogene times. Shallow reburial would be expected to produce a bimodal distribution consisting of a component of short tracks formed during the protracted slow cooling through the upper PAZ and a component of long tracks generated subsequent to the final cooling to surface temperatures. Neither of the analysed Hardangervidda samples displays such a track length distribution.

The ICE hypothesis suggests general monotonous cooling following the climax of the Caledonian orogeny. Consequently, the predicted cooling paths are not time-dependently constrained to specific thermal conditions and the ICE hypothesis therefore cannot be tested in the same detailed manner as the peneplanation-uplift model. However, the fission track and (U-Th)/He data obtained in the current study are compatible with the general exhumation scenario portrayed by the ICE hypothesis, i.e. protracted exhumation governed mainly by rift-related extension along the coast and by isostatically compensated erosion further inland. According to the flexural isostatic exhumation model presented by Nielsen et al. (2009), AFT ages of 120-140 Ma are expected at low elevations in the inner fjord regions. In the present study the majority of sea level samples exhibit ages between 120 Ma and 130 Ma, with local exceptions on the Eidfjord north flank. The slow Mesozoic cooling that is evident from the thermal history models are in agreement with the notion of Nielsen et al. (2009) of the Late Jurassic and Cretaceous as periods of relative tectonic quiescence and warm climate associated with modest erosion. The ICE hypothesis predicts accelerated exhumation in the Cenozoic, attributed to a climatically driven increase in erosion rates. Unfortunately,

thermochronological techniques cannot directly differentiate between tectonically and climatically induced exhumation. The thermal history models obtained in the present study strongly indicate accelerated Cenozoic cooling rates, but it cannot be inferred whether the cooling signals are attributed to topographic rejuvenation following uplift (as implied by the peneplanation-uplift model) or increased efficiency of surface processes as a response to climatic changes.

In light of the new thermochronological data presented in the current contribution, pre-Eocene peneplanation and subsequent uplift is suggested to provide an inadequate explanation for the morphotectonic evolution of southwestern Norway. Taking the thermal conditions required by the AFT data into account, the peneplanation scenario is found to be in conflict with independent geological observations. This assessment is based on thermal history modelling of three samples. In order to draw a firm conclusion with regard to the compatibility between the AFT record and the peneplanation-uplift model, the results obtained in the present study must be verified by additional data from the Hardangervidda plateau. It should be noted that the alternative thermal history models presented in this thesis were constructed to acknowledge the main perspectives on the age of the paleic surface portrayed in previous studies and do not cover the full range of possible scenarios. By shifting the timing of peneplanation towards the present, the compatibility between the resulting cooling paths, the AFT data and the geological observations is expected to improve. Although, the presented data are in accordance with the thermal conditions inferred by the ICE hypothesis, the most recent cooling history, which is essential for understanding the topographic evolution, cannot be resolved by the AFT and (U-Th)/He methods. Hence, the key principles of the ICE hypothesis are neither disproved nor verified.

9. CONCLUSION

From the thermochronological and structural data obtained in the present study, the following main conclusions can be drawn:

- A general correlation between AFT age and elevation is found throughout the studied area. Early Cretaceous cooling ages predominate close to sea level, while Jurassic ages are widespread on the Hardangervidda plateau. This implies that samples from high elevations reached shallower crustal depths at an earlier stage than samples from low elevations and suggests that progressive, uniform exhumation of the crustal column has exerted the main control on the thermal evolution. The age-elevation gradients from the Kjeåsen and Bu profiles imply low cooling rates of ~1°C within the time interval bracketed by the AFT ages. Short mean track lengths and mixed distribution signatures suggest a thermal history characterized by slow cooling through the temperatures associated with the upper kilometres of the crust. Surprisingly young ages and short mean track lengths within the Hardangerfjord Shear Zone may be explained by hydrothermal heating.
- The obtained (U-Th)/He ages suggest cooling through the 70-40 °C isotherms in the Cretaceous, i.e. ~50 Ma after cooling through the apatite partial annealing zone. This relation substantiates the low Jurassic-Cretaceous cooling rates estimated from the AFT age-elevation trends. The generally poor reproducibility of single grain (U-Th)/He ages may be attributed to He trapping effects associated with accumulated radiation damage.
- Thermal history modelling indicates two main time intervals characterized by rapid cooling. The first is constrained to the Permo-Triassic and is suggested to reflect accelerated denudation rates in relation to rift flank uplift and reactivation of major structures. A second cooling episode commenced in the latest Cretaceous-Paleogene, concomitant with the onset of rifting in the North Atlantic and proposed episodes of uplift attributed to the thermal effects of the Icelandic plume. Accelerated Neogene cooling is pronounced in thermal history models of samples from sea level. A substantial portion of this recent cooling is probably attributed to Quaternary fjord incision.

- Fission track ages are locally offset across lineaments. This is interpreted to reflect significant post-middle-late-Jurassic fault activity. Considerable brittle deformation has been accommodated by N-S-trending structures. Reactivation of other fracture sets is likely to have taken place, but the displacements are below the resolution of the AFT method and firm conclusions cannot be drawn. Differential fission track signatures and offset PAZ exits across the Eidfjord suggest Cenozoic displacement along a fault that underlies the fjord, possibly in combination with reactivation of smaller-scale structures within the Eidfjord north block.
- Decreasing apatite fission track ages are generally evident from the coast towards the interior of southwestern Norway. This age pattern may be explained in terms of general down-to-the-west extensional displacement along structures that dissect the coastal plain and the outer rift flank.
- The required reburial depths and possible Cenozoic fault activity inferred from thermal history modelling of samples from the Hardangervidda plateau are found to conflict with pre-Eocene peneplanation of southern Norway. However, more recent peneplanation is not precluded by the data. The obtained results are in agreement with the ICE hypothesis, but the most recent thermal history, which is essential for the understanding of the topographic evolution of the southwestern Norwegian margin, is outside the sensitivity range of the applied thermochronometers and cannot be resolved from this study alone.

10. OUTLOOK

The present study has provided new perspectives on the tectonic evolution of the inner Hardangerfjord region through low-temperature thermochronology of densely spaced samples. There are still numerous unresolved aspects regarding the morphotectonic development of the areas surrounding the Hardangerfjord and further sampling is clearly required. As a regional pattern of fission track ages in southwestern Norway has already been established, future studies should focus on detailed sampling in geographically restricted areas in order to contribute a better understanding of the structural complexity. The sampling scheme utilized in the present study (i.e. vertical profiles) is most successful when faults are avoided entirely (although this must be regarded as a nearly impossible task). Future studies should employ systematic sampling across lineaments of equal orientations in order to elucidate the displacement records of individual fault populations. In the inner Hardangerfjord region, the pervasive N-S-trending fracture set is of particular interest. Additionally, it would certainly be worthwhile studying the possible displacement records of brittle structures that parallel the Hardangerfjord Shear Zone. Granvin and Ulvik would make interesting targets for future studies attempting to reveal whether the Hardangerfjord Shear Zone has experienced post-Devonian brittle reactivation and associated circulation of hydrothermal fluids. Additional samples should be collected in the hangingwall immediately to the west of the HSZ in order to detect possible differential cooling patterns across the innermost exposed segment and thus improve the understanding of how the HSZ has influenced the topographic evolution of the area. An extensive study involving apatite fission track and apatite and zircon (U-Th)/He analysis of samples from the central Hardangerfjord region is currently in preparation and is expected to provide new insights into the exhumation history across the Hardangerfjord Shear Zone. Thermochronological studies across the transitional relay structures of the Lærdal-Gjende Fault to the north of the present study area could potentially yield valuable information on possible differences in exhumation style from southwest to northeast along the strike of the HSZ.

The samples collected from low elevations in Simadalen were unfortunately not datable. Considering the young ages obtained from relatively high elevations in this particular area, samples from sea level may provide new information about the more recent thermal history of the inner Hardangerfjord region and should be included in future studies. The Eidfjord Granite is obviously not an ideal lithology for fission track analysis, but migmatitic

gneisses are abundant directly northeast of the sampled outcrops and are generally found to contain sufficient apatite of good quality. In order to constrain the Cretaceous and Cenozoic cooling history, the vertical profiles should be extended by sampling below sea level in the fjords. The tributaries of the inner Hardangerfjord are shallow and are therefore not obvious targets for such a sampling strategy. However, the outer Eidfjord is relatively deep and may potentially hold intriguing clues to the topographic evolution of the southern Scandes.

By applying the (U-Th)/He method to closely spaced samples from lateral transects and vertical profiles it may be possible to constrain the proposed Cenozoic cooling event and determine whether the extensive fault activity that is documented in the present work also continued into the Late Cretaceous and possible even the Paleogene. However, the (U-Th)/He method still yields unreliable results for many Norwegian samples. Clearly, problems regarding the possible retentive effects of radiation damage and the nearly ubiquitous zoning observed in samples from southern Norway must be addressed in the future for this approach to be successful.

Joint modelling of samples from vertical profiles may significantly constrain the cooling paths, considering that temperature recorded by a sample at any given time is highly dependent on the temperatures of the remaining samples in the profile. In the modelling approach applied in the current study every sample is treated independently. A joint modelling approach is normally most successful if all included samples have experienced the same cooling history. It is thereby essential that sampling is accompanied by detailed structural mapping.

Although the inner Hardangerfjord region has been targeted by several detailed thermochronological studies in the past, the present contribution reveals some new aspects regarding the exhumation history and structural evolution of the area. Clearly, regional studies cannot fully elucidate the structural complexity of southern Norway and detailed studies of restricted areas are required. Despite the effort of a number of workers over the last couple of decades, a considerable amount of thermochronological and structural work thus remains for a thorough understanding of the intricate post-Permian evolution of the Norwegian North Sea margin.

REFERENCES

Allmendinger, R. W., Cardozo, N., & Fisher, D. M. (2012). *Structural Geology Algorithms: Vectors and Tensors*. New York: Cambridge University Press.

Andersen, T., Andresen, A., & Sylvester, A. G. (2002). Timing of late- to post-tectonic Sveconorwegian granitic magmatism in South Norway. *Norges Geologiske Undersøkelse Bulletin, 440*, 5-18.

Andersen, T. B. (1998). Extensional tectonics in the Caledonides of southern Norway, an overview. *Tectonophysics, 285*, 333-351.

Andersen, T. B., Torsvik, T. H., Eide, E. A., Osmundsen, P. T., & Faleide, J. I. (1999). Permian and Mesozoic extensional faulting within the Caledonides of central south Norway. *Journal of the Geological Society, London, 156*, 1073-1080.

Anderson, R. S. (2002). Modeling the tor-dotted crests, bedrock edges, and parabolic profiles of high alpine surfaces of the Wind River Range, Wyoming. *Geomorphology, 46*, 35-58.

Andriessen, P. A. M., & Bos, A. (1986). Post-Caledonian thermal evolution and crustal uplift in the Eidfjord area, Western Norway. *Norwegian Journal of Geology, 66*, 243-250.

Barbarand, J., Carter, A., Wood, I., & Hurford, T. (2003a). Compositional and structural control of fission-track annealing in apatite. *Chemical Geology, 198*, 107-137.

Barbarand, J., Hurford, A. J., & Carter, A. (2003b). Variation in apatitefission-track length measurement: implications for thermal history modelling. *Chemical Geology, 198*, 77-106.

Belton, D. X., Brown, R. W., Kohn, B. P., Fink, D., & Farley, K. A. (2004). Quantitative resolution of the debate over antiquity of the central Australian landscape: implications for the tectonic and geomorphic stability of cratonic interiors. *Earth and Planetary Science Letters, 219*, 21-34.

Bernet, M. (2009). A field-based estimate of the zircon fission-track closure temperature. *Chemical Geology, 259*, 181-189.

Bhandari, N., Bhat, S. G., Lal, D., Rajagopalan, G., Tamhane, A. S., & Venkatavaradan, V. S. (1971). Fission fragment tracks in apatite: recordable track lengths. *Earth and Planetary Science Letters, 13*, 191-199.

Bingen, B., Nordgulen, Ø., & Viola, G. (2008). A four-phase model for the Sveconorwegian orogeny. *Norwegian Journal of Geology, 88*, 43-72.

Birkeland, A., Sigmond, E. M. O., Whitehouse, M. J., & Vestin, J. (1997). From Archaean to Proterozoic on Hardangervidda, South Norway. *Norges Geologiske Undersøkelse Bulletin, 433*, 4-5.

Boundy, T. M., Essene, E. J., Hall, C. M., Austrheim, H., & Halliday, A. N. (1996). Rapid exhumation of lower crust during continent-continent collision and late extension: Evidence from 40Ar/39Ar incremental heating of hornblendes and muscovites, Caledonian orogen, western Norway. *Geological Society of America Bulletin, 108*(9), 1425-1437.

Braathen, A., Nordgulen, Ø., Osmundsen, P. T., Andersen, T. B., Solli, A., & Roberts, D. (2000). Devonian, orogen-parallel, opposed extension in the Central Norwegian Caledonides. *Geology, 28*(7), 615-618.

Bray, R. J., Green, P. F., & Duddy, I. R. (1992). Thermal history reconstruction using apatite fission track analysis and vitrinite reflectance; a case study from the UK East Midlands and southern North Sea. *Geological Society, London, Special Publications, 67*, 2-25.

Bungum, H., Alsaker, A., Kvamme, L. B., & Hansen, R. A. (1991). Seismicity and Seismotectonics of Norway and Nearby Continental Shelf Areas. *Journal of Geophysical Research, 96*(B2), 2249-2265.

Burchart, J., Butkiewicz, T., Dakowski, M., & Galazka-Friedman, J. (1979). Fission track retention in minerals as a function of heating time during isothermal experiments: a discussion. *Nuclear Tracks, 3*, 109-117.

Bursill, L. A., & Braunshausen, G. (1990). Heavy-ion irradiation tracks in zircon. *Philosophical Magazine, 62*, 395-420.

Burtner, R. L., Nigrini, A., & Donelick, R. A. (1994). Thermochronology of Lower Cretaceous source rocks in the Idaho-Wyoming Thrust Belt. *Bulletin of the American Association of Petroleum Geologists, 78*, 1613-1636.

Carlson, W. D., Donelick, R. A., & Ketcham, R. A. (1999). Variability of apatite fission track annealing kinetics: I. Experimental results. *American Mineralogist, 84*, 1213-1223.

Cederbom, C., Larson, S. Å., Tullborg, E.-L., & Stiberg, J.-P. (2000). Fission track thermochronology applied to Phanerozoic thermotectonic events in central and southern Sweden. *Tectonophysics, 316*, 153-167.

Chadderton, L. T. (1988). On the anatomy of a fission fragment track. *Nuclear Tracks, 15*, 11-29.

Chadderton, L. T. (2003). Nuclear tracks in solids: registration physics and the compound spike. *Radiation Measurements, 36*, 13-34.

Chauvet, A., & Dallmeyer, R. D. (1992). 40Ar/39Ar mineral dates related to Devonian extension in the southwestern Scandinavian Caledonides. *Tectonophysics, 210*, 155-177.

Chauvet, A., & Séranne, M. (1994). Extension-parallell folding in the Scandinavian Caledonides: implications for late-orogenic processes. *Tectonophysics, 238*, 31-54.

Cloetingh, S., Gradstein, F. M., Kooi, H., Grant, A. C., & Kaminski, M. (1990). Plate reorganization; a cause of rapid late Neogene subsidence and sedimentation around the North Atlantic. *Journal of the Geological Society, London, 147*, 495-506.

Danišík, M., Kuhlemann, J., Dunkl, I., Evans, N. J., Székely, B., & Frisch, W. (2012). Survival of Ancient Landforms in a Collisional Setting as Revealed by Combined Fission Track and (U-Th)/He Thermochronometry: A Case Study from Corsica (France). *The Journal of Geology, 120*(2), 155-173.

Davis, W. M. (1889). The rivers and valleys of Pennsylvania. *National Geographic Magazine, 1*, 183-253.

Dietler, T. N., Koestler, A. G., & Milnes, A. G. (1985). A preliminary structural profile through the Western Gneiss Complex, Sognefjord, Southwestern Norway. *Norwegian Journal of Geology, 65*, 233-235.

Dobrzhinetskaya, L. F., Eide, E. A., Larsen, R. B., Smith, D. C., Sturt, B. A., Tønnes, R. G., Taylor, W. R., & Poshukhova, T. V. (1995). Microdiamonds in high-grade metamorphic rocks from the Western Gneiss region, Norway. *Geology, 23*, 597-600.

Dodson, M. H. (1973). Closure temperature in cooling geochronological and petrological systems. *Contributions to Mineralogy and Petrology, 40*, 259-274.

Donelick, R. A. (1991). Crystallographic orientation dependence of mean etchable fission track length in apatite: An emperical model and experimental observations. *American Mineralogist, 76*, 83-91.

Donelick, R. A. (1993). U.S.A. Patent No. 5267274.

Donelick, R. A., O'Sullivan, P. B., & Ketcham, R. A. (2005). Apatite Fission-Track Analysis. *Reviews in Mineralogy & Geochemistry, 58*, 49-94.

Donelick, R. A., Roden, M. K., Mooers, J. D., Carpenter, B. S., & Miller, D. S. (1990). Etchable length reduction of induced fission tracks in apatite at room temperature (~23

ºC): crystallographic orientation effects and "initial" mean lengths. *Nuclear Tracks Radiation Measurements, 17*, 261-265.

Doré, A. G. (1992). The Base Tertiary Surface of southern Norway and the northern North Sea. *Norwegian Journal of Geology, 72*(3), 259-265.

Doré, A. G., Lundin, E. R., Jensen, L. N., Birkeland, Ø., Eliassen, P. E., & Fichler, C. (1999). Principal tectonic events in the evolution of the northwest European Atlantic margin. In A. J. Fleet & S. A. R. Boldy (Eds.), *Petroleum Geology of Northwest Europe: Proceedings of the 5th conference*: The Geological Society, London.

Duddy, I. R., Green, P. F., & Laslett, G. M. (1988). Thermal annealing of fission tracks in apatite, 3. Variable temperature behaviour. *Chemical Geology: Isotope Geoscience section, 73*, 25-38.

Dumitru, T. A. (1993). A new computer-automated microscope stage system for fission-track analysis. *Nuclear Tracks and Radiation Measurements, 21*, 557-580.

Dunkl, I. (2002). TRACKKEY: a Windows program for calculating and graphical presentation of fission track data. *Computers & Geosciences, 28*, 3-12.

Dunlap, W. J., & Fossen, H. (1998). Early Paleozoic orogenic collapse, tectonic stability, and late Paleozoic continental rifting revealed through thermochronology of K-feldspars, southern Norway. *Tectonics, 17*(4), 604-620.

Eide, E. A., Torsvik, T. H., & Andersen, T. B. (1997). Absolute dating of brittle fault movements: Late Permian and Late Jurassic fault breccias in western Norway. *Terra Nova, 9*(3), 135-139.

Eide, E. A., Torsvik, T. H., Andersen, T. B., & Arnaud, N. O. (1999). Early Carboniferous Unroofing in Western Norway: A Tale of Alkali Feldspar Thermochronology. *The Journal of Geology, 107*, 353-374.

England, P., & Molnar, P. (1990). Surface uplift, uplift of rocks, and exhumation of rocks. *Geology, 18*, 1173-1177.

Faleide, J. I., Kyrkjebø, R., Kjennerud, T., Gabrielsen, R. H., Jordt, H., Fanavoll, S., & Bjerke, M. D. (2002). Tectonic impact on sedimentary processes during Cenozoic evolution of the northern North Sea and surrounding areas. *Geological Society, London, Special Publications, 196*, 235-269.

Farley, K. A. (2000). He diffusion from apatite: General behaviour as illustrated by Durango fluorapatite. *Journal of Geophysical research, 105*(B2), 2903-2914.

Farley, K. A. (2002). (U-Th)/He Dating: Techniques, Calibrations and Applications. *Reviews in Mineralogy and Geochemistry, 47*, 819-844.

Farley, K. A., Wolf, R. A., & Silver, L. T. (1996). The effects of long alpha-stopping distances on (U-Th)/He ages. *Geochimica et Cosmochimica Acta, 60*(21), 4223-4229.

Fechtig, H., & Kalbitzer, S. (1966). The diffusion of argon in potassium bearing solids. In O. A. Schaeffer & J. Zahringer (Eds.), *Potassium-Argon Dating* (pp. 68-106). Heidelberg: Springer.

Fick, A. (1855). *Philosophical Magazine, 10*, 30-39.

Fitzgerald, P. G., & Gleadow, A. J. W. (1990). New approaches in fission track geochronology as a tectonic tool: Examples from the Transantarctic Mountains. *Nuclear Tracks Radiation Measurements, 17*(3), 351-357.

Fitzgerald, P. G., Sorkhabi, R. B., Redfield, T. F., & Stump, E. (1995). Uplift and denudation of the central Alaska Range: A case study in the use of apatite fission track thermochronology to determine absolute uplift parameters *Journal of Geophysical Research, 100*(B10), 175-191.

Fjeldskaar, W., Lindholm, C. D., Dehls, J. F., & Fjeldskaar, I. (2000). Postglacial uplift, neotectonics and seismicity in Fennoscandia. *Quarternary Science Reviews, 19*, 1413-1422.

Fleischer, R. L., & Price, P. B. (1964a). Fission track evidence for the simultaneous origin of tektites and other natural glasses. *Geochimica et Cosmochimica Acta, 28*, 755-766.

Fleischer, R. L., & Price, P. B. (1964b). Techniques for geological dating of minerals by chemical etching of fission fragment tracks. *Geochimica et Cosmochimica Acta, 28*, 1705-1714.

Fleischer, R. L., Price, P. B., & Walker, R. M. (1965a). Effects of Temperature, Pressure, and Ionization of the Formation and Stability of Fission Tracks in Minerals and Glasses. *Journal of Geophysical Research, 70*(6), 1497-1502.

Fleischer, R. L., Price, P. B., & Walker, R. M. (1965b). The ion spike explosion mechanism for formation of charged particle tracks. *Journal of Applied Physics, 36*, 3645-3652.

Fleischer, R. L., Price, P. B., & Walker, R. M. (1975). *Nuclear Tracks in Solids; Principles and Applications*. Berkeley: University of California Press.

Fossen, H. (1992). The role of extensional tectonics in the Caledonides of south Norway. *Journal of Structural Geology, 14*(8/9), 1033-1046.

Fossen, H. (1998). Advances in understanding the post-Caledonian structural evolution of the Bergen area, West Norway. *Norwegian Journal of Geology, 78*, 33-46.

Fossen, H. (2000). Extensional tectonics in the Caledonides: Synorogenic or postorogenic? *Tectonics, 19*(2), 213-224.

Fossen, H. (2010). Extensional tectonics in the North Atlantic Caledonides: a regional view. *Geological Society, London, Special Publications, 335*, 767-793.

Fossen, H., & Dunlap, W. J. (1998). Timing and kinematics of Caledonian thrusting and extensional collapse, southern Norway: evidence from 40Ar/39Ar thermochronology. *Journal of Structural Geology, 20*(6), 765-781.

Fossen, H., & Dunlap, W. J. (1999). On the age and tectonic significance of Permo-Triassic dikes in the Bergen-Sunnhordaland region, southwestern Norway. *Norwegian Journal of Geology, 79*, 169-178.

Fossen, H., & Hurich, C. A. (2005). The Hardangerfjord Shear Zone in SW Norway and the North Sea: a large scale low-angle shear zone in the Caledonian crust. *Journal of the Geological Society, London, 162*, 675-687.

Fossen, H., Mangerud, G., Hesthammer, J., Bugge, T., & Gabrielsen, R. H. (1997). The Bjorøy Formation: a newly discovered occurrence of Jurassic sediments in the Bergen Arc System. *Norwegian Journal of Geology, 77*, 269-287.

Fossen, H., & Rykkelid, E. (1992). Postcollisional extension of the Caledonide orogen in Scandinavia: Structural expressions and tectonic significance. *Geology, 20*, 737-740.

Færseth, R. B., Gabrielsen, R. H., & Hurich, C. A. (1995). Influence of basement in structuring of the North Sea basin, offshore southwest Norway. *Norwegian Journal of Geology, 75*, 105-119.

Færseth, R. B., Knudsen, B.-E., Liljedahl, T., Midbøe, P. S., & Søderstrøm, B. (1997). Oblique rifting and sequential faulting in the Jurassic development of the northern North Sea. *Journal of Structural Geology, 19*, 1285-1302.

Færseth, R. B., & Lien, T. (2002). Cretaceous evolution in the Norwegian Sea - a period characterized by tectonic quiescence. *Marine and Petroleum Geology, 19*(8), 1005-1027.

Færseth, R. B., Macintyre, R. M., & Naterstad, J. (1976). Mesozoic alkaline dykes in the Sunnhordaland region, western Norway: ages, geochemistry and regional significance. *Lithos, 9*, 331-345.

Gaál, G., & Gorbatschev, R. (1987). An Outline of the Precambrian Evolution of the Baltic Shield. *Precambrian Research, 35*, 15-52.

Gabrielsen, R. H., Braathen, A., Dehls, J. F., & Roberts, D. (2002). Tectonic lineaments of Norway. *Norwegian Journal of Geology, 82*, 153-174.

Gabrielsen, R. H., Faleide, J. I., Pascal, C., Braathen, A., Nystuen, J. P., Etzelmuller, B., & O'Donnel, S. (2010). Latest Caledonian to Present tectonomorphological development of southern Norway. *Marine and Petroleum Geology, 27*, 709-723.

Galbraith, R. F. (1981). On Statistical Models for Fission Track Counts. *Mathematical Geology, 13*(6), 471-478.

Galbraith, R. F. (1988). Graphical display of estimates having different standard errors. *Technometrics, 30*, 271-281.

Galbraith, R. F. (1990). The radial plot: graphical assessment of spread in ages. *Nuclear Tracks, 17*(207-214).

Galbraith, R. F. (2005). *Statistics for fission track analysis*. Boca Raton: Chapman & Hall/CRC.

Gallagher, K., & Brown, R. (1997). The onshore record of passive margin evolution. *Journal of the Geological Society, London, 154*, 451-457.

Gallagher, K., Brown, R., & Johnson, C. (1998). Fission track analysis and its applications to geological problems. *Annual Reviews in Earth and Planetary Sciences, 26*, 519-572.

Gallagher, K., Stephenson, J., Brown, R., Holmes, C., & Fitzgerald, P. G. (2005). Low temperature thermochronology and modelling strategies for multiple samples 1: Vertical profiles. *Earth and Planetary Science Letters, 237*, 193-208.

Gee, D. G., Fossen, H., Henriksen, N., & Higgins, A. K. (2008). From the Early Paleozoic Platforms of Baltica and Laurentia to the Caledonide Orogen of Scandinavia and Greenland. *Episodes, 31*(1), 1-8.

Gilchrist, A. R., & Summerfield, M. A. (1990). Differential denudation and flexural isostasy in the formation of rifted margin upwarps. *Nature, 346*, 739-742.

Gleadow, A. J. W., & Duddy, I. R. (1981). A natural long-term annealing experiment for apatite. *Nuclear Tracks, 5*(1/2), 169-174.

Gleadow, A. J. W., Duddy, I. R., Green, P. F., & Lovering, J. F. (1986). Confined fission tracks in apatite: a diagnostic tool for thermal history analysis. *Contributions to Mineralogy and Petrology, 94*, 405-415.

Gleadow, A. J. W., & Fitzgerald, P. G. (1987). Uplift history and structure of the Transantarctic mountains: new evidence from fission track dating of basement apatites in the Dry Valley area, southern Victoria Land. *Earth and Planetary Science Letters, 82*, 1-14.

Green, P. F. (1980). On the cause of shortening of spontaneous fission tracks in certain minerals. *Nuclear Tracks, 4*, 91-100.

Green, P. F. (1981). A new look at statistics in the fission track dating. *Nuclear Tracks, 5*, 77-86.

Green, P. F. (1988). The relationship between track shortening and fission track age reduction in apatite: combined influences of inherent instability, annealing anisotropy, length bias and system calibration. *Earth and Planetary Science Letters, 89*, 335-352.

Green, P. F., Crowhurst, P. V., Duddy, I. R., Japsen, P., & Holford, S. P. (2006). Conflicting (U/Th)/He and fission track ages in apatite: Enhanced He retention, not anomalous annealing behaviour. *Earth and Planetary Science Letters, 250*, 407-427.

Green, P. F., Duddy, I. R., Gleadow, A. J. W., Tingate, P. R., & Laslett, G. M. (1986). Thermal annealing of fission tracks in apatite 1. A qualitative description. *Chemical Geology, 59*, 237-253.

Green, P. F., Duddy, I. R., Laslett, G. M., Hegarty, K. A., Gleadow, A. J. W., & Lovering, J. F. (1989). Thermal annealing of fission tracks in apatite 4. Quantitative modelling techniques and extension to geological timescales. *Chemical Geology, 79*, 155-182.

Green, P. F., & Durrani, S. A. (1977). Annealing studies of tracks in crystals. *Nuclear Track Detection, 1*(1), 33-39.

Griffin, W. L., Austrheim, H., Brastad, K., Bryhni, I., Krill, A. G., Krogh, E. J., Mørk, M. B. E., Quale, H., & Tørudbakken, B. (1985). High-pressure metamorphism in the Scandinavian Caledonides. In D. G. Gee & B. A. Sturt (Eds.), *The Caledonide Orogen - Scandinavia and Related Areas* (pp. 783-801): J. Wiley and Sons.

Hammerschmidt, K., Wagner, G. A., & Wagner, M. (1984). Radiometric dating on research drill core Urach III: a contribution to its geothermal history. *Journal of Geophysical Research, 54*, 97-105.

Hartz, E. H., Schmid, D. W., Medvedev, S., Martinsen, B. B., Souche, A., Rüpke, L., & Faleide, J. I. (2012). Learning from broken continents: Integrating multidisciplinary onshore-offshore margin-studies across the NE Atlantic. *NGF Abstracts and Proceedings, 2*, 29-31.

Hartz, E. H., & Torsvik, T. H. (2002). Baltica upside down: A new plate tectonic model for Rodinia and the Iapetus Ocean. *Geology, 30*(3), 255-258.

Hasebe, N., Barbarand, J., Jarvis, K., Carter, A., & Hurford, A. J. (2004). Apatite fission-track chronometry using laser ablation ICP-MS. *Chemical Geology, 207*(3-4), 135-145.

Hendriks, B. W. H., Andriessen, P. A. M., Huigen, Y., Leighton, C., Redfield, T. F., Murrell, G., Gallagher, K., & Nielsen, S. B. (2007). A fission track data compilation for Fennoscandia. *Norwegian Journal of Geology, 87*, 143-155.

Hendriks, B. W. H., & Redfield, T. F. (2005). Apatite fission track and (U-Th)/He data from Fennoscandia: An example of underestimation of fission track annealing in apatite. *Earth and Planetary Science Letters, 236*, 443-458.

Hicks, E. C., Bungum, H., & Lindholm, C. D. (2000). Stress inversion of earthquake focal mechanism solutions from onshore and offshore Norway. *Norwegian Journal of Geology, 80*, 235-250.

Hourigan, J. K., Reiners, P. W., & Brandon, M. T. (2005). U/Th zonation dependent alpha ejection in (U-Th)/He thermochronometry. *Geochimica et Cosmochimica Acta, 96*, 3349-3365.

House, M. A., Wernicke, B. P., & Farley, K. A. (1998). Dating topography of the Sierra Nevada, California, using apatite (U-Th)/He ages. *Nature, 396*, 66-69.

Hurford, A. J. (1990). International Union of Geological Sciences subcommission on geochronology recommendation for the standardization of fission track dating calibration and data reporting. *Nuclear Tracks Radiation Measurements, 17*(3), 233-236.

Hurford, A. J., & Carter, A. (1991). The role of fission track dating in discrimination of provenance. In A. C. Morton, S. P. Todd & P. D. W. Haughton (Eds.), *Developments in Sedimentary Provenance Studies* (Vol. 57, pp. 67-78). London: Geological Society, London, Special Publications.

Hurford, A. J., & Green, P. F. (1982). A users' guide to fission track dating calibration. *Earth and Planetary Science Letters, 59*, 343-354.

Hurford, A. J., & Green, P. F. (1983). The zeta age calibration of fission-track dating. *Isotope Geoscience, 1*, 285-317.

Hurford, A. J., & Hammerschmidt, K. (1985). 40Ar/39Ar and K/Ar dating of the bishop and fish canyon tuffs: Calibration ages for fission-track dating standards. *Chemical Geology, 58*(1-2), 23-32.

Hurich, C. A., & Kristoffersen, Y. (1988). Deep structure of the Caledonide orogen in southern Norway: new evidence from marine seismic reflection profiling. In Y. Kristoffersen (Ed.), *Progress in studies of the lithosphere in Norway* (Vol. 3, pp. 96-101). Trondheim: Norges Geologiske Undersøkelse Special Publication.

Japsen, P. (1998). Regional velocity-depth anomalies, North Sea Chalk: a record of overpressure and Neogene uplift and erosion. *AAPG Bulletin, 82*, 2031-2074.

Japsen, P., & Chalmers, J. A. (2000). Neogene uplift and tectonics around the North Atlantic: overview. *Global and Planetary Change, 24*, 165-173.

Johansen, L. (2008). *Exhumation history across major lineaments within and around the Bergen Arc using fission track thermochronology.* MSc Thesis, University of Bergen, Bergen.

Jonckheere, R. C., & Wagner, G. (2000). On the occurence of anomalous fission tracks in apatite and titanite. *American Mineralogist, 85*, 1744-1753.

Jordt, H., Faleide, J. I., Bjørlykke, K., & Ibrahim, M. T. (1995). Cenozoic sequence stratigraphy of the central and northern North Sea Basin: tectonic development, sediment distribution and provenance areas. *Marine and Petroleum Geology, 12*(8), 845-879.

Ketcham, R. A. (2005). Forward and Inverse Modeling of Low-Temperature Thermochronometry Data. *Reviews in Mineralogy & Geochemistry, 58*, 275-314.

Ketcham, R. A., Carter, A., Donelick, R. A., Barbarand, J., & Hurford, A. J. (2007a). Improved measurement of fission-track annealing in apatite using c-axis projection. *American Mineralogist, 92*, 789-798.

Ketcham, R. A., Carter, A., Donelick, R. A., Barbarand, J., & Hurford, A. J. (2007b). Improved modeling of fission-track annealing in apatite. *American Mineralogist, 92*, 799-810.

Ketcham, R. A., Donelick, R. A., Balestrieri, M. L., & Zattin, M. (2009). Reproducibility of apatite fission-track length data and thermal history reconstruction. *Earth and Planetary Science Letters, 284*(3-4), 504-515.

Ketcham, R. A., Donelick, R. A., & Carlson, W. D. (1999). Variability of apatite annealing kinetics: III. Extrapolation to geological time scales. *American Mineralogist, 84*, 1235-1255.

Ketcham, R. A., Gautheron, C., & Tassan-got, L. (2011). Accounting for long alpha-particle stopping distances in (U-Th-Sm)/He geochronology: refinement of the baseline case. *Geochimica et Cosmochimica Acta, 75*, 7779–7791.

Kooi, H., & Beaumont, C. (1994). Escarpment evolution on high-elevation rifted margins: insights derived from a surface process model that combines diffusion, advection, and reaction. *Journal of Geophysical Research, 99*(12), 191-209.

Krabbendam, M., & Wain, A. (1997). Late-Caledonian structures, differential retrogression and structural position of (ultra)high-pressure rocks in the Nordfjord-Stadlandet area, Western Gneiss Region. *Norges Geologiske Undersøkelse Bulletin, 432*, 127-139.

Ksienzyk, A. (2012). *From mountains to basins: geochronological case studies from southwestern Norway, Western Australia and East Antarctica.* PhD Thesis, University of Bergen, Bergen.

Kullerud, L., Tørudbakken, B., & Ilebekk, S. (1986). A compilation of radiometric age determinations from the Western Gneiss Region, south Norway. *Norges Geologiske Undersøkelse Bulletin, 406*, 17-42.

Lal, D., Rajan, R. S., & Tamhane, A. S. (1969). Chemical composition of nuclei Z>22 in cosmic rays using meteoritic minerals as detectors. *Nature, 221*, 33-37.

Larsen, Ø., Fossen, H., Langeland, K., & Pedersen, R. B. (2003). Kinematics and timing of polyphase post-Caledonian deformation in the Bergen area, SW Norway. *Norwegian Journal of Geology, 83*, 149-165.

Laslett, G. M., Galbraith, R., & Green, P. F. (1994). The analysis of projected fission track lengths. *Nuclear Tracks, 23*, 103-123.

Laslett, G. M., Gleadow, A. J. W., & Duddy, I. R. (1984). The relationship between fission track length and track density in apatite. *Nuclear tracks, 9*(1), 29-38.

Laslett, G. M., Kendall, W. S., Gleadow, A. J. W., & Duddy, I. R. (1982). Bias in measurement of fission-track length distributions. *Nuclear Tracks, 6*(2/3), 79-85.

Leighton, C. A. (2007). *The thermotectonic development of southern Norway: constraints from low-temperature thermochronology.* PhD Thesis, Imperial College London, London.

Lidmar-Bergström, K., & Bonow, J. M. (2009). Hypotheses and observations on the origin of the landscape of southern Norway - A comment regarding the isostacy-climate-erosion hypothesis by Nielsen et al. 2008. *Journal of Geodynamics, 48*, 95-100.

Lidmar-Bergström, K., Ollier, C. D., & Sulebak, J. R. (2000). Landforms and uplift history of southern Norway. *Global and Planetary Change, 24*, 211-231.

Lippolt, H. J., Leitz, M., Wernicke, R. S., & Hagedorn, B. (1994). (Uranium+thorium)/helium dating of apatite: Experience with samples from different geochemical environments. *Chemical Geology, 112*, 179-191.

Løvlie, R., & Mitchell, J. G. (1982). Complete remagnetization of some Permian dykes from western Norway induced during burial/uplift. *Physics of the Earth and Planetary Interiors, 30*, 415-421.

Magerholm, T. (2010). *Exhumation history and fault tectonics across the Hardangerfjord Shear Zone, using fission track thermochronology.* MSc Thesis, University of Bergen, Bergen.

Mancktelow, N. S., & Grasemann, B. (1997). Time-dependent effects of heat advection and topography on cooling histories during erosion. *Tectonophysics, 270*, 167-195.

McDowell, F., & Keizer, R. P. (1977). Timing of mid-Tertiary volcanism in the Sierra Madre Occidental between Durango city and Mazatlan, Mexico. *Geological Society of America Bulletin, 88*, 1479-1487.

McDowell, F., McIntosh, W. C., & Farley, K. A. (2005). A precise 40Ar–39Ar reference age for the Durangoapatite (U–Th)/He and fission-track dating standard. *Chemical Geology, 214*(3-4), 249-263.

Milnes, A. G., Dietler, T. N., & Koestler, A. G. (1988). The Sognefjord northshore log - a 25 km depth section through Caledonized basement in western Norway. *Special Publication Norges Geologiske Undersøkelse, 3*, 114-121.

Mitchell, S. G., & Montgomery, D.R. (2006). Influence of a glacial buzzsaw on the height and morphology of the Cascade Range in central Washington State, USA. *Quarternary Research, 65*, 96-107.

Mosar, J. (2003). Scandinavia's North Atlantic passive margin. *Journal of Geophysical Research, 108*, 1-18.

Naeser, C. W. (1979). Thermal history of sedimentary basins: Fission-track dating of subsurface rocks. *Society of Economic Paleontologists and Mineralogists Special Publication, 26*, 109-121.

Naeser, C. W., & Forbes, R. B. (1976). Variation of fission track ages with depth in two deep drill holes. *Transactions of the American Geophysical Union, 57*, 353.

Naeser, C. W., Izett, G. A., & Obradovich, J. D. (1980). Fission-track and K-Ar ages of natural glasses. *U.S. Geological Survey Bulletin, 1489*, 1-31.

Nesje, A., & Whillans, I. M. (1994). Erosion of Sognefjord, Norway. *Geomorphology, 9*, 33-45.

Neumann, E.-R., Olsen, K. H., Baldridge, W. S., & Sundvoll, B. (1992). The Oslo Rift: a review. *Tectonophysics, 208*, 1-18.

Nielsen, S. B., Gallagher, K., Leighton, C., Balling, N., Svenningsen, L., Jacobsen, B. H., Thomsen, E., Nielsen, O. B., Heilmann-Clausen, C., Egholm, D. L., Summerfield, M. A., Clausen, O. R., Piotrowski, J. A., Thorsen, M. R., Huuse, M., Abrahamsen, N., King, C., & Lykke-Andersen, H. (2009). The evolution of western Scandinavian

topography: A review of Neogene uplift versus the ICE (isostacy-climate-erosion) hypothesis. *Journal of Geodynamics, 47*, 72-95.

Norton, M. (1986). Late Caledonian extension in western Norway: A response to extreme crustal thickening. *Tectonics, 5*, 192-204.

O'Sullivan, P. B., & Parrish, R. R. (1995). The importance of apatite composition and single-grain ages when interpreting fission track data from plutonic rocks: a case study from the Coast Ranges, British Columbia. *Earth and Planetary Science Letters, 132*, 213-224.

Ollier, C. D., & Pain, C. F. (1997). Equating the basal unconformity with the palaeoplain: a model for passive margins. *Geomorphology, 19*, 1-15.

Osmundsen, P. T., Andersen, T. B., Markussen, S., & Svendby, A. K. (1998). Tectonics and sedimentation in the hangingwall of a major extensional detachment: the Devonian Kvamshesten Basin, western Norway. *Basin Research, 10*, 213-234.

Pascal, C., Elvebakk, H., & Olesen, O. (2010). *An Assessment of Deep Geothermal Resources in Norway.* Paper presented at the World Geothermal Congress 2010, Bali, Indonesia.

Paul, T. A. (1993). Transmission electron microscopy investigation of unetched fission tracks in fluorapatite - physical process of annealing. *Nuclear Tracks Radiation Measurements, 21*(4), 507-511.

Paul, T. A., & Fitzgerald, P. G. (1992). Transmission electron microscope investigation of fission tracks in fluorapatite. *American Mineralogist, 77*, 336-344.

Pedersen, R. B., Furnes, H., & Dunning, G. (1988). Some Norwegian ophiolite complexes reconsidered: progress in studies of the lithosphere in Norway. *Norges Geologiske Undersøkelse Special Publication, 3*, 80-85.

Price, P. B., & Walker, R. M. (1962). Chemical etching of charged-particle tracks in solids. *Journal of Applied Physics, 33*, 3407-3412.

Price, P. B., & Walker, R. M. (1963). Fossil tracks of charged particles in mica and the age of minerals. *Journal of Geophysical Research, 68*, 4847-4862.

Priem, H. N. A., Boelrijk, N. A. I. M., Hebeda, E. H., Verdurmen, E. A. T., & Verschure, R. H. (1976). Isotope Geochronology of the Eidfjord Granite, Hardangervidda, West Norway. *Norges Geologiske Undersøkelse Bulletin, 327*, 35-39.

Ragnhildstveit, J., Sigmond, E. M. O., & Tucker, R. D. (1994). Early Proterozoic supracrustal rocks west of the Mandal-Ustaoset fault zone, Hardangervidda, South Norway. *Terra Nova Abstract Supplement, 2*, 15-16.

Redfield, T. F. (2010). On apatite fission track dating and the Tertiary evolution of West Greenland topography. *Journal of the Geological Society, London, 167*, 261-271.

Redfield, T. F., Braathen, A., Gabrielsen, R. H., Osmundsen, P. T., Torsvik, T. H., & Andriessen, P. A. M. (2005). Late Mesozoic to Early Cenozoic components of vertical separation across the Møre-Trøndelag fault complex, Norway. *Tectonophysics, 395*, 233-249.

Redfield, T. F., Torsvik, T. H., Andriessen, P. A. M., & Gabrielsen, R. H. (2004). Mesozoic and Cenozoic tectonics of the Møre Trøndelag Fault Complex, central Norway: constraints from new apatite fission track data. *Physics and Chemistry of the Earth, 29*, 673-682.

Reusch, H. (1901). Nogle bidrag til forstaaelsen af hvorledes Norges dale og fjelde er blevne til. *Norges Geologiske Undersøgelse 32, Aarbog for 1900*, 124-263.

Riis, F. (1996). Quantification of Cenozoic vertical movements of Scandinavia by correlation of morphological surfaces with offshore data. *Global and Planetary Change, 12*, 331-357.

Riis, F., & Fjeldskaar, W. (1992). On the magnitude of the Late Tertiary and Quarternary erosion and its significance for the uplift of Scandinavia and the Barents Sea. In R. M.

Larsen, H. Brekke, B. T. Larsen & E. Talleraas (Eds.), *Structural and Tectonic Modelling and its Application to Petroleum Geology. NPF Special Publication 1* (pp. 163-185). Amsterdam: Elsevier.

Roberts, A. M., Yielding, G., Kusznir, N. J., Walker, I. M., & Dorn-Lopez, D. (1995). Quantitative analysis of Triassic extension in the Northern Viking graben. *Journal of the Geological Society, London, 152*, 15-26.

Roberts, D., & Gee, D. G. (1985). An introduction to the structure of the Scandinavian Caledonides. In D. G. Gee & B. A. Sturt (Eds.), *The Caledonide Orogen - Scandinavia and Related Areas* (pp. 55-68). Chichester: John Wiley and Sons.

Roberts, D., Nordgulen, Ø., & Melezhik, V. (2007). The uppermost allochthon in the Scandinavian Caledonides; from a Laurentian ancestry through Taconian orogeny to Scandian crustal growth on Baltica. *Geological Society of America Memoir 200*.

Rohrman, M. (1995). *Thermal evolution of the Fennoscandian region from fission track thermochronology: An integrated approach.* PhD Thesis, Vrije Universiteit, Amsterdam.

Rohrman, M., & van der Beek, P. (1996). Cenozoic postrift domal uplift of North Atlantic margins: An astenospheric diapirism model. *Geology, 24*(10), 901-904.

Rohrman, M., van der Beek, P., & Andriessen, P. A. M. (1994). Syn-rift thermal structure and post-rift evolution of the Oslo Rift (SE Norway): New constraints from fission track thermo-chronology. *Earth and Planetary Science Letters, 127*, 39-54.

Rohrman, M., van der Beek, P., Andriessen, P. A. M., & Cloetingh, S. (1995). Meso-Cenozoic morphotectonic evolution of southern Norway: Neogene domal uplift inferred from apatite fission track thermochronology. *Tectonics, 14*(3), 704-718.

Rutherford, E. (1905). Present problems in radioactivity. *Popular Science, May*, 1-34.

Séranne, M. (1992). Late-Paleozoic kinematics of the Møre-Trøndelag fault zone and adjacent areas, central Norway. *Norwegian Journal of Geology, 72*, 141-158.

Shuster, D. L., Flowers, R. M., & Farley, K. A. (2006). The influence of natural radiation damage on helium diffusion kinetics in apatite. *Earth and Planetary Science Letters, 249*, 148-161.

Sibson, R. H. (1977). Fault rocks and fault mechanisms. *Journal of the Geological Society, London, 133*, 191-213.

Sigmond, E. M. O. (1985). The Mandal-Ustaoset line, a newly discovered major fault zone in South Norway. In A. C. Tobi & J. L. R. Touret (Eds.), *The Deep Proterozoic Crust in the North Atlantic Provinces*. Dordrecht: D. Reidel Publishing Company.

Sigmond, E. M. O. (Cartographer). (1998). Geologisk kart over Norge, berggrunnskart Odda, 1:250000.

Sigmond, E. M. O., Birkeland, A., & Bingen, B. (2000). A possible basement to the Mesoproterozoic quartzites on Hardangervidda, South-central Norway: zircon U-Pb geochronology of a migmatitic gneiss. *Norges Geologiske Undersøkelse Bulletin, 437*, 25-32.

Silk, E. C. H., & Barnes, R. S. (1959). Examination of fission fragment tracks with an electron microscope. *Philosophical Magazine, 4*, 970-972.

Skelton, A., & Jakobsson, M. (2007). Could peridotite hydration reactions have provided a contributory driving force for Cenozoic uplift and accelerated subsidence along the margins of the North Atlantic and Labrador Sea? *Norwegian Journal of Geology, 87*, 241-248.

Skogseid, J., & Lunt, I. (2012). Late Cretaceous and Cenozoic dynamic uplift and plate kinematics in the NE Atlantic realm. *NGF Abstracts and Proceedings, 2*, 70.

Steer, P., Huismans, R. S., Valla, P. G., Gac, S., & Herman, F. (2012). Bimodal Plio-Quaternary glacial erosion of fjords and low-relief surfaces in Scandinavia. *Nature Geoscience, 5*, 635-639.

Steiger, R. H., & Jäger, E. (1977). Subcommission on geochronology: Convention on the use of decay constants in geo- and cosmochronology. *Earth and Planetary Science Letters, 36*, 359-362.

Stephens, M. B. (1988). The Scandinavian Caledonides: a complexity of collisions. *Geology Today, 4*, 20-26.

Stuevold, L. M., & Eldholm, O. (1996). Cenozoic uplift of Fennoscandia inferred from a study of the mid-Norwegian margin. *Global and Planetary Change, 12*, 359-386.

Stüwe, K., White, L., & Brown, R. (1994). The influence on eroding topography on steady-state isotherms - application to fission track analysis. *Earth and Planetary Science Letters, 124*, 63-74.

Tagami, T., & O'Sullivan, P. B. (2005). Fundamentals of Fission-Track Thermochronology. *Reviews in Mineralogy & Geochemistry, 58*, 19-47.

Torske, T. (1972). Tertiary oblique uplift of western Fennoscandia; crustal warping in connection with rifting and break-up of the Laurasian continent. *Norges Geologiske Undersøkelse Bulletin, 273*, 43-48.

Torsvik, T. H., Andersen, T. B., Eide, E. A., & Walderhaug, H. J. (1997). The age and tectonic significance of dolerite dykes in western Norway. *Journal of the Geological Society, London, 154*, 961-973.

Torsvik, T. H., & Cocks, R. M. (2005). Norway in space and time: A Centennial cavalcade. *Norwegian Journal of Geology, 85*, 73-86.

Torsvik, T. H., Sturt, B. A., Swensson, E., Andersen, T. B., & Dewey, J. F. (1992). Palaeomagnetic dating of fault rocks: evidence for Permian and Mesozoic movements and brittle deformation along the extensional Dalsfjord fault, western Norway. *Geophysical Journal International, 109*, 565-580.

Tørresen, S. (2009). *Exhumation history and fault tectonics across the North Sea margin in the Nordhordaland area, from Øygarden to Masfjorden, using fission track thermochronology.* MSc Thesis, University of Bergen, Bergen.

Utami, K. J. (2012). *Exhumation history and tectonics across the Hardangerfjord Shear Zone, using apatite fission track thermochronology.* MSc Thesis, University of Bergen, Bergen.

Van den Haute, P. (1977). Apatite fission track dating of Precambrian intrusive rocks from the southern Rogaland (south-western Norway). *Bulletin van de Belgische Vereniging voor Geologie, 86*, 97-110.

Van den Haute, P., De Corte, F., Jonckheere, R., & Bellemans, F. (1998). The parameters that govern the accuracy of fission-track age determinations: a re-appraisal. In P. Van den Haute & F. De Corte (Eds.), *Advances in Fission-Track Geochronology* (pp. 33-46). Dordrecht: Kluwer Academic Publishers.

van der Beek, P., Cloetingh, S., & Andriessen, P. (1994). Mechanisms of extensional basin formation and vertical motions at rift flanks: Constraints from tectonic modelling and fission-track thermochronology. *Earth and Planetary Science Letters, 121*, 417-433.

Vineyard, G. H. (1976). Thermal Spikes and Activated Processes. *Radiation Effects, 29*, 245-248.

Vågnes, E., Gabrielsen, R. H., & Haremo, P. (1998). Late Cretaceous-Cenozoic intraplate contractional deformation at the Norwegian continental shelf: timing, magnitude and regional implications. *Tectonophysics, 300*, 29-46.

Wagner, G. (1972). The geological interpretation of fission track ages. *Transactions of the American Nuclear Society, 15*, 117.

Wagner, G., Coyle, D. A., Duyster, J., Henjes-Kunst, F., Peterek, A., Schröder, B., Stöckhert, B., Wemmer, K., Zulauf, G., Ahrendt, H., Bischoff, R., Hejl, E., Jacobs, J., Menzel, D., Lal, N., Van den Haute, P., Vercoutere, C., & Welzel, B. (1997). Post-Variscan thermal and tectonic evolution of the KTB site and its surroundings. *Journal of Geophysical Research, 102*(B8), 18,221-218,232.

Wagner, G., & Reimer, G. M. (1972). Fission track tectonics: The tectonic interpretation of fission track apatite ages. *Earth and Planetary Science Letters, 14*, 263-268.

Wagner, G., & Storzer, D. (1972). Fission track length reductions in minerals and the thermal history of rocks. *Transactions of the American Nuclear Society, 15*, 127-128.

Wagner, G., & Van den Haute, P. (1992). *Fission-track dating*. Dordrecht: Kluwer Academic Publishers.

Wendt, A. S., Olivier, V., & Chadderton, L. T. (2002). Experimental evidence for the pressure dependence of fission track annealing in apatite. *Earth and Planetary Science Letters, 201*, 593-607.

Wilks, W. J., & Cuthbert, S. J. (1994). The evolution of the Hornelen Basin detachment system, western Norway: Implications for the style of late orogenic extension in the southern Scandinavian Caledonides. *Tectonophysics, 238*, 1-30.

Wolf, R. A., Farley, K. A., & Kass, D. M. (1998). Modeling of the temperature sensitivity of the apatite (U-Th)/He thermochronometer. *Chemical Geology, 148*(1-2), 105-114.

Wölfler, A., Kurz, W., Danišík, M., & Rabitsch, R. (2010). Dating of fault zone activity by apatite fission track and apatite (U–Th)/He thermochronometry: a case study from the Lavanttal fault system (Eastern Alps). *Terra Nova, 22*(4), 274-282.

Young, E. J., Myers, A. T., Munson, E. L., & Conklin, N. M. (1969). Mineralogy and geochemistry of fluorapatite from Cerro de Mercado, Durango, Mexico. *U.S. Geological Survey Professional Paper, 650*, D84-D93.

Zeitler, P. K., Herczeg, A. L., McDoughall, I., & Honda, M. (1987). U-Th-He dating of apatite: A potential thermochronometer. *Geochimica et Cosmochimica Acta, 51*, 2865-2868.

Appendix A: List of samples

Outcrop number	Sampling date	Location	Elevation (m asl)	UTM N UTM E	Outcrop type and description	Sample description	Joints	Spacing
BG-13	07.09.2007	Ulgenes	25	371904 6701787	Freshly exposed road outcrop beween Ulgenes and Tjoflot.	Coarse-grained granite with qtz, pink kfsp and bt. Pegmatite dykes (~3 dm wide).	059/82 057/90 053/83 048/85 019/72 347/55 053/64 352/53	dm-m-spacing
BG-14	08.09.2007	Osafjellet	1055	398209 6719094	Relatively freshly exposed road outcrop.	Coarse-grained augen gneiss with fsp, qtz and bt. Fsp augen are < 5 cm. Pegmatite dykes (dm-m-scale). Felsic "schlieren" - migmatite? Well-foliated.	272/81 312/83 257/75	m- several m-spacing
BG-16	08.09.2007	Skår	510	372345 6719421	Road outcrop next to sideroad to Skår.	Augen gneiss. Grain size varies between layers. Qtz, fsp and bt are abundant. Pink kfsp augen are < 1 cm. Layers of pink kfsp and lenses of qtz.	193/82 205/81 206/82 127/74	dm-m-spacing
BG-26		Kvanndal	25	370234 6706814	Road outcrop along the Granvinfjord between Kvanndal and Granvin. ~6 m high.	Medium-grained, light grey granite with pegmatitic "schlieren" of qtz, pink kfsp and bt. Xenoliths of dark grey gneiss.	No dominant joint direction	
BG-27		Utne	130	367631 6701607	Freshly exposed road outcrop. 1-3 m high.	Medium-grained , light grey granite with qtz, fsp and bt. Light-coloured fsp-bands occur locally. Cut by qtz-fsp pegmatite dyke (~30 cm wide).	312/75	Jointing not significant

Outcrop number	Sampling date	Location	Elevation (m asl)	UTM N UTM E	Outcrop type and description	Sample description	Joints	Spacing
BG-53	04.06.2008	Jåstad	3	368998 6691882	Road outcrop.	Medium-grained, light grey granite with qtz, fsp, bt. Blocks of gneiss in the granite. Fine-grained mafic dyke.	171/20 186/31 213/39 135/42 116/45 090/10 029/86 040/87 047/85 119/56 205/41 076/16	dm-several m-spacing
KJ-1	06.07.2011	Osafjellet	950	397022 6717880	Freshly exposed road outcrop.	Augen gneiss. Coarse grained qtz. White, <10 cm fsp augen. Minor mafics, mostly bt. Well-foliated.	060/74 202/84 057/82 030/46	dm-scale
KJ-2	06.07.2011	Osafjellet, Langevatn	1115	396599 6715530	Freshly exposed road outcrop close to Langevatn.	Coarse-grained migmatitic gneiss. Light bands are dominated by qtz and fsp. Bt-rich dark bands.	018/60	2-3 m
KJ-3	06.07.2011	Osafjellet	750	395211 6717419	Steep slope close to the road to Osafjellet.	Coarse-grained, homogeneously dark-coloured granodioritic (?) gneiss with qtz, plg and abundant bt. Weak foliation. Pegmatite dykes.	216/82 144/43 146/53	>1m
KJ-4	06.07.2011	Osa	550	394777 6717210	Freshly exposed road outcrop	Migmatitic gneiss. Leococratic layers contain coarse-grained qtz and white K-fsp. Some layers contain dominantly qtz. Dark grey, finer-grained mafic layers with mainly bt and hbl. Complex folding.	206/81 202/84 028/84	dm-m-spacing

Outcrop number	Sampling date	Location	Elevation (m asl)	UTM N UTM E	Outcrop type and description	Sample description	Joints	Spacing
KJ-5	06.07.2011	Osa	330	394223 6717643	Freshly exposed road outcrop	Dark grey/black amphibolitic gneiss. Medium-grained. Abundant hbl, plg and bt. Weakly foliated. Coarse-grained fsp veins are foliated together with the host rock.	232/47	1-2 m
KJ-6	06.07.2011	Osa	195	393337 6718091	Freshly exposed road outcrop	Grey, medium-grained migmatitic gneiss with pegmatoidal fsp veins. Stromatic layers. Leocosome with qtz and plg. Bt-rich mafic layers.	224/35 228/83 036/77	Several m
KJ-7	16.07.2011	Osa	105	392936 6718446	River outcrop close to steep cliff.	Light-coloured, medium-grained gneiss with abundant plg and qtz. Thin (<1 cm), discontinuous melanocratic layers with abundant bt. Weakly foliated.	No prominent joints detected	
KJ-8	16.07.2011	Osa	45	392399 6718079	Steep cliff behind red house.	Medium-coarse-grained leococratic gneiss. Rich in qtz and fsp. Local clusters of bt. Weakly-moderately foliated.	No single dominant orientation	
KJ-9	02.08.2011	Between Brimnes and Eidfjord	30	387723 6706130	Road outcrop. Steep cliff close to the road between Brimnes and Eidfjord.	Medium-grained, dark grey gneiss. Abundant coarse-grained qtz and plg. Weakly foliated. Wide,qtz- and fsp-rich pegmatoidal veins. No preferred orientation.	270/34 110/20	>1m
KJ-10	02.08.2011	Sima	15	397384 6707611	Relatively fresh, but dirty road outcrop, located in the innermost fjord near Sima.	Coarse-grained, white granite. Massive. Mostly qtz, some fsp. Large bt-crystals, locally > 1 cm.	Exfoliation	>1m

Outcrop number	Sampling date	Location	Elevation (m asl)	UTM N UTM E	Outcrop type and description	Sample description	Joints	Spacing
KJ-11	02.08.2011	Eidfjord	15	394397 6705845	Freshly exposed, dirty road outcrop by the intersection between the road to Sima and the road to Blurneslia.	Coarse-grained, light granite. Massive. High content of qtz, plg and bt. Additional hbl and brown ttn. Pegmatoidal fsp veins (1-30 cm) occur locally.	176/40	Several m
KJ-12	04.08.2011	Bu	980	382092 6703384	Mountain outcrop on the outer margin of the Hardangervidda plateau. Steep terrain. Moderatly to strongly weathered outcrops covered by lichen.	Fine-medium-grained granite. Mainly qtz and white kfsp. Some bt. Weakly deformed.		
KJ-13	04.08.2011	Bu	790	382239 6703732	Mountain outcrop by dry river bed along a steep track from Bu to Hardangervidda.	Light grey, medium-coarse-grained granite. Abundant qtz and fsp. Some bt. Weakly deformed.	No single dominant orientation	
KJ-14	04.08.2011	Bu	640	382410 6704005	River outcrop in Budalen. Relatively fresh, but dirty surfaces.	Light grey, medium-grained granite. Mainly qtz and fsp. Fine crystals of bt. Weakly deformed.	No single dominant orientation	
KJ-15	04.08.2011	Bu	440	382646 6704522	Beneath steep cliffs in the woods slightly west of the marked track.	Light grey, medium-coarse-grained granite. Rich in qtz and fsp. Some fine bt. Weakly deformed. Abundant qtz veins.	No single dominant orientation	
KJ-16	05.08.2011	Bu	190	382574 6705192	Road outcrop by tractor road close to the farm at Bu.	Fine-grained, grey gneiss. Parallel leucocratic bands with mainly fsp and some qtz. Melanocratic bands with fine-grained bt. dm-scale pegmatitic veins (fsp).	061/65	<10 cm - dm 2
KJ-17	05.08.2011	Bu	100	382736 6705609	Road outcrop just west of Bugjelet.	Dark grey meta-dacite(?). Fine-grained. Contains plg, qtz, hbl and bt. dm- m-scale pegmatoidal veins of fsp.	039/65	1 dm- 1m

Outcrop number	Sampling date	Location	Elevation (m asl)	UTM N UTM E	Outcrop type and description	Sample description	Joints	Spacing
KJ-18	05.08.2011	Between Bu and Brimnes	1	383695 6705475	Fjord outcrop. Abrased rocks. Good quality outcrop.	Fine-medium-grained banded gneiss. Rich in fsp and qtz. Mafic layers consist mainly of bt. Pegmatoidal veins (~1 dm) of fsp. Strongly foliated.		
KJ-19	20.08.2011	Kjeavatnet	1220	397243 6711186	Mountain outcrop west of Kjeavatnet.	Medium-grained migmatitic gneiss. Abundant qtz and fsp. Prominent dark layers with bt. Stromatic.	069/87 002/86 016/71 005/78 171/78 179/72 182/89 030/84 205/65 207/76	ca 2 m
KJ-20	20.08.2011	Kjeavatnet	1025	397235 6710405	Flat mountain outcrop on the plateau north of Kjeåsen. Only flat, polished outcrops are evident in the surrounding area.	Coarse-grained banded gneiss. Light-coloured. Mainly qtz and fsp in lecocratic layers. Mafic layers are bt-rich. Prominent foliation.	078/40 077/68	
KJ-21	20.08.2011	Kjeåsen	805	397021 6709857	Mountain outcrop situated above a steep cliff. Weathered.	Medium-coarse-grained banded gneiss. Abundant qtz and kfsp. Bt and hbl in dark layers. Well-defined foliation.	313/80	0,5 m
KJ-22	21.08.2011	Kjeåsen	605	397618 6709345	Cliff face by gravel road next to tunnel.	Medium-coarse-grained banded gneiss. Leococratic layers are thick and coarse-grained. Melanocratic layers are finer-grained, but large (~0.5 cm) bt-crystals occur locally.	055/60 338/64	0,5m - 10 m

Outcrop number	Sampling date	Location	Elevation (m asl)	UTM N UTM E	Outcrop type and description	Sample description	Joints	Spacing
KJ-23	21.08.2011	Sima	1	397359 6708517	Fjord outcrop by the track to Kjeaneset.	Coarse-grained, white granite. Massive. Abundant qtz and kfsp. Some plg. Big crystals of bt occur locally.	Exfoliation	
KJ-24	23.08.2011	Nipahøgdi	1345	395733 6720845	Mountain outcrop in the valley to the southeat of the Nipahøgdi peak. Carbonaceous and micaceous phyllites are evident in the nearby areas.	Fine-grained quartzitic phyllite. Light grey, semi-shiny foliation planes. Contains mainly qtz. Thin bands of ms and bt. Abundant qtz-segregations. Meso- and microfolds.		
KJ-25	23.08.2011	Nipahøgdi	1210	397460 6720443	Mountain outcrop between Nipahøgdi and Rundavatnet. First outcrop with augen gneiss when approaching from the west.	Coarse-grained augen gneiss. Large (<5 cm) fsp pophyroclasts, qtz and fine-grained bt. Well defined foliation is cross-cut by granitoid.	009/74 026/55 028/56	1m - >10 m
KJ-26	23.08.2011	Osafjellet	1045	398231 6719552	Road outcrop by gravel road next to Rundavatnet. Good quality outcrop.	Dark-coloured augen gneiss with large (< 5 cm), elongate feldspar porphyroclasts. Fine-medium-grained dark layers rich in bt. Well-foliated.	228/85 042/85 028/56 038/76 178/72 165/56 338/61	0,5 m - 1 m
KJ-27	23.08.2011	Bruravik	50	383168 6707545	Road outcrop close to the ferry terminal. Oxidized meta-volcanics with felsic dykes are found in the same area.	Coarse-grained, light grey granite. Qtz, fsp, hbl and bt. Massive.	082/90	Several m

Outcrop number	Sampling date	Location	Elevation (m asl)	UTM N UTM E	Outcrop type and description	Sample description	Joints	Spacing
KJ-28	01.09.2011	Vatnasetenuten	1310	383333 6702043	Mountain outcrop close to the summit of Vatnasetenuten. Weathered.	Medium-coarse-grained migmatitic gneiss. Light-coloured due to high content of qtz and fsp. Large (~0.5 cm) crystals of hbl and px. Some bt.	034/84 027/80 100/90 030/70 018/74 030/64 030/64	
KJ-29	02.09.2011	Kjeåsen	170	397291 6708672	Cliff face on the track from Simadalen to Kjeåsen. Right before log bridge and extremely steep track with ladders.	Coarse-grained, white granite with large (> 1 cm) bt crystals. High content of qtz. Some fsp. Pinkish weathering colour.	Exfoliation	
KJ-30	02.09.2011	Kjeåsen	410	397343 6708863	Cliff face below Kjeåsen.	Coarse-grained, white granite. Big crystals and qtz and bt. Some fsp. Pinkish weathering colour.	348/78	1 m - several m
KJ-31	02.09.2011	Osa	15	391372 6718152	Road outcrop along steep cliff directly west of Osa. Abundant scree material.	Banded gneiss. Variable grain size. Large bt crystals (several cm) occur locally. Lecocratic bands consist mainly of qtz and kfsp. Melanocratic bands are rich in bt and hbl.	189/68	2 m - several tens of m

Appendix B: Container positions and track density gradients

a)

Irradiation NoB-008		
Position	**NoB-017**	**ρd (10^5)**
1	IRMM 3-1	21.522
2	BG-01T	21.443
3	BG-87	21.364
4	BG-86	21.285
5	BG-83	21.206
6	BG-78	21.127
7	BG-88	21.048
8	BG-112	20.969
9	BG-111	20.890
10	BG-107	20.811
11	BG-84	20.731
12	BG-108	20.653
13	**IRMM 3-2**	20.574
14	**Dur 1**	20.495
15	**Dur 2**	20.416
16	FCT 1	20.337
17	**FCT 2**	20.258
18	NPD 16/1-4	20.179
19	NPD 16/3-2	20.100
20	NPD 16/5-1	20.021
21	NPD 36/1-1	19.942
22	**IRMM 3-3**	19.863
23	BG-103	19.784
24	BG-104	19.704
25	BG-105	19.625
26	BG-106	19.546
27	BG-113	19.467
28	BG-114	19.388
29	BG-24	19.309
30	BG-25	19.230
31	BG-28	19.151
32	**BG-27**	19.072
33	**BG-53**	18.993
34	**BG-13**	18.914
35	BG-49	18.835
36	BG-50	18.756
37	BG-51	18.677
38	BG-52	18.598
39	**IRMM 3-4**	18.519

b)

Irradiation NoB-011		
Position	**NoB-017**	**ρd (10^5)**
1	**IRMM 1**	17.927
2	TM 04	17.880
3	TM 05	17.833
4	TM 06	17.786
5	TM 07	17.739
6	TM 08	17.692
7	TM 12	17.645
8	TM 13	17.598
9	TM 14	17.552
10	TM 15	17.505
11	TM 17	17.458
12	TM 18	17.411
13	BG-32	17.364
14	IRMM 2	17.317
15	BG-70	17.270
16	BG-72	17.223
17	BG-73	17.177
18	BG-75	17.130
19	BG-05	17.083
20	BG-08	17.036
21	BG-11	16.989
22	**BG-14**	16.942
23	**BG-16**	16.895
24	BG-17	16.848
25	DUR	16.802
26	**FCT**	16.755
27	**IRMM 3**	16.708
28	**BG-26**	16.6610
29	BG-42	16.614
30	PMM 03019	16.567
31	PZ 03005	16.520
32	PMM 0325	16.473
33	PZ 03057	16.427
34	PZ 03062	16.380
35	PZ 99	16.333
36	**IRMM 4**	16.286

c)

Irradiation NoB-017		
Position	**NoB-017**	**ρd (10^5)**
1	**IRMM 3-1**	21.375
2	**KJ-1**	21.257
3	**KJ-3**	21.140
4	**KJ-4**	21.022
5	**KJ-5**	20.904
6	**KJ-6**	20.786
7	**KJ-7**	20.668
8	**KJ-8**	20.550
9	**KJ-9**	20.432
10	**KJ-11**	20.314
11	**KJ-12**	20.196
12	**KJ-13**	20.078
13	**KJ-14**	19.960
14	**KJ-15**	19.842
15	**KJ-16**	19.724
16	**KJ-17**	19.606
17	**KJ-18**	19.488
18	**KJ-19**	19.370
19	DUR 1	19.252
20	FCT 1	19.134
21	**IRMM 3-2**	19.016
22	DUR 2	18.898
23	FCT 2	18.780
24	**KJ-20**	18.662
25	**KJ-21**	18.544
26	**KJ-22**	18.426
27	**KJ-24**	18.308
28	**KJ-25**	18.190
29	**KJ-26**	18.072
30	**KJ-27**	17.955
31	**KJ-28**	17.837
32	**KJ-31**	17.719
33	PMM03014	17.600
34	**IRMM 3-3**	17.482

Position of standard glasses, age standards and samples in irradiation tube **a)** NoB-008, **b)** NoB-011 and **c)** NoB-017, numbered according to distance from the neutron source. Estimated ρ_d values are displayed in the right column. Counted samples and standard glasses are marked in bold font.

Appendix C: Radial plots

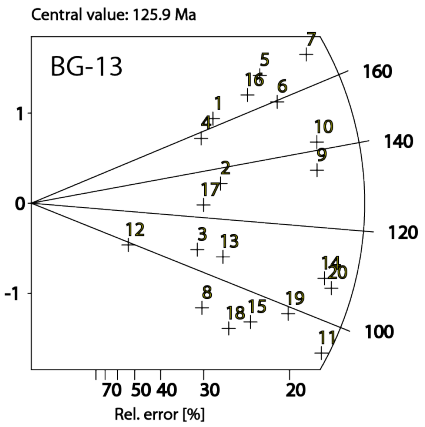

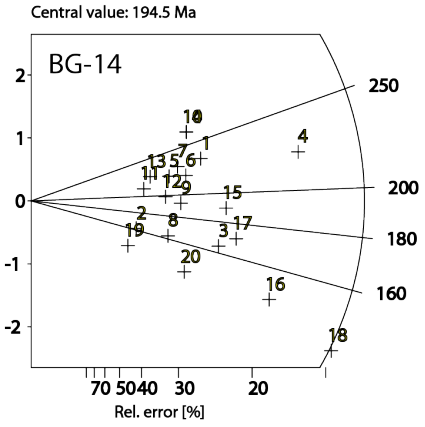

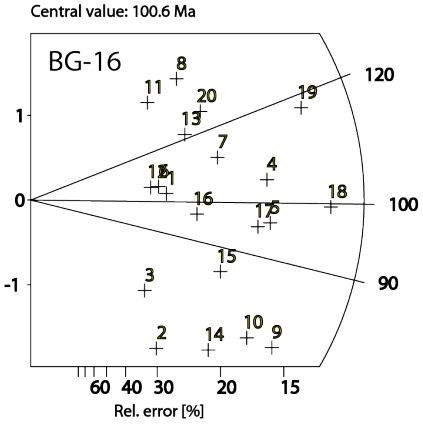

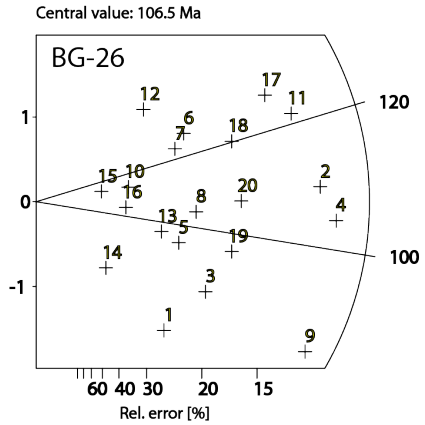

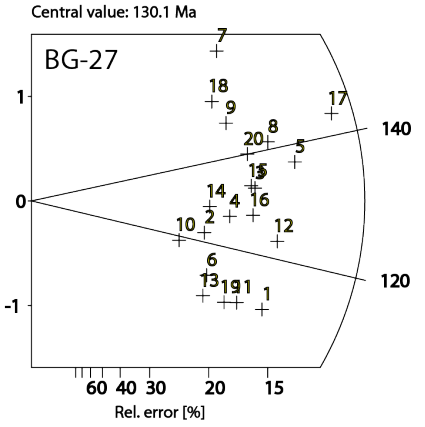

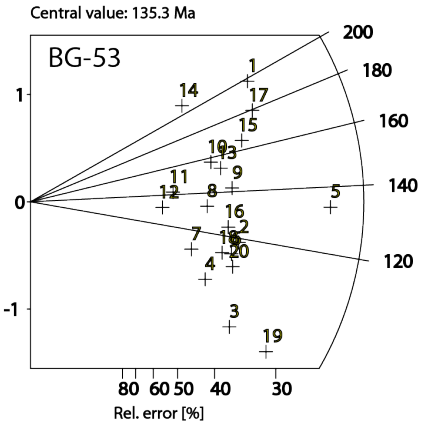

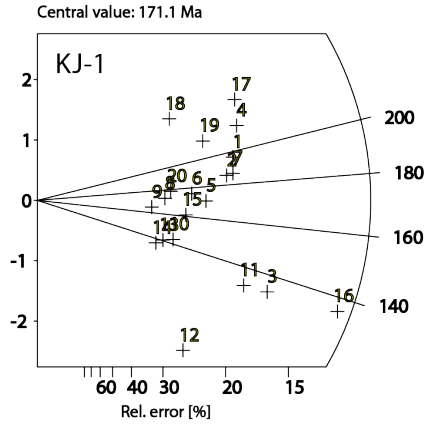

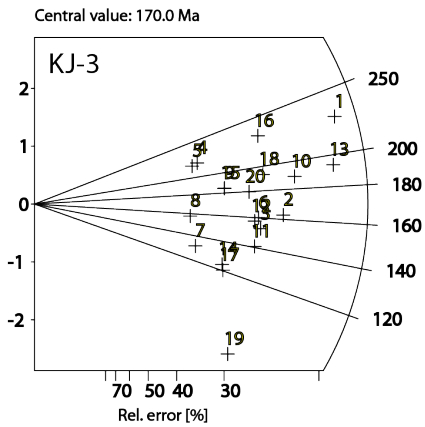

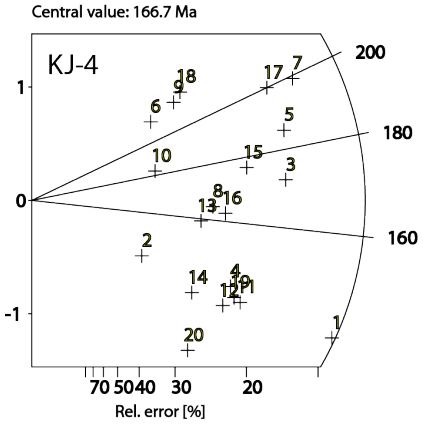

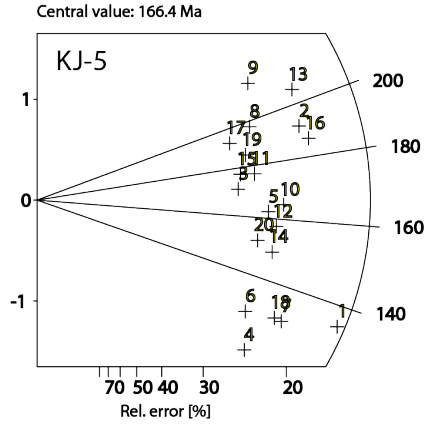

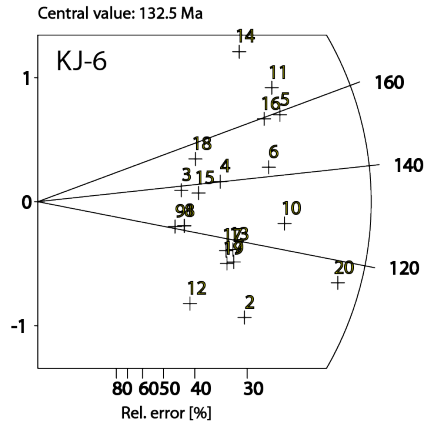

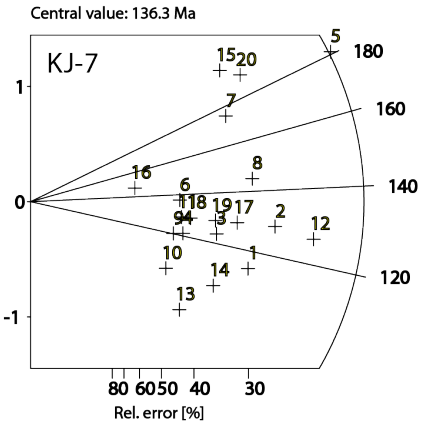

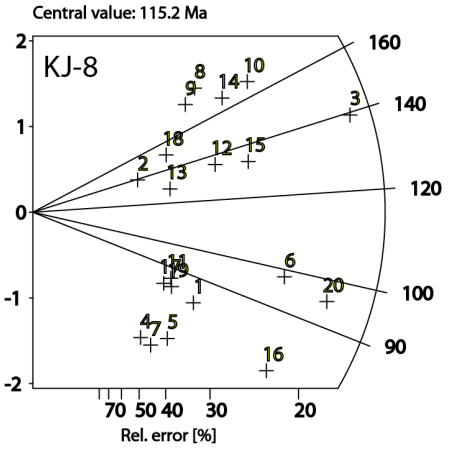
Central value: 115.2 Ma
KJ-8
Rel. error [%]

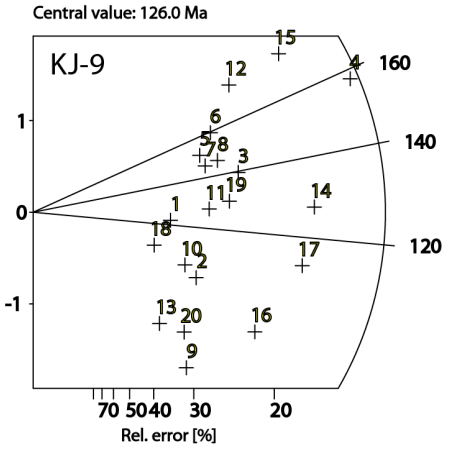
Central value: 126.0 Ma
KJ-9
Rel. error [%]

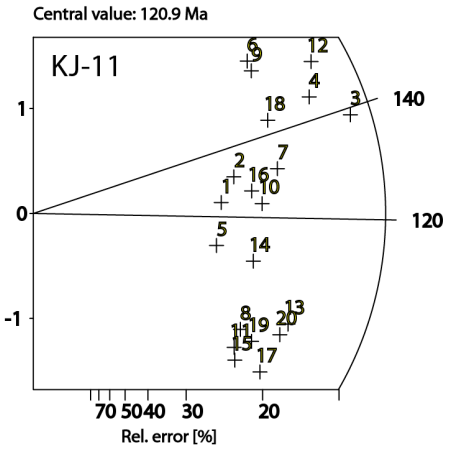
Central value: 120.9 Ma
KJ-11
Rel. error [%]

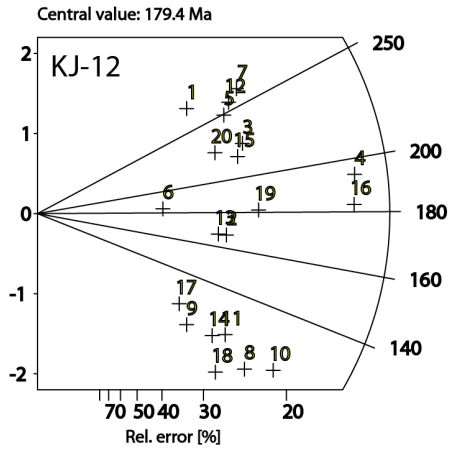
Central value: 179.4 Ma
KJ-12
Rel. error [%]

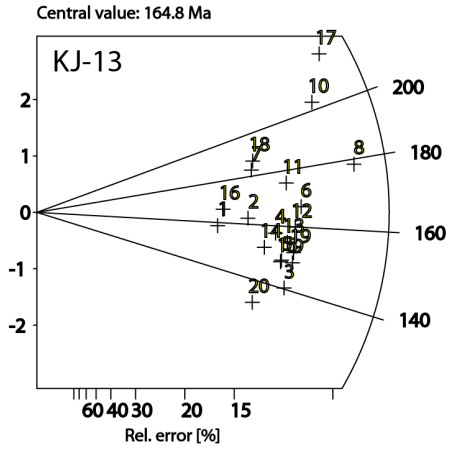
Central value: 164.8 Ma
KJ-13
Rel. error [%]

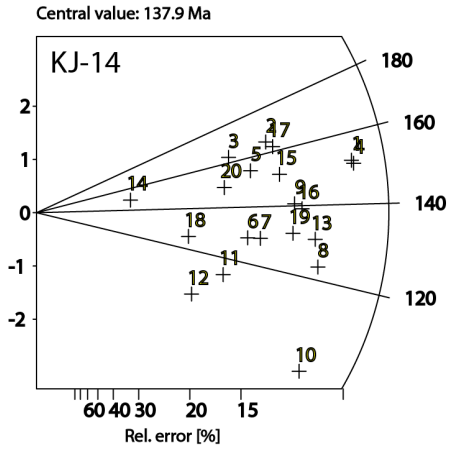
Central value: 137.9 Ma
KJ-14
Rel. error [%]

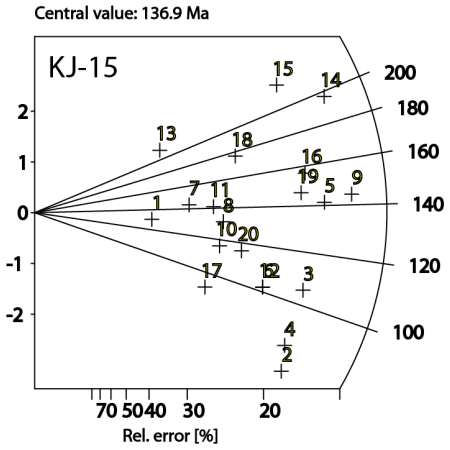
Central value: 136.9 Ma
KJ-15
Rel. error [%]

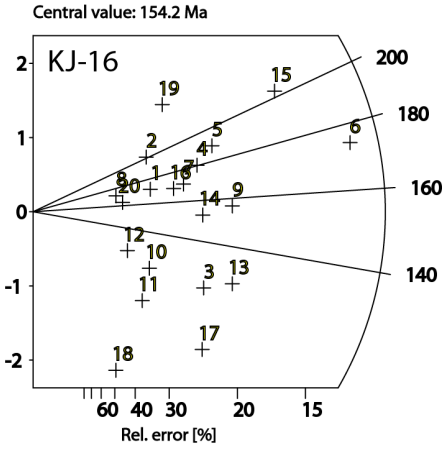
Central value: 154.2 Ma
KJ-16
Rel. error [%]

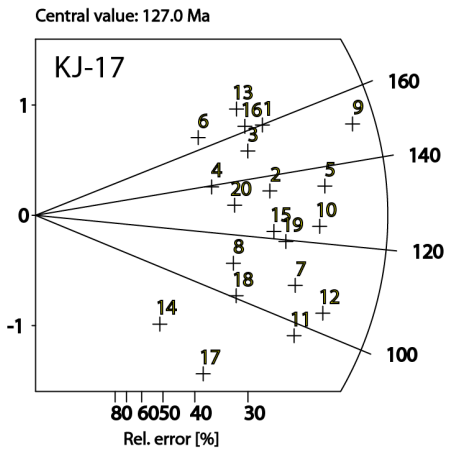
Central value: 127.0 Ma
KJ-17
Rel. error [%]

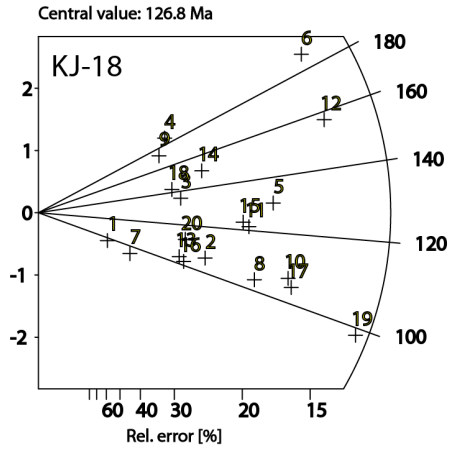
Central value: 126.8 Ma
KJ-18
Rel. error [%]

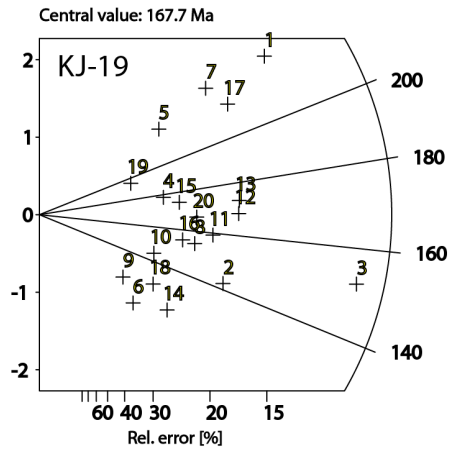
Central value: 167.7 Ma
KJ-19
Rel. error [%]

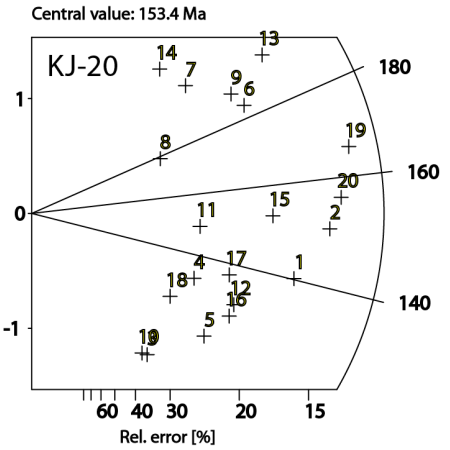
Central value: 153.4 Ma
KJ-20
Rel. error [%]

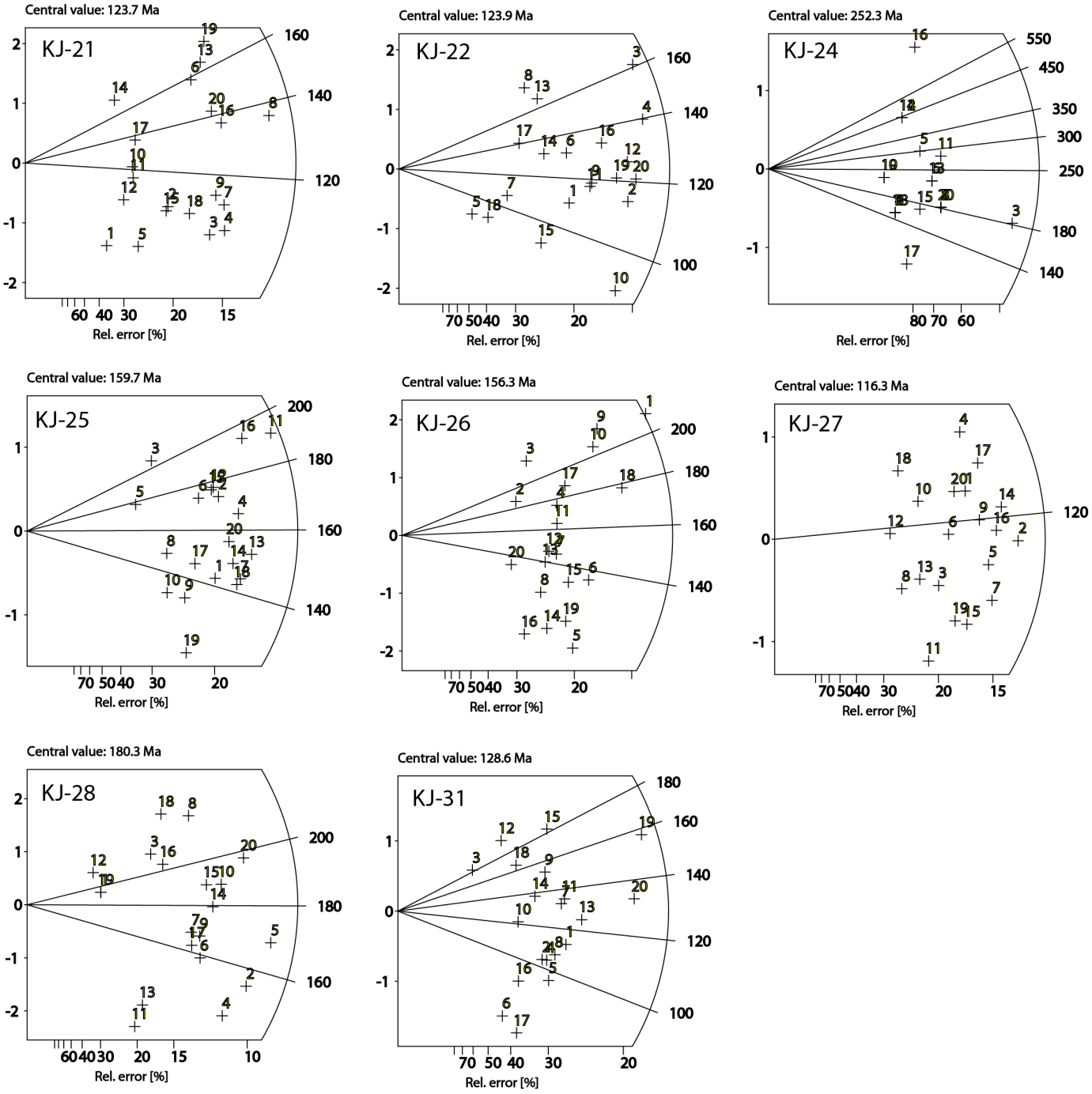

Radial plots from TrackKey, showing the distribution of single grain ages from apatite fission track analysis. Ages are read of the radial logarithmic scale in the outer right part of the diagram by extrapolating a line from the origin through the grain coordinate. The most precise grain ages are located furthest from the origin.

Appendix D: (U-Th)/He analytical data

Grain no.	TAU (%)	Estim. error on F_T (%)	First He re-extract (%)
KJ-8a	3.2	4.5	0.1
KJ-8b	2.5	4.5	0.3
KJ-11a	3.0	4.3	0.0
KJ-11b	3.1	4.0	0.1
KJ-11c	2.5	3.9	0.0
KJ19a	2.4	4.0	1.7
KJ-19b	2.9	3.3	0.0
KJ-19c	2.5	3.4	4.1
KJ-25a	2.7	3.5	0.3
KJ-25b	2.7	4.9	0.3

Aalytical data indicative of the quality of (U-Th)/He measurements for individual grains. TAU is the total analytical uncertainty in percent. Elevated first He re-extracts are evident for two of the grains in KJ-19.

Appendix E: Alternative inverse models

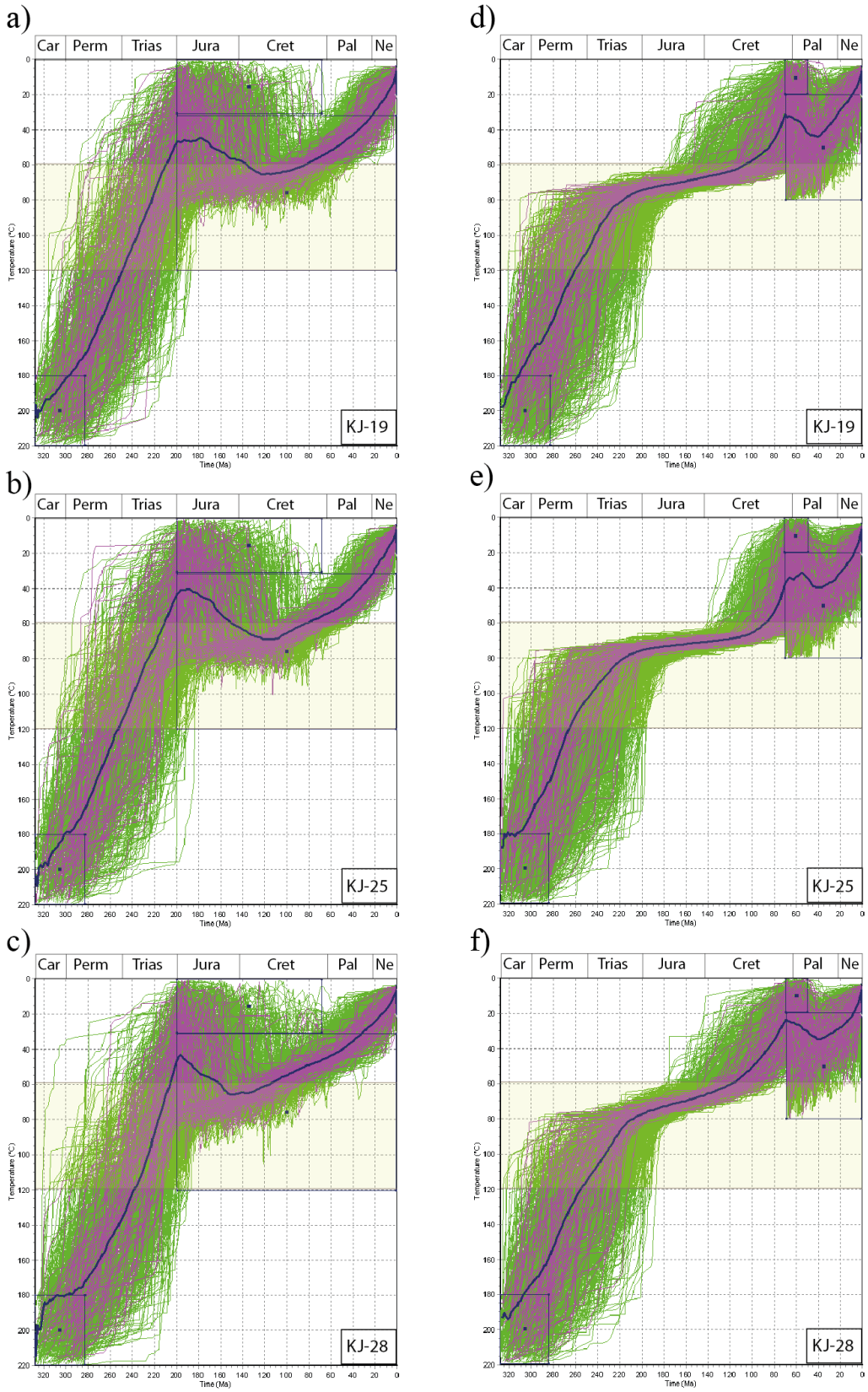

Alternative thermal history models for samples from the Hardangervidda plateau: **a-c)** Mesozoic peneplanation and reburial; **d-f)** Paleogene peneplanation and reburial.

Appendix F: Forward models for KJ-19

a)

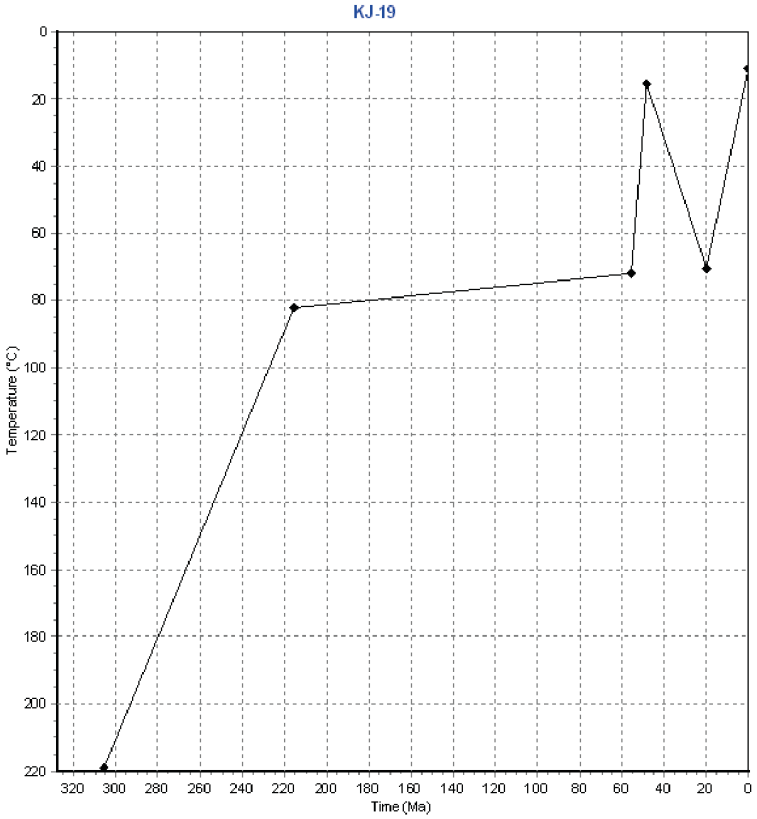

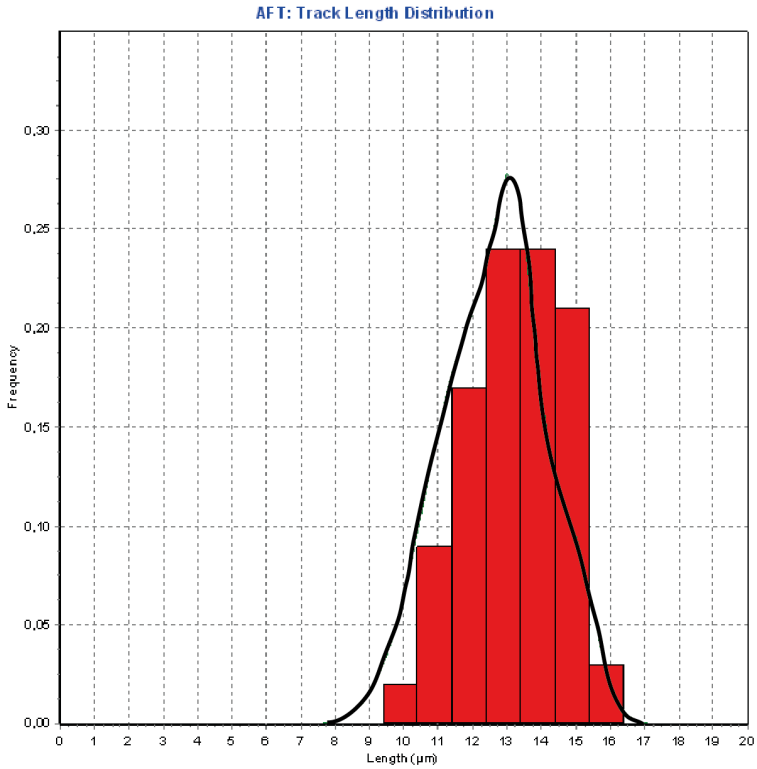

b)

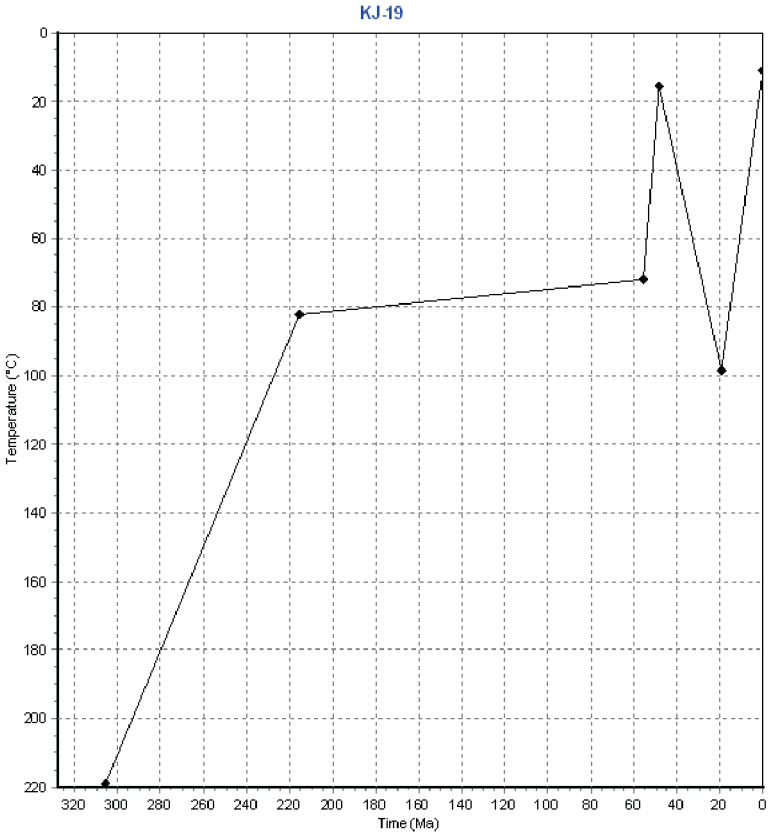
KJ-19
Temperature (°C)
Time (Ma)
0
20
40
60
80
100
120
140
160
180
200
220
320 300 280 260 240 220 200 180 160 140 120 100 80 60 40 20 0

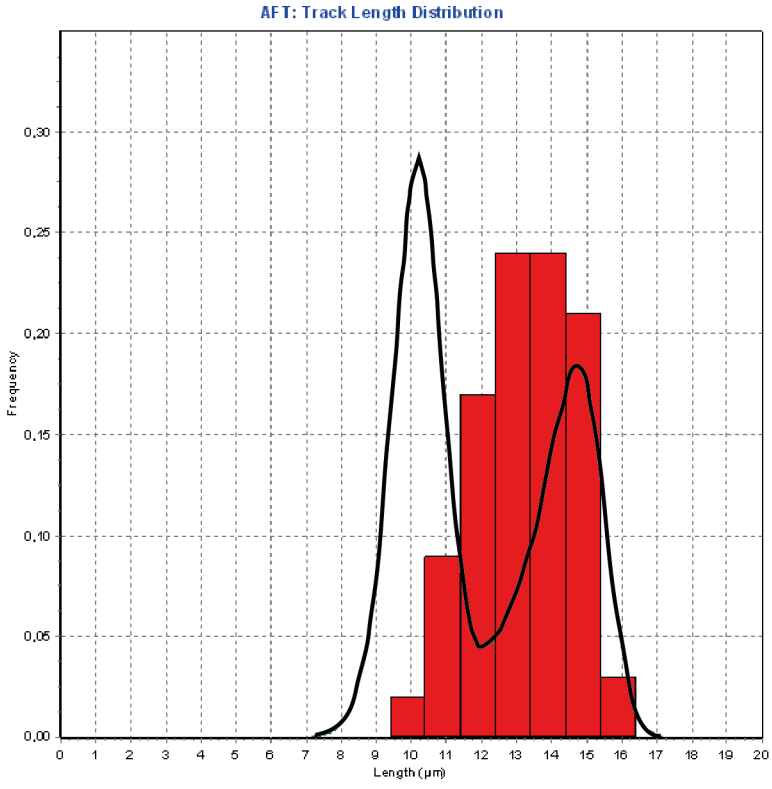
AFT: Track Length Distribution
Frequency
Length (µm)
0,30
0,25
0,20
0,15
0,10
0,05
0,00
0 1 2 3 4 5 6 7 8 9 10 11 12 13 14 15 16 17 18 19 20

c)

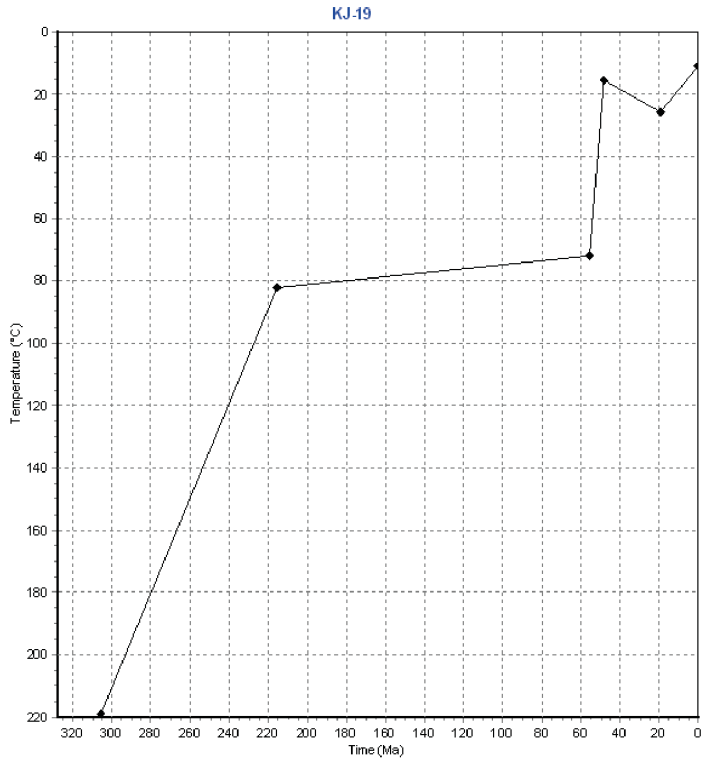

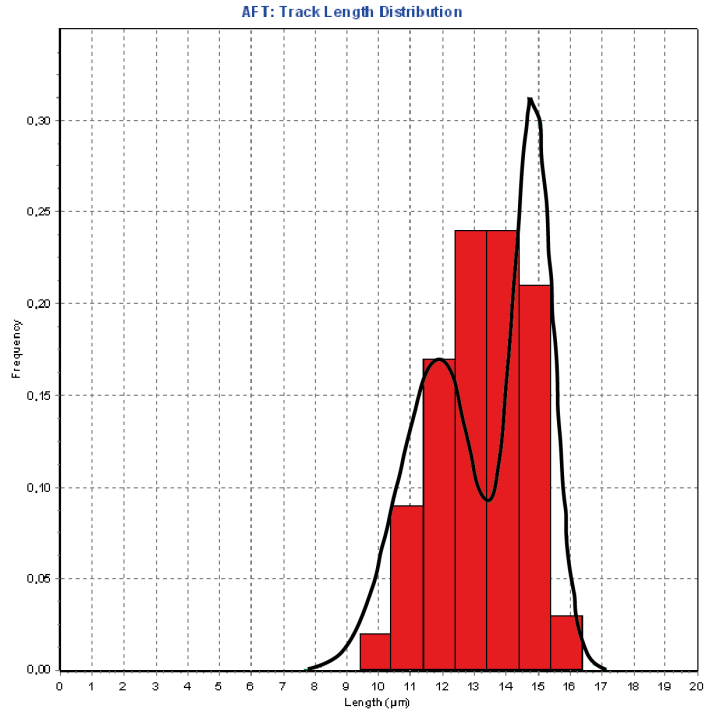

Forward modelling of KJ-19, assuming Paleogene peneplanation and reburial: **a)** Maximum burial depth as suggested by the inverse model. No bimodal track length distribution. **b)** Deep reburial. Bimodal track length distribution with a majority of short tracks. **c)** Shallow reburial. Bimodal track length distribution with a majority of long tracks. Red histograms show the c-axis projected track length distribution. Thick, black lines represent predicted distribution signature for the given thermal history.